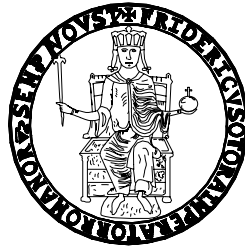


UNIVERSITY OF NAPLES FEDERICO II

PH.D. PROGRAMME IN SEISMIC RISK
COORDINATOR PROF. PAOLO GASPARINI
XIX CYCLE



PH.D. THESIS

MARCO DI LUDOVICO

**COMPARATIVE ASSESSMENT OF SEISMIC
REHABILITATION TECHNIQUES ON THE FULL
SCALE SPEAR STRUCTURE**

TUTOR PROF. GAETANO MANFREDI

*“Deep thinking is attainable only
by a man of deep feeling”*

S.T. Coleridge

Aknowledgments

At the end of this wonderful adventure that has been the Ph.D., the satisfaction for the developed work is associated to the keenly need to express my sincere gratitude to those that made it possible.

First of all I would like to thank Edoardo Cosenza and Gaetano Manfredi for their clear and irreplaceable guidance and for their deep and valuable teachings. To me they are a vivid example both in the research and life.

I am deeply grateful to Andrea Prota who influenced my perspectives in the research since my universities studies and for his generous devotion and continuous collaboration.

Thanks to Antonio Nanni who nourished my enthusiasm for research when I spent a period of study at the University of Missouri Rolla, U.S., before my graduation.

Thanks to Gerardo Verderame and Giovanni Fabbrocino and to all the members of the Department of Structural Analysis and Design with whom I shared interesting and constructive discussion about my research field.

I also wish to express my thanks to Paolo Negro, Elena Mola, Javier Molina and the whole staff of the ELSA Laboratory of the JRC where the entire experimental activity of the SPEAR project was carried out.

Thanks to my friends who have made my work less hard by sharing with me discouraging and joyful moments. To Gabriella for her continuous encouragement and comprehension; her love brings joy into my life making it brighter and brighter. To my brother that always reminded me to do the best and that ambition is not a fault.

Finally a special thanks to my parents: to my father for teaching me equilibrium and rationality and for transmitting me the passion for the research and to my mother that always has understood me and opened my mind with her originality and fantasy. Despite their diversity, they have always been united in their unshakable faith in me and in my dreams.

Marco

INDEX

Introduction	11
Chapter I	
1.1 DESCRIPTION OF THE STRUCTURE	19
1.2 PSEUDODYNAMIC TEST: RATIONALE AND SETUP	23
1.3 INSTRUMENTATION	26
1.4 EXPERIMENTAL CAMPAIGN	29
Chapter II	
2.1 EXPERIMENTAL BEHAVIOUR OF THE ‘AS-BUILT’ STRUCTURE	31
2.1.1 As-Built Structure: PGA = 0.15g.....	31
2.1.2 As-Built Structure: PGA = 0.20g.....	36
Chapter III	
3.1 MODELLING OF THE STRUCTURE	45
3.1.1 Geometrical model.....	45
3.1.2 Material Properties.....	48
3.1.3 Gravity loads and masses.....	49
3.2 LUMPED PLASTICITY MODEL.....	54
3.2.1 Lumped plasticity model assumptions.....	54
3.2.2 Plastic hinges characterization	56
3.3 NON LINEAR STATIC (PUSHOVER) ANALYSIS.....	59
3.3.1 Capacity	59
3.3.2 Seismic Demand	68
3.3.3 Theoretical vs. Experimental results.....	81
Chapter IV	
4.1 REHABILITATION INTERVENTION STRATEGIES	79
4.2 DESIGN OF REHABILITATION WITH COMPOSITES.....	81
4.2.1 Columns Confinemnt	81
4.2.2 Design of shear strengthening: Beam column joints.....	85
4.2.3 Design of shear strengthening: wall type column, C6	88
4.2.4 Assessment of the Rehabilitated Structure.....	89
4.3 FRP INSTALLATION PROCEDURE	97
4.4 EXPERIMENTAL BEHAVIOUR OF THE FRP RETROFITTED STRUCTURE	101
4.4.1 FRP retrofitted structure: PGA=0.20g	101
4.4.2 FRP retrofitted structure: PGA=0.30g	105
4.4.3 Theoretical vs. experimental results.....	111
4.5 ‘AS BUILT’ vs. FRP RETROFITTED: COMPARISON OF THE	
EXPERIMENTAL RESULTS	113

Chapter V

5.1	REHABILITATION WITH RC JACKETING	121
5.1.1	Design of the intervention with RC Jacketing	121
5.1.2	Assessment of the Rehabilitated Structure.....	124
5.2	RC JACKETING CONSTRUCTION PHASES	138
5.3	EXPERIMENTAL BEHAVIOUR OF THE RCJACKETED STRUCTURE....	143
5.3.1	RC Jacketed structure: PGA = 0.20g	143
5.3.2	RC Jacketed structure PGA = 0,30g	146
5.3.3	Theoretical vs. experimental results.....	152
5.4	‘AS-BUILT’ vs. RC JACKETED: COMPARISON OF THE EXPERIMENTAL RESULTS	153

Chapter VI

6.1	COMPARISON BETWEEN LAMINATES AND RC JACKETING	159
6.2	CONCLUSIVE REMARKS.....	161

Appendix A	167
-------------------------	-----

Appendix B	173
-------------------------	-----

Appendix C	179
-------------------------	-----

Appendix D	187
-------------------------	-----

INTRODUCTION

From a literature review it has been possible to point out, starting from greek and latin literature references, the development of at least 160 catastrophic seismic events in the Mediterranean area. Studies and researches have shown that about 60% of such events have been recorded in Italy as well as more than 50% of the recorded damages. Such data can be ascribed to the high intensity of the recorded earthquakes in Italy but also to both the high density of population and the presence of many structures under-designed or designed following old codes and construction practice; among them, plan-wise asymmetric structures are quite common.

Recent earthquakes have confirmed the inadequate protection level regarding both damages and collapse of the existing reinforced concrete (RC) structures; casualties and losses have been mainly due to deficient RC buildings not adequately designed for earthquake resistance.

Thus, in the last decades, seismic rehabilitation of the existing structures, and in particular of RC structures, has risen as a theme of a primary interest both in the academic and working sphere.

By analysing the data provided by the 14th census of population and buildings (2001) in Italy, it is possible to have a clear idea regarding the maintenance state of the existing reinforced concrete buildings (see Table 1); such data show that more than 10% of the existing buildings urgently need of rehabilitation interventions and about one million (35%) have been built before the redaction of the first code with seismic provisions, Legge 2/2/74 n.64 [1].

Given the economic costs of demolishing and re-building under-designed structures, it is nowadays necessary to enforce a more rational approach for the seismic assessment and rehabilitation of existing structures in order to reliably identify hazardous buildings and conceive rehabilitation interventions aimed at the most critical deficiencies only.

Such considerations caused the progressive change of the seismic provisions from simple suggestions and constructive indications to exhaustive guidelines with

theoretical approaches more and more complexes in order to exactly take into account, in the modelling of the structure, the seismic actions and the effective structural response.

PERIOD OF COSTRUCTION	Maintenance state				
	<i>Good</i>	<i>Quite good</i>	<i>Bad</i>	<i>Very bad</i>	<i>Total</i>
<i>Before 1919</i>	0	0	0	0	0
<i>From 1919 to 1945</i>	14374	44540	21759	2740	83413
<i>From 1946 to 1961</i>	59290	169830	55808	3856	288784
<i>From 1962 to 1971</i>	148878	360053	79191	3580	591702
<i>From 1972 to 1981</i>	251055	457426	77578	3104	789163
<i>From 1982 to 1991</i>	277105	305423	36745	1425	620698
<i>After 1991</i>	294223	90157	9545	520	394445
Total	1044925	1427429	280626	15225	2768205

RC Building Maintenance state in Italy

Maintenance State	Percentage
Good	38%
Quite good	51%
Bad	10%
Very bad	1%

Rc Buildings period of construction in Italy

Period of Construction	Percentage
From 1919 to 1945	14%
From 1946 to 1961	22%
From 1962 to 1971	30%
From 1972 to 1981	21%
From 1982 to 1991	3%
After 1991	10%

Table 1 - Buildings maintenance state and period of construction- Italy - census of 2001.

A strong impulse in such way has been provided, in Italy, by the development of a new seismic guideline, Ordinanza 3431 [2], especially developed with the aim of ensuring that, in the event of earthquakes, the human lives are protected, damage is limited and structure important for civil protection remain operational (hospitals, schools, barracks, prefectures etc.).

According to the European Standard seismic provisions, Eurocode 8, Part I [3], the main innovative aspects of such guideline can be summarized as follows:

- the possibility of choosing various analysis techniques for the structural calculation:
 - Static Linear Analysis
 - Dynamic Analysis
 - Non-Linear static analysis
 - Non-Linear Dynamic Analysis

each analysis can be selected according to various criteria and limitations outlined in the document; in this way, for each structural system, it is possible to guarantee an adequate level of investigation;

- the introduction of the importance factors to take into account reliability differentiation; buildings are classified in importance classes, depending on the consequences of collapse for human life, on their importance for public safety and civil protection in the immediate post-earthquake period, and on the social and economic consequences of collapse;
- the introduction of two ductility classes (CD”A” and CD”B”) depending on the structural hysteretic dissipation capacity;
- the presence of a section exclusively addressed to the existing structures in order to provide criteria for the assessment of their seismic performances and for the design of the repair/strengthening measures.

The development of such code has provided to the structural engineers an effective tool for a more rationale and safety design approach to the design of the structures in seismic regions and for the assessment of the existing ones. Furthermore, the definition of such provisions, have pointed out the deficiencies of the existing RC buildings designed with reference to old seismic codes.

Thus, studies in the field of repair/strengthening schemes that will provide cost-effective and structurally effective solutions have focused the interest of the research community; traditional methods used in the past have to be revised and developed in the light of the new seismic code requirements as well as the study of new methods, also based on the use of new materials (i.e. Fiber Reinforced Polymers, FRPs), need to be further investigated. The most common strategies adopted in the field of seismic rehabilitation of existing structures are the restriction or change of use of the building, partial demolition and/or mass reduction, removal or lessening of existing irregularities and discontinuities, addition of new lateral load resistance systems, local or global modification of elements and systems.

In particular, the *local intervention methods* are aimed at increasing the deformation capacity of deficient components so that they will not reach their specified limit state as the building responds at the design level. Common approaches include:

- *Steel jacketing*: mainly used in the case of columns, involves the total encasement of the column with thin steel plate placed at a small distance from the column surface or alternatively a steel cage with steel angles in the corners of the existing cross-section and transversal straps welded on them; it is aimed at increasing both the flexural and shear strength of the member, its deformation capacity and improving the efficiency of lap splice zones;
- *Steel plate adhesion*: mainly used in the case of beams, it allows increasing shear and flexural strength of the member;
- *Externally Bonded FRPs*: is regarded as a selective intervention technique, aiming at: a) increasing the flexural capacity of deficient members, with and without axial load, through the application of composites with the fibers placed parallel to the element axis, b) increasing the shear strength through the application of composites with the fibers placed transversely to the element axis, c) increasing the ductility (or the chord rotation capacity) of critical zones of beams and columns through FRP wrapping (confinement), d) improving the efficiency of lap splice zones, through FRP wrapping, e) preventing buckling of longitudinal rebars under compression through FRP wrapping, f) increasing the tensile strength of the panels of partially confined beam-column joints through the application of composites with the fibers placed along the principal tensile stresses.

On the other hand, ***global intervention methods*** involve a global modification of the structural system; such modification is designed so that the design demands (often denoted by target displacement) on the existing structural and nonstructural components are less than structural capacities. Common approaches include:

- *RC jacketing*: is a widely used and cost-effective technique for the rehabilitation of concrete members; it is considered a global intervention if the added longitudinal reinforcement placed in the jacket passes through holes drilled in the slab and new concrete is placed in the beam-column joint (in the case of longitudinal reinforcement stopped at the

floor level it is classified as a member intervention technique). It has multiple effects on stiffness, flexural/shear resistance and deformation capacity;

- *Addition of walls*: it is commonly used in the existing structures by introducing new shear walls with a partial or full infill of selected bays of the existing frame; such method allows decreasing the global lateral drift and thus reducing the damages in frame members. A drawback of the method is the need for strengthening the foundations and for integrating the new walls with the rest of the structure;
- *Steel bracing*: is one effective way of increasing the strength and earthquake resistance of a building; advantages of such technique are the possibility of pursue such strengthening by a minimal added weight to the structure and, in the case of external steel systems, by a minimum disruption to the function of the buildings and its occupants. On the other hand, particular attention need to be paid regarding the connections between the steel braces and the existing structure;
- *Base isolators*: are becoming an increasingly applied structural design technique for rehabilitation of buildings especially in the case of buildings with expensive and valuable contents; the objective of seismic isolation systems is to decouple the structure from the horizontal components of the earthquake ground motion by interposing a layer with low horizontal stiffness between the structure and the foundation in order to prevent the superstructure of the building from adsorbing the earthquake energy. Displacement and yielding are concentrated at the level of the isolation devices, and the superstructure behaves very much like a rigid body.

The overview of the rehabilitation strategies outlined, shows that the structural performances of an existing building can be enhanced in different ways by acting on ductility, stiffness or strength (separately or, in many cases, at the same time); in each case, a preliminary analysis of the existing structure performances and the

evaluation of the analysis results are strictly necessary to select the rehabilitation method that meets the required performance targets. Nevertheless, numerous factors influence the selection of the most appropriate technique and therefore no general rules can be applied. Moreover, it is noted that while the effect of the rehabilitation methods above recalled have been extensively investigated, in the past, with regard to a single structural member or sub-assembly, real data of the seismic performances on full scale tests are still severely lacking.

The above considerations clearly highlight the importance of research studies specifically targeted at the evaluation of current assessment and rehabilitation methods and at development of new assessment and retrofitting techniques.

In such context, the SPEAR (Seismic Performance Assessment and Rehabilitation) research project, funded by the European Commission, with the participation of many European and overseas Partners, has been developed with the aim of throwing light onto the behaviour of existing RC frame buildings lacking seismic provisions. In the framework of the research activity of the European Laboratory for Structural Assessment (ELSA) of the Joint Research Centre (JRC) in Ispra, Italy, a series of full-scale bi-directional pseudo-dynamic tests on a torsionally unbalanced three storey RC framed structure have been carried out as the core of such research project. The structure, that represents a simplification of a typical old construction in Southern Europe, was designed to sustain only gravity loads with deficiencies typical of non-seismic existing buildings as plan irregularity, poor local detailing, scarcity of rebars, insufficient column confinement, weak joints and older construction practice. The experimental activity consisted in three rounds of tests on the structure in three different configurations: 'as-built', FRP retrofitted and rehabilitated by RC jacketing. In this doctoral thesis each phase of the developed experimental campaign along with its results are presented and illustrated; furthermore, the philosophy and the calculation procedures followed to carry out the design of the rehabilitation interventions and their construction phases are extensively treated.

In particular, *Chapter I* involves the description of the structure and of the experimental campaign; *Chapter II* presents the experimental results obtained by the tests on the 'as-built' structure under the Montenegro Herceg-Novı accelerogram scaled to peak ground acceleration (PGA) of 0.15g and 0.20g. In *Chapter III*, a post-

test lumped plasticity model of the structure is presented along with the theoretical assessment of the seismic capacity of the structure by using a non linear static pushover analysis. **Chapter IV** describes the design of the first rehabilitation method investigated that is the use of FRP laminates to increase the global deformation capacity of the structure; the calculation procedures adopted in the design of the local interventions, the theoretical prediction in terms of global performances of the retrofitted structure by using a non linear static pushover analysis as well as the construction phases and the experimental results are presented and discussed. In **Chapter V**, the RC jacketing intervention design is illustrated in detail; theoretical prediction, construction phases and experimental results are again described and presented. Finally, **Chapter VI** deals with a conclusive remarks regarding the comparison between the two different rehabilitation strategies adopted in the experimental activity as well as the theoretical predictions reliability.

Chapter I

1.1 DESCRIPTION OF THE STRUCTURE

The SPEAR structure represents a three-storey RC structure typical of old constructions built in southern European Countries without specific provisions for earthquake resistance. Its design aimed at obtaining a gravity load designed (GLD) frame and was performed using the concrete design code enforced in Greece between 1954 and 1995 as well as both construction practice and materials typical of the early 70s. The structure is regular in elevation with a storey height of 3 meters and 2.5 m clear height of columns between the beams; it is non symmetric in both directions, with 2-bay frames spanning from 3 to 6 meters (see Figure 1.1-1). The 3D view of the structural model and of the completed structure are shown in Figure 1.1-2.

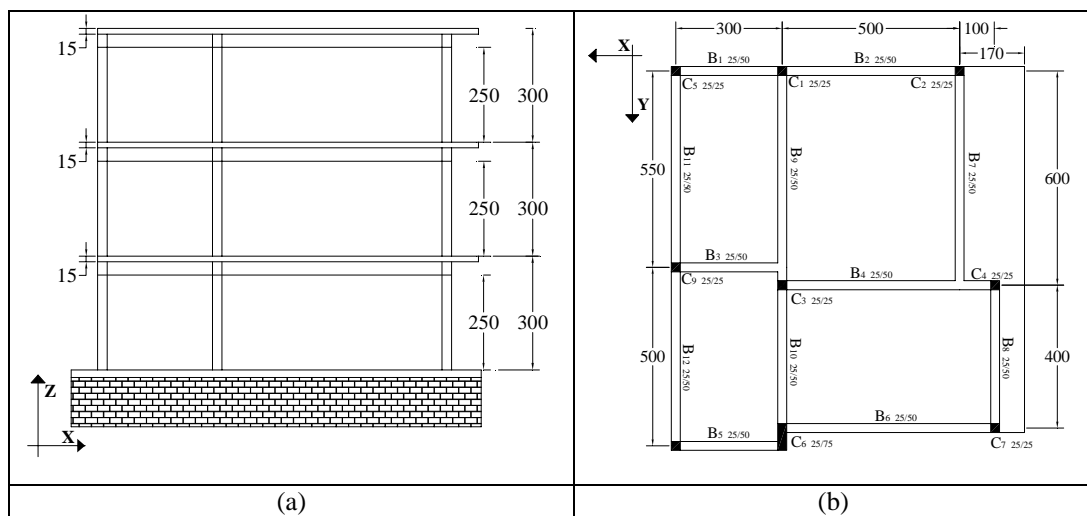


Figure 1.1-1 – Structure elevation (a) and plan (b) view, (dimensions in cm).

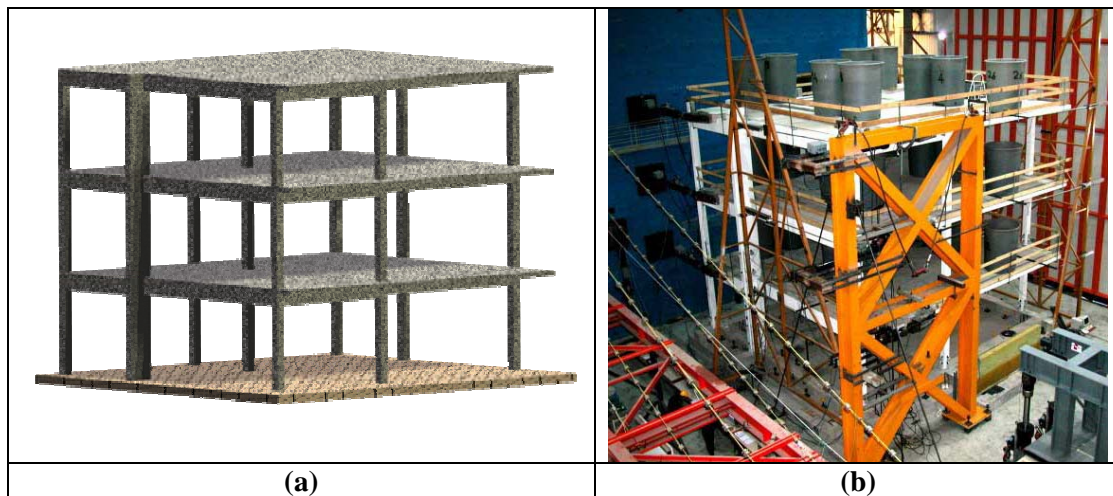


Figure 1.1-2 – Structure model (a) and 3D (b) view.

The concrete floor slabs are 150 mm thick, with bi-directional 8 mm smooth steel rebars, at 100, 200 or 400 mm spacing.

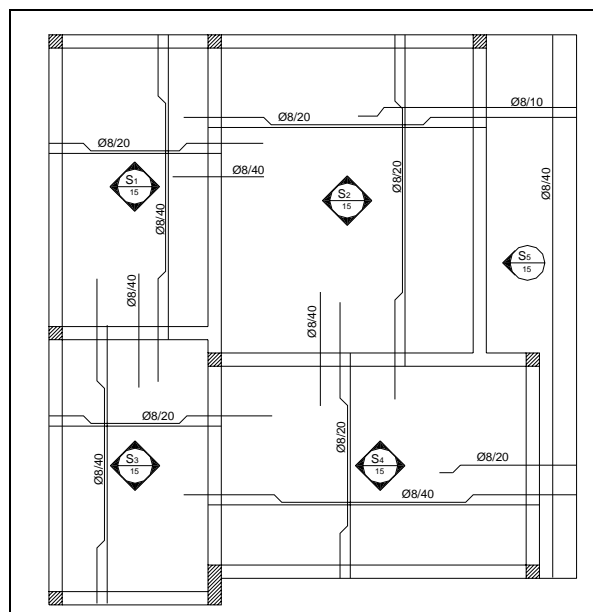


Figure 1.1-3 – Slab reinforcement layout.

The structure has the same reinforcement in the beams and columns of each storey. Beam cross-sections are 250 mm wide and 500 mm deep. They are reinforced by means of 12 and 20 mm smooth steel bars, both straight and bent at 45 degrees angles, as typical in older practice; 8 mm smooth steel stirrups have 200 mm spacing (see Figure 1.1-4). The confinement provided by this arrangement is thus very low. Eight out of the nine columns have a square 250 by 250 mm cross-section; the ninth

(column C6) has a rectangular cross-section of 250 by 750 mm, which makes it much stiffer and stronger than the others along the Y direction, (as defined in Figure 1.1-1) which is the strong direction for the whole structure. All columns have longitudinal reinforcement provided by 12 mm bars (4 in the corners of the square columns, 10 along the perimeter of the rectangular one) (see Figure 1.1-4). Their longitudinal bars are lap-spliced over 400 mm at floor level. Column stirrups consist in 8 mm bars, spaced at 250 mm, which is equal to the column width, meaning that the confinement effect is again very low.

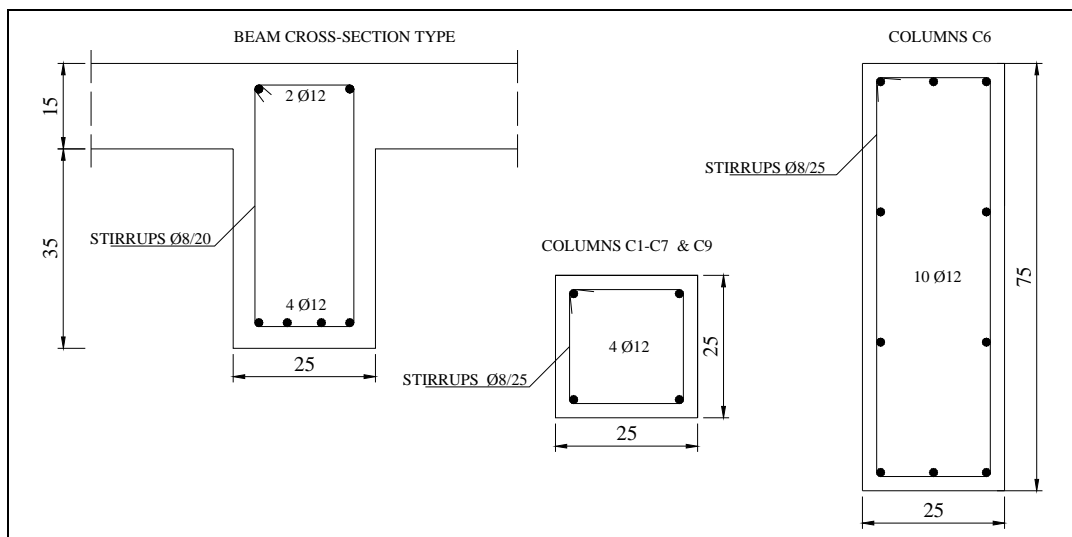


Figure 1.1-4 – Typical beam and column cross-sections, dimension in cm.

Details about beams longitudinal reinforcement are reported in Appendix A.

The joints of the structure are one of its weakest points: neither beam nor column stirrups continue into them, so that no confinement at all is provided. Moreover, some of the beams directly intersect other beams (see joint close to columns C3 and C4 in Figure 1.1-1) resulting in beam-to-beam joints without the support of the column.

The foundation system is provided by strip footings; column longitudinal reinforcement is lap spliced over 400 mm at each floor level including the first one (see Figure 1.1-5)

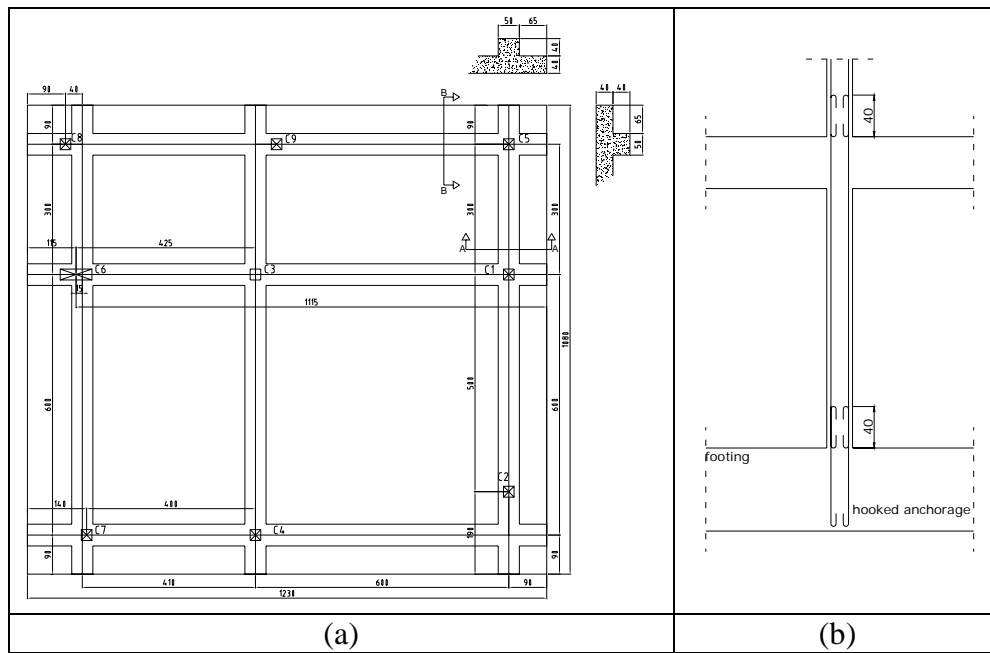


Figure 1.1-5 – Footings plan view (a) and longitudinal reinforcement lap splice

The materials used for the structure were those typical of older practice: concrete and smooth steel bars strength were equal to $f'_c = 25$ MPa and $f_y = 320$ MPa, respectively.

1.2 PSEUDODYNAMIC TEST: RATIONALE AND SETUP

The PsD method is an on-line computer controlled testing technique devoted to the evaluation of structures subjected to dynamics loads, typically earthquakes. It is an hybrid testing technique that combines on-line computer simulation of the dynamic aspects of the problem with experimental outcomes of the structure in order to provide realistic dynamic response histories, even for the non linear structural behaviour. The PsD method is based on the analytical techniques used in the structural dynamics considering the structure as an assemblage of elements interconnected at a finite number of nodes. The motion of the structure is governed by the following equations:

$$\mathbf{M}\mathbf{a}(t)+\mathbf{C}\mathbf{v}(t)+\mathbf{r}(t) = \mathbf{f}(t) \quad (1)$$

where \mathbf{M} and \mathbf{C} are the structural mass and damping, $\mathbf{a}(t)$ and $\mathbf{v}(t)$ are the acceleration and velocity vectors, $\mathbf{r}(t)$ is the structural restoring force vector and $\mathbf{f}(t)$ is the internal force vector applied to the system.

In the case of framed buildings (in which masses can be concentrated in the floor slabs) the equations (1) can be expressed in terms of a reduced number of degrees of freedom (DoFs) that are the horizontal displacements in the floor slabs; thus the PsD method application is simplified because the number of points of the structure to be controlled (in general equal to the number of actuators attached to the structure) is reduced.

In order to solve equations (1), it is necessary to compute the restoring force vector, $\mathbf{r}(t)$, by using appropriate subroutines which represent the structural behaviour of each element. Such computation is the major source of uncertainty because adequate refined models for the structural behaviour of the elements is still lacking. The main advantage of the PsD method is that in the numerical solution of the discretized equations of motions, the evaluation of the restoring force vector, $\mathbf{r}(t)$, is not evaluated numerically, but directly measured on the structure at certain controlled locations; mass and viscous damping of the test structure are analytically modelled.

Once the restoring force vector has been computed, the numerical algorithms in the on-line computer solve the equations of motion by numerical time integration methods. The calculation results are the displacements that have to be imposed to the

structure at the next time step; then the test structure is loaded by actuators until the imposed target displacements is achieved and the restoring force vector is measured again. At this stage the procedure follows the same steps above illustrated in an iterative way. A more detailed description of both the method and the mathematical approach can be found in Molina et al. [4] and Molina et al. [5].

A sketch of the PsD method procedure is reported in Figure 1.2-1.

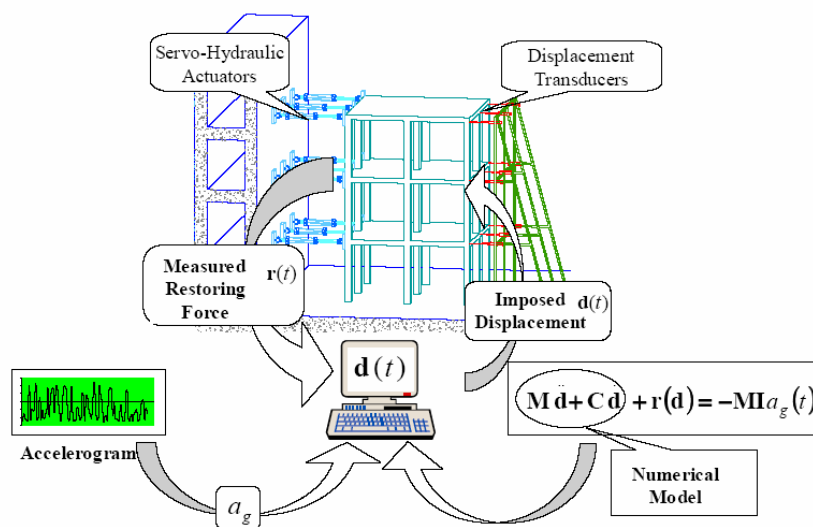


Figure 1.2-1 – Schematic representation of the pseudo-dynamic test method

In the case of the SPEAR structure a bi-directional PsD test method was used, consisting in the simultaneous application of the longitudinal and the transverse earthquake components to the structure. The bidirectionality of the test introduces a higher degree of complexity as the DoFs to be considered are three per storey (two translations and one rotation along the vertical axis) as opposed to single one in the case of unidirectional PsD tests. Thus four actuators (MOOG) with load capacity of 0.5 MN and $\pm 0.5\text{m}$ ($\pm 0.25\text{m}$ for the first floor) stroke were installed at each floor; three of which were strictly necessary. Each actuator was equipped with a strain-gauge load cell and a Temposonics internal displacement transducer.

In order to implement the time integration algorithm, it is necessary to estimate the structural mass that takes into account the presence of the finishing and of the quota of the live loads which is assumed to act at the time of the earthquake.

In the case of the structure discussed in the present doctoral thesis, the full-scale test did not have finishing and live load on it; thus in order to reproduce the

corresponding stress on the structural elements, a distribution of water tanks on each floor was applied. The tanks were distributed to simulate the presence of finishing and of 30% of live loads so that the gravity loads on columns would be the closest to the value used in the design. The tanks distribution is reported in Figure 1.2-2.

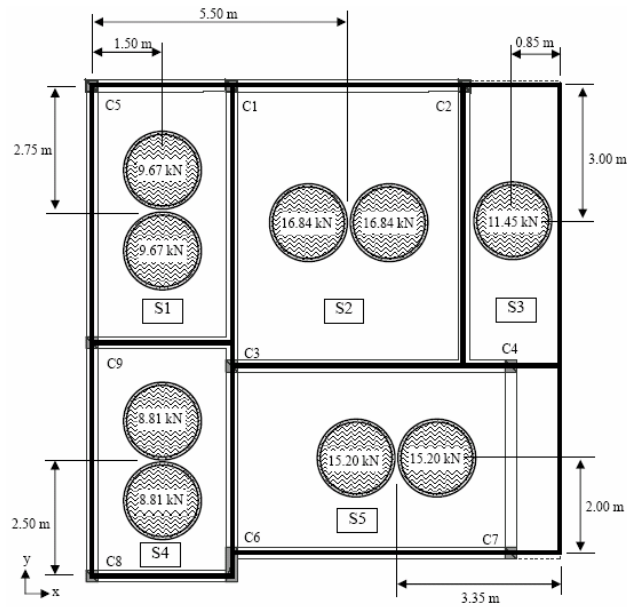


Figure 1.2-2 – Water tanks distribution (Jeong, S.-H. and Elnashai, A. S. [6] part II)

1.3 INSTRUMENTATION

The layout of the instrumentation on the structure responded to different needs and considerations, both numerical and experimental. Based on the extensive preliminary numerical simulations (Jeong and Elnashai, [7] part I), the expected damage pattern had been defined, and the elements likely to exhibit the most significant behaviour had been identified. Such analysis showed that the failure were expected mainly on columns and thus the local instrumentation was focused on the columns at the first and second floor, with inclinometers mounted at the member ends. To capture the effects of the hooks of the bars, inclinometers were also placed above the splice level (see Figure 1.3-1).

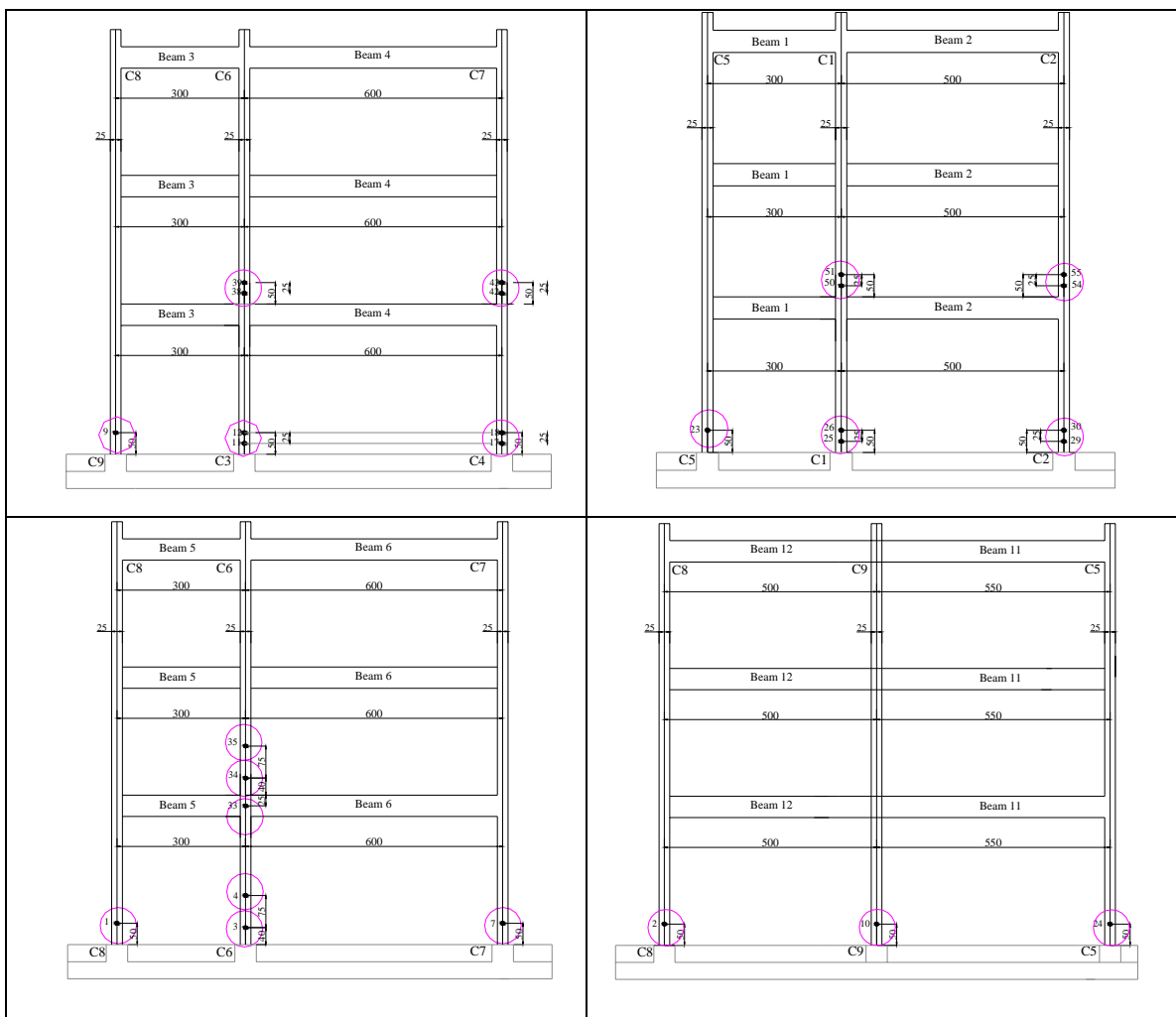


Figure 1.3-1 – Inclinometers on the square columns

Moreover, on the two large faces of column C6, displacement transducers were located to measure the shear deformation of the column, without including the effects of bar slippage at the bottom (see Figure 1.3-2).

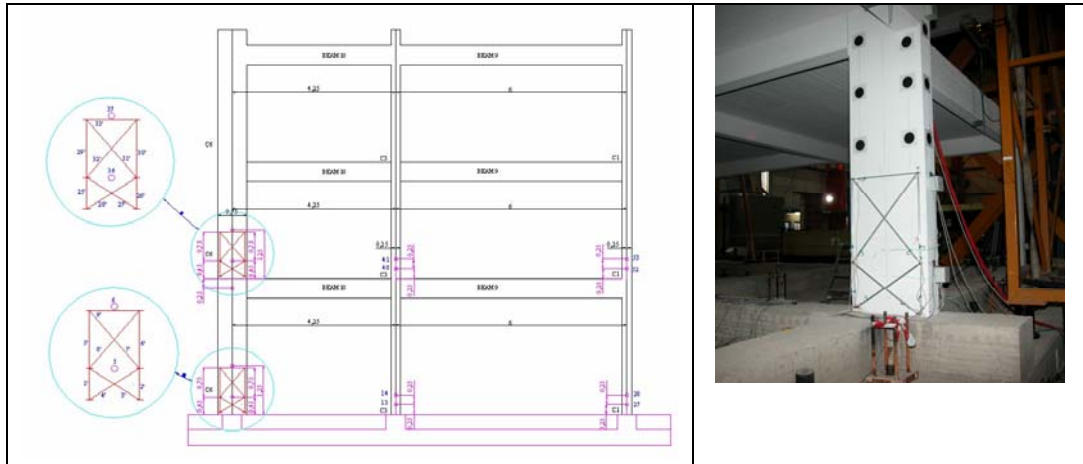


Figure 1.3-2 - Inclination meters on the rectangular column C6.

Finally, the beam-on-beam intersections (close to columns C3 and C4) on the soffit of the first and second floor were chosen to be more carefully investigated because they could have experienced local torsional effects. They were both instrumented with two inclinometers (one in each direction) and two crossed displacement transducers (see Figure 1.3-3).

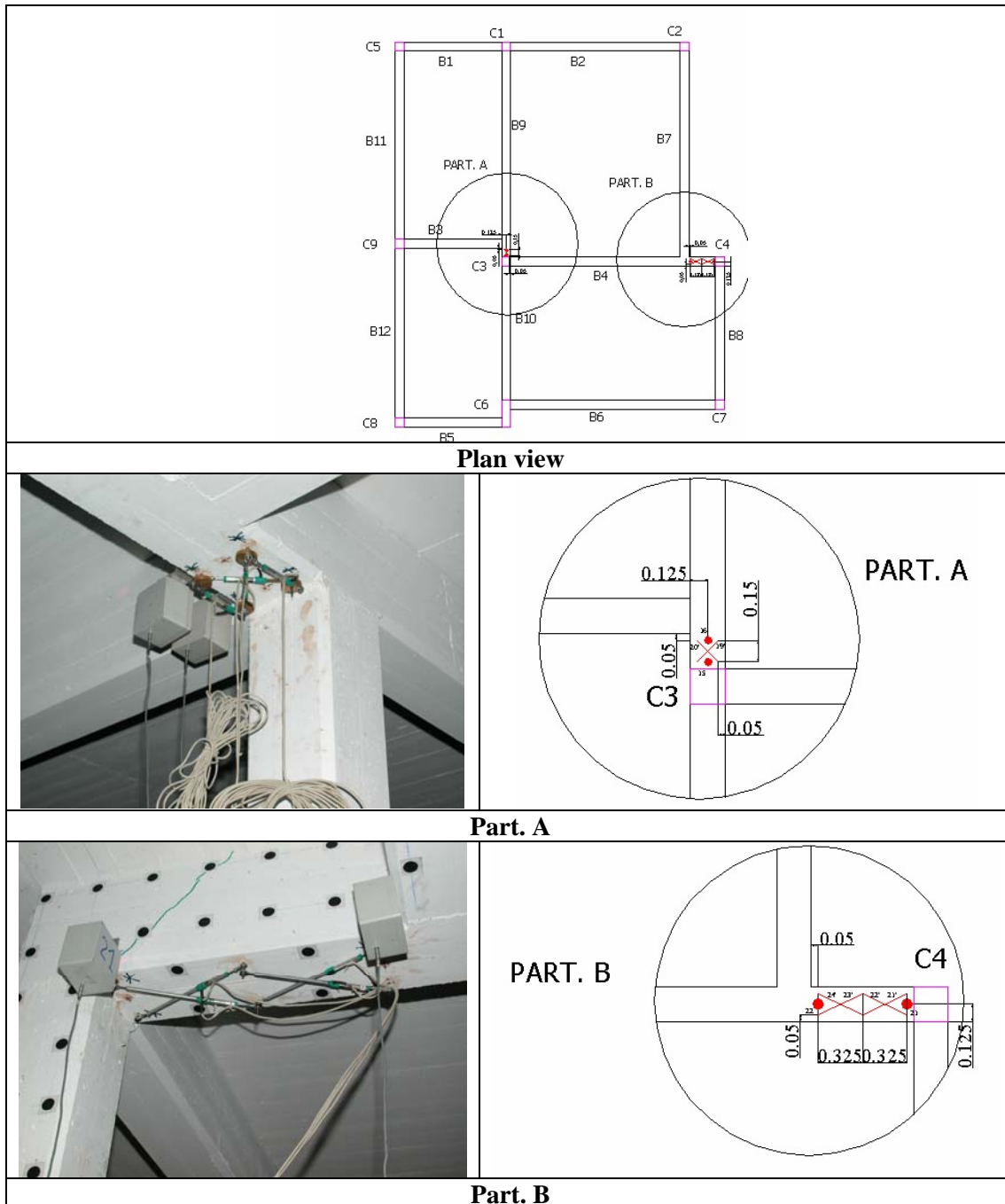


Figure 1.3-3 - Inclinerometers on beam-on-beam intersections.

1.4 EXPERIMENTAL CAMPAIGN

The experimental program consisted in a series of bi-directional PsD tests, each of them entailing the simultaneous application of the longitudinal and the transverse earthquake components to the structure.

In order to provide comprehensive experimental data for the investigation of the structure, after extensive preliminary numerical activity (Fajfar et al. [8]; Jeong and Elnashai, [7] part I), the Montenegro 1979 Herceg Novi ground motion record was selected for the test. The two orthogonal components of horizontal accelerations of such record were modified from natural records to be compatible to the Eurocode 8 [3] Part 1, Type 1 design spectrum, soil type C and 5% damping (see Figure 1.4-1).

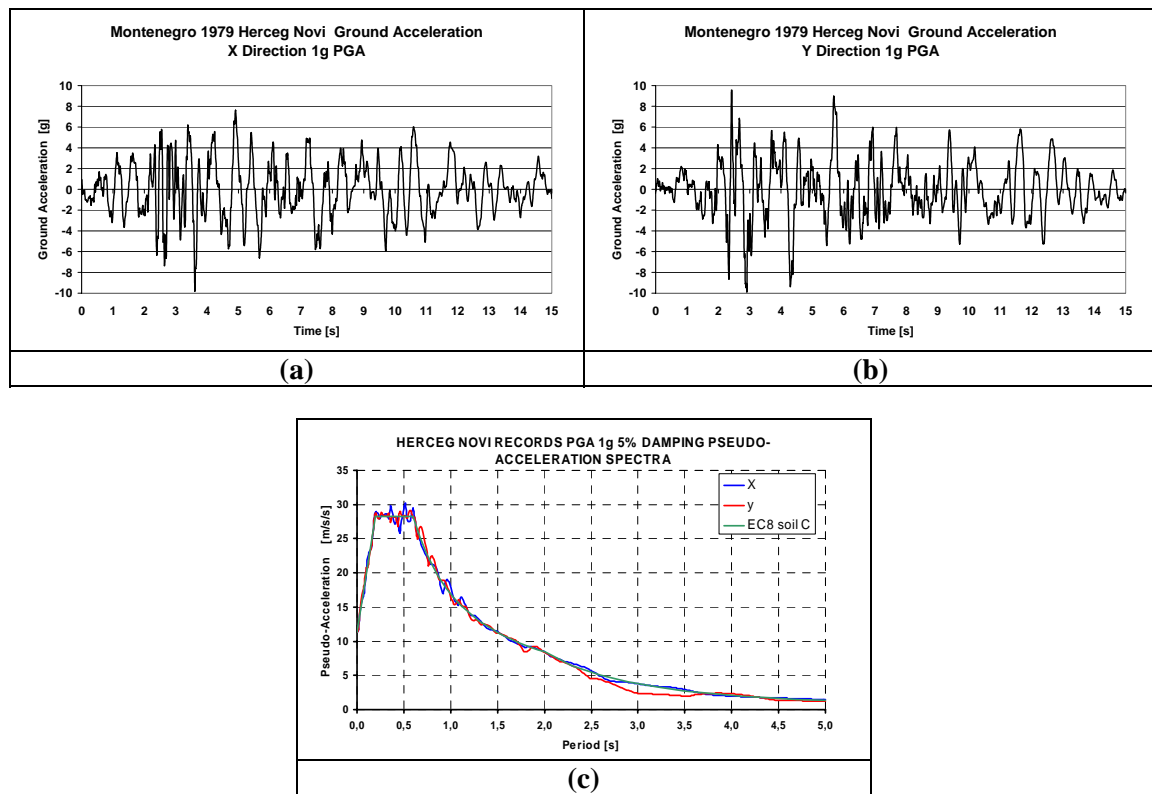


Figure 1.4-1 - Herceg-Novi records PGA = 1g; (a) longitudinal component, (b) transverse component, (c) acceleration response spectra of X and Y components and EC8 soil c spectrum.

A series of preliminary analyses were run to define the most appropriate direction of application for the chosen signal. To maximize the effect of the torsion on the response, it was decided to adopt the pair of signals that consisted in the application

of the X signal component in the $-X$ direction of the reference system of Figure 1.1-1, and of the Y signal component in the $-Y$ direction of the same reference system.

The structure was subjected to three rounds of bi-directional PsD tests in three different configurations:

- Tests on the ‘as-built’ structure;
- Tests on the FRP retrofitted structure;
- Tests on the RC Jacketed structure

As the retrofit phases were intended to consist into a light interventions, the appropriate intensity of PGA was chosen in order to obtain a level of damage in the first round of test that would be significant but not so severe as to be beyond repair; thus, it was decided to run the first test in the ‘as-built’ configuration with a scaled PGA level of 0.15g. Since the inspection of the structure soon after the test revealed that only minor damage had occurred for such PGA level, then one more test at the increased intensity of 0.2g PGA was run.

After that, the structure was retrofitted by using FRP laminates and then tested under the same input ground motion of the ‘as-built’ structure, with a PGA level of 0.20g, in order to have a direct comparison with the previously executed experiment. In order to investigate the effectiveness of the retrofit technique adopted, another test was carried out with a PGA level of 0.30g. Finally two tests were performed on the structure retrofitted by RC Jacketing with the same PGA level intensity of the previous round of tests. The tests phases of the whole experimental activity are summarized in Table 1.4-1.

Test	PGA Level	Configuration
ABs 0.15	0.15 g	‘As-built’
ABs 0.20	0.20 g	
FRPs 0.20	0.20 g	“FRP Retrofitted”
FRPs 0.30	0.30 g	
RCJs 0.20	0.20 g	“RC Jacketed”
RCJs 0.30	0.30 g	

Table 1.4-1 – Experimental campaign

Chapter II

2.1 EXPERIMENTAL BEHAVIOUR OF THE ‘AS-BUILT’ STRUCTURE

The first round of tests involved the ‘as-built’ structure subjected to levels of PGA in order to obtain significant damages but not so severe as to be beyond repair. Thus, based on a series of preliminary analyses, it was decided to run the first test in the ‘as-built’ configuration with a scaled PGA level of 0.15g.

In the following section a detailed description of the test results in terms of both global and local behaviour is reported.

2.1.1 As-Built Structure: PGA = 0.15g

Global Behaviour

During the first test on the ‘as built’ structure, at PGA level equal to 0.15g, the structure showed a damage level lower than that expected from analytical predictions (Fajfar et al. [8], Jeong et al., part I [7,]); in particular, the inspection of the structure after the test, showed only the development of light cracking, mainly at columns ends and in correspondence of the beams-columns joints (see Figure 2.1.1-1). More significant cracks were detected on the rectangular column C6 as reported in Figure 2.1.1-2

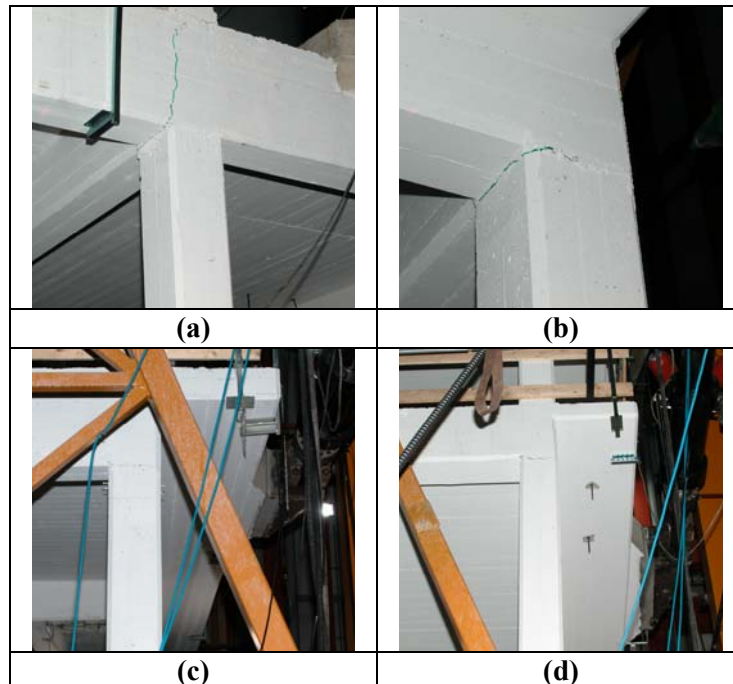


Figure 2.1.1-1 – Cracks on columns C1 (a) and C2 (b) at 1st floor, C7 at 1st floor (c) and 2nd floor (d).

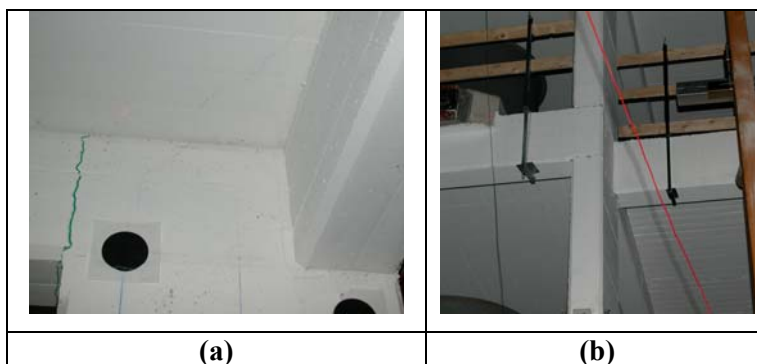


Figure 2.1.1-2 - Cracks on column C6 at 1st floor (a) and 2nd floor (b).

In Figure 2.1.1-3, the base shear-top displacement curves related to such test for the X and Y direction are presented (top displacement is referred to the centre of mass, CM, of the third storey). By comparing the average slopes of the curves, it is possible to assess the stiffness of the structure in the longitudinal and transverse direction; the comparison shows that the stiffness was greater in the Y direction than in the X one; this is consistent with the arrangement of the wall type column C6 placed with its strong axis in such direction. As a consequence, the maximum base shear reached along the Y direction, 261 kN, was larger than that reached in the X direction, 176

kN. On the contrary, much larger top displacements were reached in the X direction rather than in the Y one (70.1 mm vs. 47.0 mm).

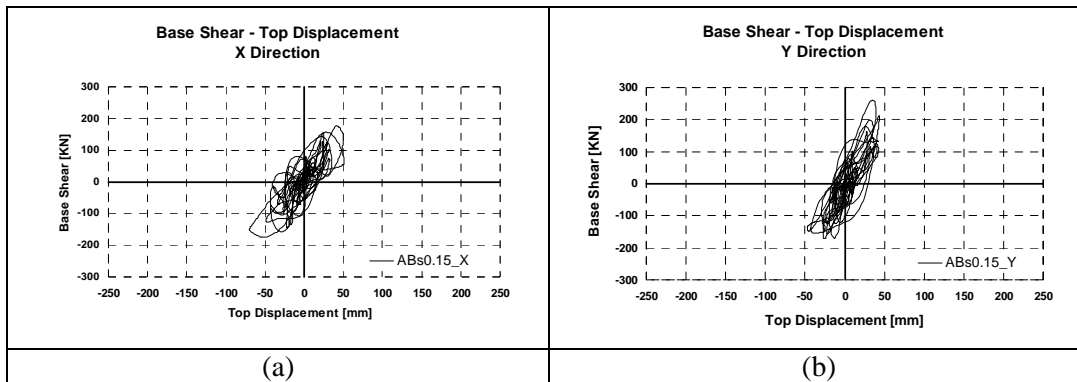


Figure 2.1.1-3 - Base Shear-Top Displacement hysteresis loops; (a) X direction, (b) Y direction

By totalling up the areas under hysteretic cycles of base shear-top displacement relationships, it is possible to obtain information about the energy dissipation; in particular, comparable values of adsorbed energy were recorded in the two directions, 29.61 kJ in the X direction and 31.81 kJ in the Y one, equal to 48% and 52% of the total adsorbed energy, respectively. It is underlined that the absolute value of the rotational adsorbed energy is equal to the kinetic energy as, during the test, the rotational input energy was equal to zero; thus the rotational adsorbed energy is not reported in terms of energy adsorption.

The torsional behaviour of the structure is represented in Figure 2.1.1-4 in which the base-torsion vs. top rotation is reported; the diagram shows that the maximum base torsion achieved during the test was equal to 878 kNm and the maximum top rotation was equal to 12.54 mrad.

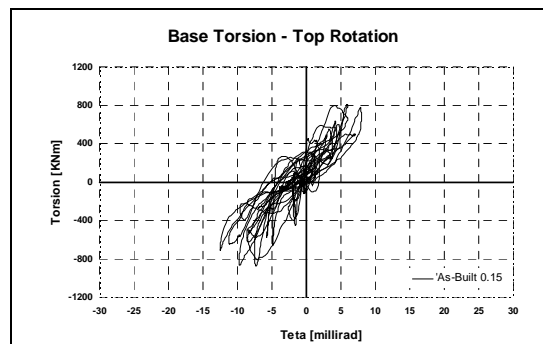


Figure 2.1.1-4 - Base Torsion-Top Rotation

A summary of the main experimental results recorded during such test are reported in Table 2.1.1-1 and Table 2.1.1-2; the first table clearly shows that the maximum inter-storey displacement were reached at the second floor.

DIRECTION	Total Absorbed Energy	Max Base Shear	Max Top Displ.	Level	Max I-S Shear	Max I-S Displ.
	[KJ]	[KN]	[mm]		[kN]	[mm]
X	29.61	PX: 175	PX: 70.1	1	176	15.1
		NX: 176	NX: 51.1	2	161	36.2
				3	126	24.2
Y	31.81	PY: 172	PY: 47.5	1	261	11.6
		NY: 261	NY: 43.6	2	235	19.9
				3	147	18.2

Table 2.1.1-1 - Experimental outcomes

	Max Base Torsion	Max Base Rotation	Level	Max I-S Torque	Max I-S Rotation
	[KNm]	[millirad]		[kNm]	[millirad]
TETA	Positive: 803	Positive: 7.96	1	878	3.35
	Negative: -878	Negative: -12.54	2	738	5.91
			3	613	4.06

Table 2.1.1-2 - Experimental outcomes

Local Behaviour

In order to analyze the local dissipation capacity of the central column C3, where the major damages were found, the base shear-Y axis rotation curves, with reference to the inclinometers placed at the base of such column (named #1 and #2, respectively), are reported in Figure 2.1.1-5. The inclinometer #1, in particular, was located at the beam-column intersection whereas the inclinometer #2 was placed at a distance equal to 500 mm from the column end in order to investigate the member rotation above the lap splice length of the longitudinal reinforcement (equal to 400 mm and indicated in Figure 2.1.1-5 by the dashed line). The figure shows that the rotations recorded by the inclinometer #2 were larger than those achieved in correspondence of the inclinometer #1. In both cases an horizontal plateau was recorded highlighting the presence of plastic deformations. The constant branch, that indicates increasing rotations with respect to a constant external action, is wider in correspondence of the curve related to the inclinometer #2. Such effect could be due to the strength

discontinuity provided by the double amount of longitudinal steel reinforcement along the lap splice; the strength discontinuity, in fact, implied a significant difference in terms of deformation capacity between the cross sections above and below the lap splice. Thus, the formation of the plastic hinge occurred at the cross section immediately after the lap splice length and then it propagated at the base of the member. The maximum rotations recorded were $1.91 \mu\text{rad}$ and $2.43 \mu\text{rad}$ for inclinometer #1 and #2, respectively.

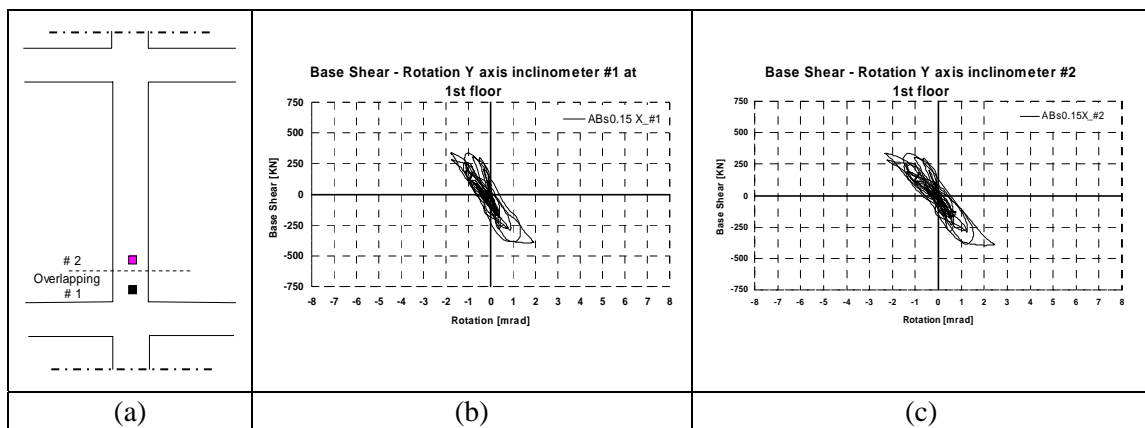


Figure 2.1.1-5 – ABs 0.15 local hysteresis loops for column C3: (a) Inclinometers positions, (b) Base Shear-Rotation Y axis inclinometer #1, (c) Base Shear-Rotation Y axis inclinometer #2.

2.1.2 As-Built Structure: PGA = 0.20g

Since the inspection of the structure soon after the test at the PGA level of 0.15g revealed only minor damage as above illustrated, then one more test at the increased intensity of 0.2g PGA was run.

Global Behaviour

During the test on the ‘as built’ structure, at PGA level equal to 0.20g, the structure showed a more significant level of damage. Columns were again the most damaged members of the structure, especially at the second storey; significant inclined cracks were observed on their compressive sides and on the tensile side at the beam-column interface. In particular, the central column C3, where the axial load is maximum, along with the corner column C4 showed the major damages as reported in Figure 2.1.2-1 and Figure 2.1.2-2. The damage on the rectangular column C6 was less significant even though crushing of concrete and cracks at the interface with beams were observed (see Figure 2.1.2-3).



Figure 2.1.2-1 - Damages on column C3 at 1st floor (a) and 2nd floor (b)



Figure 2.1.2-2 – Damages on column C4 at 1st floor (a) and 2nd floor (b)

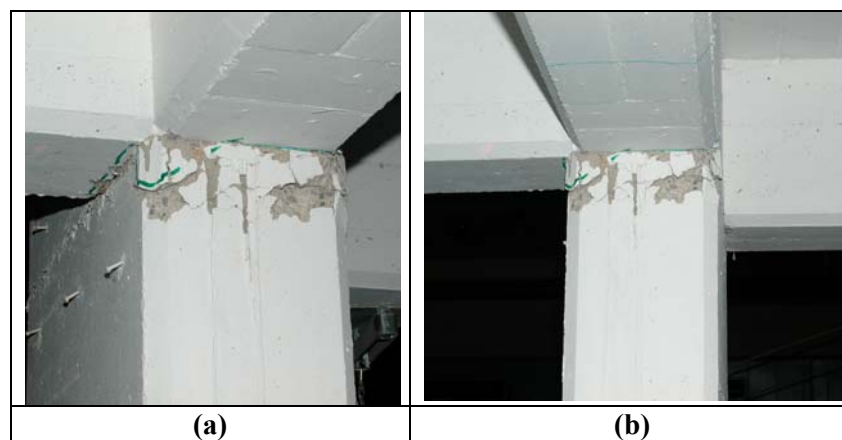


Figure 2.1.2-3 – Damages on column C6 at 1st floor (a) and 2nd floor (b)

In Figure 2.1.2-4, the base shear-top displacement curves related to such test for the X and Y direction are presented. The same trend of the previous test was observed in terms of stiffness confirming that the maximum base shear was reached along the Y direction, 276 kN, rather than in the X one, 195 kN. The maximum top displacement recorded was again greater along the X direction, 105.7 mm, rather than in the Y direction where a maximum top displacement equal to 103.1 mm was achieved.

By totalling up the areas under hysteretic cycles of base shear-top displacement relationships, it was observed that the 40% of the total energy, equal to 44 kJ, was adsorbed in the X direction, whereas the remaining 60% was adsorbed in the Y direction, 65 kJ; it can thus be concluded that, as the seismic intensity level increased, the stiffer direction was more involved in the energy adsorption.

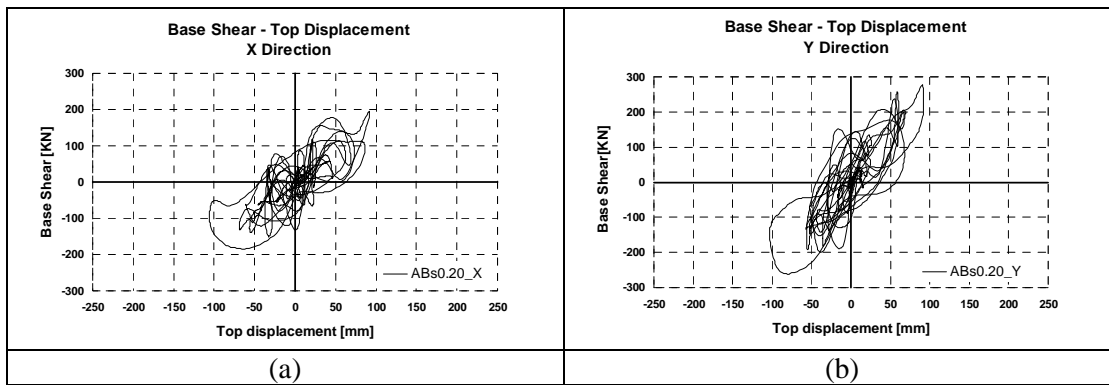


Figure 2.1.2-4 – Base Shear-Top Displacement hysteresis loops; (a) X direction, (b) Y direction.

The torsional behaviour of the structure is represented in Figure 2.1.2-6 in which the base-torsion vs. top rotation is reported; the diagram shows that the maximum base torsion achieved during the test was equal to 963 kNm and the maximum top rotation was equal to 19.91 mrad.

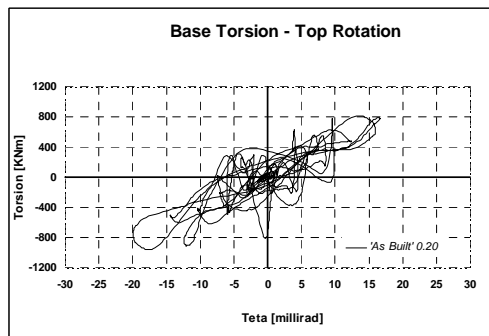


Figure 2.1.2-5 - Base Torsion-Top Rotation

In order to highlight the behavior of each storey of the structure during the test, interstorey shears are plotted against the interstorey drifts for each floor in Figure 2.1.2-6, it is clearly visible that the maximum interstorey drifts were reached at the second storey (57.0mm in the X direction and 47.2 mm in the Y direction) with an increment of 130% in the X direction and of about 57% in the Y direction with respect to the first storey. Comparing the interstorey drift of the second storey with those of the third one, an increment equal to 60% and 43%, for X and Y direction respectively, was recorded. Furthermore, it can be observed that the second storey adsorbed more energy with respect to the others, followed by the third storey and then by the first one. Such results were confirmed also by the inspection of the

structure after the test as major damages were observed at the columns ends of the second storey.

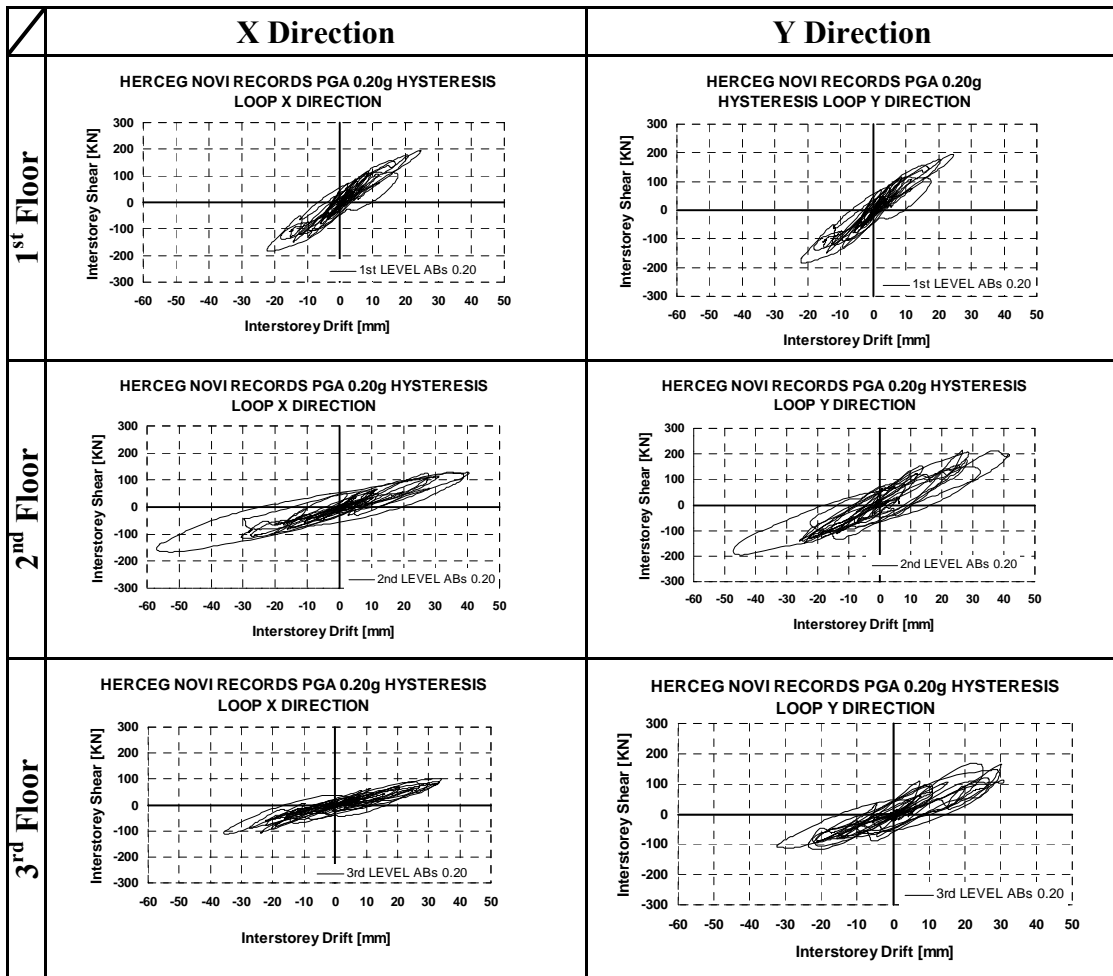


Figure 2.1.2-6 - ABs 0.20: Interstorey Shear–Interstorey Drift hysteresis loops

The same trend was observed by plotting the curves related to the interstorey torque vs. the interstorey rotation; the second floor was again the most involved in the torsional behaviour of the structure with an increment of 76% and of about 44% with respect to the first and third storey, respectively.

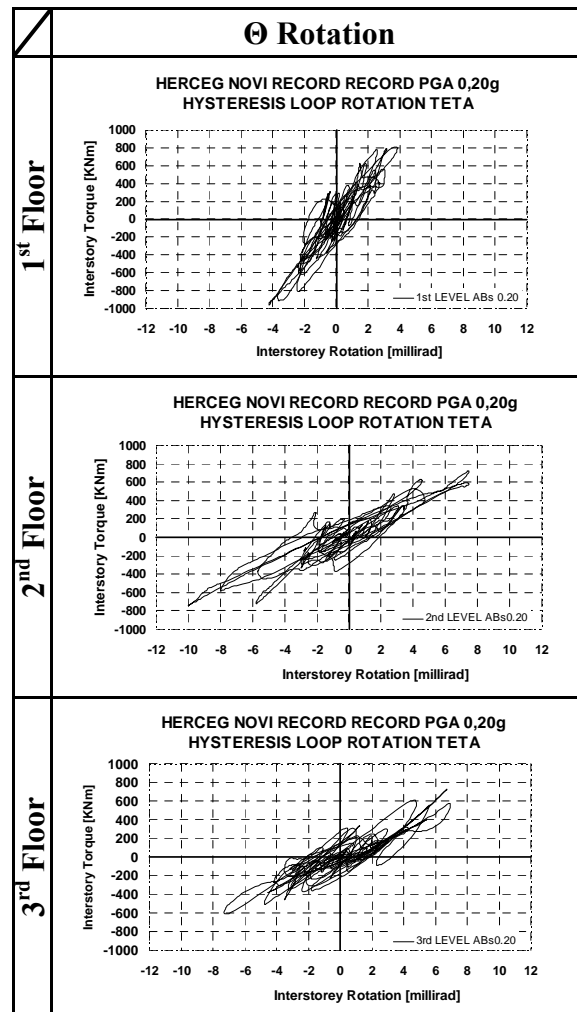


Figure 2.1.2-7 - ABs 0.20: Interstorey Torque – Interstorey Rotation hysteresis loops

The plan irregularity of the structure caused the presence of significant rotations once the structure was subjected to bidirectional seismic actions; in order to investigate on the extent of such torsional effects, the absolute interstorey drifts of each column of the structure have been compared with those of its centre of the mass. As the previous diagrams have highlighted that in each case the second storey showed the maximum interstorey drifts, the comparison is reported only for such storey. In order to have a global idea of the torsional effects on the entire structure the diagrams have been arranged so that the column plan disposition is reproduced (see Figure 2.1.2-8)

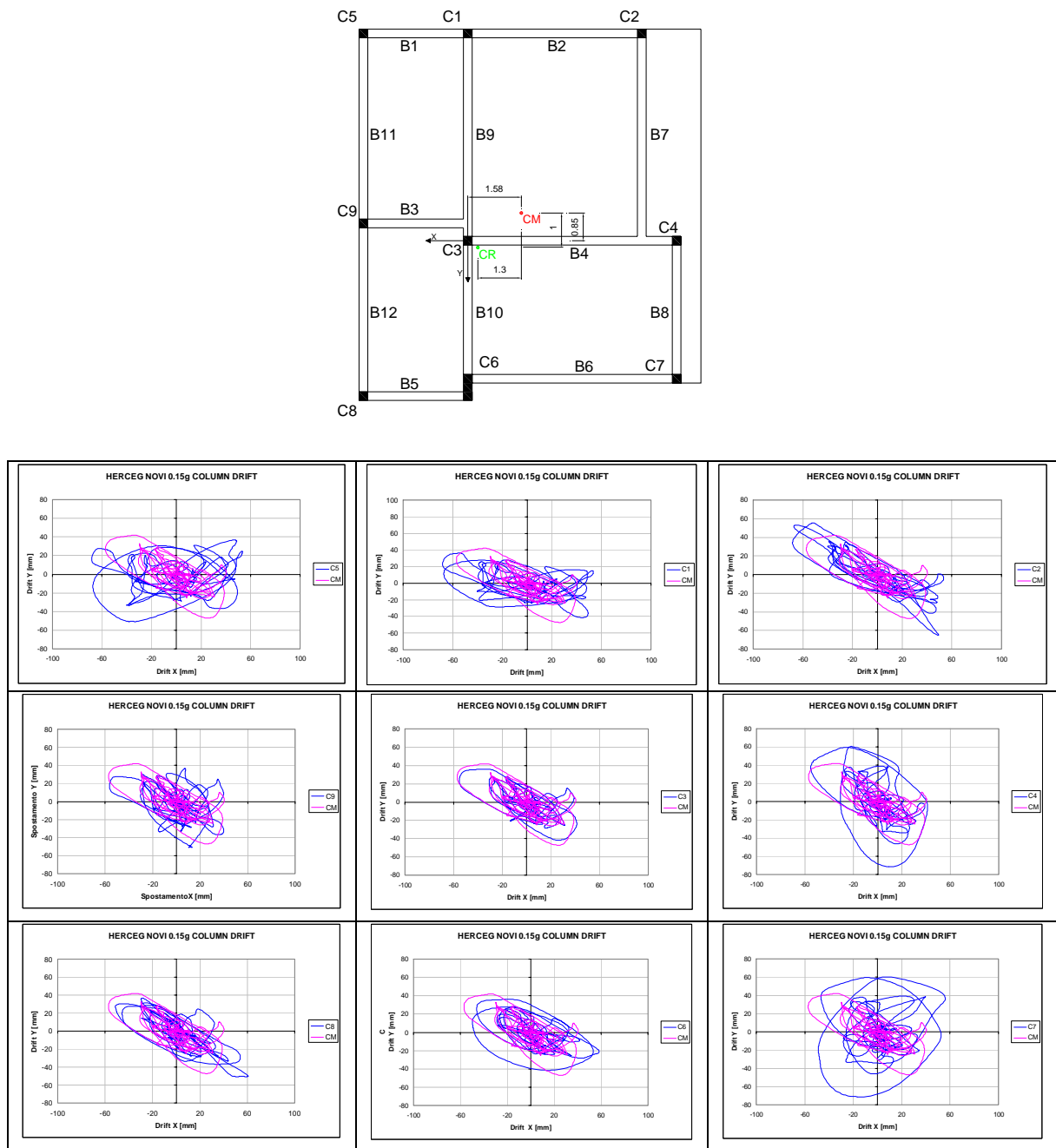


Figure 2.1.2-8 – Column Drifts compared to CM drifts in X and Y direction at second storey.

The diagram shows that in the case of columns C8, C3 and C2, the drifts are substantially equal to those recorded in correspondence of the centre of mass; such result is due to the low eccentricity in this direction between the centre of the mass and of stiffness; on the other hand such eccentricity becomes higher in the opposite direction (the diagonal of columns C5, C3, and C7) and thus the maximum torsional

effects have been recorded on columns C5 and C7. In particular, from the experimental data analysis it has been possible to determine the instant in which the maximum rotation of the second storey was achieved; with reference to such instant the plane deformed shape of the structure is reported in Figure 2.1.2-9 (to have a clear view, drifts have been amplified by a factor of 1000); the figure shows that the maximum displacement due to the torsion have been achieved, in the direction orthogonal to that obtained by connecting the centre of the mass, columns C5 and C7. Such observation explains the difference between the areas under the diagrams of columns C5 and C7 with respect to those of columns C2 and C8.

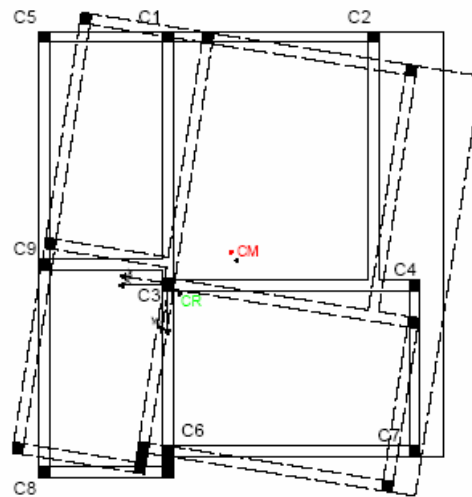


Figure 2.1.2-9 – Maximum torsional effect, deformed shape of the second storey.

A summary of the main experimental results recorded in such test are reported in Table 2.1.2-1 and .Table 2.1.2-2

DIRECTION	Total Absorbed Energy	Max Base Shear	Max Top Displ.	Level	Max I-S Shear	Max I-S Displ.
	[KJ]	[KN]	[mM]		[kN]	[mm]
X	44.00	PX: 184	PX: 105.7	1	195	24.6
		NX: 195	NX: 91.9	2	165	57.0
				3	112	35.8
Y	65.00	PY: 261	PY: 103.1	1	276	30.6
		NY: 276	NY: 92.0	2	214	47.2
				3	167	32.6

Table 2.1.2-1 - Experimental outcomes

	Max Base Torsion	Max Base Rotation	Level	Max I-S Torque	Max I-S Rotation
	[KNm]	[millirad]		[kNm]	[millirad]
TETA	Positive:812	Positive: 16.66	1	963	4.26
	Negative: -963	Negative: -19.91	2	742	9.98
			3	723	7.30

Table 2.1.2-2 - Experimental outcomes

Local Behaviour

The base shear-Y axis rotation curves, with reference to the inclinometers #1 and #2, are reported in Figure 2.1.2-10. After the first test at 0.15g PGA intensity it was already observed the formation of the plastic hinge at the first floor in correspondence of the bottom column end C3, at first above the lap splice length, then also below such length. Increasing the seismic intensity it was noted a very similar trend of the rotation recorded by the two inclinometers placed below and above the lap splice length. Such behaviour can be explained considering that the plasticization had probably already propagated along the entire lap splice length. The two inclinometers recorded comparable maximum rotations, 3.86 μ rad the inclinometer #1 and 4.26 μ rad the #2 one, with an increment of about 100% and 75% with respect to the maximum rotations achieved in the previous test in correspondence of the same inclinometers.

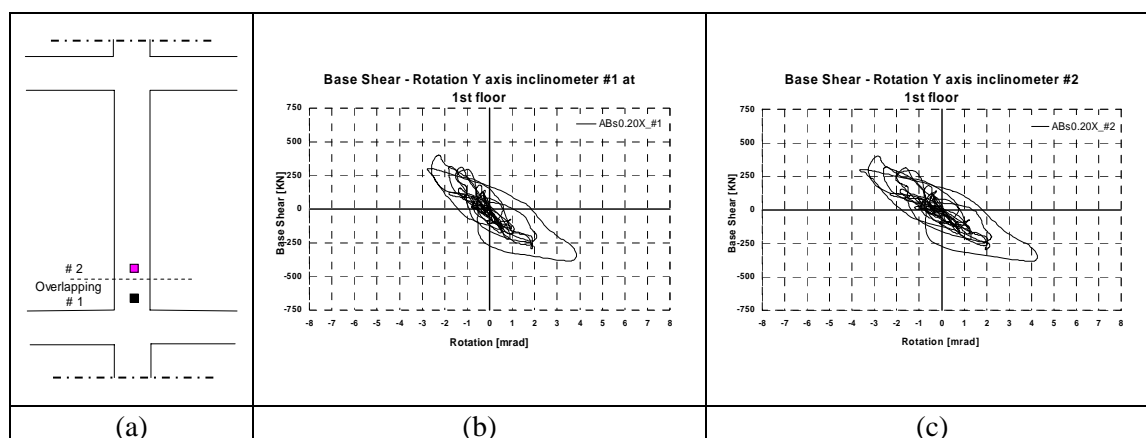


Figure 2.1.2-10 - ABs 0.20 local hysteresis loops for column C3: (a) Inclinometers positions, (b) Base Shear-Rotation Y axis inclinometer #1, (c) Base Shear-Rotation Y axis inclinometer #2.

Chapter III

3.1 MODELLING OF THE STRUCTURE

In order to assess the theoretical seismic capacity of the ‘as-built’ structure, a post-test assessment of the structural global capacity was performed by a non-linear static pushover analysis on the lumped plasticity structural model.

3.1.1 Geometrical model

The finite element analysis program SAP2000 [9] was utilized to run the theoretical analyses. First step consisted in the cross-section definition and implementation for the geometrical modelling of the structure.

In the analytical model, slabs were omitted and their contribution to beam stiffness and strength was considered assuming a T cross section for the beams with the effective flange width equal to the rectangular beam width (250 mm) plus 7% of the clear span of the beam on either side of the web (Fardis M.N. [10]). Such assumption provides flange width values between the conservative flange width indicated in the Eurocode 8, *Part I* [3] for design purposes and the width recommended for gravity load design. According to such assumption, the values of effective flange width of T-sections assumed in the model are summarized in Table 3.1.1-1.

BEAM	Clear Span [mm]	Width added to a web [mm]	Effective flange width [mm]
B1	2750	1x192,5	442,5
B2	4750	1x332,5	582,5
B3	2750	2x192,5	635
B4	5750	2x402,5	1055
B5	2750	1x192,5	442,5
B6	5750	1x402,5	652,5
B7	5750	2x402,5	1055
B8	3750	2x262,5	775
B9	5750	2x402,5	1055
B10	3750	2x262,5	775
B11	5250	1x367,5	617,5
B12	4750	1x332,5	582,5

Table 3.1.1-1- Effective flange width of T-sections

In Figure 3.1.1-1, a plan and 3D view of the structure as well as their models are reported.

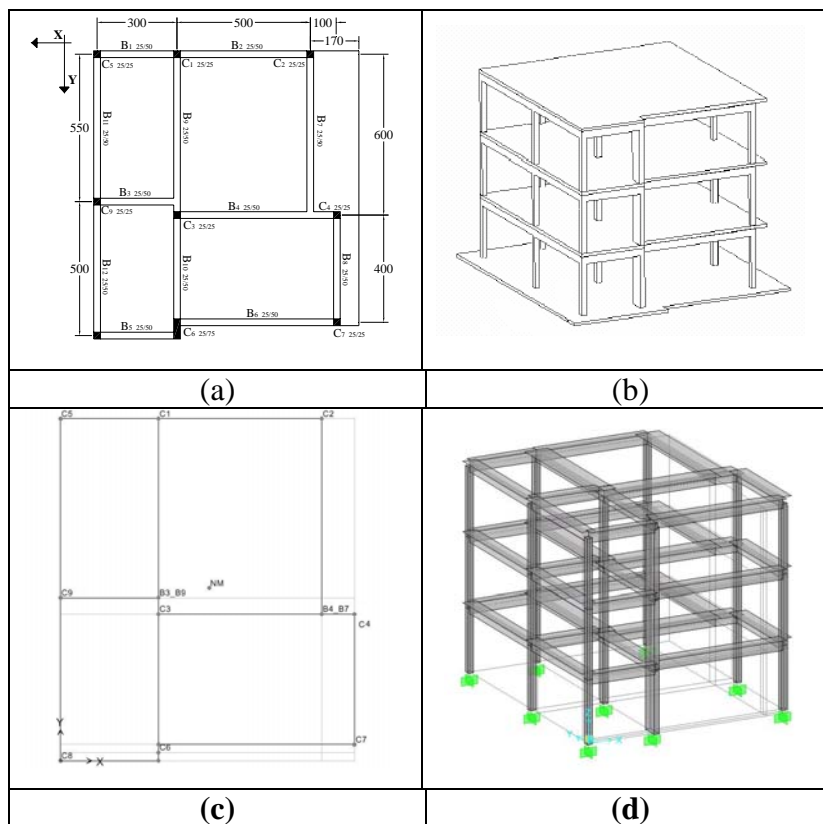


Figure 3.1.1-1 – Plan (a) and 3D view (b) of the structure, plan model (c) and 3D model of the structure (d)

Moreover, in order to take into account the effect of the slabs, a rigid diaphragm was assumed at each storey of the model. The diaphragm constraint causes all of its constrained joints to move together as a planar diaphragm that is rigid against membrane (in-plane) deformation; it is typically used for modelling concrete floors in building structures because they are characterized by a high in-plane stiffness (see Figure 3.1.1-2).

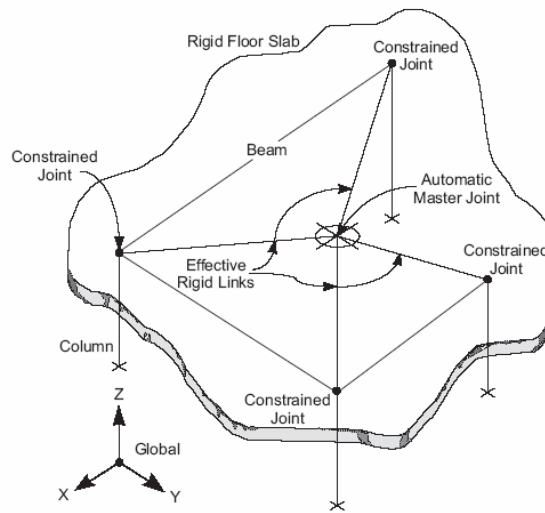


Figure 3.1.1-2- Use of the Diaphragm Constraint to Model a Rigid Floor Slab (SAP2000 manual [9])

By observing the plan view of the structure, it is shown that beams adjacent to the rectangular column C6 are not in alignment; thus the gap between center lines of beams (B5 and B6) and the column (C6) have been considered in the modelling of the beam-column connection at C6. In particular, to prevent plastic hinges development inside such beam-column intersections, rigid elements were used in the structural model (Jeong and Elnashai, [7] part I)

In Figure 3.1.1-3, a 3D view of the structure model is reported.

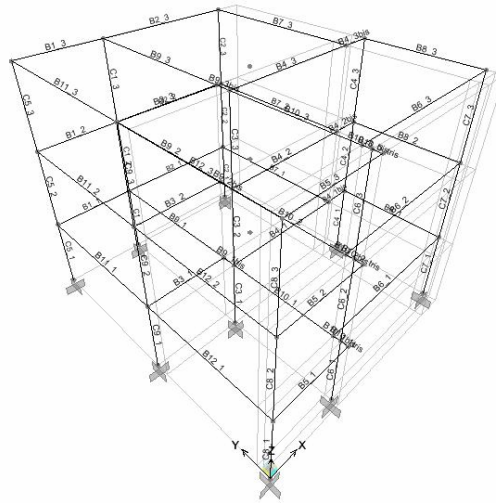


Figure 3.1.1-3-3D view of the model

3.1.2 Material Properties

In order to characterize both concrete and reinforcing steel used in the structure, tests were performed on concrete and steel samples. In particular, concrete samples were provided with reference to both slabs and columns of each floor; five steel samples were tested for each diameter used. Based on laboratory tests results, average strength values are reported in Table 3.1.2-1.

Concrete			Steel	
Floor	Member	f_{cm} (N/mm ²)	Bars Diameter	f_{ym} (N/mm ²)
1°	columns	24.73	8mm	320
	slab	26.7		
2°	columns	26.7	12mm	320
	slab	27.53		
3°	columns	25.32	20mm	320
	slab	27.39		

Table 3.1.2-1 - Average concrete and steel strength.

Thus, in the structural modelling, concrete and steel average strength equal to $f_{cm} = 25 \text{ N/mm}^2$ and $f_{ym} = 320 \text{ N/mm}^2$ have been assumed.

As concern the Young's Modulus, it has been computed as:

$$E_c = 5700 \sqrt{R_{ck}} = 24681 \text{ (N/mm}^2\text{)}$$

where R_{ck} it has assumed as $0.75f_{cm}$.

3.1.3 Gravity loads and masses

The theoretical assessment of the structure seismic capacity has been performed with reference to the Italian code, Ordinanza 3431 [2].

According to such code, the design value F_d of the effects of actions in the seismic design situation can be expressed as:

$$F_d = \gamma_I E + G_K + \sum_i (\psi_{2i} Q_{Ki})$$

where E is the horizontal loading which can be represented by the inertia forces due to the mass of the building exposed to an earthquake, γ_I is the importance factor, G_K is the characteristic value of the permanent actions, Q_{Ki} represent the characteristic value of the variable action Q_i and ψ_{2i} is the reduction factor used for the quasi-permanent characteristic of Q_{ki} .

- *Permanent Actions G_K*

In the structural modelling dead loads due to the columns has been automatically considered by the program while beams dead loads were assigned as an external distributed load. Loads acting on slabs (finishing equal to $50KN/m^2$ at first and second storey) and due to slab self-weight were distributed to the nearest beam by considering trapezoidal areas as shown in Figure 3.1.3-1.

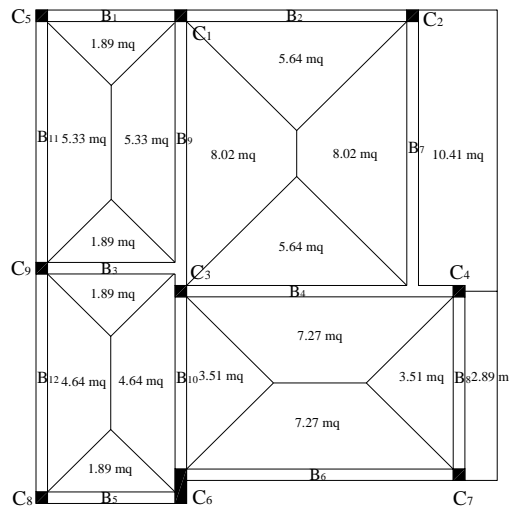


Figure 3.1.3-1 –Slabs gravity loads distribution

The permanent actions values obtained for each beam at each storey are reported in Table 3.1.3-1.

1 st and 2 nd STOREY						
Member	Length [m]	Ainf. Slab. [m ²]	Gk slab [kN/m]	Gk finishing. [kN/m]	Gk p.p.beam [kN/m]	Gk TOT [kN/m]
Beam B1	3,00	1,89	2,36	0,32	3,125	5,80
Beam B2	5,00	5,64	4,23	0,56	3,125	7,92
Beam B3	3,00	3,78	4,73	0,63	3,125	8,48
Beam B4	6,00	12,91	8,07	1,08	3,125	12,27
Beam B5	3,00	1,89	2,36	0,32	3,125	5,80
Beam B6	6,00	7,27	4,54	0,61	3,125	8,27
Beam B7	6,00	18,43	11,52	1,54	3,125	16,18
Beam B8	4,00	6,4	6,00	0,80	3,125	9,93
Beam B9	6,00	13,35	8,34	1,11	3,125	12,58
Beam B10	4,25	8,15	7,19	0,96	3,125	11,28
Beam B11	5,50	5,33	3,63	0,48	3,125	7,24
Beam B12	5,00	4,64	3,48	0,46	3,125	7,07
3 rd STOREY						
Member	Length [m]	Ainf. Slab. [m ²]	Gk slab [kN/m]	Gk finishing. [kN/m]	Gk p.p.beam [kN/m]	Gk TOT [kN/m]
Beam B1	3,00	1,89	2,36	0,00	3,125	5,49
Beam B2	5,00	5,64	4,23	0,00	3,125	7,36
Beam B3	3,00	3,78	4,73	0,00	3,125	7,85
Beam B4	6,00	12,91	8,07	0,00	3,125	11,19
Beam B5	3,00	1,89	2,36	0,00	3,125	5,49
Beam B6	6,00	7,27	4,54	0,00	3,125	7,67
Beam B7	6,00	18,43	11,52	0,00	3,125	14,64
Beam B8	4,00	6,40	6,00	0,00	3,125	9,13
Beam B9	6,00	13,35	8,34	0,00	3,125	11,47
Beam B10	4,25	8,15	7,19	0,00	3,125	10,32
Beam B11	5,50	5,33	3,63	0,00	3,125	6,76
Beam B12	5,00	4,64	3,48	0,00	3,125	6,61

Table 3.1.3-1- Permanent actions on beams

- *Variable Actions Q_K*

Water tanks were utilized to apply the design gravity loads (2kN/m^2) to the test structure (Jeong, S.-H. e Elnashai, A. S. [6] part II); tanks distribution has been reported in Chapter I, Figure 1.2 – 2.

The same procedure described for the case of the permanent action was used for the computation of the distributed loads Gk on beams due to such variable actions. The Q_K values obtained have been multiplied by the reduction factor, ($\psi_{2i} = 0.3$ for each storey) as prescribed for civil constructions by Ordinanza 3431 [2].

The variable actions values obtained for each beam at each storey are reported in Table 3.1.3-2.

1st, 2nd and 3rd STOREY				
Member	Length [m]	Ainf. Slab. [m ²]	Qk TOT [KN/m]	$\psi_{2i}Q_k$ [KN/m]
Beam B1	3,00	1,89	1,26	0,38
Beam B2	5,00	5,64	2,26	0,68
Beam B3	3,00	3,78	2,52	0,76
Beam B4	6,00	12,91	4,30	1,29
Beam B5	3,00	1,89	1,26	0,38
Beam B6	6,00	7,27	2,42	0,73
Beam B7	6,00	18,43	6,14	1,84
Beam B8	4,00	6,4	3,20	0,96
Beam B9	6,00	13,35	4,45	1,34
Beam B10	4,25	8,15	3,84	1,15
Beam B11	5,50	5,33	1,94	0,58
Beam B12	5,00	4,64	1,86	0,56

Table 3.1.3-2- Variable actions on beams

- *Masses*

The structural model is characterized by three dynamics degree of freedom (two translations along X and Y direction, respectively, and one rotation along the vertical axis) for each storey. A mass is correlated at each degree of freedom; in particular, the storey mass is correlated to the X and Y translations and the storey mass multiplied by the square of the radius of inertia (computed assuming that masses are distributed on the storey surface) for the rotational degree of freedom.

According to the Ordinanza 3431 [2], seismic actions shall be computed taking into account the masses associated with all gravity loads appearing in the following combination of actions:

$$G_K + \sum_i (\psi_{Ei} Q_{Ki})$$

where ψ_{Ei} is the combination coefficient for variable action Q_i , computed as $\psi_{2i} \times \varphi$. It takes into account the probability that all actions Q_{Ki} are present when earthquake occurs as well as the reduced participation of masses in the motion of the structure due to the non-rigid connection between them. The recommended values for the coefficient φ are reported in Ordinanza 3431 [2] and they depend by the type of

variable action and by the storey. Thus, for a three storey existing building, such coefficient should be equal to:

$$\psi_{Ei} = \psi_{2i} \cdot \varphi = 0,3 \times 0,5 = 0,15 \text{ for the 1}^{\text{st}} \text{ and the 2}^{\text{nd}} \text{ storey ,}$$

$$\psi_{Ei} = \psi_{2i} \cdot \varphi = 0,2 \times 1 = 0,2 \text{ for the 3}^{\text{rd}} \text{ storey } (\psi_{2i} = 0,2 \text{ for roof with snow}).$$

However, in the case of the SPEAR structure, the value of φ has been assumed equal to 1 and $\psi_{2i} = 0.3$ because the likelihood of the loads Q_{Ki} being present over the entire structure during the simulated earthquake was known. According to such assumptions in Table 3.1.3-3 the masses values computed with reference to each storey of the structure are listed ($Q_{slabs} = 2500 * 0,15 = 375 \text{ kg/m}^2$; $Q_{var.} = 50 + 0,3 * 200 = 110 \text{ kg/m}^2$).

1 st and 2 nd STOREY	A _{infl.} [m ²]	W _{slab} [kg]	A _{infl.} [m ²]	W _{var.} [kg]	L _{beam} [m]	W _{beam} [kg]	L _{col.} [m]	P _{col.} [kg]	W _{TOT} [kg]	Masses [KN/(m/s ²)]
C5	3,61	1353,5	4,13	453,8	4	1250	3	468,75	3526,0	3,53
C1	9,84	3691,4	11,00	1210,0	6,375	1992	3	468,75	7362,3	7,36
C2	11,16	4183,6	11,55	1270,5	5	1563	3	468,75	7485,3	7,49
C9	6,88	2578,1	7,88	866,3	5	1563	3	468,75	5475,6	5,48
C3	20,53	7699,2	23,63	2598,8	9	2813	3	468,75	13579,2	13,58
C4	19,41	7277,3	19,43	2136,8	7,625	2383	3	468,75	12265,7	12,27
C8	3,27	1224,6	3,75	412,5	3,750	1172	3	468,75	3277,7	3,28
C6	8,66	3246,1	9,75	1072,5	6,125	1914	3	1406,25	7638,9	7,64
C7	6,61	2479,7	7,40	814,0	4,75	1484	3	468,75	5246,8	5,25
TOT									65857,7	65,86

3 rd STOREY	A _{infl.} [m ²]	W _{slab} [kg]	A _{infl.} [m ²]	W _{var.} [kg]	L _{beam} [m]	W _{beam} [kg]	L _{col.} [m]	P _{col.} [kg]	W _{TOT} [kg]	Masses [KN/(m/s ²)]
C5	3,61	1353,5	4,13	453,8	4	1250	1,5	234,375	3291,6	3,29
C1	9,84	3691,4	11,00	1210,0	6,375	1992	1,5	234,375	7128,0	7,13
C2	11,16	4183,6	11,55	1270,5	5	1563	1,5	234,375	7251,0	7,25
C9	6,88	2578,1	7,88	866,3	5	1563	1,5	234,375	5241,3	5,24
C3	20,53	7699,2	23,63	2598,8	9	2813	1,5	234,375	13344,8	13,34
C4	19,41	7277,3	19,43	2136,8	7,625	2383	1,5	234,375	12031,3	12,03
C8	3,27	1224,6	3,75	412,5	3,750	1172	1,5	234,375	3043,4	3,04
C6	8,66	3246,1	9,75	1072,5	6,125	1914	1,5	703,125	6935,8	6,94
C7	6,61	2479,7	7,40	814,0	4,75	1484	1,5	234,375	5012,4	5,01
TOT									63279,5	63,28

Table 3.1.3-3- Masses values for each storey.

The storey masses have been assigned in correspondence of the master joints of the structural model; such joints have been assumed as the centre of the mass of each storey. Coordinates of the centre of mass (with reference to the coordinate system of Figure 3.1.1-1) and correlated translational and rotational masses are listed in the following Table 3.1.3-4.

	X_G [m]	Y_G [m]	Masses in X e Y dir. [KN/(m/s ²)]	Modulus of Inertia in Z dir. [KNm ² /(m/s ²)]
1st and 2nd STOREY	4,55	5,30	65,86	1249
3rd STOREY	4,58	5,34	63,28	1170

Table 3.1.3-4- Centre of mass coordinates and masses

3.2 LUMPED PLASTICITY MODEL

Two main approaches can be used in order to take into account the inelastic behaviour of materials:

- Lumped plasticity model
- Distributed plasticity model

In the present study, it was decided to use the lumped plasticity model that allows concentrating the member non-linear behaviour in correspondence of their ends; such simplification is particularly indicated in the case of frame structures where the potential plastic hinges are located at the member ends.

3.2.1 Lumped plasticity model assumptions

In a frame structure, the moment distribution due to the horizontal loads, assuming to neglect the gravity loads effects, is linear as reported in Figure 3.2.1-1 and thus, each member can be considered as a fixed end member, with a span equal to L_V , subjected to a force on the free end.

L_V is defined as the shear span and it is delimited by the inflexion point of the member deformed shape corresponding to the point in which the moment diagram is equal to zero. During the linear behavior of the structure it is possible to exactly estimate the location of such inflexion point; however, once first plastic regions develop, a redistribution of the flexural moments and a consequent translation of the inflexion point happens. Thus the estimation of the shear span length is not a simple task. In order to simplify the problem, the shear span can be assumed constant during the horizontal loading process and equal to $L_V=0,5L$. Such assumption has been adopted in the modeling of the structure. Furthermore, the stiffness in the plastic region it is assumed constant and equal to that of the cross-section at the beam-column interface.

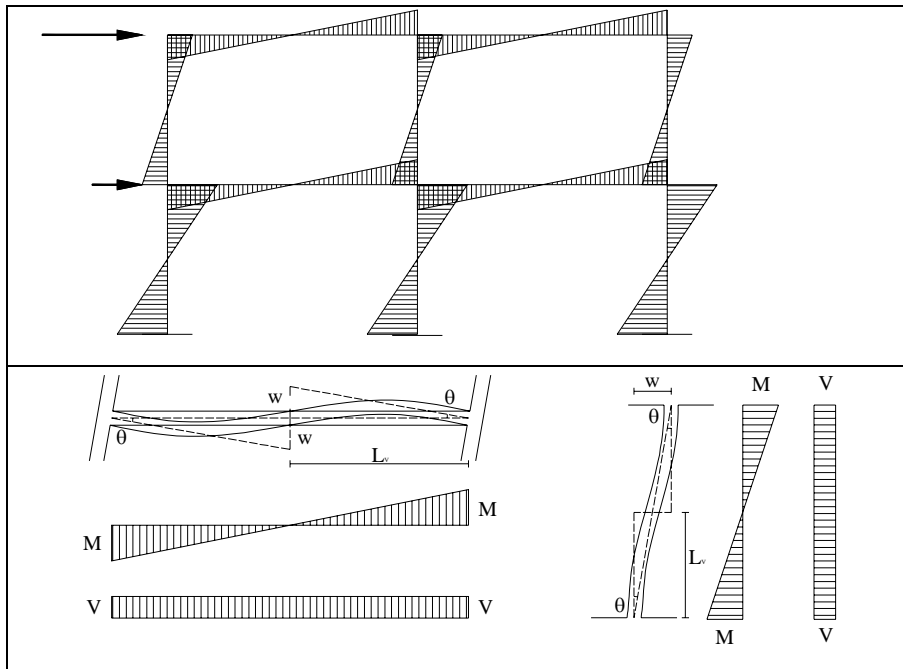


Figure 3.2.1-1- Moments and deformed shape of frame beams and columns under horizontal loads (Verderame, G. [11])

The model used is known as “*one component model*”; it consists in the coupling of an elastic element with a constant stiffness equal to EI (representative of the elastic behavior of the member until it reaches the plasticity) with a rigid-plastic one (representative of the plastic phase) as indicated in Figure 3.2.1-2.

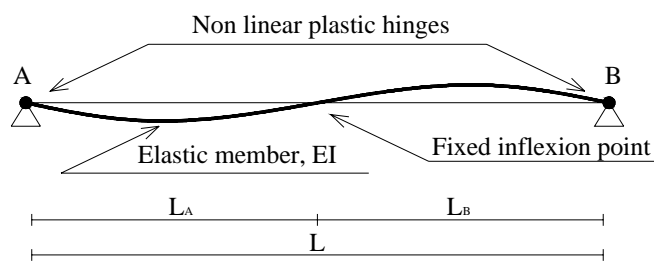


Figure 3.2.1-2- Member modeling (Verderame, G. [11])

Plastic hinges are activated once the yielding moment is achieved; a schematic representation of the elastic-rigid plastic member is reported in Figure 3.2.1-3.

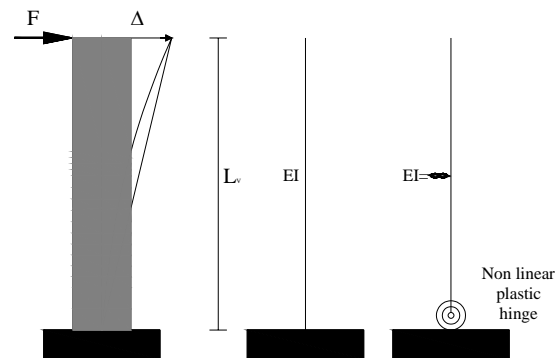


Figure 3.2.1-3- Modeling of the elastic-rigid plastic member (Verderame, G. [11])

The main advantage of the model is its simplicity and computational efficiency; on the other hand, the assumption of a constant shear span, L_v , can be considered not very realistic if it is taken into account that yielding moments at the members ends are generally different (due to different reinforcement ratio). Moreover, the model does not allow computing the formation of plastic hinges along the member due to the horizontal and gravity load interaction.

3.2.2 Plastic hinges characterization

To characterize the plastic hinges it is necessary to define the moment-rotation relationship that is strictly connected to the moment –curvature relationship. Thus, for each structural member (beams and columns), the moment-curvature diagram of its end cross-section has to be determined.

Generally, a tri-linear moment-rotation relationship may be used to characterize plastic hinge (see Figure 3.2.2-1 (a)); such diagram is defined by three points representative of the attainment of yielding (yielding moment, M_y , and rotation θ_y), of maximum moment and rotation in the post-elastic phase (M_{max} , and rotation θ_{max}), and ultimate condition in the softening branch (M_u , and rotation θ_u). In order to simplify the plastic hinge characterization, a bilinear elasto-plastic relationship moment-rotation diagram it has been assumed in the modelling (see Figure 3.2.2-1 (b)); such simplification can be assumed without strongly affecting the analysis results, (Verderame, G. [11]).

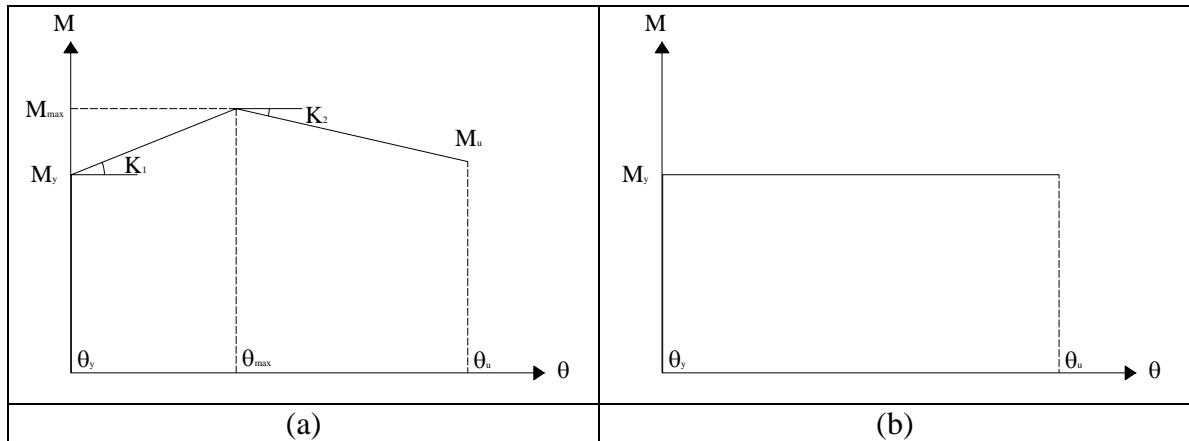


Figure 3.2.2-1- Typical (a) and adopted (b) moment-rotation relationship

The moment rotation relationship was obtained based on the moment curvature analysis performed for each element cross-section. It is noted that yielding curvature, ϕ_y and moment M_y , were computed in correspondence of the attainment of the tensile steel yielding strain; the ultimate curvature, ϕ_u , and ultimate moment, M_u , were determined in correspondence of the attainment of ultimate strains in concrete or steel (concrete ultimate strain was conventionally assumed equal to 3.5‰; the steel ultimate strain was conventionally assumed equal to 40‰).

Plastic hinge length, L_{pl} , yielding and ultimate rotation, θ_y and θ_u , were computed according to the Eurocode 8, Part III [12] type expressions:

$$L_{pl} = \alpha_{flex} L_V + \alpha_{shear} h + \alpha_{slip} d_{bL} f_y \quad (1)$$

$$\theta_y = \beta_{flex} \phi_y L_V + \beta_{shear} + \beta_{slip} \frac{d_{bL} f_y}{\sqrt{f_c}} \quad (2)$$

$$\theta_u = \gamma \left[\theta_y + (\phi_u - \phi_y) L_{pl} \left(1 - \frac{0.5 L_{pl}}{L_V} \right) \right] \quad (3)$$

where L_V is the shear span, h is the cross-section depth, d_{bL} is the diameter of longitudinal bars, f_y and f_c are the average steel and concrete strength, respectively; factors α_{flex} , α_{shear} , α_{slip} along with β_{flex} , β_{shear} , β_{slip} and γ , have been provided with reference to the latest seismic guideline developed by the Italian Department of Civil Protection, Ordinanza 3431 [2]:

$$\left\{ \begin{array}{l} \alpha_{flex.} = 0.1 \\ \alpha_{shear} = 0.17; \\ \alpha_{slip} = \frac{0.24}{\sqrt{f_c}} \end{array} \right. \left\{ \begin{array}{l} \beta_{flex.} = 1/3 \\ \beta_{shear} = 0.0013 \left(1 + 1.5 \frac{h}{L_V} \right); \\ \beta_{slip} = 0.13\phi_y \end{array} \right. \left\{ \begin{array}{l} \gamma = \frac{1}{\gamma_{el.}} \end{array} \right. \quad (4)$$

where $\gamma_{el.}$ is a coefficient equal to 1.5 or 1 for primary or secondary members, respectively.

Considering that original detailed construction drawings were known and comprehensive material testing was performed, it was assumed, according to the Ordinanza 3431 [2], a knowledge level equal to 3, KL3, corresponding to a confidence factor (i.e., CF) equal to 1. As consequence of this knowledge level, average values of strength for materials ($f_{cm} = 25 \text{ N/mm}^2$ and $f_{ym} = 320 \text{ N/mm}^2$) were assumed in the analysis.

Based on the above discussed assumptions and expressions, the moment rotation relationship was obtained for each element cross-section considering section properties and constant axial loads (due to gravity loads, $G_K + \sum_i (\psi_{Ei} Q_{Ki}) = G_K + 0.3Q_K$) for columns and axial forces equal to zero for the beams.

In Appendix B, axial load values obtained for each column due to gravity loads are reported as well as yielding and ultimate rotations and moments obtained for each plastic hinge at each member end. Frames models of the structure with the plastic hinge labels are also reported in Appendix B.

3.3 NON LINEAR STATIC (PUSHOVER) ANALYSIS

The conventional static pushover is a nonlinear procedure in which monotonically increasing lateral loads along with constant gravity loads are applied to a framework until a control node (usually referred to the building roof) sways to a predefined 'target' lateral displacement, or to a 'target' base shear, which corresponds to a performance level. The target displacement is the maximum roof displacement likely to be experienced during the design earthquake.

Structural deformation and internal forces are monitored continuously as the model is displaced laterally. The method allows tracing the sequence of yielding and failure at the member and system levels, and can determine the inelastic drift distribution along the height of the building and the collapse mechanism of the structure. The strength and ductility demands at the target displacement (or target base shear) are used to check the acceptance of the structural design. The base shear versus roof displacement relationship, referred to as a capacity curve, is the fundamental product of the pushover analysis because it characterizes the overall performance of the building. The prescribed lateral inertia load pattern for pushover analysis is based on the premise that the response of the structure is controlled by a single frequency mode, and that the shape of this mode remains constant throughout the time history response. Generally, the fundamental mode of the structure is selected as the dominant response mode of the MDOF system and the influence of the other modes is ignored.

3.3.1 Capacity

Initially, an eigenvalue analysis was performed on the structural model in order to determine the elastic period, T , of the structure and the fundamental modal displacements of the structure. The first six modal periods and participating masses along with in plan deformed shapes are reported in the following Figure 3.3.1-1.

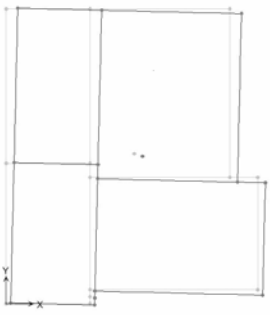


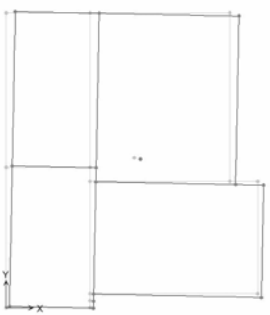

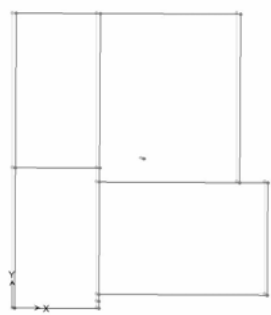
		
1° mode of vibration T=0,623 s; M _{%X} =71,8%; M _{%Y} =5,8%	2° mode of vibration T=0,535 s; M _{%X} =12,4%; M _{%Y} =60,5%	3° mode of vibration T=0,430 s; M _{%X} =2,9%; M _{%Y} =16,5%
		
4° mode of vibration T=0,219 s; M _{%X} =8,7%; M _{%Y} =0,5%	5° mode of vibration T=0,179 s; M _{%X} =1,5%; M _{%Y} =6,7%	6° mode of vibration T=0,150 s; M _{%X} =2,0%; M _{%Y} =0%

Figure 3.3.1-1- Fundamental modes of vibration, modal periods and participating masses for X and Y direction.

After that, pushover analyses in the longitudinal and transverse directions were performed by subjecting the structure to a monotonically increasing pattern of lateral forces proportional to the 1st and 2nd modes of vibration (in X and Y direction, respectively) and mass distribution; lateral loads were applied at the location of the centre of masses in the model. Centre of mass at each storey, masses values, modal displacements in correspondence of each centre of mass in the X and Y direction along with the corresponding normalized lateral loads are summarized in Table 3.3.1-1 and Table 3.3.1-2.

1° mode of vibration				
	displ. in dir. X [m]	mass [ton]	mass*displ.	F ^X _{mod} [KN]
1° storey	0,0102	65,86	0,6693	0,362
2° storey	0,0222	65,86	1,4602	0,791
3° storey	0,0292	63,28	1,8471	1

Table 3.3.1-1- Lateral forces proportional to the 1st mode of vibration.

2° mode of vibration				
	displ. in dir. Y [m]	mass [ton]	mass*displ.	F ^Y _{mod} [KN]
1° storey	-0,0081	65,86	-0,5328	0,297
2° storey	-0,0201	65,86	-1,3251	0,739
3° storey	-0,0284	63,28	-1,7940	1

Table 3.3.1-2- Lateral forces proportional to the 2nd mode of vibration.

A constant distribution of lateral loads was also investigated as indicated in the Ordinanza 3431 [2], and the main results are reported in Appendix C.

- **Limit states (LS)**

Building performance is a combination of both structural and non-structural components, and it is expressed in terms of *discrete damage states*. There are different performance levels (or particular damage states) defined in the literature (i.e., four such levels are: Operational (OP), Immediate Occupancy (IO), Life Safety (LS), and Collapse Prevention (CP) (FEMA-273, 1997, [13]); in the present study, according to Eurocode 8 [12], Part 3, and Ordinanza 3431 [2], the state of damage in the structure has been evaluated with reference to the following Limit States (LS):

- LS of damage limitation (DL): the building has sustained minimal or no damage to its members and only minor damage to its non-structural components that could however be economically repaired; the building is safe to be reoccupied immediately following the earthquake;
- LS of significant damage (SD): the building has experienced extensive damage to its structural and non-structural components and, while the risk to life is low, repairs may be required before re-occupancy can occur, and the repair may be deemed economically impractical;

- LS of near collapse (NC): the building has reached a state of impending partial or total collapse, where the building may have suffered a significant loss of lateral strength and stiffness with some permanent lateral deformation, but the major components of the gravity load carrying system should still continue to carry gravity load demands; the building may pose a significant threat to life safety as a result of the failure of non-structural components.

The damage limitation limit state (LSDL) corresponds to design seismic actions with a probability of exceedance of 20% in 50 years; the LSSD and LSNC are characterized by seismic actions with a probability of exceedance equal to 10% and 2% in 50 years, respectively.

In the present case of study, the three limit states above mentioned are treated with particular attention to the LSDL and LSSD that have to be analyzed in the case of civil buildings. It is noted that, according to the Ordinanza 3431 [2], each limit state is achieved, in the structural model, in correspondence of the attainment of a specific rotation value in the plastic hinge: 1) the LSDL corresponds to the first attainment of θ_y in one of the plastic hinges; 2) the LSSD corresponds at the first attainment of the $0.75\theta_u$ in one of the plastic hinges and 3) the LSNC corresponds at the first attainment of the θ_u in one of the plastic hinges.

- ***Pushover curves***

Based on such limit states, pushover analyses on the ‘as-built’ structure were performed in the longitudinal direction (positive and negative X-direction, named PX and NX, respectively) and in the transverse direction (positive and negative Y-direction, named PY and NY, respectively). The capacity curves obtained along with the point representative of each limit state investigated are reported in Figure 3.3.1-2. The same curves related to a constant lateral load distribution are reported in Appendix C.

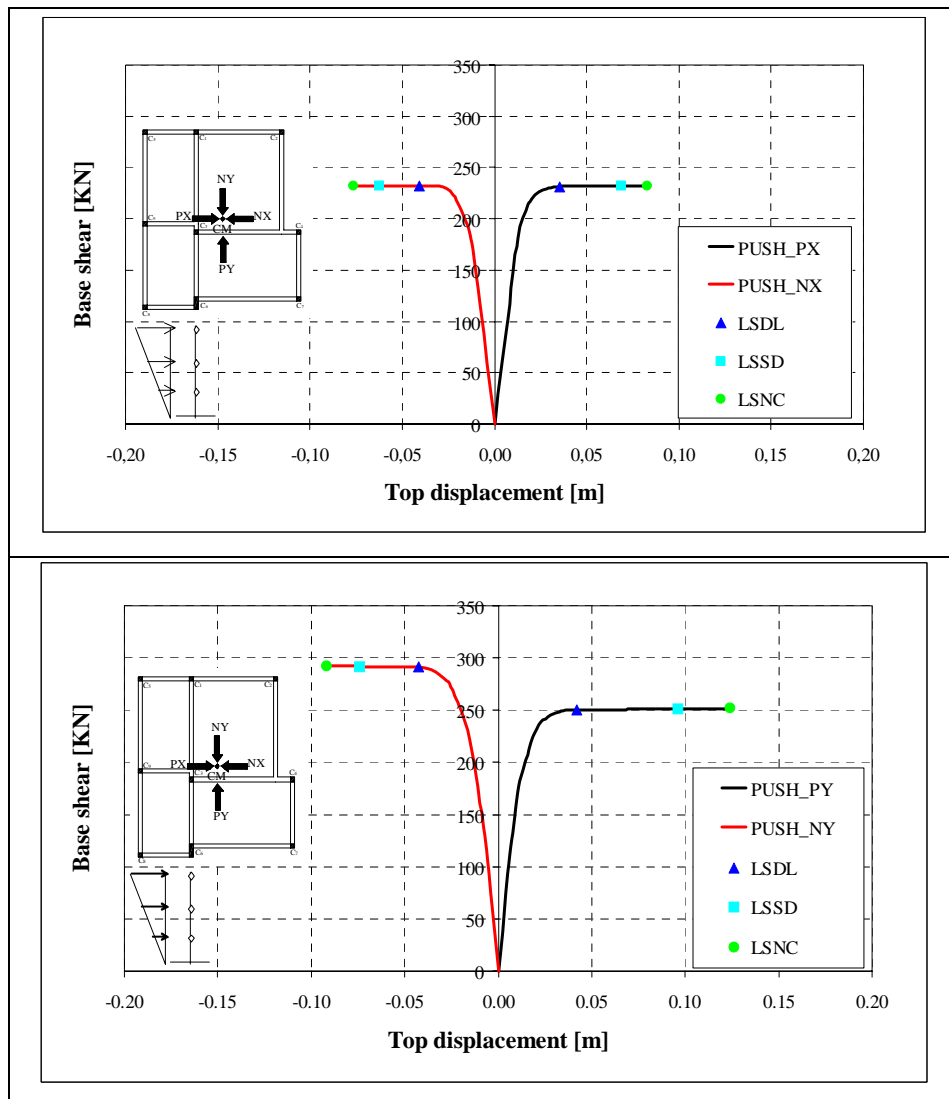


Figure 3.3.1-2– Pushover curves in positive and negative X and Y direction

According to the presence of the wall type column C6, the pushover curves clearly show that the structural strength is higher in direction Y rather than in the X one. The theoretical results in terms of rotation achieved in correspondence of the attainment of each limit state, the member on which such rotation has been recorded, as well as the maximum base shear, F_{max} , top displacement, d_{max} , and absolute inter-storey displacements, I-D, and drifts ξ , are summarized in Table 3.3.1-3 and Table 3.3.1-4. The same tables related to a constant lateral load distribution are reported in Appendix C.

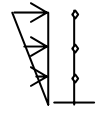
		TRIANGULAR FORCE DISTRIBUTION							
		θ [rad]	MEMBER	F_{max} [KN]	d_{max} [m]	d_i [m]	h [m]	$I-D=d_i-d_{i-1}$ [m]	$\xi=I-D/h$
PUSH_PX	LSDL	0,0042	B1_1	231	0,0355	0,0118	2,75	0,0118	0,004
						0,0312	3,00	0,0193	0,006
						0,0355	3,00	0,0043	0,001
	LSSD	0,0150	C4_2	232	0,0690	0,0124	2,75	0,0124	0,005
						0,0630	3,00	0,0505	0,017
						0,0690	3,00	0,0060	0,002
LSNC	0,0201	C4_2	232	0,0830	0,0124	2,75	0,0124	0,005	
					0,0782	3,00	0,0651	0,022	
					0,0830	3,00	0,0043	0,001	
PUSH_NX	LSDL	0,0076	C5_2	232	0,0406	-0,0094	2,75	-0,0094	-0,003
						-0,0366	3,00	-0,0272	-0,009
						-0,0406	3,00	-0,0040	-0,001
	LSSD	-0,0135	C3_2	232	0,0626	-0,0093	2,75	-0,0093	-0,003
						-0,0578	3,00	-0,0485	-0,016
						-0,0617	3,00	-0,0048	-0,002
	LSNC	-0,0181	C3_2	232	0,0766	-0,0093	2,75	-0,0093	-0,003
						-0,0714	3,00	-0,0621	-0,021
						-0,0766	3,00	-0,0052	-0,002

Table 3.3.1-3- Summary of the results in terms of capacity (direction X)

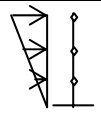
		TRIANGULAR FORCE DISTRIBUTION							
		θ [rad]	MEMBER	F_{max} [KN]	d_{max} [m]	d_i [m]	h [m]	$I-D=d_i-d_{i-1}$ [m]	$\xi=I-D/h$
PUSH_PY	LSDL	0,0047	B10_1	250	0,0422	0,0114	2,75	0,0114	0,004
						0,0271	3,00	0,0157	0,005
						0,0422	3,00	0,0151	0,005
	LSSD	0,0093	C6_1	251	0,0962	0,0287	2,75	0,0287	0,010
						0,0632	3,00	0,0344	0,011
						0,0962	3,00	0,0330	0,011
LSNC	0,0126	C6_1	252	0,1242	0,0372	2,75	0,0372	0,014	
					0,0808	3,00	0,0436	0,015	
					0,1242	3,00	0,0434	0,014	
PUSH_NY	LSDL	-0,0050	B10_1	291	0,0425	-0,0133	2,75	-0,0133	-0,005
						-0,0291	3,00	-0,0158	-0,005
						-0,0425	3,00	-0,0134	-0,004
	LSSD	-0,0093	C6_1	292	0,0740	-0,0284	2,75	-0,0284	-0,010
						-0,0740	3,00	-0,0323	-0,011
						-0,0732	3,00	-0,0133	-0,004
LSNC	-0,0125	C6_1	292	0,0940	-0,0370	2,75	-0,0370	-0,013	
					-0,0786	3,00	-0,0417	-0,014	
					-0,0940	3,00	-0,0154	-0,005	

Table 3.3.1-4- Summary of the results in terms of capacity (direction Y)

The tables show that, with reference to the LSDL, the plastic hinge limit is almost always attained on the beams. As concerns the LSSD and LSNC, the plastic hinge rotation limits are achieved at the second storey (column C5 and C3) for the analysis in the X direction and on the rectangular column C6 at first storey for the analysis in the Y direction. The maximum base shear is 232 kN and 292 kN for the longitudinal and transversal direction, respectively.

The structure deformed shape with reference to the limit states investigated as well as the plastic hinges rotation states (i.e. blue is used for indicating the attainment of θ_y in one of the plastic hinges corresponding to the LSDL, cyan and green for the attainment of rotations equal to $0.75\theta_u$ and θ_u , corresponding to the LSSD and LSNC) are reported in Figure 3.3.1-3 and Figure 3.3.1-4. (for the constant lateral load distribution, see Appendix C).

From such figures it is possible to have a clear idea of the structural behaviour under an increasing pattern of seismic actions.

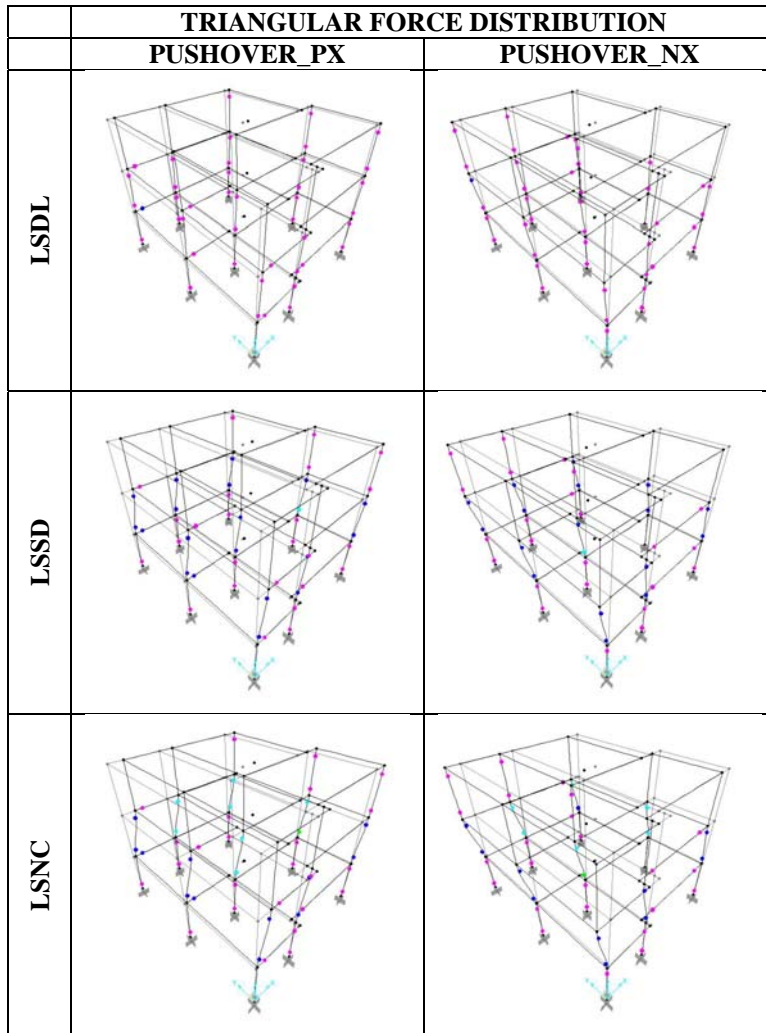


Figure 3.3.1-3- Plastic hinges distribution (triangular lateral loads, direction X)

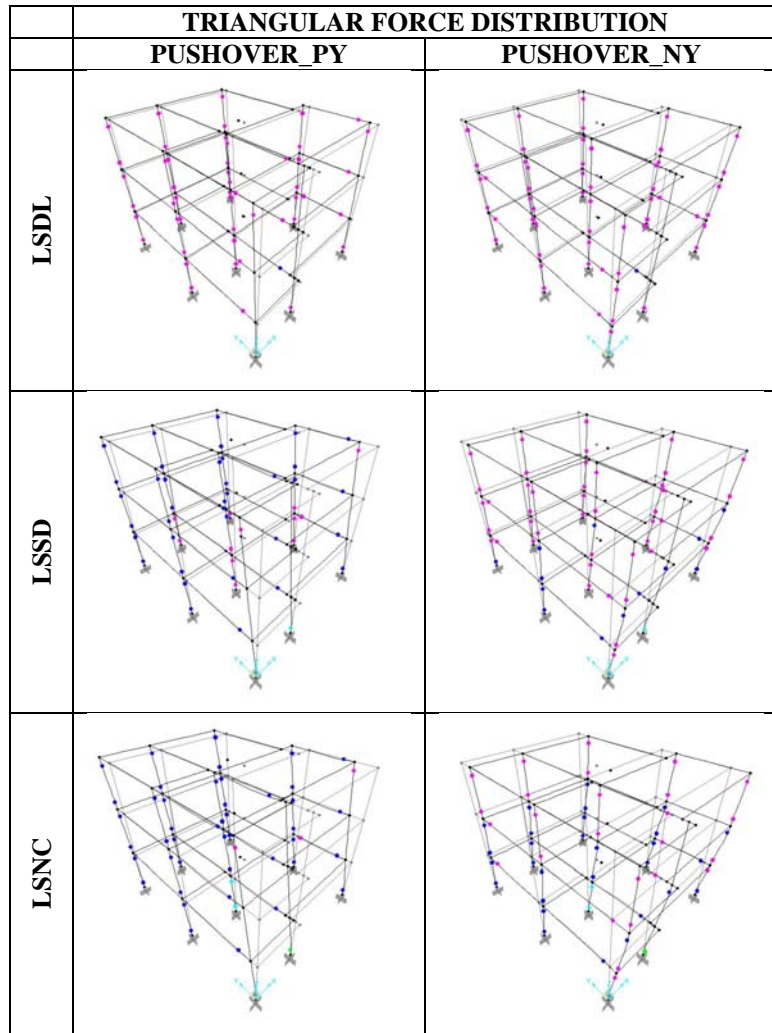


Figure 3.3.1-4- Plastic hinges distribution (triangular lateral loads, direction Y)

The inter-storey displacements referred to the limit states investigated are also reported in Figure 3.3.1-5. From such diagrams it is clear that the second storey it is the most involved in terms of displacement. The same diagrams related to a constant lateral load distribution are reported in Appendix C.

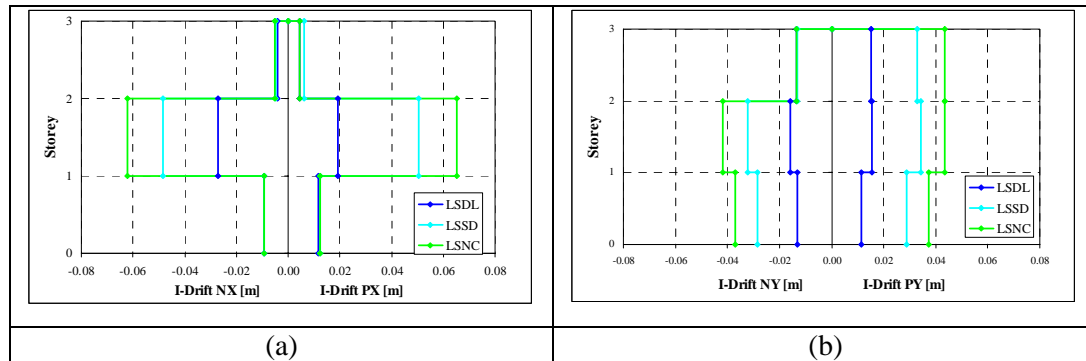


Figure 3.3.1-5- Inter-storey displacements: (a) X direction, (b) Y direction.

3.3.2 Seismic Demand

Once the seismic capacity of the structure has been determined with reference to each direction, the next step has been the computation of the seismic demand related to seismic actions with a PGA level equal to both 0,20g (in order to have a direct comparison with the experimental test executed) and 0,30g (in order to analyse the structural seismic behaviour under increased horizontal actions).

- **Definition of the elastic design spectrum**

The experimental tests on the ‘as-built’ structure were conducted with reference to the accelerogram of Montenegro 1979 Herceg-Novi in both X and Y direction (see Figure 3.3.2-1); such accelerogram was scaled to a PGA level equal to 0,15g and 0,20 g in the first and second test, respectively.

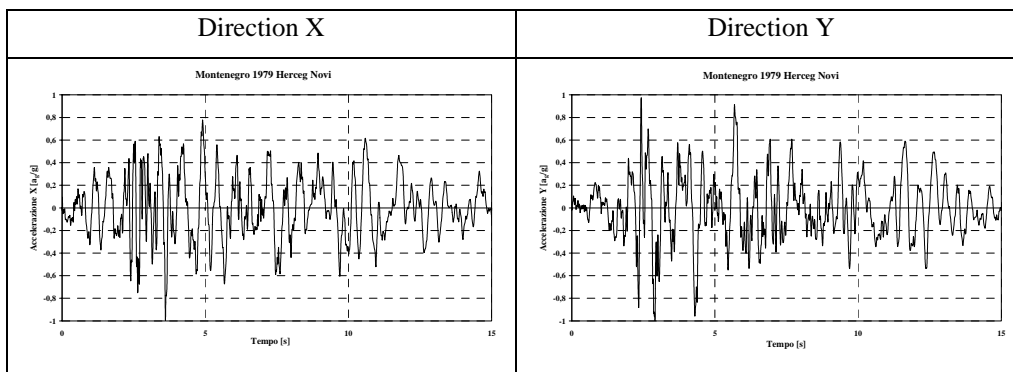


Figure 3.3.2-1 - Montenegro 1979 Herceg-Novi accelerogram (PGA 1g)

From the accelerogram it is possible to determine the corresponding elastic design spectrum by a numerical integration procedure; the elastic spectrum is, in fact, the

interpolation curve representative of the maximum responses in terms of acceleration, velocity or displacement of a Single Degree of Freedom (SDoF) system as a function of its fundamental period.

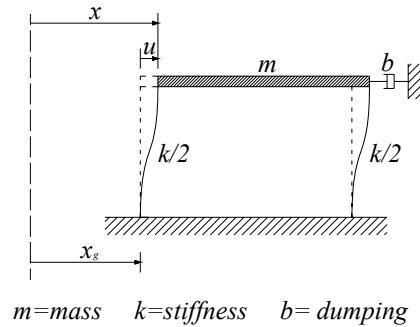


Figure 3.3.2-2- Single degree of freedom (SDoF) system

For a SDoF system under a seismic action, the equation of the motion is the following:

$$m\ddot{u} + b\dot{u} + ku = -\ddot{x}_g(t)m \Rightarrow \ddot{u} + 2v\omega\dot{u} + \omega^2u = -\ddot{x}_g(t)$$

where $\ddot{x}_g(t)$ is the accelerogram. The solution of such equation is provided by the Duhamel's integral:

$$u(t) = \frac{1}{\omega} \int_0^t \ddot{x}_g(\tau) \cdot e^{-v\omega(t-\tau)} \text{sen} \omega(t-\tau) d\tau$$

By derivating such expression it is possible to derive the relative velocity and acceleration; from the relative acceleration it is then possible to compute the total acceleration by the expression:

$$\ddot{x}(t) = \ddot{x}_g + \ddot{u}$$

By repeating such procedure for the oscillator with different values of the period and in correspondence of the accelerogram peaks it has been obtained the elastic acceleration spectra reported in Figure 3.3.2-3 (a).

Moreover by using the equation:

$$S_{de}(T) = S_{ae}(T) \left(\frac{T}{2\pi} \right)^2$$

it has been derived the related displacement elastic spectra reported in Figure 3.3.2-3 (b).

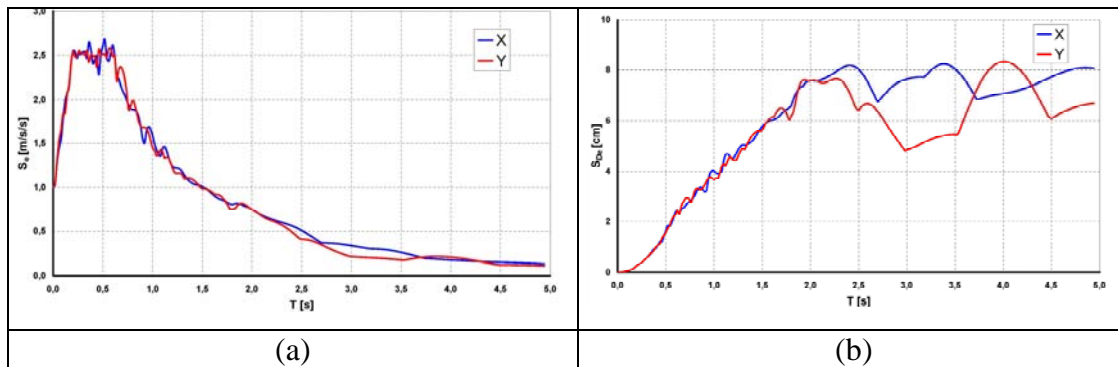


Figure 3.3.2-3- Elastic acceleration (a) and displacement (b) spectra for the Montenegro 1979, Herceg Novi accelerogram

Both the design spectrum of the Eurocode 8 [3] Part I and of the Ordinanza 3431 [2](soil type C, 5% damping), provide a pseudo-acceleration spectrum compatible with that obtained by the experimental ground motion record, Montenegro Herceg-Novu (see Figure 3.3.2-4). Thus, the seismic demand was computed with reference to the Ordinanza 3431 [2] design spectrum.

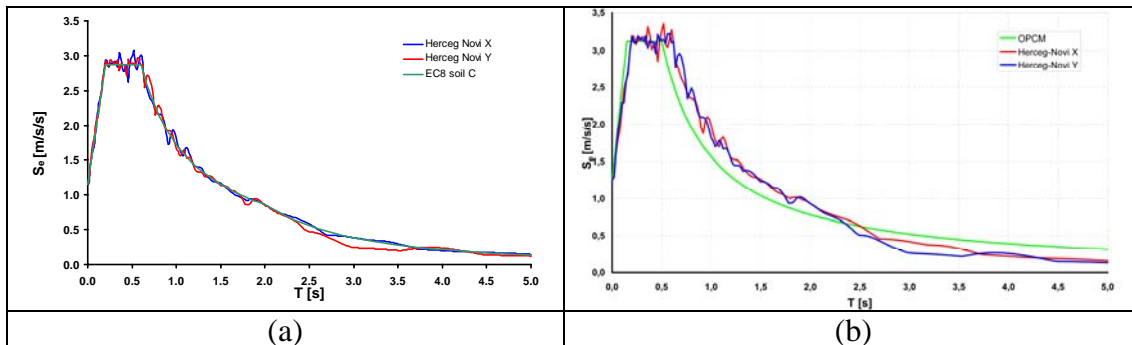


Figure 3.3.2-4- Acceleration response spectra (5% damping) of X and Y components and Eurocode 8 (a) - Ordinanza (b) soil C spectrum

As indicated in the Ordinanza 3431 [2], such response spectrum has been multiplied by a factor equal to 0.4, 1 and 1.5 for the LSDL, LSSD and LSNC, respectively.

- ***Determination of the target displacement***

Once the capacity curve, which represents the relation between base shear force and control node displacement, is known, the target displacement is determined from the elastic response spectrum. In order to determine such displacement for a structure, that is a Multi Degree of Freedom system (MDoF), it is necessary to consider an equivalent SDoF by using the transformation factor:

$$\Gamma = \frac{\sum m_i \Phi_i}{\sum m_i \Phi_i^2}$$

where m_i is the mass in the i -th storey and Φ_i are the normalized displacement (relative to the first mode of vibration); the displacement are normalized in such a way that $\Phi_n = 1$, where n is the control node (usually, n denotes the roof level)

The force F^* and displacement d^* of the equivalent SDoF system are computed as follows:

$$F^* = F/\Gamma; \quad d^* = d/\Gamma$$

where F and d are the base shear force and the control node displacement of the MDoF system, respectively (see Figure 3.3.2-5). Once the characteristic curve of the MDoF system has been scaled to the factor Γ , the characteristic curve (force-displacement, F^*-d^*) of the SDoF system can be obtained by tracing an idealized elasto-perfectly plastic bilinear curve in such a way that the areas under the actual and the idealized force-displacement curve are equal (that implies $A_1=A_2$, see Figure 3.3.2-5). The yielding force, F_y^* , represents the ultimate strength of the idealized system and it is equal to the base shear force at the formation of the plastic mechanism; k^* , is the initial stiffness of the idealized system determined by the areas equivalence.

The period, T^* , of the idealized equivalent SDoF system is determined by:

$$T^* = 2\pi \sqrt{\frac{m^*}{k^*}} = 2\pi \sqrt{\frac{m^* d_y^*}{F_y^*}}$$

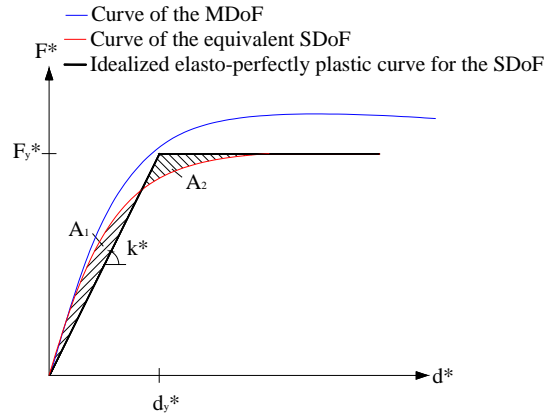


Figure 3.3.2-5- Determination of the idealized elasto-perfectly plastic force-displacement relationship

The target displacement of the inelastic system can be computed as a function of the period T^* and of the assumed response spectrum. In particular, if $T^* \geq T_C$ (medium and long period range), the target displacement of the inelastic system is equal to that one with unlimited elastic behaviour and is given by:

$$d_{\max}^* = d_{e,\max}^* = S_{de}(T^*)$$

In Figure 3.3.2-6 (a) the equivalent graphical procedure to obtain such displacement is reported in the ADRS (*Acceleration-Displacement Response Spectrum*) format, period T^* is represented by the radial line from the origin of the coordinate system to the point at the elastic response spectrum defined by the point d_{\max}^* and $S_{de}(T^*)$.

If $T^* < T_C$, the displacement of the inelastic system is larger than that with unlimited elastic behaviour (with the same period) and it is computed as follows:

$$d_{\max}^* = \frac{d_{e,\max}^*}{q^*} \left[1 + (q^* - 1) \frac{T_C}{T^*} \right] \geq d_{e,\max}^*$$

where $q^* = S_{ae}(T^*)m^*/F_y^*$ is the ratio between the acceleration in the structure with unlimited elastic behaviour, $S_e(T^*)$ and in the structure with limited strength F_y^*/m^* . The equivalent graphical procedure is reported in Figure 3.3.2-6 (b).

Once the target displacement for the equivalent SDoF system has been computed, the target displacement of the MdoF system is given by:

$$d_{\max} = \Gamma d_{\max}^*$$

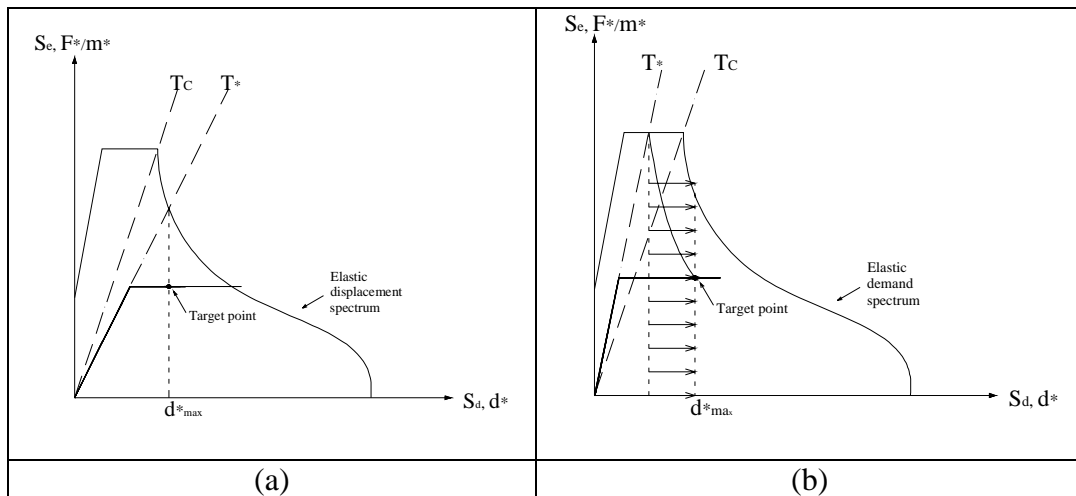


Figure 3.3.2-6- Graphical procedure for computing the target displacement in the case of $T^* \geq T_C$ (a), and $T^* < T_C$, (b).

The displacement demand due to the seismic actions can be compared to the structural displacement capacity computed by the nonlinear static pushover.

By using such procedure, it has been possible to plot the seismic capacity and demand for both seismic action at 0.20g and 0.30g PGA level and for the three limit states investigated. The results are reported in Figure 3.3.2-7. In Appendix C, such curves are reported with reference to a constant distribution of lateral loads.

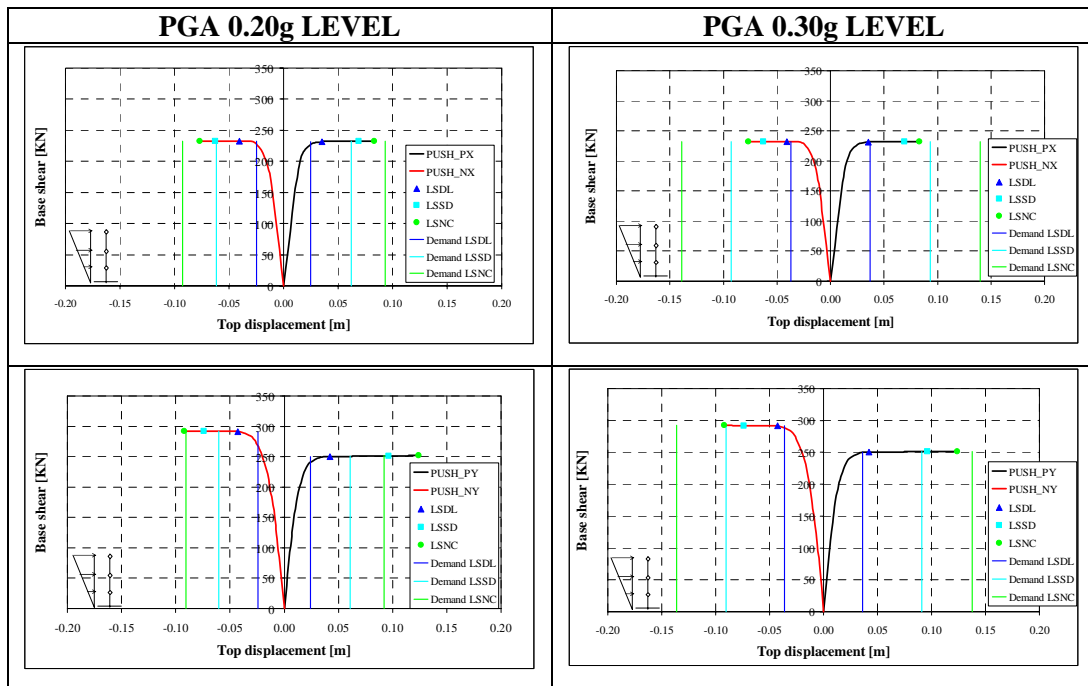


Figure 3.3.2-7- Demand vs. capacity comparison for PGA level equal to 0.20g and 0.30g at LSDL, LSSD and LSNC.

Such results are summarized in a numerical form in the following tables.

		CAPACITY	DEMAND	
			0,20g	0,30g
		d_{max} [m]	d_{max} [m]	d_{max} [m]
PUSH_PX	LSDL	0,0355	0,0248	0,0372*
	LSSD	0,0690	0,0623	0,0934*
	LSNC	0,0825	0,0934*	0,1401*
PUSH_NX	LSDL	0,0406	0,0247	0,0371
	LSSD	0,0626	0,0618	0,0927*
	LSNC	0,0753	0,0927	0,1391

		CAPACITY	DEMAND	
			0,20g	0,30g
		d_{max} [m]	d_{max} [m]	d_{max} [m]
PUSH_PY	LSDL	0,0422	0,0240	0,0360
	LSSD	0,0962	0,0607	0,0910
	LSNC	0,1225	0,0919	0,1379*
PUSH_NY	LSDL	0,0425	0,0240	0,0361
	LSSD	0,0740	0,0603	0,0904*
	LSNC	0,0912	0,0907	0,1360*

(*Demand displacements not satisfied by the structure)

Table 3.3.2-1- Demand vs. capacity comparison for PGA level equal to 0.20g and 0.30g at LSDL,LSSD and LSNC.

The above reported Figure 3.3.2-7 and (*Demand displacements not satisfied by the structure)

Table 3.3.2-1 show that the ‘as-built’ structure is able to satisfy both LSDL and LSSD in each direction with reference to the 0.20g PGA level even if, especially in the positive and negative X direction for the LSSD, the capacity is only slightly larger than the demand. Moreover, increasing the seismic action up to a 0.30g, the LSDL verification is not satisfied in the PX direction; with regards to the LSSD, the capacity is larger than demand only in the PY direction. At this PGA level for the LSSD the maximum gap in terms of maximum top displacement is provided in the NX direction where the difference between the seismic demand and the displacement capacity is equal to 0.0301 m (0.0927 m minus 0.0626 m) corresponding to a percentage performance gap equal to 48%. Such result can be is also clearly visualized by using a capacity spectrum approach (CSA), Fajfar P. [14] as reported below:

• ***Capacity Spectrum Approach, CSA - N2 Method***

The N2 method, Fajfar P. [14], is a simply nonlinear method for the seismic analysis of structures that combines the pushover analysis of a MDoF system with the response spectrum analysis of a SDoF system. Such method yields exactly the same results obtained by the procedure above adopted, but the formulation of the method in the acceleration – displacement (AD) format, enables the visual interpretation of the procedure and of the relations between the basic quantities controlling the seismic response. A brief description of the method is below reported.

For an elastic SDoF system, the elastic acceleration spectrum, S_{ae} and displacement spectrum, S_{de} , are related by the expression:

$$S_{de} = \frac{T^2}{4\pi^2} S_{ae}$$

thus, the elastic acceleration spectrum (for a fixed damping ratio) can be plotted as a function of the elastic displacement spectrum as reported in Figure 3.3.2-8 (blue curve).

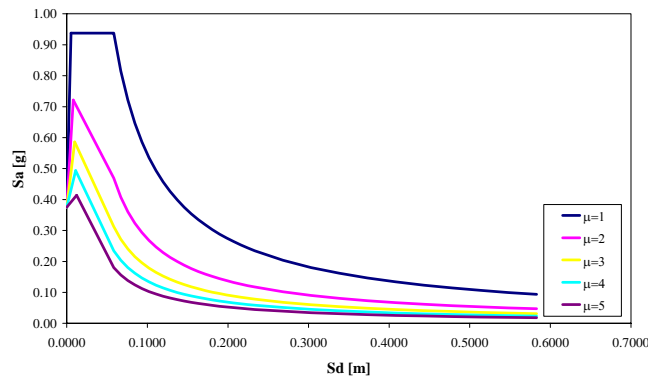


Figure 3.3.2-8-Elastic and inelastic acceleration and displacement spectrum in AD format

In the case of an inelastic SDoF system with a bilinear force-displacement relationship, the relation between the acceleration spectrum, S_a and displacement spectrum, S_d , can be determined by the expression:

$$S_a = \frac{S_{ae}}{R_\mu} ; S_d = \frac{\mu}{R_\mu} S_{de}$$

from which can be determined the relation between them:

$$S_d = \frac{\mu}{R_\mu} S_{de} = \frac{\mu}{R_\mu} \frac{T^2}{4\pi^2} S_{ae} = \mu \frac{T^2}{4\pi^2} S_a$$

where μ is the ductility factor defined as the ratio between the maximum displacement and the yield displacement, and R_μ is the reduction factor due to the ductility. Such factors in the N2 method are computed as:

$$R_\mu = (\mu - 1) \frac{T}{T_C} + 1 \text{ for } T < T_C;$$

$$R_\mu = \mu \text{ for } T \geq T_C$$

where T_C is the characteristic period of the ground motion (see Figure 3.3.2-9)

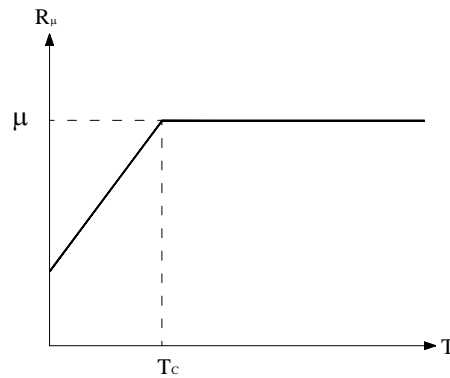


Figure 3.3.2-9- Reduction factor, R_μ as a function of T .

Based on such expressions, it is possible, starting from the elastic design spectrum to determine the demand spectra for different values of the ductility factor, μ (see Figure 3.3.2-8).

The idealized elasto-perfectly plastic force-displacement relationship of the equivalent SDoF system (SDoF capacity diagram) can be plotted in the AD format by dividing the forces in the force-deformation diagram by the equivalent mass, m^* :

$$S_a = \frac{F^*}{m^*}$$

Then, plotting in the same graph the elastic demand spectrum ($\mu = 1$) and the bilinear curve of the equivalent SDoF system (SDoF capacity diagram) it is possible to determine the acceleration and the corresponding elastic displacement demand (named S_{ae} and S_{de} , respectively), required in the case of elastic behaviour, by

intersecting the radial line corresponding to the elastic period of the idealized bilinear system T^* with the elastic demand spectrum (see Figure 3.3.2-10 and Figure 3.3.2-11). At this point, the inelastic demand in terms of accelerations and displacements is provided by the intersection point of the capacity diagram with the demand spectrum corresponding to the ductility demand, μ (defined as the ratio between $S_d =$ requested displacement, and $D_y^* =$ yield displacement of the idealized bilinear system of the equivalent SDOF system). Depending if T^* is larger or less of T_C , the ductility demand, μ , and the requested displacement, S_d , are given by:

for $T^* < T_C$	for $T^* \geq T_C$
$\mu = (R_\mu - 1) \frac{T_C}{T} + 1$	$\mu = R_\mu$
$S_d = \frac{S_{de}}{R_\mu} \left(1 + (R_\mu - 1) \frac{T}{T_C} \right)$	$S_d = S_{de}$

where R_μ can be computed as the ratio between the acceleration corresponding to the elastic and inelastic system, $R_\mu = \frac{S_{ae}(T^*)}{S_{ay}}$.

In this way it is possible to perform the verification in a graphical manner by checking if the capacity curve exceeds or not the demand spectrum curve (see Figure 3.3.2-10 and Figure 3.3.2-11).

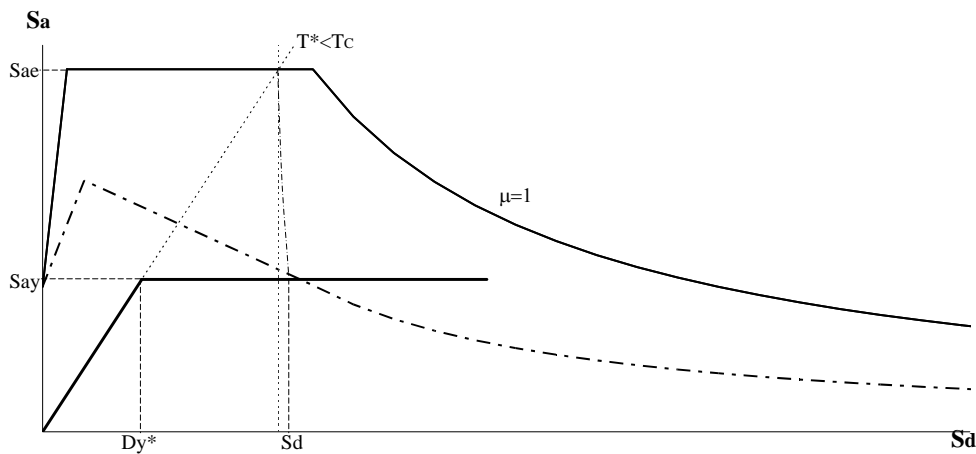


Figure 3.3.2-10- N2 method, elastic and inelastic spectra vs. capacity diagram ($T^* < T_C$)

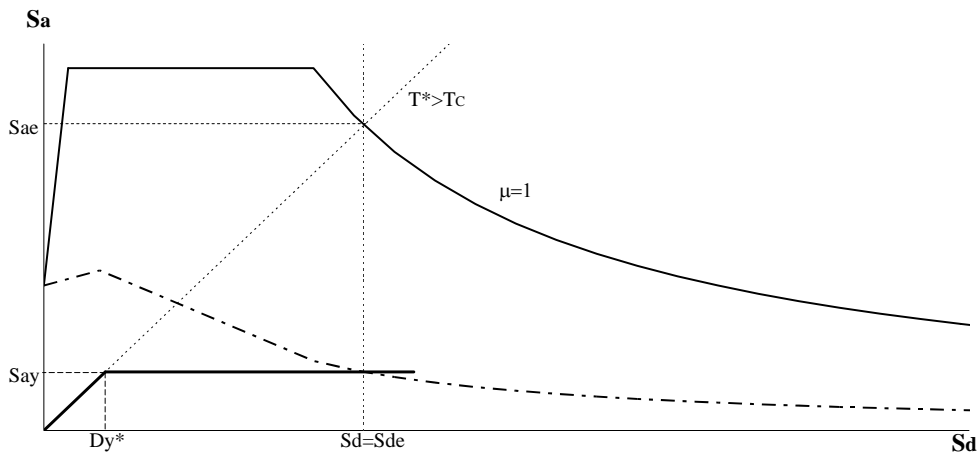


Figure 3.3.2-11- N2 method, elastic and inelastic spectra vs. capacity diagram ($T^* \geq T_C$)

In the following Figure 3.3.2-12, the seismic verification at the LSSD for a PGA equal to both 0.20g and 0.30g are reported by using such procedure. In each case, it is reported the value of the ductility demand, μ , and of the structural ductility, μ_s , obtained as the ratio between the maximum displacement of the equivalent SDOF system, d^*_{\max} and its yield displacement, D^*_y .

In Appendix C the same graphs are reported with reference to the constant lateral distribution of seismic forces.

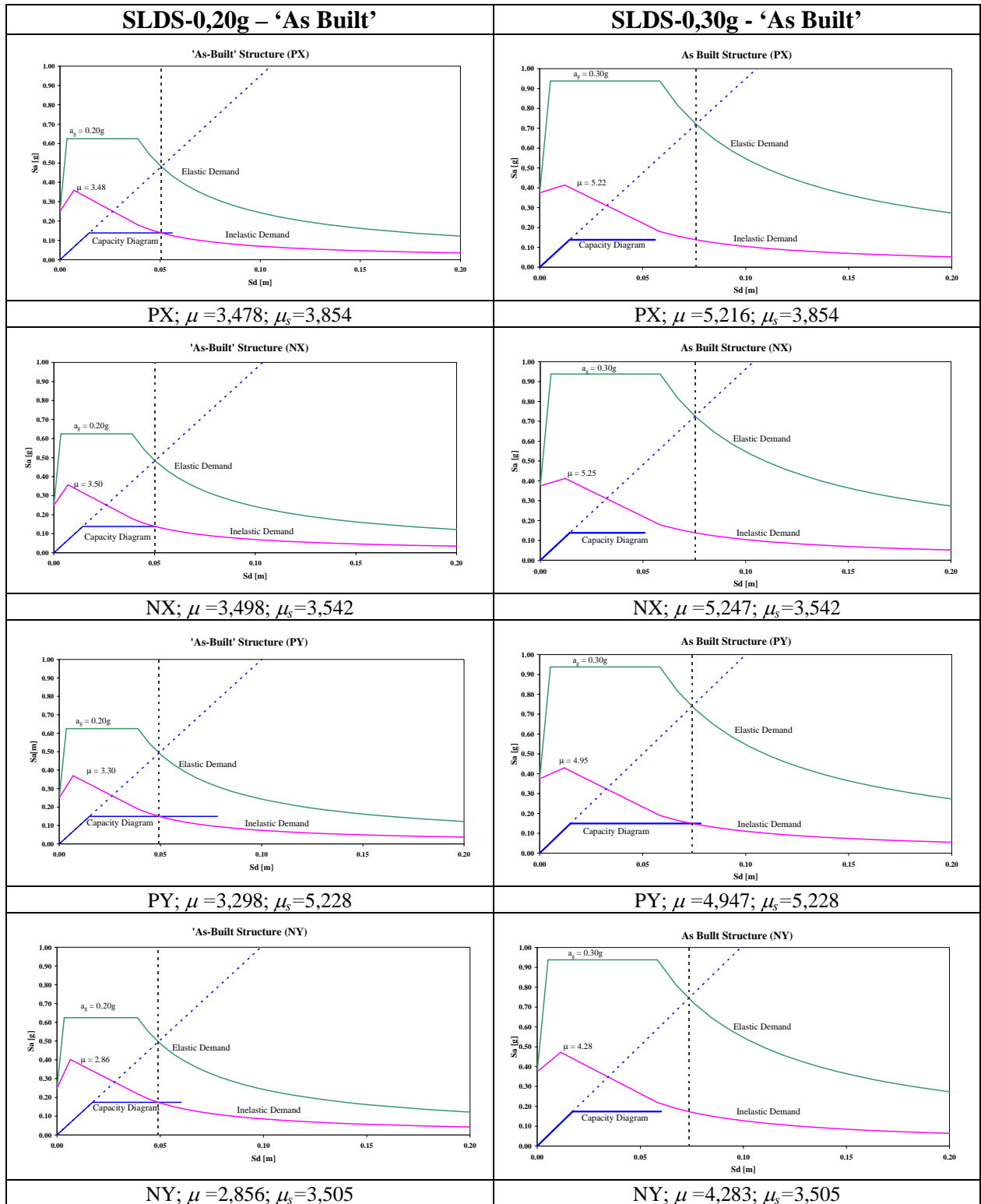


Figure 3.3.2-12 - N2 method, capacity vs. demand

As above mentioned the results obtained by using such procedure are the same that can be provided numerically. In particular it is recalled that the maximum gap in terms of maximum top displacement is provided in the NX direction.

Such result is clearly highlighted by Figure 3.3.2-13 in which the seismic demand, for the two levels of ground motion analysed for the equivalent SDOF system in the NX direction, is determined by using the N2 method.

Figure 3.3.2-13 highlights that the ‘as-built’ structure in the NX direction, hardly able to satisfy the demand corresponding to the 0.20g PGA level ($\mu = 3.49$ against $\mu_s = 3.54$), is totally lacking the appropriate capacity to resist the 0.30g PGA level as the requested ductility is about $\mu = 5.24$ against the structural ductility equal to $\mu_s = 3.54$ ($d^*_{max} = 0.0509$ m, and $D^*_y = 0.0143$ m).

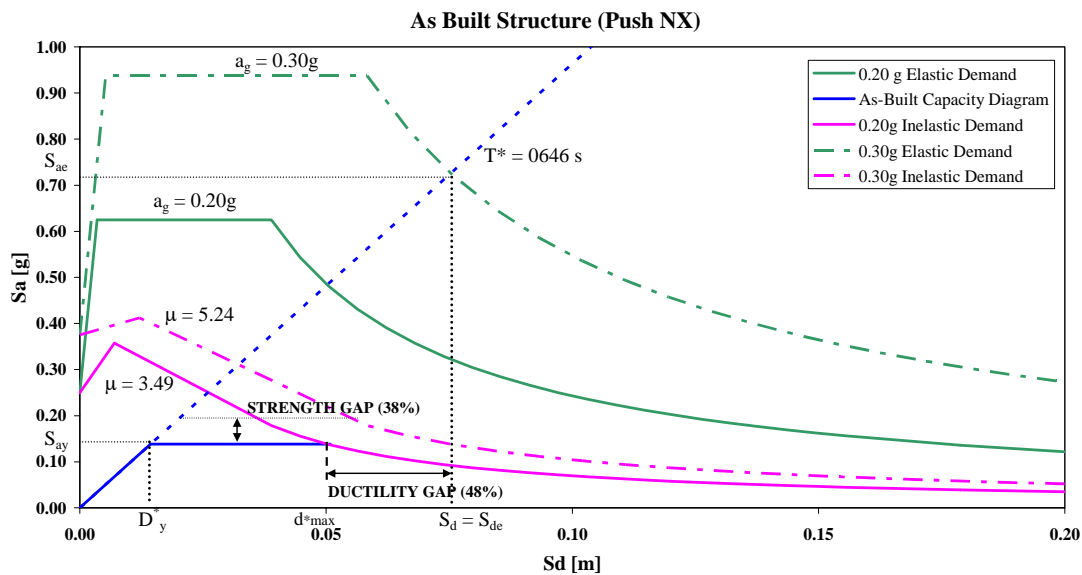


Figure 3.3.2-13 – ‘As-built’ structure elastic and inelastic demand spectra vs. capacity diagram

3.3.3 Theoretical vs. Experimental results

The theoretical analysis provided results very close to the experimental ones as it predicted the first attainment of the significant damage limit state (i.e. $0.75\theta_u$ in the plastic hinge) in correspondence of the columns ends at the second floor (i.e. at column C3 and C4 in the PX and NX direction, respectively) where the most significant damages were found during the test. The accuracy of the model is confirmed, in terms of global behaviour of the structure, by plotting the theoretical (for the LSSD) vs. experimental envelop of inter-storey drifts (see Figure 3.3.3-1).

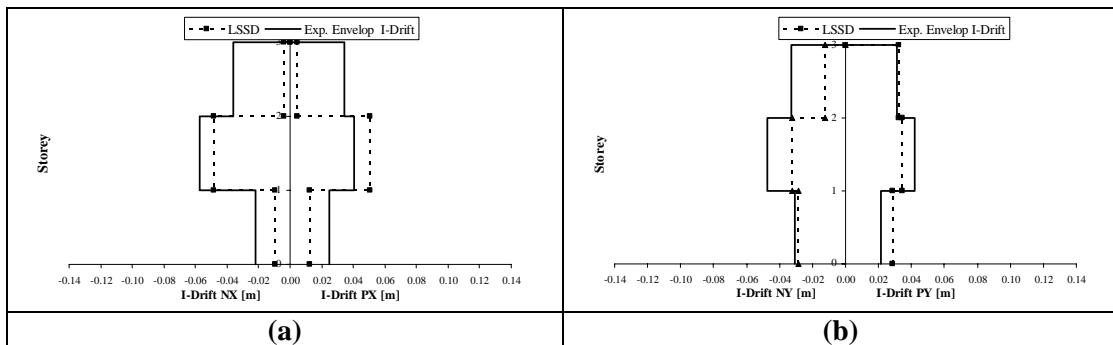


Figure 3.3.3-1– Theoretical vs. experimental envelop inter-storey drift: ‘as-built’ structure at PGA level 0.20g in the X direction (a) and Y direction (b)

Although the experimental inter-storey displacements are reported in terms of envelope and thus were not reached at the same time, it is possible to underline the model compatibility with test results: the theoretical results were in compliance with the experimental ones in assessing the second storey as the one more involved in the seismic structural behaviour.

Moreover, it is noted that the theoretical analysis was in good agreement with the experimental outcomes because, according to the damage pattern found on the structure after the test, it provides a 0.20g as a limit acceleration value for the verification of the LSSD.

Chapter IV

4.1 REHABILITATION INTERVENTION STRATEGIES

Both the experimental activity and the lumped plasticity analysis indicate that the ‘as-built’ structure was able to sustain seismic actions at LSSD up to a 0.20g level, but, in order to increase the seismic actions without inducing the collapse of the structure, a rehabilitation intervention was necessary.

In order to increase the seismic capacity of an existing building, different strategies can be followed; in particular if the structural capacity, represented by a point in the Strength-Ductility plan, is lower than the requested seismic capacity, represented by a curve in the same plan, three main strategies can be followed to allow moving such point beyond the curve representative of the demand: (a) by acting on ductility only, increasing the global deformation capacity of the structure (the point can be moved beyond the curve demand in a horizontal way), (b) by increasing both strength and ductility (the point can be moved over the curve demand in a diagonal way) and (c) by increasing the structural strength only (the point can be moved beyond the curve demand in a vertical way) (Sugano, S. [15], see Figure 4.1-1)

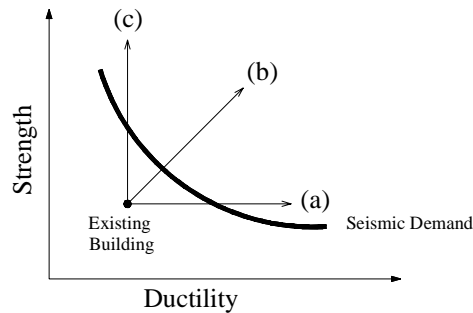


Figure 4.1-1–Rehabilitation strategies (Sugano, S. [15])

In the case of the investigated structure it has been shown, from the theoretical analysis results reported in the previous chapter, that the target design PGA level equal to 0.30g could have been sustained by 1) increasing the global deformation capacity by a factor of 48%); 2) improving both strength and ductility capacity of the

structure; 3) increasing only the strength capacity of the structure by a factor of 38%. (see Figure 3.3.2–13). It is noted that such percentage values are computed according to the hypothesis that the elastic period of the idealized bilinear system, T^* , remains constant after the rehabilitation intervention.

The first two strategies outlined were chosen and pursued by using FRP laminates and RC jacketing, respectively. The design criteria used for the retrofit, the analytical predictions as well as the construction phases and the experimental results related to the first investigated technique are reported in the following sections. The design criteria and experimental results related to the second strategy are reported in Chapter V.

4.2 DESIGN OF REHABILITATION WITH COMPOSITES

Selection of fiber texture and retrofit design criteria were based on deficiencies underlined by both test on the ‘as-built’ structure and theoretical results provided by the post-test assessment. The results provided by such analyses indicate that, in order to increase the seismic capacity of the structure, a retrofit intervention was necessary; in particular, the theoretical results showed that the target design PGA level equal to 0.30g could have been sustained by the structure if its displacement capacity is increased by a factor of 48%. In order to pursue such objective, the retrofit design strategy was focused on two main aspects, 1) increasing the global deformation capacity of the structure and thus its dissipating global performance and 2) allowing to fully exploit the increased deformation capacity by avoiding brittle collapses modes. Thus, the retrofit design was aimed at optimising the benefits of the externally bonded FRP reinforcement along the direction of dominant stresses by increasing either the column confinement or the shear capacity of exterior beam-column joints and of the wall-type column, C6. The design principles of the rehabilitation strategy are outlined in the following sections with reference to two main issues: 1) design of column confinement; 2) exterior beam column joints and wall-type column shear strengthening design.

4.2.1 Columns Confinement

Both experimental activity and theoretical assessment of the ‘as-built’ structure highlighted that columns cross-sectional dimensions and amount of longitudinal steel reinforcement were inadequate to satisfy the demand generated by the biaxial bending associated to the axial load; the weak column-strong beam condition led to the formation of plastic hinges in the columns. In order to provide a seismic retrofit of the structure, it was decided to increase the ductility of the plastic hinges at column ends, rather than establishing a correct hierarchy of strength by their relocalization.

Such objective was pursued by GFRP columns confinement that allows enhancing

the ultimate concrete compressive strain. This corresponds to an increase of curvature ductility that, assuming a plastic hinge length not significantly affected by the retrofit intervention, determines a proportional increase of the plastic hinge rotation capacity. As design hypothesis, concrete stress-strain diagram it was assumed to be parabolic-rectangular and calculations procedures usually adopted for uniaxial bending were extended to the case of biaxial bending.

In order to compute the ultimate axial strain of a FRP confined member, calculation were carried out by using the equation provided by the latest guideline developed by Italian National research Council, CNR-DT 200 [16]:

$$\varepsilon_{ccu} = 0.0035 + \sqrt{\frac{f_{l,eff}}{f_{cd}}} \quad (1)$$

where the ultimate axial strain for FRP-confined concrete, ε_{ccu} , is computed as a function of the effective lateral confining pressure, $f_{l,eff}$ and the design compressive concrete strength, f_{cd} . In order to account that calculations are referred to an existing structure the design compressive concrete strength was assumed as the average compressive concrete strength obtained by the tests on the field, $f_c = 25$ MPa.

In order to quantify the amount of FRP to be installed, the central column, C3, was selected for calculations since it carries the maximum axial force due to the gravity loads ($P = 409$ kN at first storey) and thus it has the minimum rotational capacity. In Table 4.2.1-1 the theoretical results in terms of concrete ultimate axial strain provided by equation (5), along with the ultimate curvature, for one, two and three plies of uniaxial GFRP or CFRP confinement, with density of 900 gr/m^2 and 300 gr/m^2 and thickness of 0.48 mm/ply and 0.166 mm/ply , respectively, are summarized. In the last two columns the ultimate rotation and the percentage rotation increase with respect to the original unconfined cross-section, $\Delta_{abs.}$, are reported. It is noted that the ultimate rotation values were computed with reference to the expression (3) reported in Chapter III.

FRP type	FRP thickness	FRP volumetric ratio	Ultimate Strain	Ultimate Curvature	Ultimate Rotation	Ultimate Rotation Abs. Increase
	t_f (mm)	$\rho_{frp} = \frac{\rho_{frp}}{2t_f(b+d)/bd}$	ϵ_{ccu} (‰)	ϕ_u (rad/mm $\times 10^5$)	θ_u (rad)	$\Delta_{abs.}$ (%)
Original	-	-	3.50	4.325	0.0125	0
1 GFRP ply	0.480	0.00768	7.30	10.129	0.0248	98
2 GFRP plies	0.960	0.01536	8.87	12.527	0.0298	138
3 GFRP plies	1.440	0.02304	10.08	14.376	0.0337	169
1 CFRP ply	0.166	0.00266	7.12	9.854	0.0242	93
2 CFRP plies	0.332	0.00531	8.62	12.145	0.0290	131
3 CFRP plies	0.498	0.00797	9.77	13.902	0.0327	161

Table 4.2.1-1- Influence of GFRP and CFRP confinement on concrete ultimate axial strain, ultimate curvature and ultimate rotation.

In Figure 4.2.1-1, on the right-hand side, the moment-curvature relationship with reference to the original C3 column cross section (continuous line), under axial load acting at first storey due only to the gravity loads ($P= 409$ kN), is plotted; the dashed line represents the moment-curvature progress by adding one ply at a time of GFRP confinement. The same graph is plotted in the left-hand side of the diagram with respect to CFRP confinement.

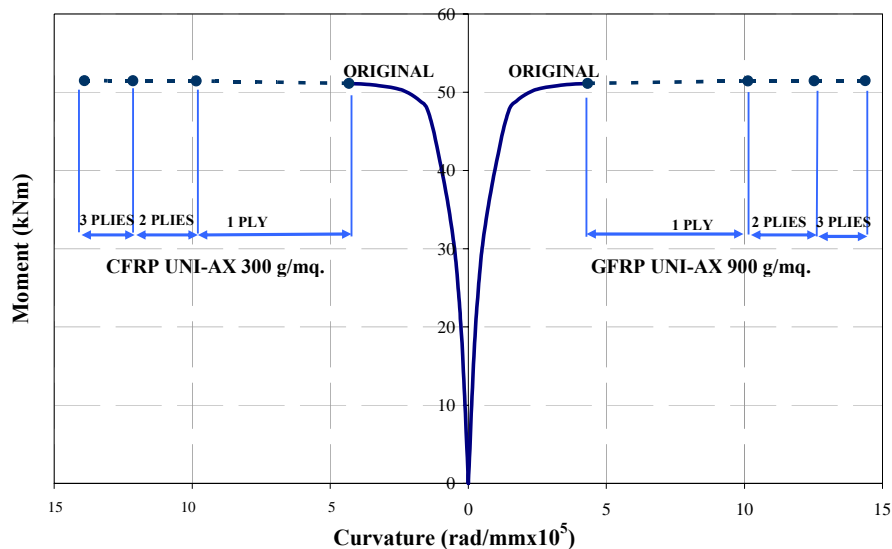


Figure 4.2.1-1- Moment-curvature for original, GFRP and CFRP upgraded C3 column cross section.

Figure 4.2.1-1 shows that both GFRP and CFRP confinement causes a negligible increment of cross-section ultimate moment (the ultimate moment goes from a value of $M_u = 51.14$ kNm in the original configuration up to value $M_u = 51.48$ kNm in the retrofitted one, either for GFRP or CFRP confinement); on the other hand, theoretical calculations clearly highlight that, with reference to the glass and carbon fibers selected, the curvature increase and the related ultimate rotation increase (see Table 4.2.1-1) is very significant but not substantially affected by the two different kind of laminates analyzed.

Once established that both materials were able to increase almost equally the ultimate concrete axial strain and thus both the ultimate curvature and ultimate rotation of the cross-section, considering that in the case of interior application in buildings, durability performance is not the driving design criterion, the choice of the fibers to be utilized was essentially governed by economic evaluations. Comparing the application costs per square meter, it was calculated that by using uniaxial glass fibers with density of 900 gr/m^2 , instead of uniaxial carbon fibers with density of 300 gr/m^2 , the costs were reduced by a factor of about 30%; this was the reason for selecting glass laminates.

By using GFRP laminates, the percentage ultimate rotation increase goes from 98% for one GFRP ply installed and becomes about 138% and 169% for two and three GFRP plies, respectively (see Table 4.2.1-1).

Since the design goal was to allow the structure withstanding a 0.3g PGA level and considering that theoretical analysis indicate that a 48% of structural deformation capacity increase was necessary to pursue such objective, it was estimated that an increase of the local rotation capacity of the plastic hinge at least twice that of the original member could have been necessary. It is noted, in fact, that the local increase of the rotation capacity is not proportional to the global deformation capacity enhancement; thus, based on such considerations, the first trial in the design of the GFRP confinement was chosen as two plies of laminates with density of 900 gr/m^2 applied to all the square columns and extended for a length greater than the effective plastic hinge length, about 380 mm, computed following expression (1) of Chapter III, given by the latest Italian seismic guideline, Ordinanza 3431 [2].

Furthermore, in order to validate such design choice, a non linear static pushover on the FRP retrofitted structure was provided at the end of the design process.

4.2.2 Design of shear strengthening: Beam column joints

In order to avoid that increasing the ductility of the columns could cause the attainment of shear strength of exterior joints, that is brittle and could be detrimental to the global performance, further FRP was designed on beam-column joints corresponding to the corner square columns C2, C5, C7 and C8. The original shear strength of the exterior joints was computed by using equations provided by Ordinanza 3431 [2].

Such seismic guideline, allows assessing the principal tensile stress of an exterior joint, σ_{nt} , by using the following expression:

$$\sigma_{nt} = \left| \frac{N}{2A_g} - \sqrt{\left(\frac{N}{2A_g}\right)^2 + \left(\frac{V_n}{A_g}\right)^2} \right| \leq 0.3\sqrt{f_c} \quad (2)$$

where N , is the axial force in the upper column, A_g , is the horizontal joint area, V_n , is the acting shear on the joint due to the contributions of both shear force on the upper column and tensile reinforcement on the beam, and finally f_c , is the compressive concrete strength.

By using such expression with first member equal to the second one, it was possible to compute, with reference to each exterior joint of the structure, the horizontal ultimate shear force and the corresponding shear strength, $v_{o,max}$, under which tensile joint failure is achieved. Theoretical results, in terms of original joint shear strength, $v_{o,max}$ with reference to the external joints, at each storey, along with the axial force due only to gravity loads, are summarized in Table 4.2.2-1.

Since theoretical simulations of the first round of tests predicted shear stresses on the exterior joints comparable with those reported in Table 4.2.2-1 (i.e. 1.87 MPa and 2.01 MPa versus 1.82 MPa and 2.44 MPa for exterior joint in correspondence of columns C8 and C2 at first floor, respectively), as confirmed by shear cracks observed on joints after the tests, it was decided to preserve the corners joints by installing FRP laminates.

The shear improvement provided by FRP laminates was assessed according to the approach proposed by Antonopoulos&Triantafillou [17] that, based on equilibrium considerations, allows following the possible states of the joint behavior up to failure. Once geometric, bond and material properties are given and the acting axial forces are evaluated, the equations provide the inclination of the principal tensile stress, θ , and the shear stress, ν , corresponding to any given state of joint strains. The failure of the FRP strengthened joint occurs when either concrete crushes (i.e., the principal compressive stress attains the crushing strength of concrete) or FRP fails (i.e., the ultimate stress is attained or debonding occurs). In order to take into account that increasing the joint strains, the inclination of principal tensile stresses, θ , change considerably, it was decided to upgrade the exterior joints by using quadriaxial laminates; according to the columns retrofit, glass fibers were chosen. As the Antonopoulos&Triantafillou [17] model was referred to uniaxial laminates, only fibers placed along the axial direction of columns and beams and those having a component on them were taken into account for calculations. With those assumptions the Antonopoulos&Triantafillou [17] model was used to compute the shear improvement due to external FRP reinforcement. The amount of the FRP needed on the joints was designed with reference to the weakest joint of the structure in correspondence of column C8 (i.e. the original shear strength was 1.82 MPa, 1.65 MPa and 1.62 MPa at first, second and third storey, respectively). The target design was to improve its shear strength up to a value of at least equal to 4.00 MPa, about 2.5 times more than the original shear strength at third storey. With reference to the joint in correspondence of column C8, at third storey (axial load $P=15650$ N), Figure 4.2.2-1 shows the relationship between the inclination of the principal tensile stress, θ , and the shear stress, ν , corresponding to any given state of joint strains for one ply of FRP reinforcement installed (continuous line) and its progress by adding one ply at time of GFRP quadriaxial laminates up to three plies (dashed line).

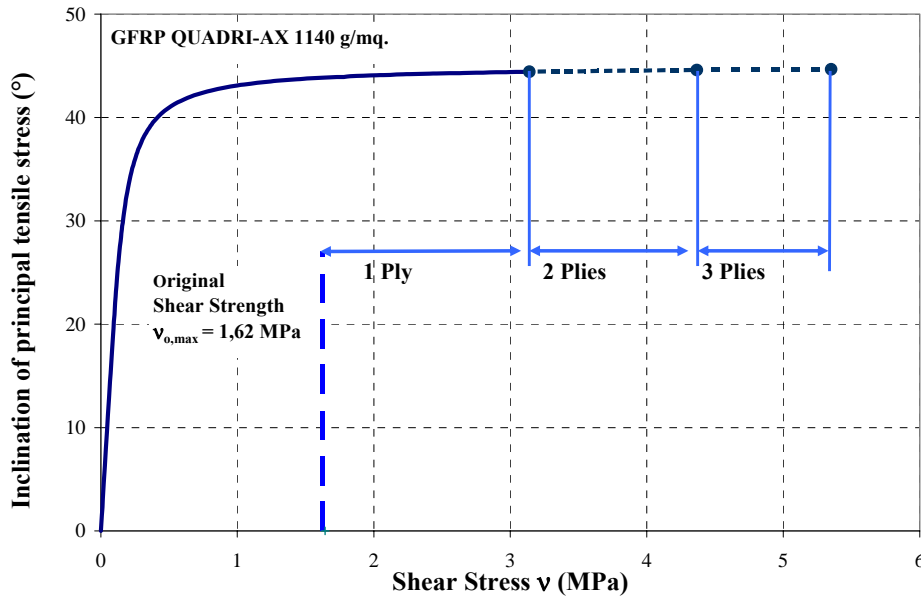


Figure 4.2.2-1– Principal tensile stress inclination – shear stress relationship for different amount of external GFRP reinforcement (corner joint C8- third storey).

It is noted that the theoretical failure mode was always concrete crushing, provided that proper anchorage would be ensured to prevent FRP debonding. The figure clearly shows that the amount of external FRP necessary to pursue the proposed target shear strength was corresponding at two plies of GFRP quadriaxial laminates with density of 1140 g/m². The results in terms of shear strength, v_{max} , with reference to each exterior joint, obtained by installing one, two and three plies of quadriaxial GFRP laminates having each a balanced density of 1140 gr/m², were computed and reported in the last three columns of Table 4.2.2-1. Table results confirm that, in every case, two plies of GFRP laminates are adequate to achieve shear strength at least equal to 4.00 MPa.

Floor	Exterior joint column	Axial Force, N (N)	Original Joint Shear strength $v_{0,max}$ (MPa)	GFRP Retrofitted joint shear strength v_{max} (Mpa)		
				1 ply	2 plies	3 plies
1 st storey	C5	59100	1.92	3.40	4.46	5.34
	C8	44280	1.82	3.26	4.48	5.47
	C2	154090	2.44	3.67	4.81	5.72
	C7	91520	2.11	3.53	4.72	5.43
2 nd storey	C5	28010	1.71	3.25	4.43	5.27
	C8	20060	1.65	3.16	4.39	5.37
	C2	72740	2.00	3.41	4.56	5.38
	C7	43360	1.81	3.39	4.52	5.44
3 rd storey	C5	23590	1.68	3.23	4.41	5.26
	C8	15650	1.62	3.14	4.37	5.35
	C2	68320	1.97	3.42	4.60	5.44
	C7	38940	1.78	3.37	4.50	5.42

Table 4.2.2-1 – Shear strength of the un-strengthened and GFRP retrofitted corners joints

4.2.3 Design of shear strengthening: wall type column, C6

Since rectangular column C6 has a sectional aspect ratio equal to 3, shear could have controlled its behavior rather than flexure. For this reason, shear FRP retrofit it was considered necessary. It was computed (by using CNR-DT 200 [16] provisions) that totally wrapping of rectangular column C6 for its entire length with two plies of the same quadri-axial GFRP laminates used for the above mentioned joints, was able to increase the sectional shear strength by a factor of about 50% (i.e. the shear strength goes from 196 kN taking into account the concrete and stirrups shear contribution only up to a value of 286 kN by considering the GFRP effect). It is noted that only fibers placed perpendicular to the longitudinal axis of the column and those having a component on that direction were taken into account for calculations; thus, the same expressions provided for uni-axial laminates shear strengthening were used in calculations.

4.2.4 Assessment of the Rehabilitated Structure

A non-linear static pushover analysis was performed with reference to the FRP confined structure in order to estimate the effectiveness of the proposed retrofit technique on the structural global behaviour. Assuming that the story masses remain constant after the FRP retrofit intervention, the modal displacements values in correspondence of each centre of mass in the X and Y directions along with the corresponding normalized lateral loads are the same of those referred to the 'as-built' structure (reported in Chapter III).

The FRP confinement was taken into account by modifying the inelastic flexural behaviour of the elements in correspondence of the member ends, where the lumped plasticity is assumed. The bilinear moment – rotation relationship used for each plastic hinge was, in fact, modified by considering the increase of the ultimate curvature ϕ_u (and the related increase of the ultimate rotation capacity) due to the FRP confinement.

In particular, it is noted that yielding curvature, ϕ_y and moment M_y , were not modified by the FRP confinement, while the ultimate curvature, ϕ_u , and ultimate moment, M_u , were determined in correspondence of the attainment of the increased ultimate strains in concrete, ϵ_{ccu} (determined from expression (1)) or in the steel reinforcement, assumed equal to 40‰ as in the 'as-built' structure.

Plastic hinge length, yielding and ultimate rotation were computed by using expressions (1), (2), (3) and (4) of Chapter III; the knowledge level was again assumed equal to 3, KL3, with a corresponding confidence factor, CF, equal to 1. The three limit states, LSDL, LSSD and LSNC, with particular attention to the first two were investigated for the assessment of the structural capacity at both 0.20g and 0.30g PGA level in the PX - NX and PY - NY directions, respectively. The pushover curves on the FRP retrofitted structure for each analysed direction are reported in Figure 4.2.4-1.

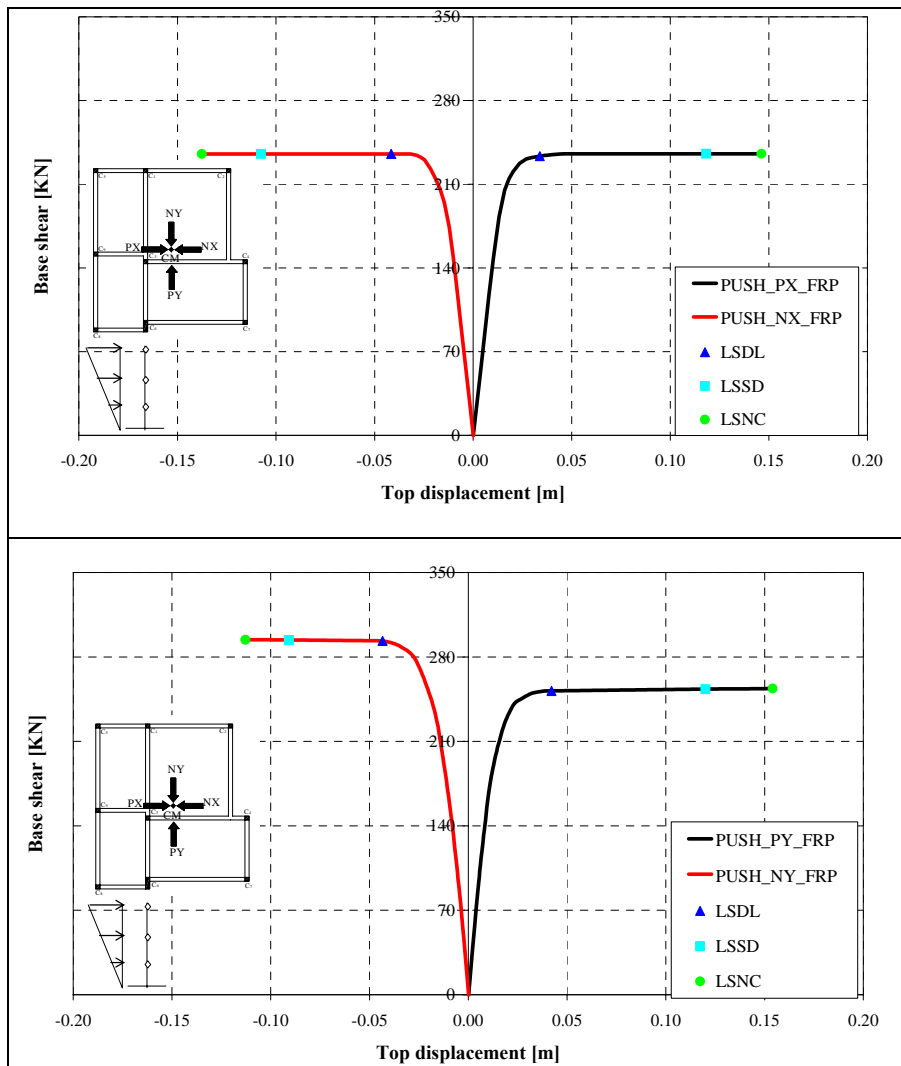


Figure 4.2.4-1- Pushover curves for the assessment of the FRP retrofitted structure

The capacity theoretical results of the rehabilitated structure in terms of maximum base shear, F_{max} top displacement, d_{max} , and absolute inter-storey drift, ξ , are summarized on the right-hand side of Table 4.2.4-1 and Table 4.2.4-2 for the LSDL and LSSD. The seismic demand was computed with reference to the same design spectra analysed in the ‘as-built’ configuration scaled at 0.20g and 0.30g PGA level. The results in terms of maximum top displacement required for each investigated PGA level and direction at LSDL and LSSD are summarized in Table 4.2.4-1 and Table 4.2.4-2. On the left-side of such table, the theoretical results in terms of both capacity and demand related to the ‘as-built’ structure are also recalled. The comparison between the seismic demand and capacity for the retrofitted structure is also reported in a graphical form in Figure 4.2.4-2.

Push Direction	Limit State	Level	'AS BUILT' STRUCTURE					FRP RETROFITTED STRUCTURE				
			CAPACITY			DEMAND		CAPACITY			DEMAND	
			F_{max}	d_{max}	$\xi=I-D/h$	d_{max}	d_{max}	F_{max}	d_{max}	$\xi=I-D/h$	d_{max}	d_{max}
			[KN]	[m]	[-]	[m]	[m]	[KN]	[m]	[-]	[m]	[m]
PX	LSDL	1	231	0,0355	0,004	0,0248	0,0372*	233	0,0338	0,004	0,0248	0,0372*
		2			0,006					0,006		
		3			0,001					0,001		
NX	LSDL	1	232	0,0406	-0,003	0,0247	0,0371	235	0,0416	-0,004	0,0247	0,0371
		2			-0,009					-0,009		
		3			-0,001					-0,001		
PY	LSDL	1	250	0,0409	0,004	0,0240	0,0360	252	0,0421	0,004	0,0240	0,0360
		2			0,005					0,005		
		3			0,005					0,005		
NY	LSDL	1	291	0,0412	-0,005	0,0240	0,0361	293	0,0434	-0,005	0,0240	0,0361
		2			-0,005					-0,006		
		3			-0,004					-0,004		

(*Demand displacements not satisfied by the structure)

Table 4.2.4-1– Summary of the results in terms of capacity and demand for the ‘as-built’ and the FRP retrofitted structure at LSDL

Push Direction	Limit State	Level	'AS BUILT' STRUCTURE					FRP RETROFITTED STRUCTURE				
			CAPACITY			DEMAND		CAPACITY			DEMAND	
			F_{max}	d_{max}	$\xi=I-D/h$	d_{max}	d_{max}	F_{max}	d_{max}	$\xi=I-D/h$	d_{max}	d_{max}
			[KN]	[m]	[-]	[m]	[m]	[KN]	[m]	[-]	[m]	[m]
PX	LSSD	1	232	0,0690	0,005	0,0623	0,0934*	235	0,1182	0,006	0,0626	0,0939
		2			0,017					0,032		
		3			0,001					0,001		
NX	LSSD	1	232	0,0626	-0,003	0,0618	0,0927*	235	0,1076	-0,004	0,0618	0,0927
		2			-0,016					-0,031		
		3			-0,001					-0,001		
PY	LSSD	1	251	0,0962	0,010	0,0607	0,0910	253	0,1201	0,013	0,0610	0,0917
		2			0,011					0,014		
		3			0,011					0,014		
NY	LSSD	1	292	0,0740	-0,010	0,0603	0,0904	294	0,0908	-0,013	0,0604	0,0906
		2			-0,011					-0,014		
		3			-0,004					-0,004		

(*Demand displacements not satisfied by the structure)

Table 4.2.4-2– Summary of the results in terms of capacity and demand for the ‘as-built’ and the FRP retrofitted structure at LSSD

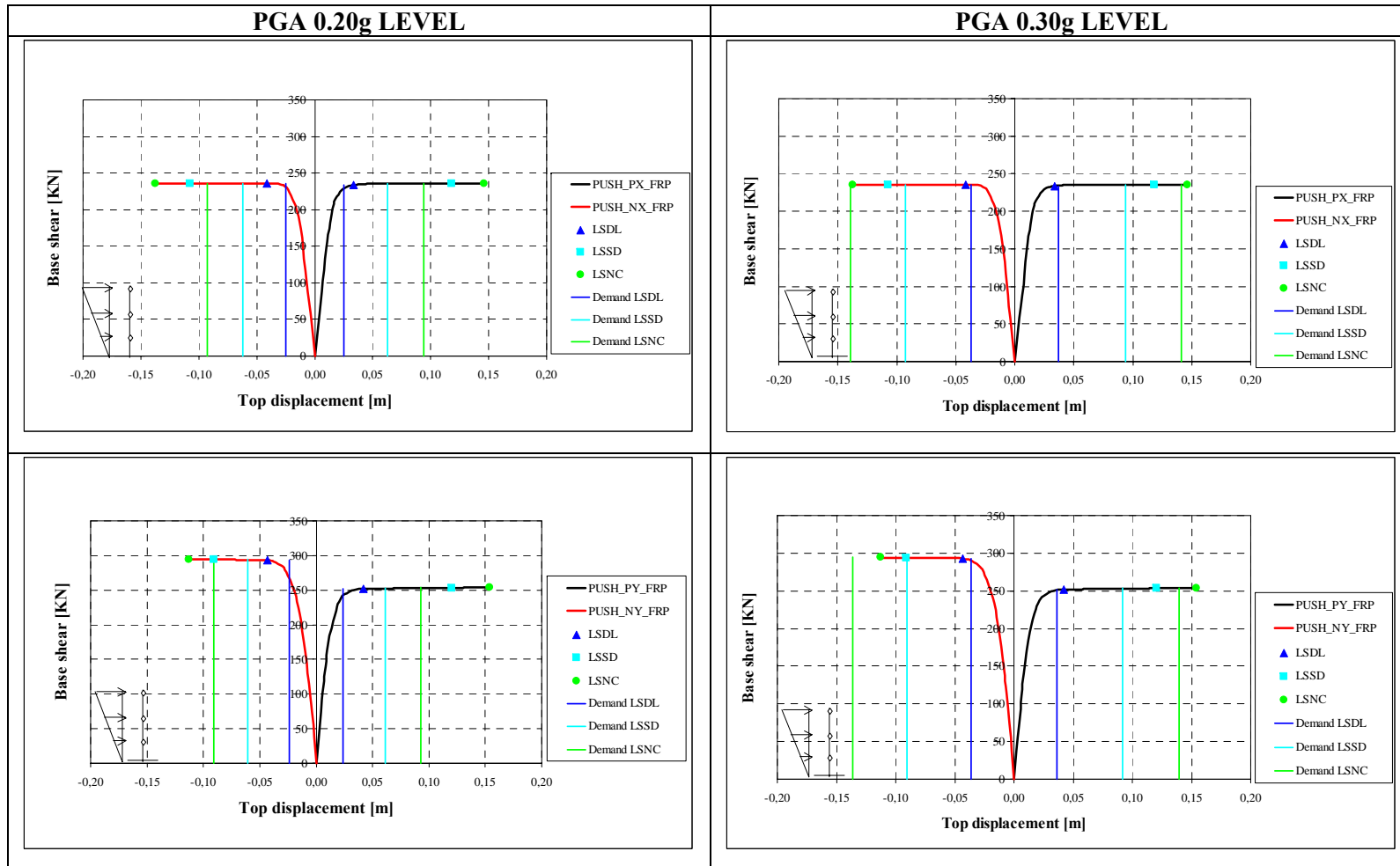


Figure 4.2.4-2 - FRP retrofitted structure, Demand vs. capacity comparison for PGA level equal to 0.20g and 0.30g at LSDL, LSSD and LSNC.

Such tables and figures show that the FRP retrofitted structure is able to satisfy the LSSD in each direction with reference to both 0.20g and 0.30g PGA level; in particular it is underlined that the verification is satisfied also in the NX direction where the maximum gap in terms of displacement demand was recorded for the ‘as-built’ structure. The capacity is, in fact, increased up to a value of 0.1076 m (0.0626 m in the ‘as-built structure’) while the demand at the target seismic level intensity, 0.30g, is equal to 0.0927 m. The visualization of such result is reported in Figure 4.2.4-3 where the seismic demand and structural capacity of the FRP retrofitted structure, for the two levels of ground motion analysed, is determined in the NX direction by using the capacity spectrum approach, CSA.

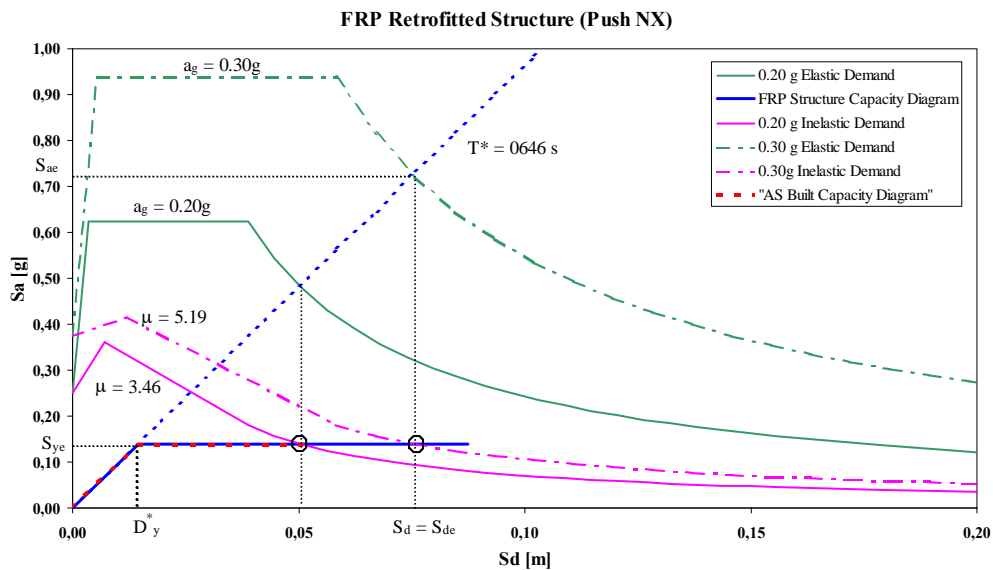


Figure 4.2.4-3– FRP retrofitted structure elastic and inelastic demand spectra vs. capacity diagram

It is noted, however, that in the case of the retrofitted structure at the 0.30g PGA level, the most critical verification is in the NY direction for which the capacity displacement is 0.0908 m whereas the demand is equal to 0.0906 m. In order to show the increase in terms of ductility provided by the FRP confinement in each direction, the LSSD verification at 0.30g PGA by using the CSA is reported in Figure 4.2.4-4; in the left side-hand the ‘as-built’ structure is analysed while on the right side-hand the theoretical prediction related to the FRP retrofitted structure are plotted. The figure clearly shows that the column confinement provide the structure with a

significant extra ductility allowing it to sustain the demand by only playing on the plastic branch of the base shear - top displacement curve.

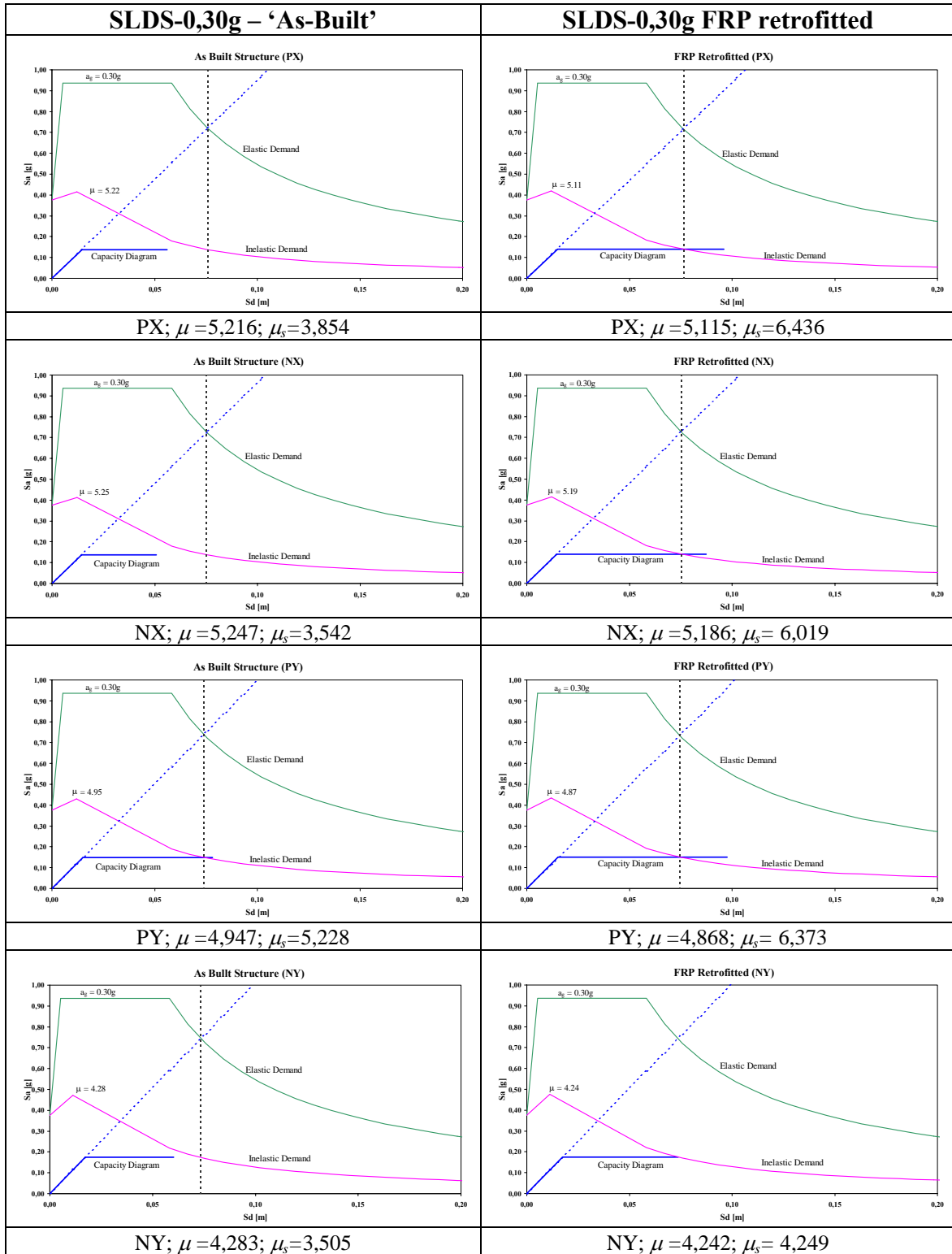


Figure 4.2.4-4– Theoretical seismic performance comparison at 0.3g PGA between ‘as-built’ and FRP retrofitted structure.

Finally, it is important to note that although the retrofit intervention provides the structure with the necessary ductility to sustain the 0.30g PGA seismic actions at the LSSD, it is not effective with reference to the damage limit state (i.e. the LSDL verification in the PX direction is again not satisfied also in the retrofitted configuration). Such effect is obviously due to the fact that the intervention does not modify the structural mass and stiffness and thus both capacity and seismic demand are the same of that computed in the case of the 'as-built' structure.

4.3 FRP INSTALLATION PROCEDURE

Once testing of the ‘as-built’ structure and the design of the FRP retrofit was completed, prior to laminates installation, unsound concrete was removed in all zones of the elements where crushing was detected; then the original cross-sections were restored using a non-shrinking mortar. In addition, all cracks caused by the first round of test were epoxy-injected (see Figure 4.3-1).



Figure 4.3-1 – Original cross section restoration (a) and injection of cracks

After that, the designed amount of GFRP laminates on columns ends, corner joints and the wall-type column C6 were installed.

- ***Columns end confinement***

According to the design of the retrofit above illustrated, the eight square columns were all confined at the top and bottom using 2 plies of GFRP uniaxial laminates having each a density of 900 gr/m^2 . At each storey, the GFRP confinement was extended for 800 mm (with 30 mm of overlapping) from the beam-column interface; in some cases, where more larger cracks were detected during the previous rounds of tests, such length was increased up to 1000 mm in order to account for the more extended concrete damage, Balsamo et. al. [18] (see Figure 4.3-2).

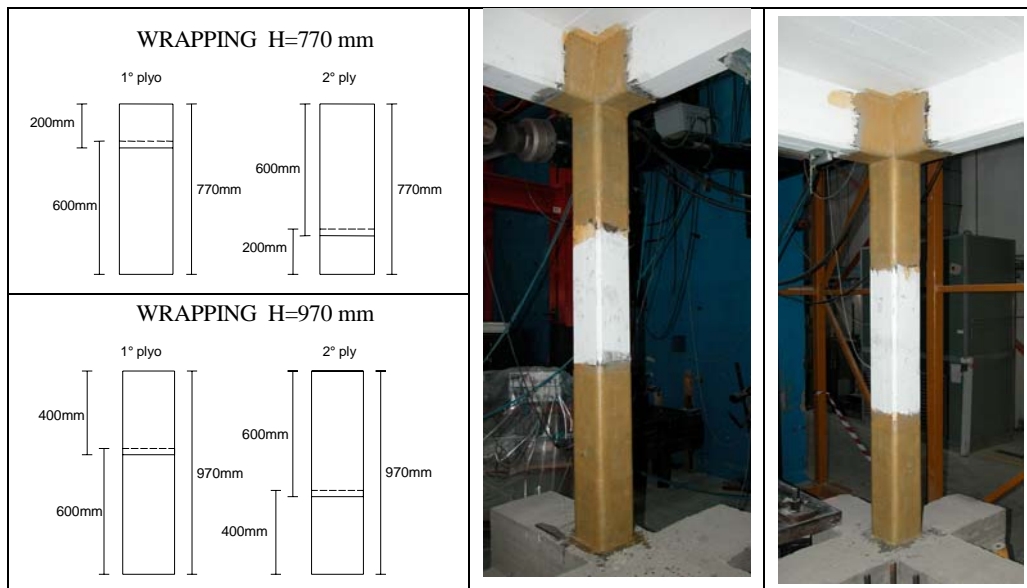


Figure 4.3-2 – Columns confinement (1000 mm left-hand side, 800 mm right-hand side)

- ***Beam-column corner joints***

Beam-column joints corresponding to the corner square columns (C2, C5, C7 and C8) were strengthened using 2 plies of quadriaxial GFRP laminates having each a balanced density of 1140 gr/m^2 . Such joint reinforcement was extended on the beams by 200 mm on each side in order to U-wrap it and to ensure a proper bond. The joint strength intervention scheme along with the joint internal and external view after the retrofit is presented in Figure 4.3-3. The external reinforcement on the joints was not connected to the columns. In fact the continuity of external reinforcement can vary the strength hierarchy of the connection and reduce the contribution of fixed end rotation to the rotation capacity of column. Therefore the plastic hinge length of rehabilitated columns was assumed comparable with those of the ‘as-built’ structure.

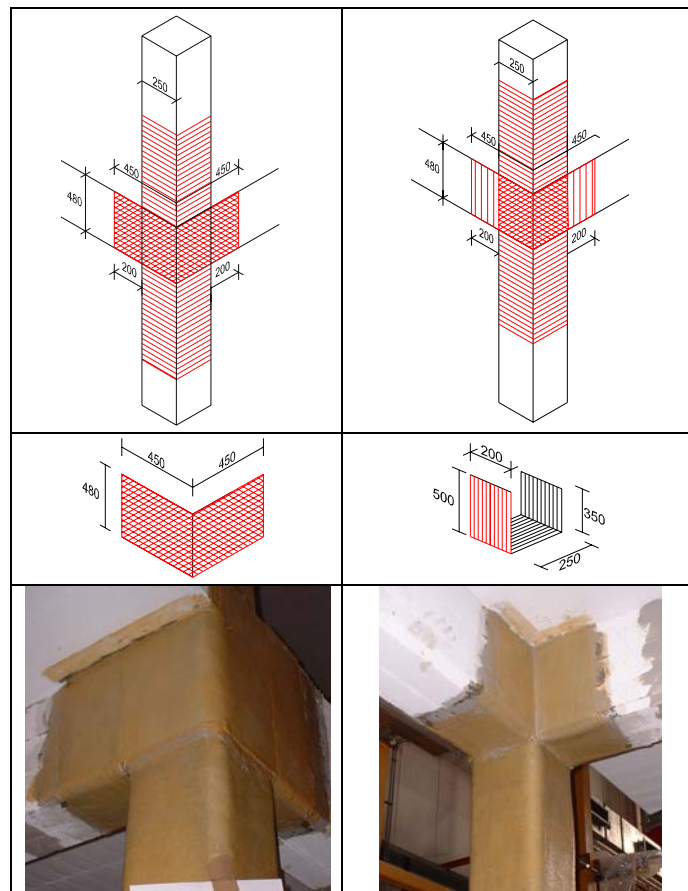


Figure 4.3-3 – Shear strength of exterior joints

- **Wall-type column C6**

Finally, column C6 was wrapped for its entire height by using two plies of the same quadriaxial laminates used for the retrofit of the corner joints. The shear strength scheme of column C6 and an overview of the whole structure after the retrofit intervention are presented in Figure 4.3-4.

As concerns the joints in correspondence of such wall-type column, both outer and inner parts of the joint were strengthened by quadriaxial GFRP reinforcement; for the outer part, the joint reinforcement had the height of the beam and was extended for 200 mm on the adjacent members, while for the inner part, even though the presence of the slab determined an height of the external reinforcement equal to 350 mm, the extension of adjacent beams and the U-wrap were equal to those of the outer part (see Figure 4.3-5).

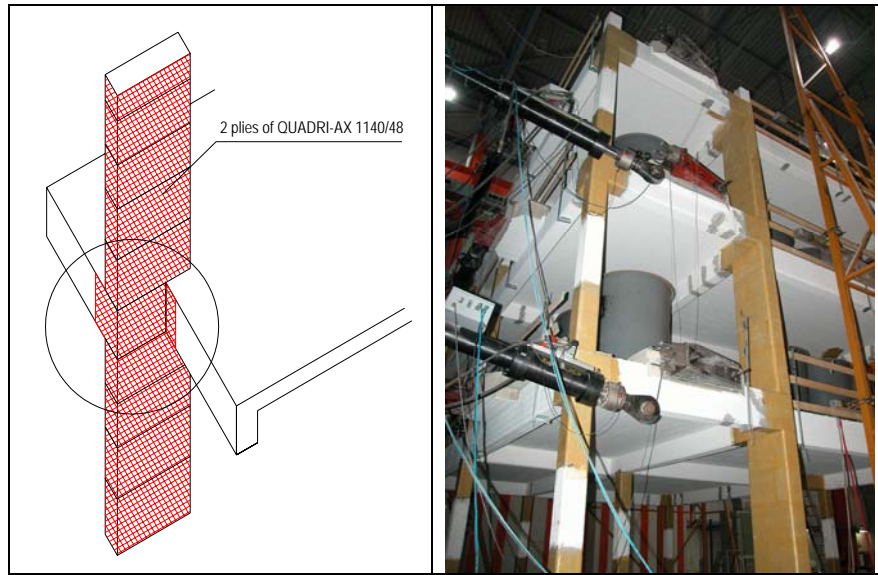


Figure 4.3-4 – Shear strength of wall-type column C6 and retrofitted structure overview

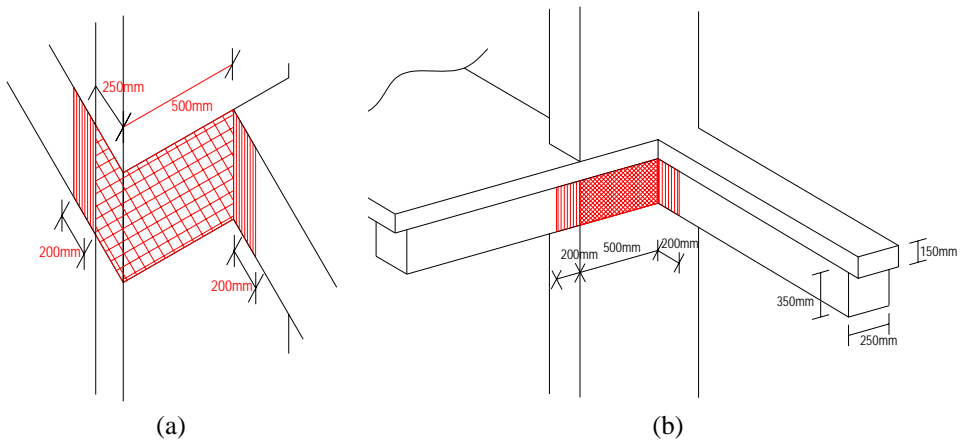


Figure 4.3-5 – Outer (a) and inner (b) portion of joint of column C6

4.4 EXPERIMENTAL BEHAVIOUR OF THE FRP RETROFITTED STRUCTURE

Once FRP-retrofitted, the structure was first tested under the same input ground motion of the ‘as-built’ structure, with a PGA level of 0.20g, to have a direct comparison with the previously executed experiment on the ‘as-built’ structure, then with a PGA level of 0.30g.

4.4.1 FRP retrofitted structure: PGA=0.20g

Global Behaviour

During the test at 0,20g PGA level, the retrofitted structure showed a global behaviour very similar to the ‘as-built’ structure but the damage level recorded, by the inspection after the test, was very limited. In particular, new cracks were not recorded on the columns ends and the laminates applied remained substantially undamaged. The only visible effect was the presence of some local defects in correspondence of the laminates used to confine the column ends (see Figure 4.4.1-1).

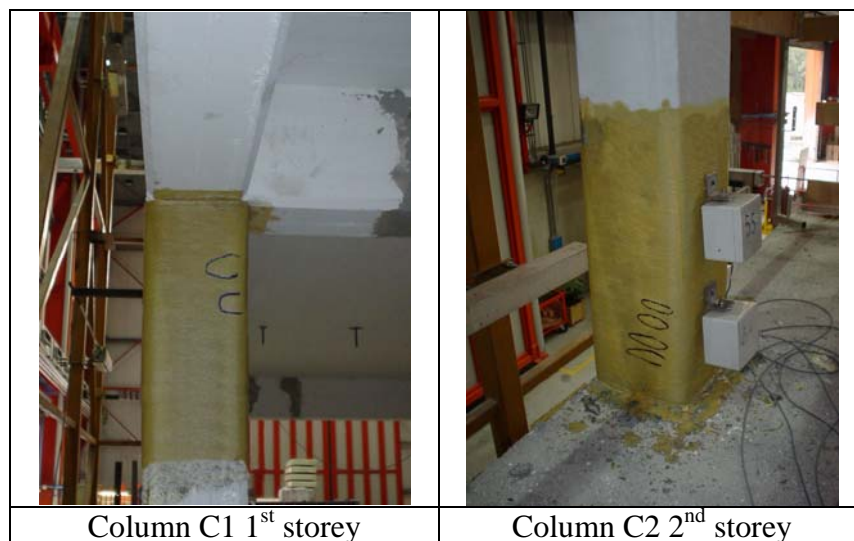


Figure 4.4.1-1 – Defects recorded after the test

No other damages were found neither on the joints panel or on the wall-type column C6. Thus, no visible cracks or damages at all were recorded.

In Figure 4.4.1-2, the base shear-top displacement curves related to such test for the X and Y direction are presented.

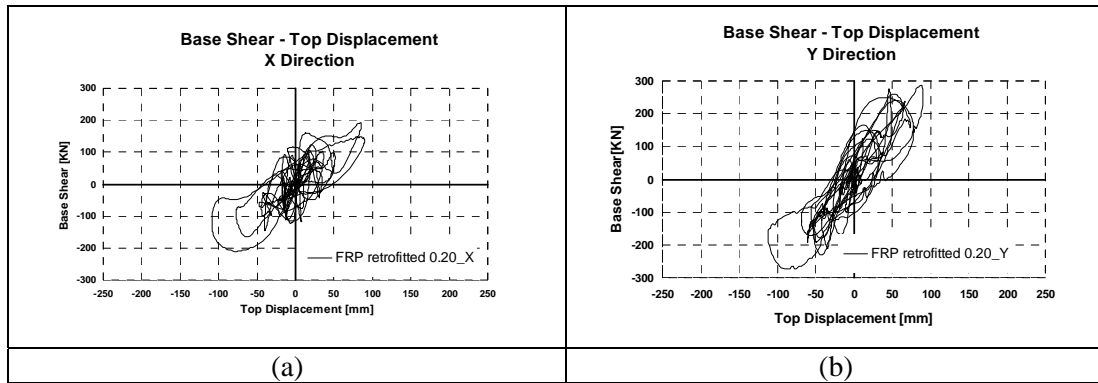


Figure 4.4.1-2– FRP retrofitted structure, 0.20g: Base Shear-Top Displacement hysteresis loops; (a) X direction, (b) Y direction.

By assessing the average slope of the two curves it is clear that the structure was again stiffer in the Y direction than in the X one as the FRP retrofit did not modify significantly the stiffness of the entire structure. Hence, the maximum base shear reached along the Y direction, 287 kN, was larger than that reached in the X direction, 211 kN. It is underlined, however, that the maximum top displacement was recorded in the stiffer direction as the top displacement in the Y direction was equal to 112.5 mm against the 108.8 mm recorded in the X direction; such result was in contrast with the outcomes provided by the two tests on the ‘as-built’ structure. As for the energy dissipation, by totaling up the areas under the hysteretic cycles of the base shear-top displacement relationships of the two reported curves, it is possible to point out only a slight difference with reference to the ‘as-built’ structure; in particular the maximum dissipation was recorded with reference to the Y direction, 68.66 kJ, equal to 62% of the total absorbed energy.

The torsional behaviour of the structure is represented in Figure 4.4.1-3 in which the base-torsion vs. top rotation is reported; the diagram shows that the maximum base torsion achieved during the test was equal to 1087 kNm and the maximum top rotation was equal to 25,18 mrad, that are close to the values recorded on the original structure (963 kNm and 19,91 mrad, respectively).

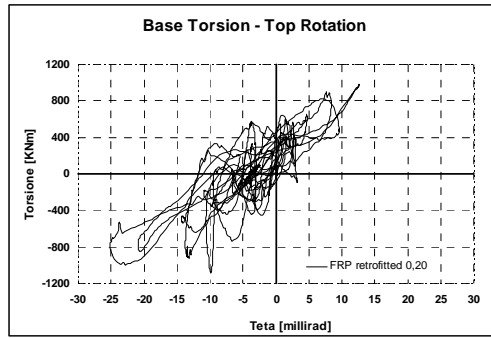


Figure 4.4.1-3 - Base Torsion-Top Rotation

A summary of the main experimental results recorded in such test are reported in Table 4.4.1-1 and Table 4.4.1-2; the first table clearly shows that the maximum inter-storey displacements were again reached at the second floor.

DIRECTION	Total Absorbed Energy	Max Base Shear	Max Top Displ.	Level	Max I-S Shear	Max I-S Displ.
	[KJ]	[KN]	[mM]		[kN]	[mm]
X	42.2	PX: 211	PX: 108.8	1	211	32.0
				2	164	55.4
		NX: 193	NX: 89.5	3	116	34.3
Y	68.66	PY: 273	PY: 112.4	1	287	39.7
				2	260	47.6
		NY: 287	NY: 90.5	3	173	31.1

Table 4.4.1-1 – FRP retrofitted structure: experimental outcomes at 0,20g level.

	Max Base Torsion	Max Base Rotation	Level	Max I-S Torque	Max I-S Rotation
	[kNm]	[millirad]		[kNm]	[millirad]
TETA	Positive: 985	Positive: 12.65	1	1087	7.1
			2	827	12.1
	Negative: -1087	Negative: -25.18	3	726	7.8

Table 4.4.1-2 - FRP retrofitted structure: experimental outcomes at 0,20g level

Local Behaviour

With reference to the same inclinometers used during the tests on the ‘as-built’ structure, the base shear-Y axis rotation curves are reported in Figure 4.4.1-4. Such figure shows that both inclinometers #1 and #2, recorded significant values of rotations in correspondence of an almost constant value of the base shear, indicating that plastic deformations were achieved. The similar trend of the two curves highlights that the plasticization propagated along the entire lap splice length. The maximum rotations were equal to $4.02 \mu\text{rad}$ and $4.17 \mu\text{rad}$, for inclinometer #1 and #2, respectively. Such values were very close to that ones observed during the test on the ‘as built’ configuration at the same PGA level; thus, since the two curves of Figure 4.4.1-4 also show the same pattern of those recorded on the ‘as built’ structure, it is possible to underline that the FRP retrofit has not modified the structural hierarchy of strength as the plastic hinges were not relocated.

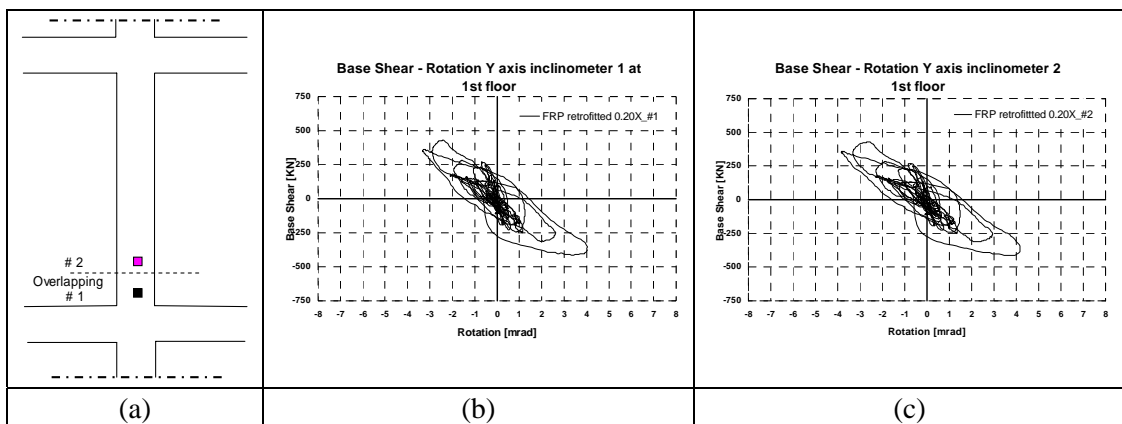


Figure 4.4.1-4– FRP retrofitted at 0,20g level local hysteresis loops for column C3: (a) Inclinometers positions, (b) Base Shear-Rotation Y axis inclinometer #1, (c) Base Shear-Rotation Y axis inclinometer #2.

4.4.2 FRP retrofitted structure: PGA=0.30g

Global Behaviour

At this stage, another test at PGA level of 0.30g was performed in order to examine the validity of the designed GFRP retrofit. After the test, only light damages were founded on the retrofitted structure mainly localized on the unstrengthened joints (see Figure 4.4.2-1). On these ones an incoming failure of beams, due to crushing of concrete, and the initiation of a shear crack pattern were observed.

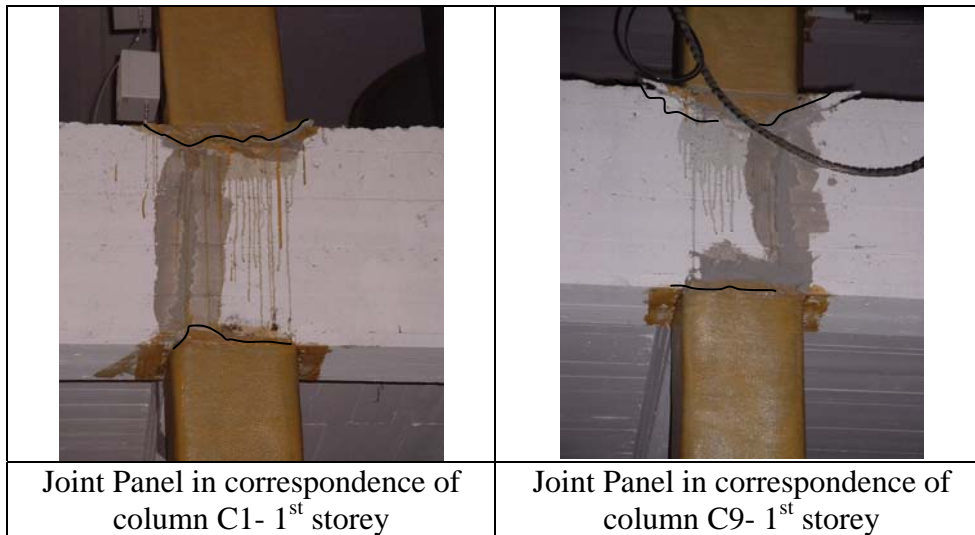


Figure 4.4.2-1 –Cracks on the unstrengthened joint panels

In Figure 4.4.1-2, the base shear-top displacement curves related to such test for the X and Y direction are presented.

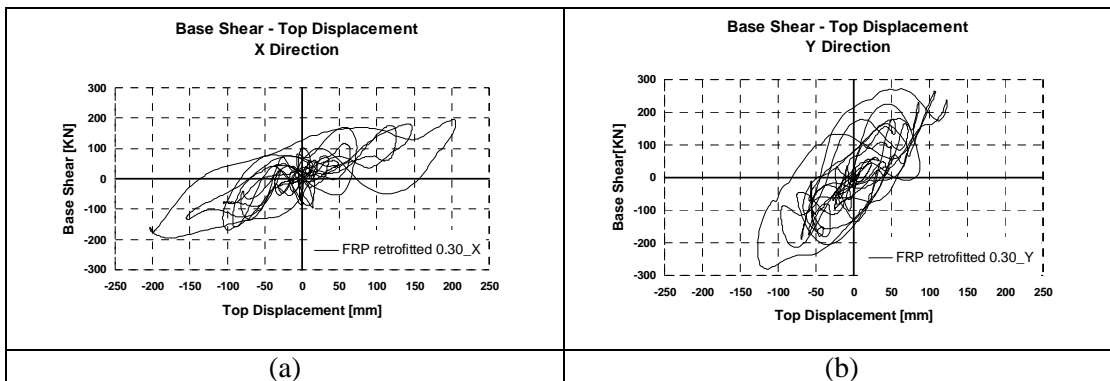


Figure 4.4.2-2 - FRP retrofitted at 0,30g level: Base Shear-Top Displacement hysteresis loops; (a) X direction, (b) Y direction.

The same trend of the previous tests was observed in terms of stiffness and thus the maximum base shear was reached along the Y direction, 281 kN, rather than in the X direction, 196 kN. With reference to the maximum top displacement, a very significant value of displacement was recorded in the X direction where a maximum value of 205.3 mm was achieved; such value was in percentage 62% higher than that achieved along the Y direction, equal to 126.6 mm. The width of the base shear-top displacement hysteretic cycles showed that high values of energy dissipation in both directions were recorded: 83.36 kJ and 104.38 kJ in the X and Y direction, respectively.

The torsional behaviour of the structure is represented in Figure 4.4.2-3 in which the base-torsion vs. top rotation is reported; the diagram shows that the maximum base torsion and the maximum top rotation achieved were equal to 1017 kNm and 26.72 mrad, respectively.

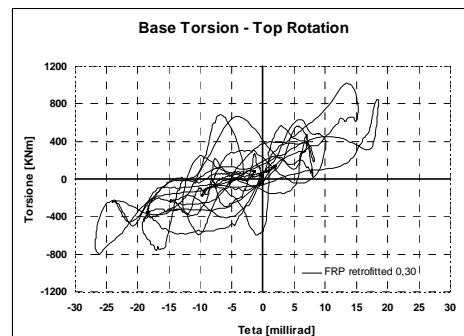


Figure 4.4.2-3 - Base Torsion-Top Rotation

Finally, with reference to the behavior of each storey of the structure, in Figure 4.4.2-4 the interstorey shears are plotted against the interstorey drifts. From the analysis of such curves, it can be noted that the maximum interstorey drifts were achieved at the second storey as observed in the 'as-built' structure. The maximum interstorey drifts at the second storey were equal to 106.0 mm in the X direction and 55.9 mm in the Y one, with an increment of 78% and 32% with respect to the drifts recorded at the first storey along the two analysed direction. The comparison of the interstorey drifts of the second storey with those achieved at the third one shows a percentage increment of 67% and 9%, for X and Y direction, respectively; such results highlight that, especially in the Y direction, the third storey was more involved into the global structural mechanisms than during the test on the original

structure. Moreover, the width of the hysteretic cycles presented in Figure 4.4.2-4 clearly confirms that the seismic actions were mainly adsorbed by the second storey.

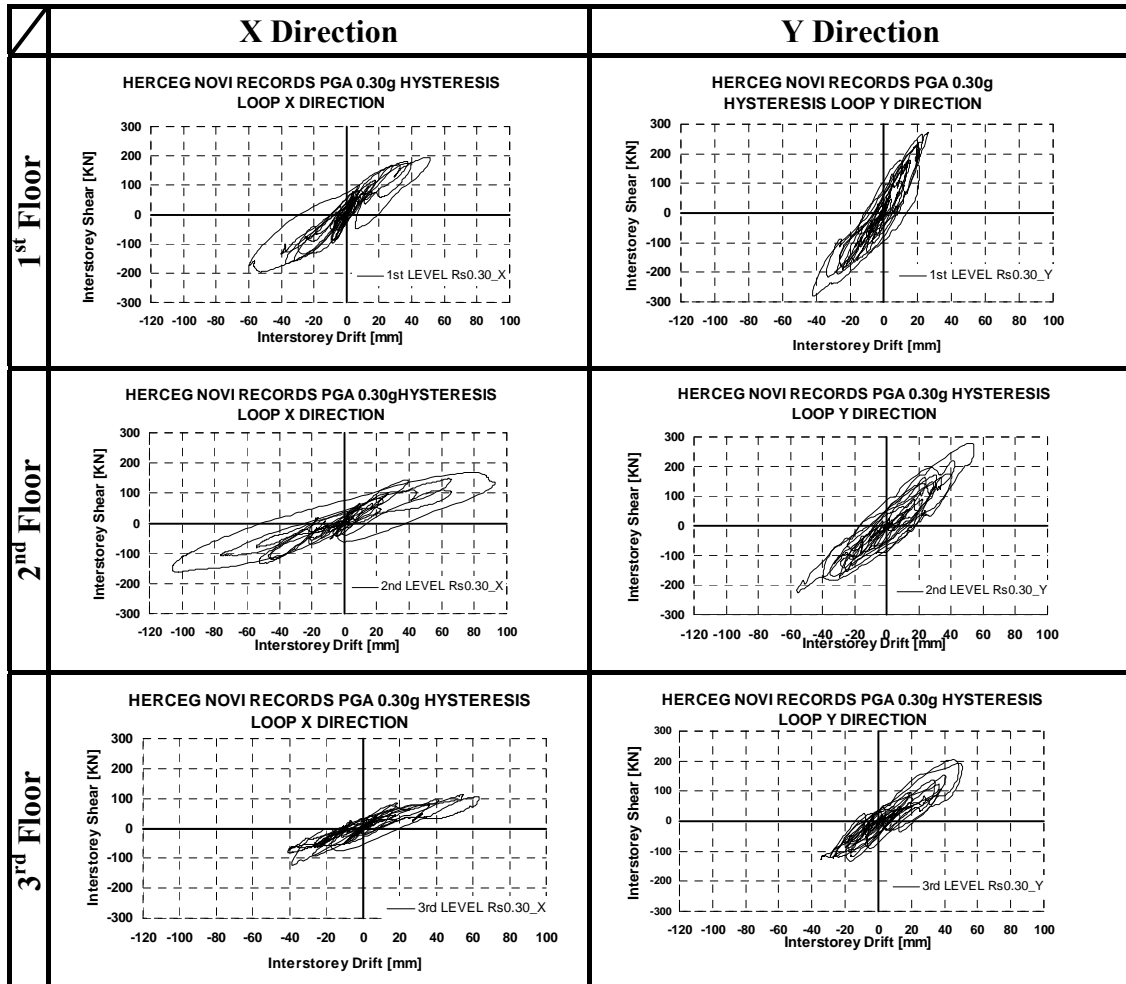


Figure 4.4.2-4 – FRP retrofitted structure at 0,30g level: Interstorey Shear –Interstorey Drift hysteresis loops

The same trend was observed by plotting the curves related to the interstorey torque vs. the interstorey rotation (see Figure 4.4.2-5); the second floor was again the most involved in the torsional behaviour of the structure with an increment of 69% and of about 80% with respect to the first and third storey, respectively.

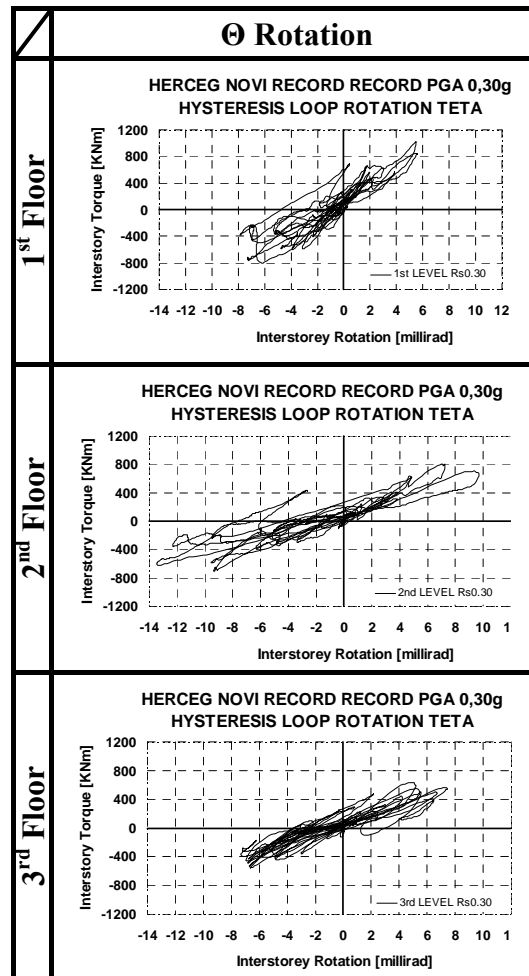


Figure 4.4.2-5 - FRP retrofitted structure at 0,30g level: Interstorey Torque – Rotation hysteresis loops

As FRP does not change the structural mass and stiffness, the effect of the plan irregularity was again significant and caused the presence of large rotations once the structure was subjected to bidirectional seismic actions; in order to investigate on the extent of such torsional effects, the absolute interstorey drifts of each column of the structure have been compared with those of its centre of the mass. As the previous diagrams have highlighted that in each case the second storey showed the maximum interstorey drifts, the comparison is reported only for such storey. In order to have a global idea of the torsional effects on the entire structure the diagrams have been arranged so that the column disposition in plan is represented (see Figure 4.4.2-6)

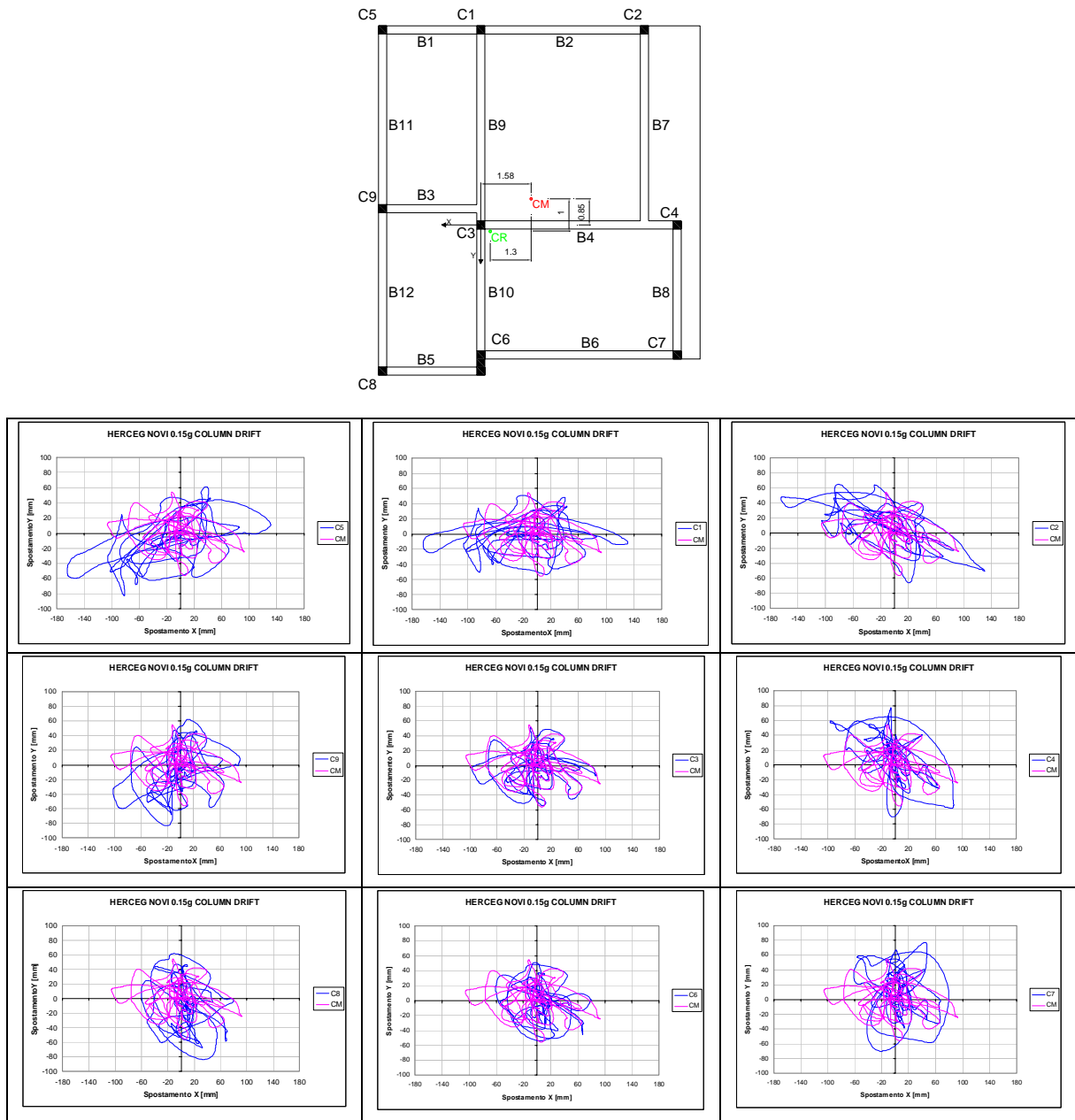


Figure 4.4.2-6 - Column Drifts compared to CM drifts in X and Y direction at second storey.

The diagrams point out that, increasing the seismic actions, the recorded columns drifts were very different by those of the centre of mass confirming a very pronounced torsional behaviour of the whole structure.

A summary of the main experimental results recorded during such test are reported in Table 4.4.2-1 and Table 4.4.2-2.

DIRECTION	Total Absorbed Energy	Max Base Shear	Max Top Displ.	Level	Max I-S Shear	Max I-S Displ.
	[KJ]	[KN]	[mM]		[kN]	[mm]
X	83.36	PX: 196	PX: 203.6	1	197	59.4
		NX: 197	NX: 205.3	2	168	106.0
				3	123	63.5
Y	104.38	PY: 281	PY: 126.6	1	281	42.3
		NY: 273	NY: 123.3	2	279	55.9
				3	104	50.7

Table 4.4.2-1 – FRP retrofitted structure: experimental outcomes at 0,30g level

	Max Base Torsion	Max Base Rotation	Level	Max I-S Torque	Max I-S Rotation
	[KNm]	[millirad]		[kNm]	[millirad]
TETA	Positive: 1017	Positive: 18.54	1	1017	7.8
	Negative: -800	Negative: -26.72	2	805	13.4
			3	631	7.4

Table 4.4.2-2 - FRP retrofitted structure: experimental outcomes at 0,30g level

Local Behaviour

The base shear-Y axis rotation curves, with reference to the inclinometers #1 and #2, are reported in Figure 4.4.2-7. By increasing the seismic action up to a PGA level equal to 0.30g, it was observed that the complete plasticization of the column end was achieved, with rotation values much higher than those recorded during the previous tests. In particular, both curves recorded a very similar trend with maximum values of rotations equal to 7.51 μ rad and 7.71 μ rad for inclinometers #1 and #2, respectively. By comparing the maximum rotation value achieved in the retrofitted configuration with that recorded on the ‘as-built’ configuration, an increment of 81% was founded; such result confirms the effectiveness of the column end confinement in providing a significant extra ductility to the member.

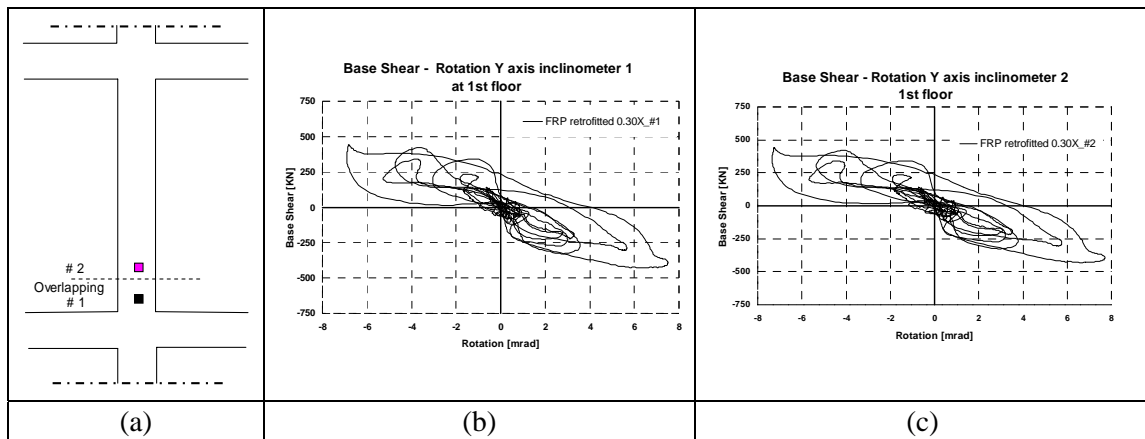


Figure 4.4.2-7 - FRP retrofitted at 0,30g level local hysteresis loops for column C3: (a) Incliner positions, (b) Base Shear-Rotation Y axis inclinometer #1, (c) Base Shear-Rotation Y axis inclinometer #2.

4.4.3 Theoretical vs. experimental results

A comparison between the experimental results and the theoretical prediction is performed in this section; however, it is noted that the performed nonlinear static pushover analysis implemented on the structure lumped plasticity model has not been developed as a direct comparison tool with the experimental results but in the way of an effective rehabilitation design methodology supported by a qualitative experimental feed-back.

The experimental behaviour of the rehabilitated structure was very close to that expected according to the rehabilitation design: 1) columns showed a very ductile behaviour; 2) no brittle mechanisms occurred (i.e., shear failure or significant damage of joints). The accuracy of the model is confirmed, in terms of global behaviour of the structure, by plotting the theoretical (at LSSD) vs. experimental envelop of inter-storey drifts (see Figure 4.4.3-1)

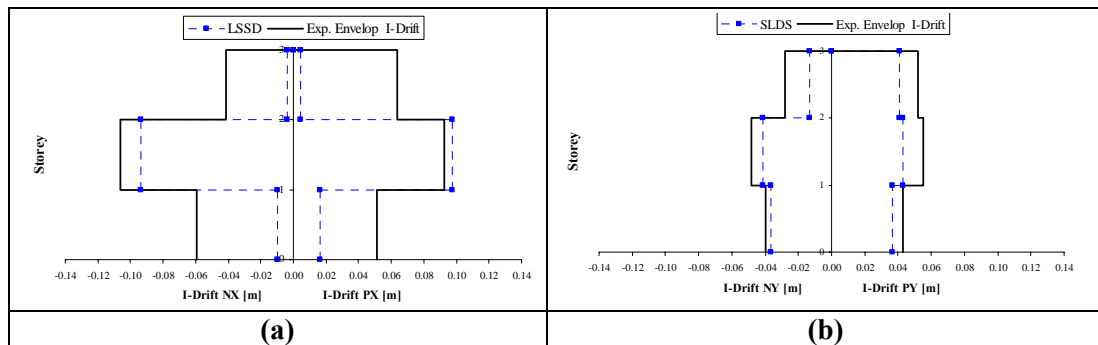


Figure 4.4.3-1 – Theoretical vs. experimental envelop inter-storey drift FRP retrofitted structure at PGA level 0.30g in the X direction (a) and Y direction (b)

As for the ‘as-built’ structure, recalling that the experimental inter-storey drifts are reported in terms of envelope and thus were not reached at the same time, the figure highlights a good agreement between the predicted inter-storey drifts and the experimental ones, especially for the second storey.

4.5 ‘AS BUILT’ vs. FRP RETROFITTED: COMPARISON OF THE EXPERIMENTAL RESULTS

The experimental activity highlighted that the retrofitting intervention provided the structure with a very significant supply of extra ductility with respect to the ‘as built’ configuration, which was almost totally lacking the appropriate capacity to resist even the 0.20g PGA level of excitation. Such result is clearly pointed out in Figure 4.5-1 where the base shear-top displacement curves (for the X and Y direction) are presented for the FRP retrofitted structure at 0.30g PGA level and compared with those recorded in the test performed on the ‘as-built’ structure (0.20g).

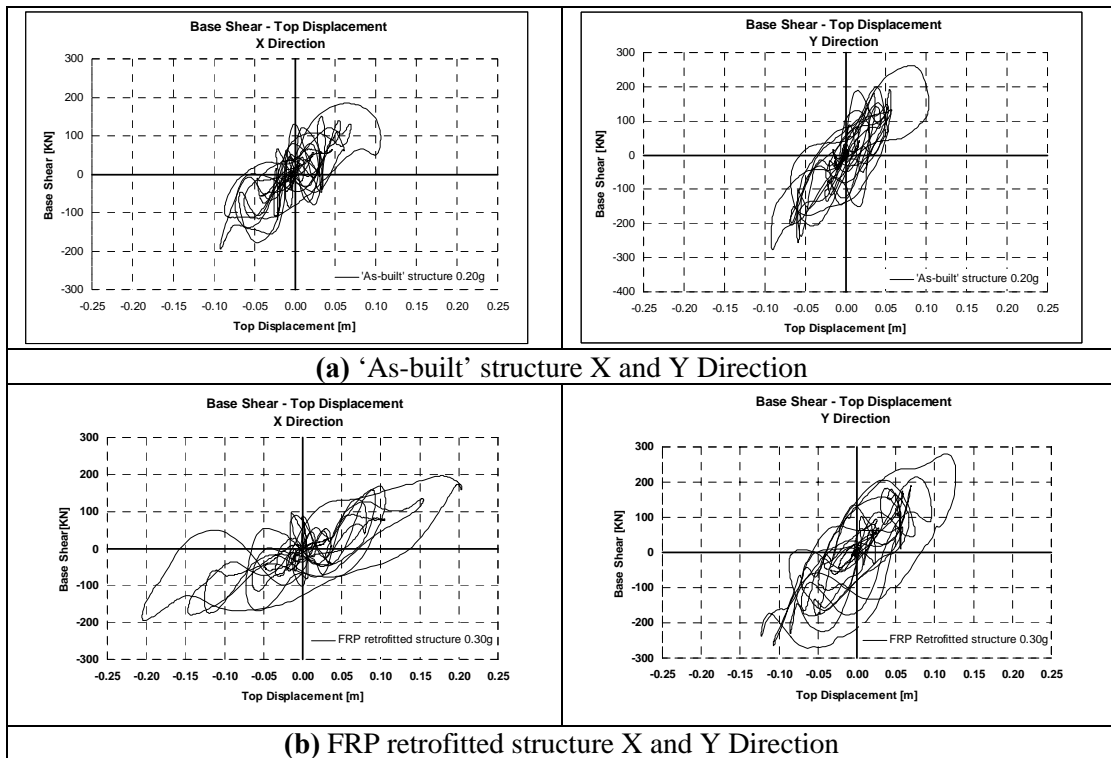


Figure 4.5-1 – Experimental Base-Shear Top-Displacement curves for the ‘as-built’ structure at PGA level 0.20g (a); and for the FRP retrofitted at PGA level 0.30g (b)

The retrofitted structure was able, after the vertical elements and the joints were wrapped with glass fibers, to withstand the higher (0.30g PGA) level of excitation without exhibiting relevant damage; after tests, in fact, FRP was removed and it was showed that the RC core was neither cracked nor damaged. A comparison of the

columns damage state after tests on both ‘as-built’ and FRP retrofitted structure is reported in Figure 4.5-2

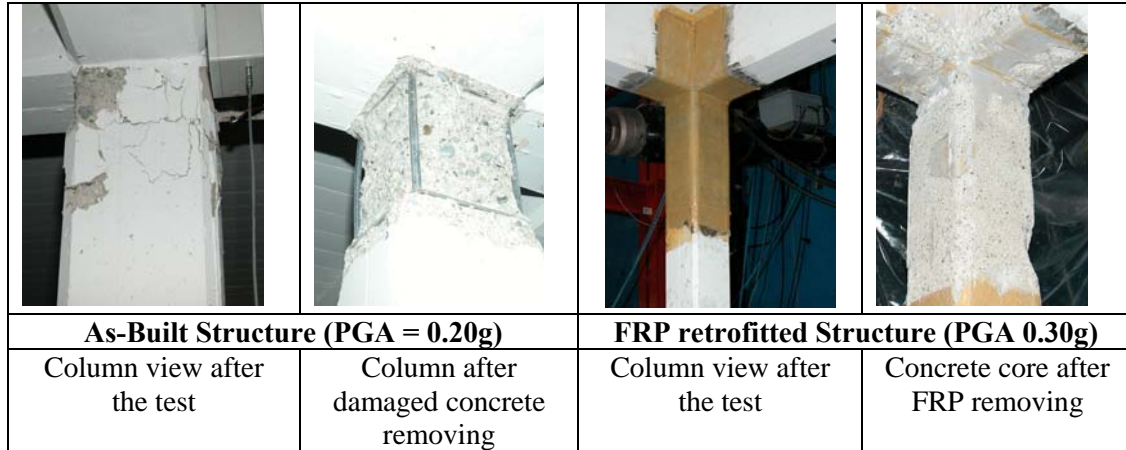


Figure 4.5-2 - Damage on columns: comparison after the test on the ‘as-built’ and FRP retrofitted configuration

Furthermore, a comparison between the experimental results recorded on the ‘as-built’ structure and FRP retrofitted in terms of total adsorbed energy, maximum base shear and top displacement, maximum inter-storey shear and inter-storey displacement are reported in Table 4.5-1 and Table 4.5-2 for the X and Y directions, respectively.

	TEST	Total Absorbed Energy	Max Base Shear	Max Top Displ.	Level	Max I-S Shear	Max I-S Displ.
		[KJ]	[KN]	[mm]		[KN]	[mm]
Direction X	'As-Built' 0.15g	29.61	176	70.1	1	176	15.1
					2	161	36.2
					3	126	24.2
	'As-Built' 0.20g	44.00	195	105.7	1	195	24.6
					2	165	57.0
					3	112	35.8
	FRP retrofitted 0.20g	42.20	211	108.8	1	211	32.0
					2	164	55.4
					3	116	34.3
FRP retrofitted 0.30g	83.36	196	205.3	1	196	59.4	
				2	168	106.0	
				3	123	63.5	

Table 4.5-1– Experimental outcomes, X direction.

	TEST	Total Absorbed Energy	Max Base Shear	Max Top Displ.	Level	Max I-S Shear	Max I-S Displ.
		[KJ]	[KN]	[mm]		[KN]	[mm]
Direction Y	'As-Built' 0.15g	31.81	261	47.0	1	260	11.6
					2	235	19.9
					3	147	18.2
	'As-Built' 0.20g	65.00	276	103.1	1	276	30.6
					2	214	47.2
					3	167	32.6
	FRP retrofitted 0.20g	68.66	287	112.5	1	287	39.7
					2	260	47.6
					3	173	31.1
	FRP retrofitted 0.30g	104.38	281	126.6	1	281	42.3
					2	279	55.9
					3	104	50.7

Table 4.5-2- Experimental outcomes, Y direction.

By comparing the experimental outcomes provided by the tests on the ‘as-built’ and GFRP retrofitted structure, at the same PGA level equal to 0.20g, it is possible to observe a very similar structural behaviour as the maximum recorded base shear was almost equal (195 kN vs 211 kN in X direction, 276 kN vs 287 kN in the Y one). Even less significant was the difference in terms of top displacement: the maximum difference recorded was about 9% in Y direction (112.5 mm vs 103.1 mm).

However, increasing the seismic level intensity up to a value of 0.30g, the displacement capacity of the retrofitted structure was significantly enhanced, especially in the X direction, where the maximum recorded top displacement was equal to 205.3 mm, about twice that reached during the previous test (105.7mm). Such result was confirmed by the data recorded in terms of energy dissipation: the absorbed energy was equal to 83.36 kJ and 104.38 kJ for the X and Y direction respectively with an increment of the 89% and 61% compared to the results obtained during the test at 0,20g on the ‘as-built’ structure, 44.0 kJ and 65.0 kJ in longitudinal and transverse direction. Thus, in terms of total adsorbed energy (by adding the adsorbed energy in both X and Y direction) , GFRP retrofit provided an increase of dissipating capacity equal to 72%; in terms of maximum base shear, however, the percent differences between tests at 0,20g and 0,30g PGA level were equal to only 10% and 12% for X and Y direction, respectively. The presented results confirm the effectiveness of the proposed retrofit technique in increasing considerably the global

structural ductility without affecting the strength, which was the objective of the adopted retrofit methodology.

Further remarks can be made if the absolute inter-storey drift and shear related to the structure in the two configurations are analysed. The comparison between the maximum values of absolute inter-storey drifts achieved during the tests on the ‘as-built’ structure at 0,20g and the FRP retrofitted one at 0.30g in correspondence of the second floor (where the maximum drifts were achieved) shows that an increase of about 85% in the weak direction was recorded (106.0mm vs. 57.0mm). On the contrary, the shear increase, with reference to the same storey and direction, was equal to 2% (i.e. 168 kN in the FRP retrofitted configuration instead of 165 kN for the ‘as built’ one).

In order to evaluate the structural stiffness during the four tests, the frequency-time relationships related to the structural mode 1 are reported in Figure 4.5-3.

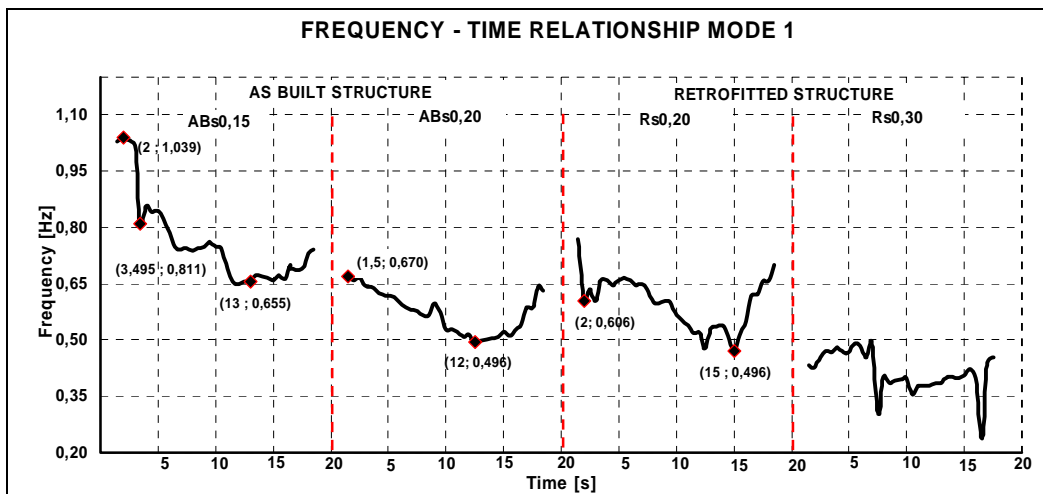


Figure 4.5-3 - Frequency-Time Relationship Mode 1.

Considering that the structural mass was constant during each test phase, it is possible to evaluate the structural stiffness progress as a direct function of the frequency; in particular, Figure 4.5-3 shows that the initial structural frequency of the ‘as-built’ structure, related to the first mode of vibration, was equal to 1.039 Hz. With reference to the first test, named ABs 0.15 in the figure, the initial frequency value drastically decreased after few seconds down to a value of 0.811 Hz, as cracking of the structural members was achieved and it became equal to 0.655 Hz at the end of the test. During the second test, named ABs 0.20 in the figure, the frequency value, starting from almost the same final value of the previous test,

showed a further decrease because the level of damage increased proportionally to the enhanced external seismic excitation. After the retrofit, an apparent stiffness increase was recorded, as confirmed by the initial frequency value recorded in the FRP retrofitted structure at 0,20g PGA level, named Rs 0.20 test in the figure, equal to 0.768 Hz; such increase can be justified by considering that, before installing the laminates, the original cross-sections of the damaged members were restored using a non-shrinking mortar and cracks were epoxy-injected. Then, as soon as the cracking load was achieved, the frequency was abruptly reduced up to a value 0.606 Hz, attaining, at the end of the test, a value equal to that recorded in the ABs 0.20 test (i.e. 0.496 Hz). Such frequency-time progress highlights the effectiveness of the FRP retrofit in repairing the damaged 'as-built' structure and ensuring very similar global structural performance. Finally, a further decrease of the structural frequency, and then of its stiffness, was recorded during the test on the retrofitted structure at 0,30 PGA level, named Rs 0.30, where the average frequency value was about 0.375 Hz. In Figure 4.5-4 the period-time relationship curves for each test, along with the elastic acceleration and displacement spectra related to the Herceg-Novik accelerogram, are plotted; the period is computed as the inverse of the frequency. By drawing an horizontal line from the initial structural period of each test phase, the figure allows quantifying both design elastic spectral acceleration and displacement demand, that would correspond to a design performed using the Herceg-Novik accelerogram scaled at PGA level equal to 1g. The figure shows that, from a design point of view, according to the initial period of the 'as-built' structure, 0.98s, the elastic demand in terms of acceleration is equal to about 1.7g and the related elastic displacement demand is about 40 mm. By considering the structure after a seismic event, at PGA level of 0.15g, the initial period becomes equal to 1.50s and the corresponding elastic acceleration demand decreases up to a value of about 1.2g with about 60 mm of displacement demand. At this stage, with reference to the structure after another seismic event at PGA level intensity of 0.20g, the figure shows that, since FRP laminates provide a negligible mass increase and then preserve the initial structural period, their adoption could allow engineers to design the retrofit intervention with reference to seismic acceleration equal to that used for the original structure. On the contrary, if a traditional retrofit technique is chosen, the consequent

mass increase might imply a lower initial period, possibly inducing an elastic acceleration demand greater than that computed on the original structure.

Finally, from the figure it is clearly shown that after the test Rs 0.20 the initial period increases and thus the seismic actions become lower and lower up to a value of 0.75g; the elastic displacement demand, however, increases up to a value of about 90 mm. In conclusion, the curves indicate that the FRP laminates allow the design of the retrofit intervention to be made considering seismic excitations equal to those computed on the 'as-built' structure but, at the same time, require a structural deformation capacity improvement in order to withstand the larger global displacement demand.

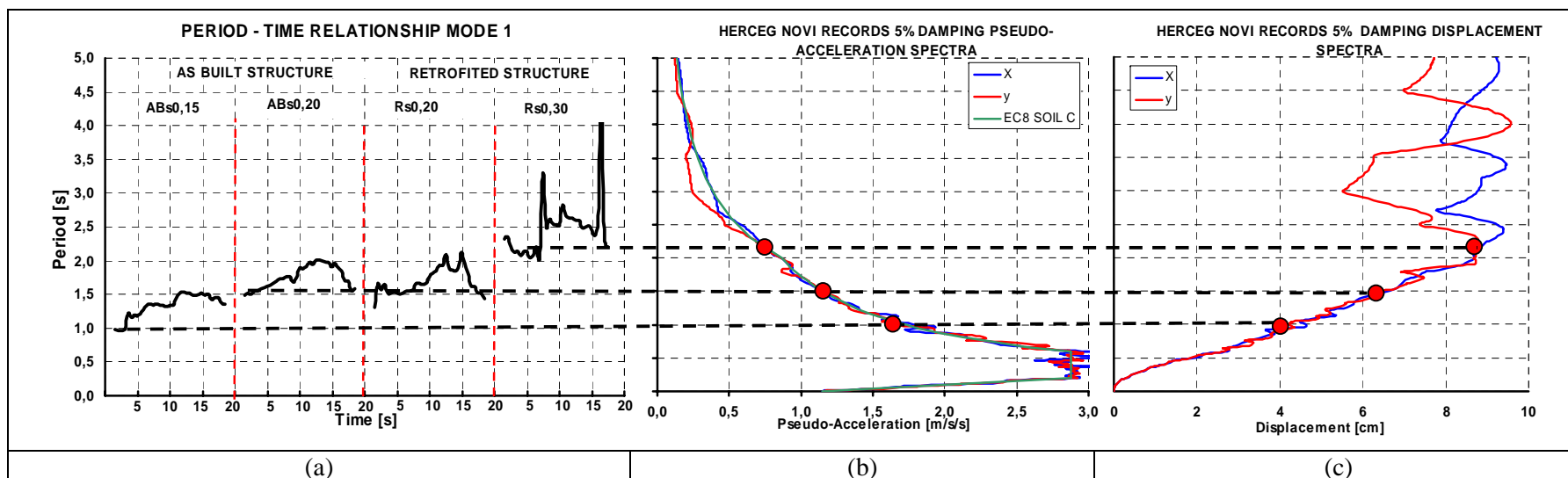


Figure 4.5-4 - (a) Frequency-Time Relationship Mode 1, (b) elastic acceleration spectra, (c) elastic displacement spectra

Chapter V

5.1 REHABILITATION WITH RC JACKETING

The aim of the second rehabilitation strategy was to increase both strength and ductility capacity of the ‘as-built’ structure by the RC jacketing of selected vertical elements. The choice of the columns to be strengthened was aimed at minimizing the structural torsional effects due to the doubly non-symmetric plan configuration of the ‘as-built’ structure; in this way, it is possible, in fact, to reduce the displacement demand on the external columns.

5.1.1 Design of the intervention with RC Jacketing

According to previous research in the field, Rutenberg et al. [19], it was found that, in the inelastic range of the response, the torsional effects are mainly governed by strength eccentricity rather than stiffness eccentricity; thus, the design was aimed at decreasing both the eccentricity between the centre of mass, CM, and the centre of strength and stiffness, CP and CR respectively, at each floor of the structure. The centre of strength was considered as the centre of the columns yielding moments.

The coordinate of such mass, stiffness and strength centre for each storey in the case of the ‘as-built’ structure are summarized in the first three rows of Table 5.1.1-1; the eccentricity between centre of stiffness and strength with regard to the centre of the mass are represented in Figure 5.1.1-1.

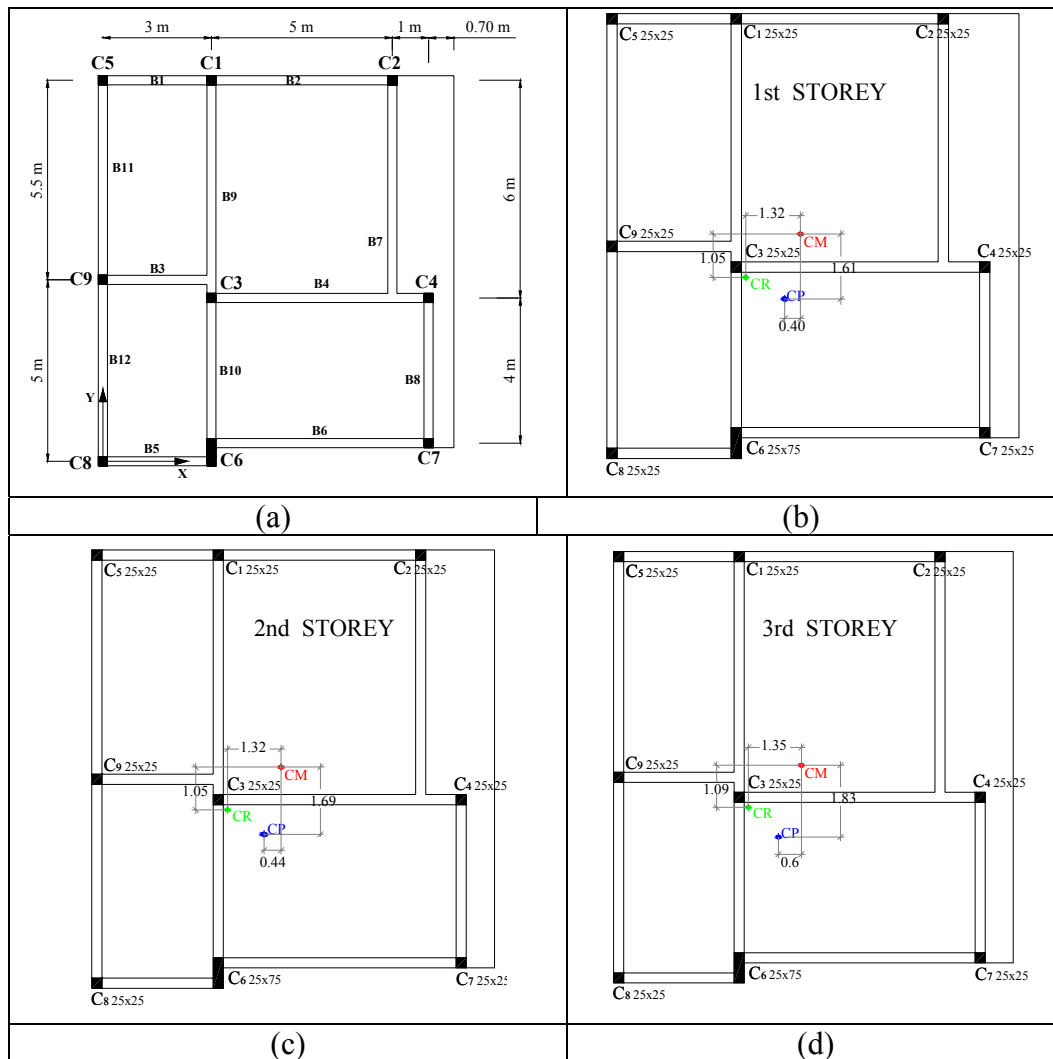


Figure 5.1.1-1 – ‘As-built’ structure: Plan layout (a), centre of stiffness and strength eccentricity at 1st (b) and 2nd storey (c) and at 3rd storey (d)

According to such goal, it was decided to increase the original cross-section of columns C4 and C1 from 250x250 mm to the jacketed 400x400 mm.

The enlargement of such columns allows, in fact, strongly reducing the eccentricity of the centre of strength and stiffness at each storey of the structure (i.e. the eccentricity of the CP at first and second storey becomes 0.32m and 0.42m instead of 0.44m and 1.69m in the X and Y direction, respectively as shown in Figure 5.1.1-2 (c)). Moreover, it is noted that such intervention is also effective in reducing the eccentricity of the centre of stiffness, CR, especially in the X direction. The coordinate of the centre of mass, of stiffness and strength for each storey in the case of the RC jacketed structure are summarized in the last three rows of Table 5.1.1-1.

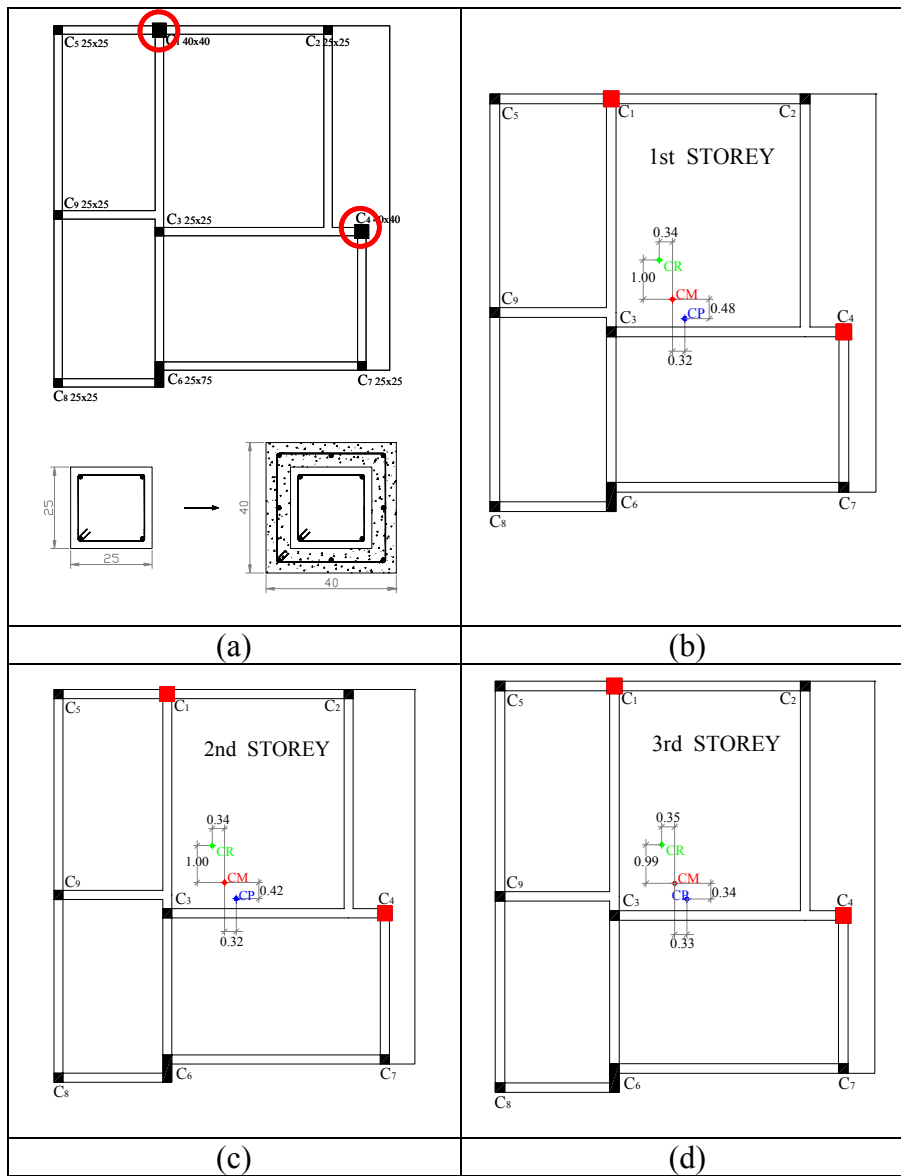


Figure 5.1.1-2 – RC rehabilitated structure: Plan layout and cross section enlargement (a), centre of stiffness and strength eccentricity at 1st (b), 2nd storey (c) and 3rd storey (d)

		Mass centre		Stiffness Centre		Strength Centre	
		X _M [m]	Y _M [m]	X _R [m]	Y _R [m]	X _P [m]	Y _P [m]
‘AS-BUILT’ structure	1 st STOREY	4,55	5,30	3,23	4,25	4,15	3,69
	2 nd STOREY	4,55	5,30	3,23	4,25	4,11	3,61
	3 rd STOREY	4,58	5,34	3,23	4,25	3,98	3,51
RC JACKETED structure	1 st STOREY	4,58	5,35	4,24	6,35	4,90	4,87
	2 nd STOREY	4,58	5,35	4,24	6,35	4,90	4,93
	3 rd STOREY	4,59	5,36	4,24	6,35	4,92	5,02

Table 5.1.1-1- ‘As-built’ and RC Jacketed structure: coordinate of centre of mass, stiffness and strength.

The RC concrete jacketing of column C4 and C1 was designed with shrinkage-compensated concrete design strength equal to $f'_c=50$ MPa. The longitudinal reinforcement of the jacketed columns was designed as 3 bars 16 mm diameter for each side of the column and a single leg 8 mm stirrups at 100 mm o.c. at the top and the bottom of the columns (for a length equal to 700 mm starting from the slab) and 150 mm o.c. for the remaining column length; steel bars and stirrups design strength were $f_y = 430$ MPa.

5.1.2 Assessment of the Rehabilitated Structure

In order to investigate the performances of the RC jacketed structure, a non linear static pushover was conducted on a lumped plasticity model of the structure. First, to model the RC jacketed structure, it was necessary to consider that, as a consequence of the columns enlargement, storey masses and centre of masses at each floor change significantly.

According to the assumptions reported in Chapter III, in Table 5.1.2-1, the masses values computed with reference to each storey of the rehabilitated structure are listed ($Q_{slabs}=2500*0,15=375kg/m^2$; $Q_{var.}=50+0,3*200=110kg/m^2$).

The table shows that the storey mass increases from 65.9 tons up to 67.2 tons for the 1st and 2nd floor and from 63.3 tons up to 63.9 tons for the 3rd floor

As for the 'as-built' structure, the storey masses have been assigned in correspondence of the master joints of the structural model; such joints have been assumed as the centre of the mass of each storey.

1st and 2nd STOREY	A_{infl.} [m ²]	W_{slab} [kg]	A_{infl.} [m ²]	W_{var.} [kg]	L_{beam} [m]	W_{beam} [kg]	L_{col.} [m]	Pcol. [kg]	W_{TOT} [kg]	Masses [KN/(m/s ²)]
C5	3,61	1353,5	4,13	453,8	4	1250	3	468,75	3526,0	3,53
C1	9,84	3691,4	11,0	1210,0	6,150	1922	3	1200	8023,3	8,02
C2	11,16	4183,6	11,6	1270,5	5	1563	3	468,75	7485,3	7,49
C9	6,88	2578,1	7,9	866,3	5	1563	3	468,75	5475,6	5,48
C3	20,53	7699,2	23,6	2598,8	9	2813	3	468,75	13579,2	13,58
C4	19,41	7277,3	19,4	2136,8	7,475	2336	3	1200	12950,0	12,95
C8	3,27	1224,6	3,8	412,5	3,750	1172	3	468,75	3277,7	3,28
C6	8,66	3246,1	9,8	1072,5	6,125	1914	3	1406,25	7638,9	7,64
C7	6,61	2479,7	7,4	814,0	4,75	1484	3	468,75	5246,8	5,25
TOT									67203,0	67,20

3rd STOREY	A_{infl.} [m ²]	W_{slab} [kg]	A_{infl.} [m ²]	W_{var.} [kg]	L_{beam} [m]	W_{beam} [kg]	L_{col.} [m]	Pcol. [kg]	W_{TOT} [kg]	Masses [KN/(m/s ²)]
C5	3,61	1353,5	4,13	453,8	4	1250	1,5	234,375	3291,6	3,29
C1	9,84	3691,4	11,0	1210,0	6,150	1922	1,5	600	7423,3	7,42
C2	11,16	4183,6	11,6	1270,5	5	1563	1,5	234,375	7251,0	7,25
C9	6,88	2578,1	7,9	866,3	5	1563	1,5	234,375	5241,3	5,24
C3	20,53	7699,2	23,6	2598,8	9	2813	1,5	234,375	13344,8	13,34
C4	19,41	7277,3	19,4	2136,8	7,475	2336	1,5	600	12350,0	12,35
C8	3,27	1224,6	3,8	412,5	3,750	1172	1,5	234,375	3043,4	3,04
C6	8,66	3246,1	9,8	1072,5	6,125	1914	1,5	703,125	6935,8	6,94
C7	6,61	2479,7	7,4	814,0	4,75	1484	1,5	234,375	5012,4	5,01
TOT									63893,6	63,89

Table 5.1.2-1- RC rehabilitated structure: masses values for each storey.

As the structural mass is enhanced the elastic period of the rehabilitated structure decreases and the first six modal periods and corresponding participating masses along with plane deformed shape are changed with respect to both the ‘as-built’ and FRP retrofitted structure. Hence an eigenvalue analysis was again performed on the RC rehabilitated structure; the results are reported in the following Figure 5.1.2-1. The figure highlights that the elastic period correlated to the first mode of vibration decrease up to a value of 0,465s against the 0,623s of the ‘as-built’ structure. It is also noted that the designed RC jacketing of columns C1 and C4 allows minimising the plan irregularity as the participating mass related to the first two modes of vibration are, in such case, almost completely represented by the mass in the X and Y direction (i.e. in the first mode $M_{%Y}=0,1\%$ and in the second mode $M_{%X}=0\%$ while in the ‘as-built’ structure they achieved the values of $M_{%Y}=5,8\%$ and $M_{%X}=12,4\%$,

respectively). Such result clearly shows that the inertial coupling of the structure can be strongly reduced by the adopted rehabilitation intervention.

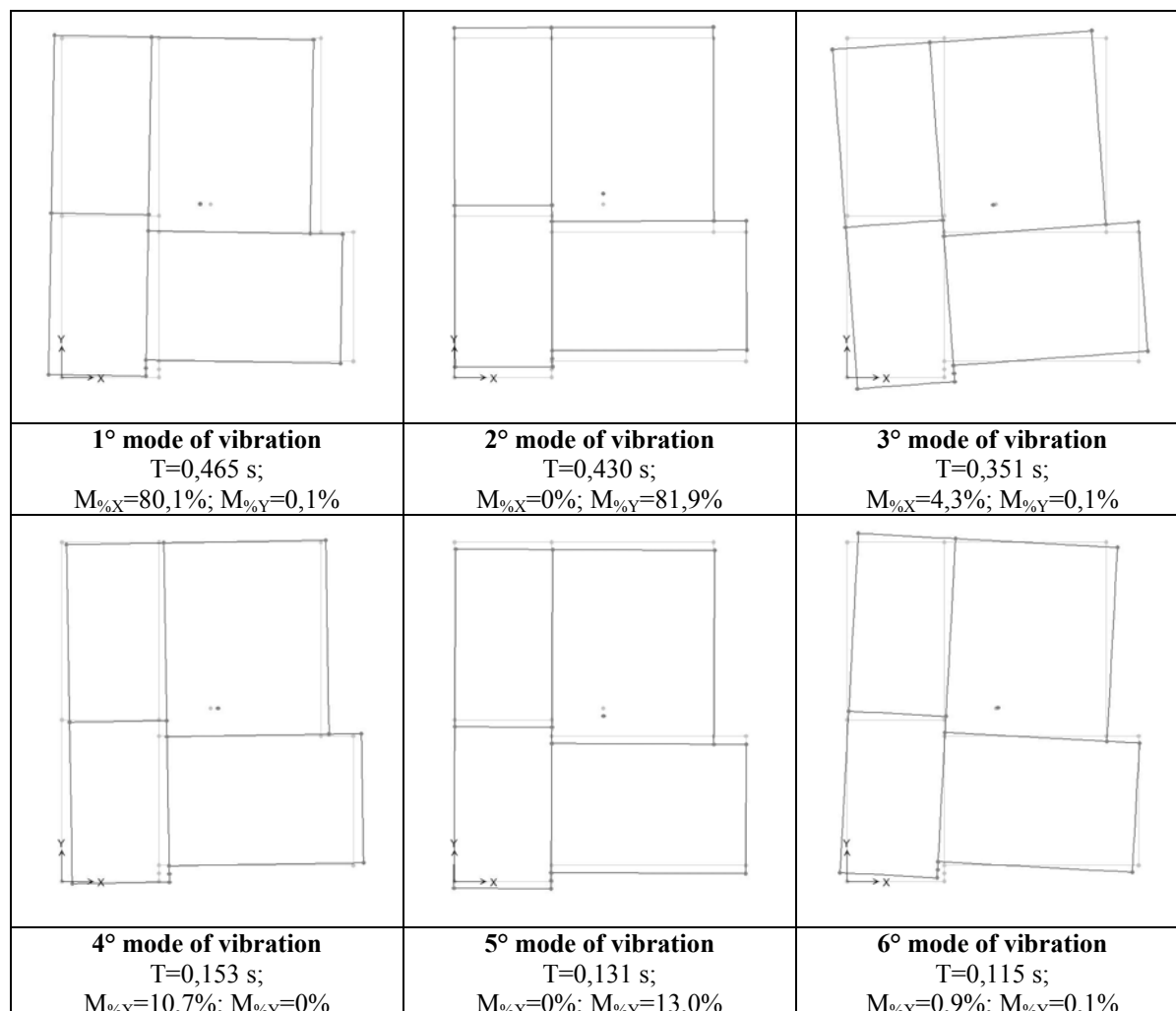


Figure 5.1.2-1 – RC rehabilitated structure: fundamental modes of vibration, modal periods and participating masses for X and Y direction.

The change of both structural masses and first and second mode of vibration induces different initial values of lateral forces to take into account for the pushover curve determination; in particular the distribution of lateral forces in the case of the RC rehabilitated structure is reported in the following Table 5.1.2-2 and Table 5.1.2-3.

1° mode of vibration				
	displ. in dir. X [m]	mass [ton]	mass*displ.	F_{mod}^X [KN]
1° storey	-0,0096	67,20	-0,6428	0,316
2° storey	-0,0232	67,20	-1,5610	0,768
3° storey	-0,0318	63,89	-2,0313	1

Table 5.1.2-2- Lateral forces proportional to the 1st mode of vibration.

	2° mode of vibration			
	displ. in dir. Y [m]	mass [ton]	mass*displ.	F _{mod} ^Y [KN]
1° storey	0,0088	67,20	0,5905	0,277
2° storey	0,0232	67,20	1,5586	0,730
3° storey	0,0334	63,89	2,1354	1

Table 5.1.2-3- Lateral forces proportional to the 2nd mode of vibration.

Moreover considering that the enlargement of the column C1 and C4 implies different axial loads values on the columns (due to gravity loads only), a different characterization of the plastic hinge at the member end was necessary.

In particular, in the bilinear moment – rotation relationship used for modelling the lumped plasticity at the members ends, both ϕ_y and M_y as well as ϕ_u and M_u were modified according to the following assumptions (Ordinanza 3431 [2], 2005 and *fib* Bulletin 24, [20]):

- 1) the member was considered as monolithic with full composite action between old and new concrete;
- 2) concrete strength was taken as that of the old column because the large differences in strength between old and new concrete;
- 3) axial load was considered acting on the full composite section;
- 4) only the longitudinal reinforcement of the jacket was considered as the reinforcement of the whole cross-section whereas the reinforcement of the existing column was neglected.

Based on such assumptions, with reference to the axial load due to only gravity loads, yielding and ultimate curvatures (and the corresponding moments) were determined in correspondence of the attainment of the tensile steel yielding strain and of ultimate strains in concrete (conventionally assumed equal to 3.5 ‰) or steel (assumed equal to 40‰), respectively for each structural member. Plastic hinge length, yielding and ultimate rotation were again computed by using the expression provided by Ordinanza 3431 [2] (expressions (1), (2), (3) and (4) of Chapter III); the knowledge level was again assumed equal to 3, KL3, with a corresponding confidence factor, CF, equal to 1.

In Appendix D, axial load values obtained for each column due to gravity loads are reported as well as the yielding and ultimate rotations and moments obtained for each plastic hinge at each member end.

As for the previous analysed cases, the three limit states, LSDL, LSSD and LSNC, with particular attention to the first two were investigated for the assessment of the structural capacity at both 0.20g and 0.30g PGA level in the PX - NX and PY - NY directions, respectively. The pushover curves on the RC jacketed structure for each direction analysed are reported in Figure 5.1.2-2.

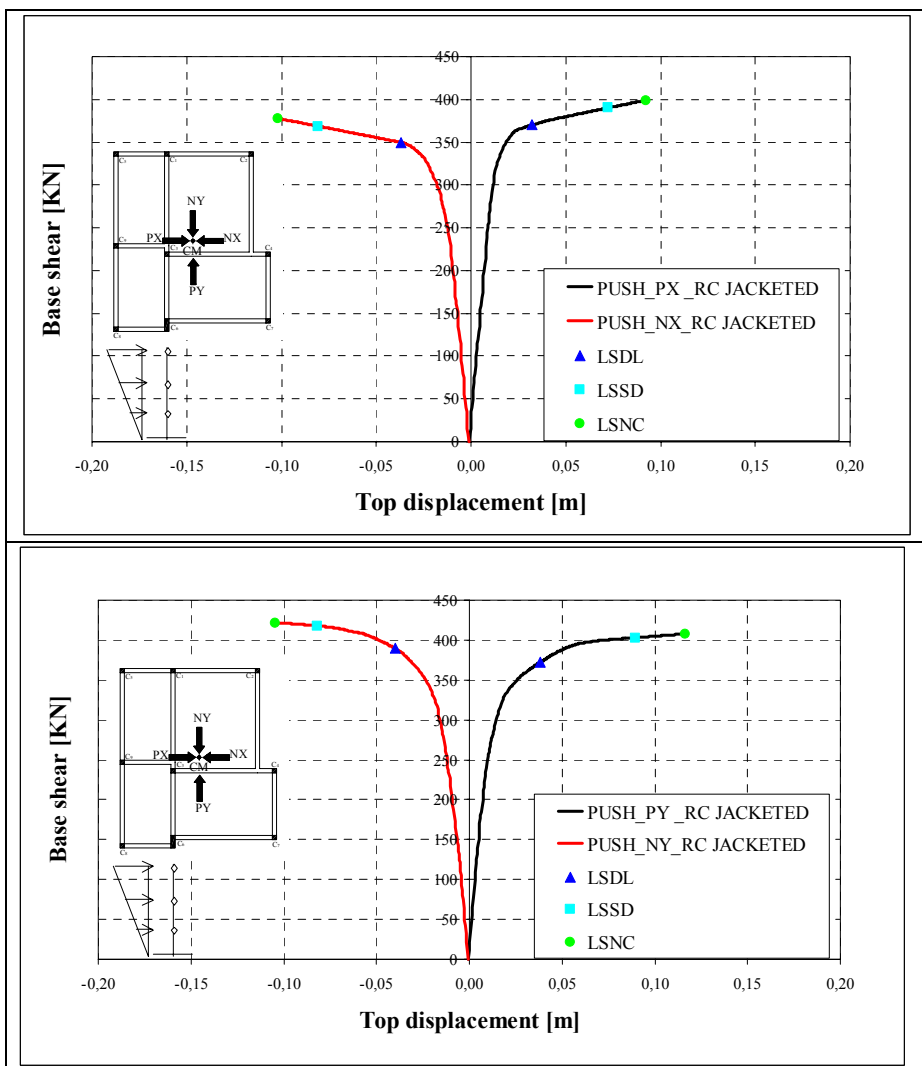


Figure 5.1.2-2- Pushover curves for the assessment of the RC jacketed structure

The capacity theoretical results of the rehabilitated structure in terms of maximum base shear, F_{max} top displacement, d_{max} , and absolute inter-storey drift, ξ , are summarized on the right-hand side of Table 5.1.2-4 and Table 5.1.2-5 for the damage

limitation and significant damage limit states, respectively. The seismic demand was computed with reference to the same design spectra analysed in the other configurations scaled at 0.20g and 0.30g PGA level.

The results in terms of maximum top displacement demand for each investigated PGA level and direction at LSDL and LSSD are also summarized in Table 5.1.2-4 and Table 5.1.2-5. On the left-side of such table, the theoretical results in terms of both capacity and demand related to the ‘as-built’ structure are recalled. The comparison between the seismic demand and capacity is also reported in a graphical form in Figure 5.1.2-3 for both seismic level intensity of 0,20g and 0,30g.

Push Direction	Limit State	Level	'AS BUILT' STRUCTURE					RC JACKETED STRUCTURE				
			CAPACITY			DEMAND		CAPACITY			DEMAND	
			F_{max}	d_{max}	$\xi=I-D/h$	d_{max}	d_{max}	F_{max}	d_{max}	$\xi=I-D/h$	d_{max}	d_{max}
			[KN]	[m]	[-]	[m]	[m]	[KN]	[m]	[-]	[m]	[m]
PX	LSDL	1	231	0,0355	0,004	0,0248	0,0372*	370	0,0321	0,005	0,0164	0,0253
		2			0,006					0,005		
		3			0,001					0,001		
NX	LSDL	1	232	0,0406	-0,003	0,0247	0,0371	350	0,0367	-0,005	0,0215	0,0322
		2			-0,009					-0,005		
		3			-0,001					-0,003		
PY	LSDL	1	250	0,0409	0,004	0,0240	0,0360	372	0,0385	0,004	0,0196	0,0294
		2			0,005					0,005		
		3			0,005					0,004		
NY	LSDL	1	291	0,0412	-0,005	0,0240	0,0361	389	0,0401	-0,005	0,0212	0,0318
		2			-0,005					-0,005		
		3			-0,004					-0,004		

(*Demand displacements not satisfied by the structure)

Table 5.1.2-4– Summary of the results in terms of capacity and demand for the ‘as-built’ and the RC jacketed structure

Push Direction	Limit State	Level	'AS BUILT' STRUCTURE					RC JACKETED STRUCTURE				
			CAPACITY			DEMAND		CAPACITY			DEMAND	
			F_{max}	d_{max}	$\xi=I-D/h$	d_{max}	d_{max}	F_{max}	d_{max}	$\xi=I-D/h$	d_{max}	d_{max}
			[KN]	[m]	[-]	[m]	[m]	[KN]	[m]	[-]	[m]	[m]
PX	LSSD	1	232	0,0690	0,005	0,0623	0,0934*	390	0,0721	0,012	0,0493	0,0740*
		2			0,017					0,012		
		3			0,001					0,002		
NX	LSSD	1	232	0,0626	-0,003	0,0618	0,0927*	367	0,0807	-0,012	0,0584	0,0876*
		2			-0,016					-0,012		
		3			-0,001					-0,004		
PY	LSSD	1	251	0,0962	0,010	0,0607	0,0910	403	0,0893	0,010	0,0552	0,0828
		2			0,011					0,011		
		3			0,011					0,010		
NY	LSSD	1	292	0,0740	-0,010	0,0603	0,0904*	418	0,0817	-0,010	0,0578	0,0867*
		2			-0,011					-0,010		
		3			-0,004					-0,007		

(*Demand displacements not satisfied by the structure)

Table 5.1.2-5– Summary of the results in terms of capacity and demand for the ‘as-built’ and the RC jacketed structure

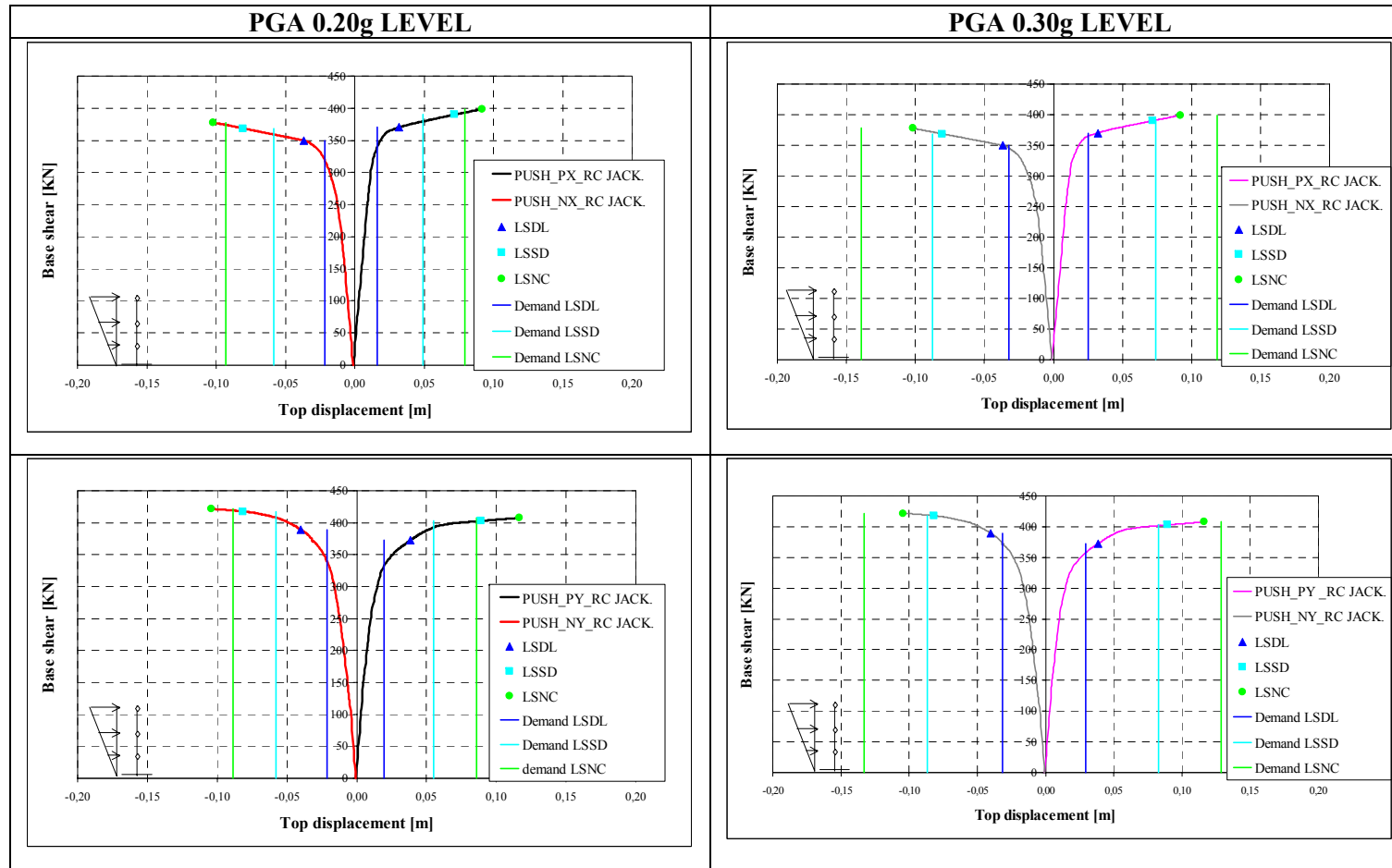


Figure 5.1.2-3 – RC jacketed structure, demand vs. capacity comparison for PGA level equal to 0.20g and 0.30g at LSDL,LSSD and LSNC.

Such tables and figures show that RC jacketing allows the structure satisfying the LSDL at both 0.20g and 0.30g in each direction; it is shown, in fact, that in the PX direction for the 0.30g PGA level (for which the ‘as-built’ structure was unable to satisfy the seismic demand) even though the top displacement capacity is less than that of the ‘as-built’ structure (0.0321m vs. 0.0355m), the structure can sustain the displacement demand that is now strongly decreased from a value of 0.0372 m up to 0.0253 m. Such effect is obviously due to the stiffness increase provided by the RC jacketing that produces an elastic period decrease and thus allows reducing the seismic demand.

As concerns the LSDS verifications, the theoretical results show that the rehabilitation intervention, although increases significantly both ductility and strength of the ‘as-built’ structure, it is slightly insufficient to allow the structure, except for the PY direction, withstanding the demand due to the seismic action at 0.30g PGA level. Such result can be clearly observed for the NX direction in Figure 5.1.2-4 in which the seismic demand and the structural capacity are plotted and compared by using the CSA approach; the requested ductility at 0.30g PGA level is equal to 3.49 against the structural ductility $\mu_s = d^*_{max} / D^*_y = 0.0651 / 0.0202 = 3.21$ (ductility gap equal to 9%).

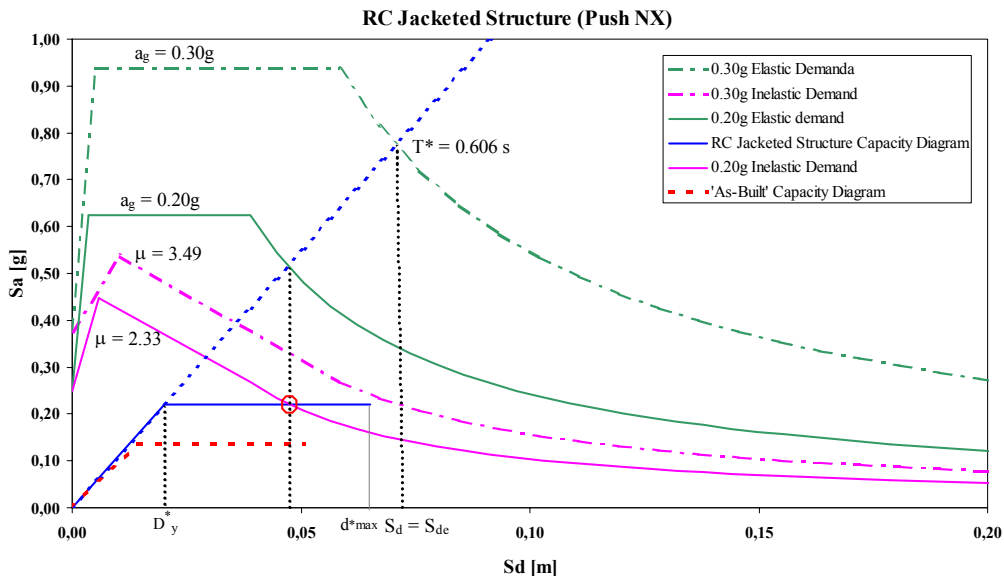


Figure 5.1.2-4– RC Jacketed structure elastic and inelastic demand spectra vs. capacity diagram

The comparison of the LSSD verifications at 0.30g PGA for the ‘as-built’ and RC retrofitted structure by using the CSA is reported in Table 5.1.2-5

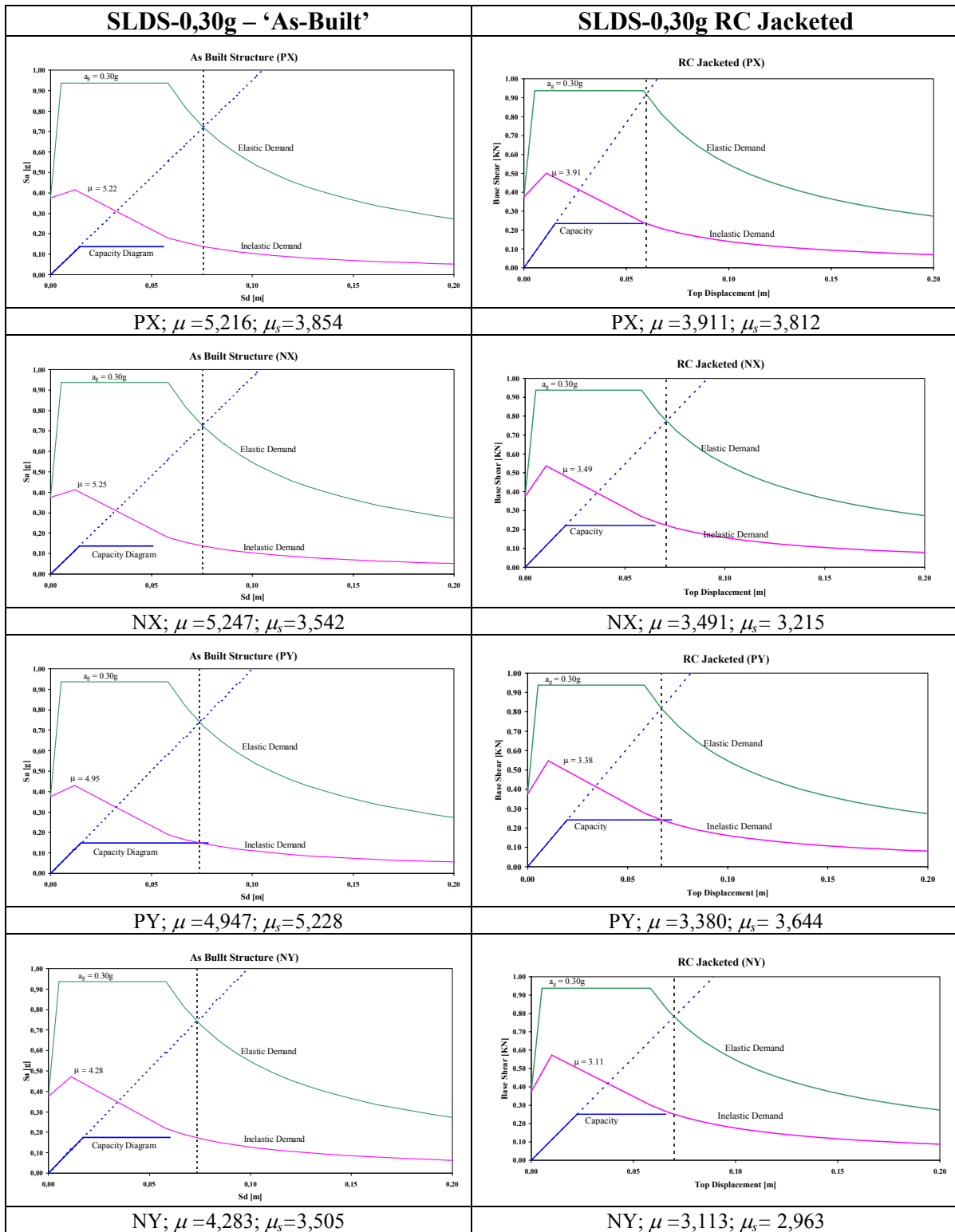


Figure 5.1.2-5 - Theoretical seismic performance comparison at 0.3g PGA between ‘as-built’ and RC jacketed structure.

The figure confirms that not only in the NX direction but also in the NY and PY the retrofitted structure shows a seismic capacity slightly insufficient. As a consequence, it was decided to investigate on the effectiveness of a more invasive scheme of RC jacketing with the aim of a further mitigation of the strength eccentricities and increase of the global deformation capacity of the structure. Thus, it was analysed the effect of the jacketing of the seven square perimeter columns to 400x400 mm (Kosmopoulos et al., [21]).

By such intervention, in fact, the eccentricity of the CP in the Y direction for the second storey could be minimised up to a value of 0.25 m (it was 1.69m for the ‘as-built’ structure and 0.42m in the case of RC jacketing of columns C1 and C4)

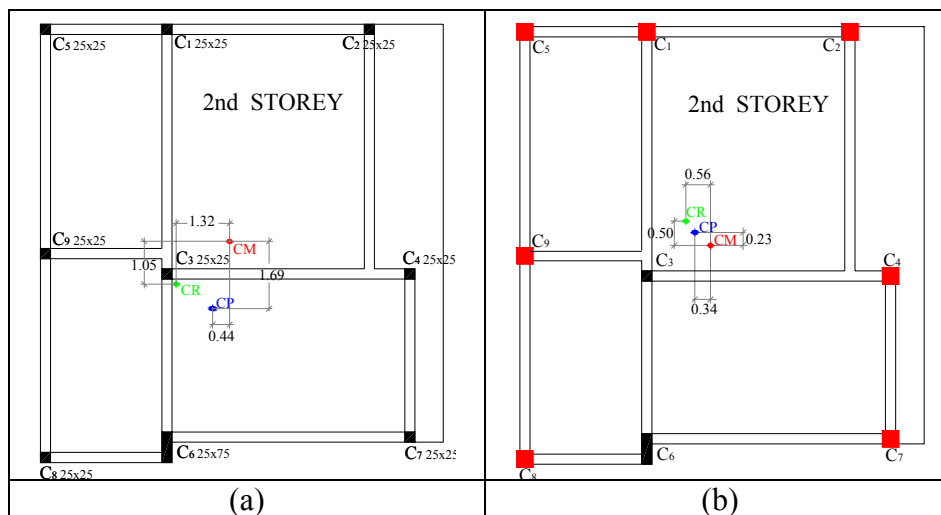


Figure 5.1.2-6 - Eccentricity of stiffness and strength centre: ‘as-built’ structure (a); structure with RC jacketing of all square perimeter columns (b) (dimensions in meters)

A non linear static pushover was again performed and it was found that such retrofit resulted much more effective in preventing structural damage because it could determine a substantial increase of the structural global deformation capacity. However, it appeared quite excessive providing the structure in the NX direction (that one in which the verification it was more far to be satisfied) with an available ductility equal to $\mu_s = d_{max}^* / D_y^* = 0.0887 / 0.0207 = 4.28$ that is about 44% larger than the requested one at 0.30g, $\mu = 2.97$ (see Figure 5.1.2-7).

Taking into account also that the first RC jacketing option is lighter as far as the impact of the retrofitting and it is much easier and faster to implement both in the

field and in the laboratory, it was decided to follow the first RC jacketing option outlined (enlargement of square columns C4 and C1 to 400x400 mm).

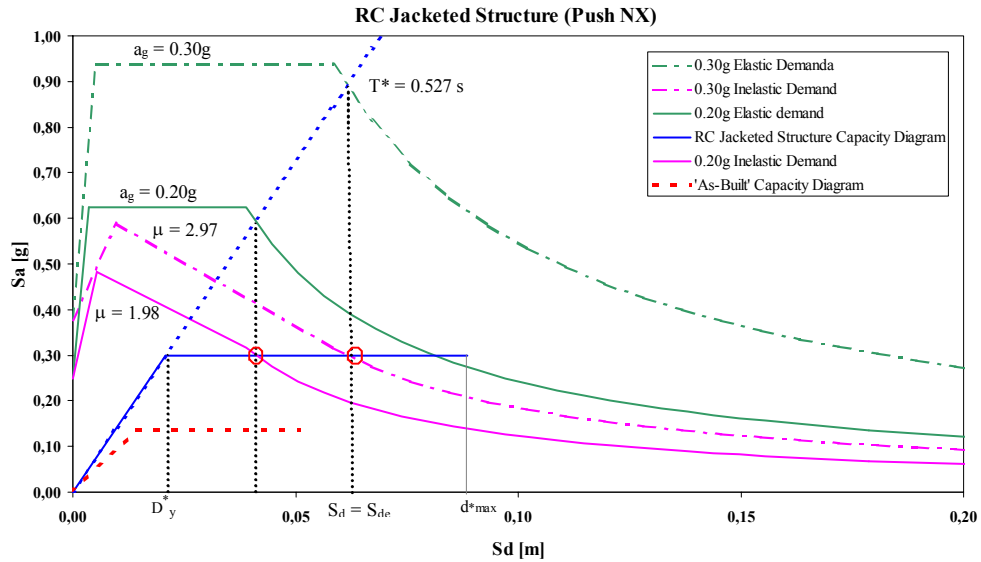


Figure 5.1.2-7– Square perimeter columns RC Jacketed structure: elastic and inelastic demand spectra vs. capacity diagram

5.2 RC JACKETING CONSTRUCTION PHASES

Once the design of the rehabilitation was completed, the third round of experimental tests started. After the test on the FRP retrofitted structure, prior to RC concrete jacketing, the FRP laminates installed in the previous phase of tests were removed; in order to easily complete such phase, a transverse cut was performed along the corner of the columns (see Figure 5.2-1). The complete integrity of the concrete under the laminates confirmed the effectiveness of the previous retrofit strategy; moreover the possibility of easily removing the laminates highlighted the reversibility of the intervention (very important aspect especially in the case of application in historic buildings).

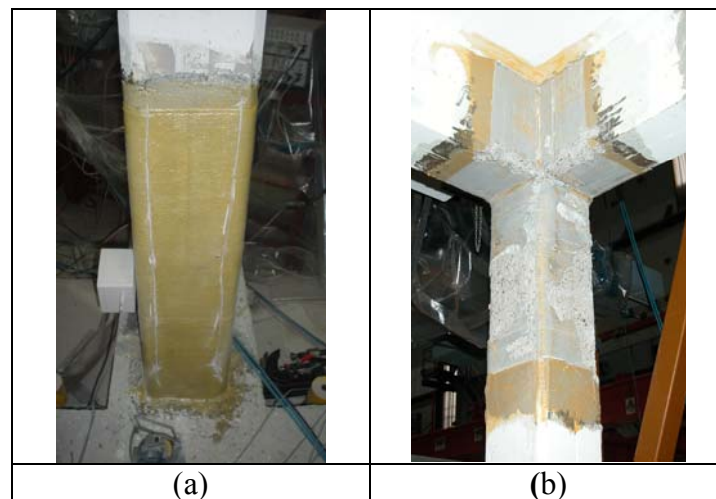


Figure 5.2-1 – FRP laminates removing

At this stage the RC jacketing of columns C4 and C1 started following the design drawings that foresee the original cross-section enlargement from 250x250 mm up to 400x400mm, 3 bars 16 mm diameter for each side of the column as longitudinal reinforcement and a single leg 8 mm stirrups at 100 mm o.c. at the top and the bottom of the columns (for a length equal to 700 mm starting from the slab) and 150 mm o.c. for the remaining column length. The complete schemes of the rehabilitation intervention designed are reported in the following Figure 5.2-2 and Figure 5.2-3.

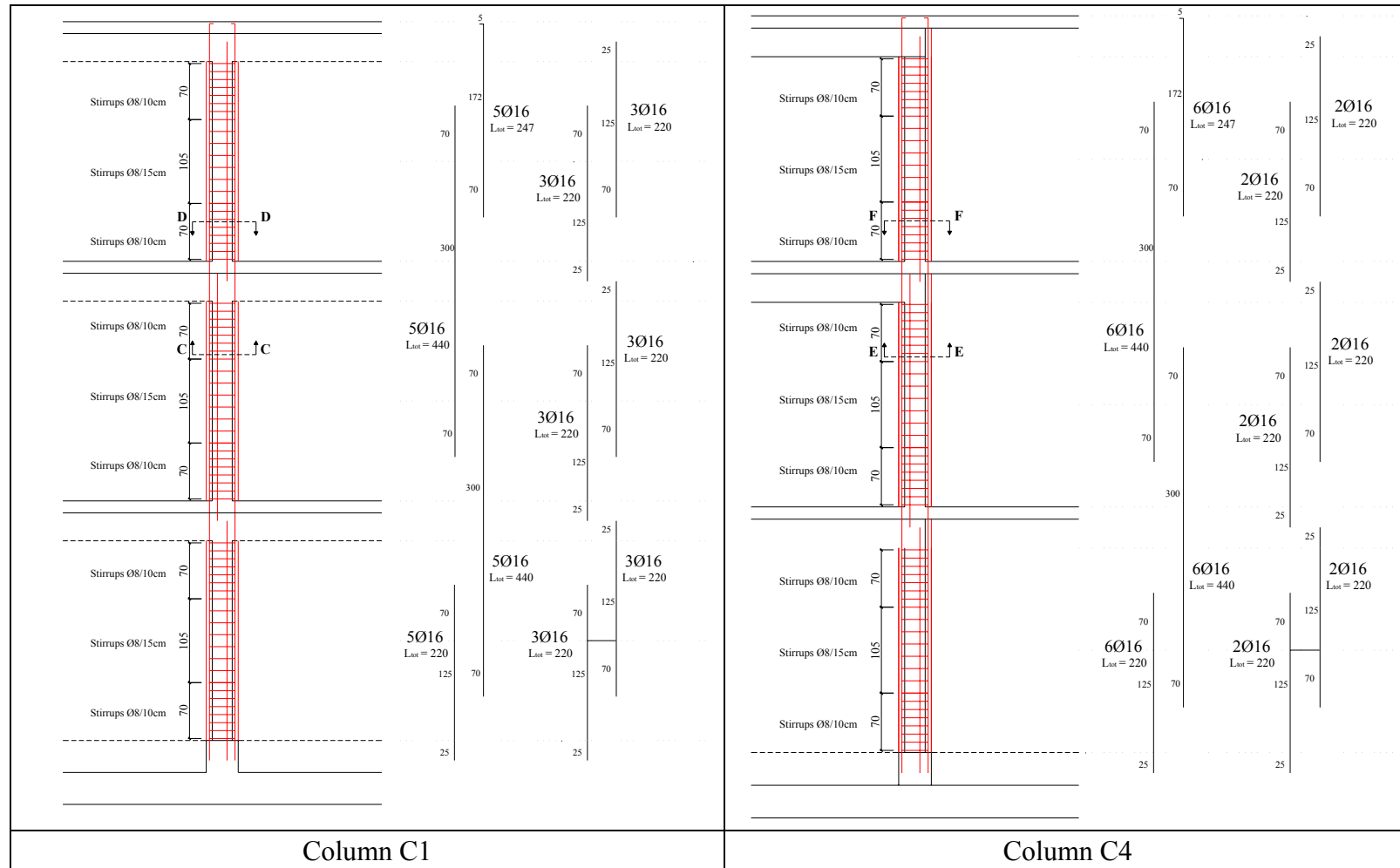


Figure 5.2-2 – RC jacketed columns reinforcement details

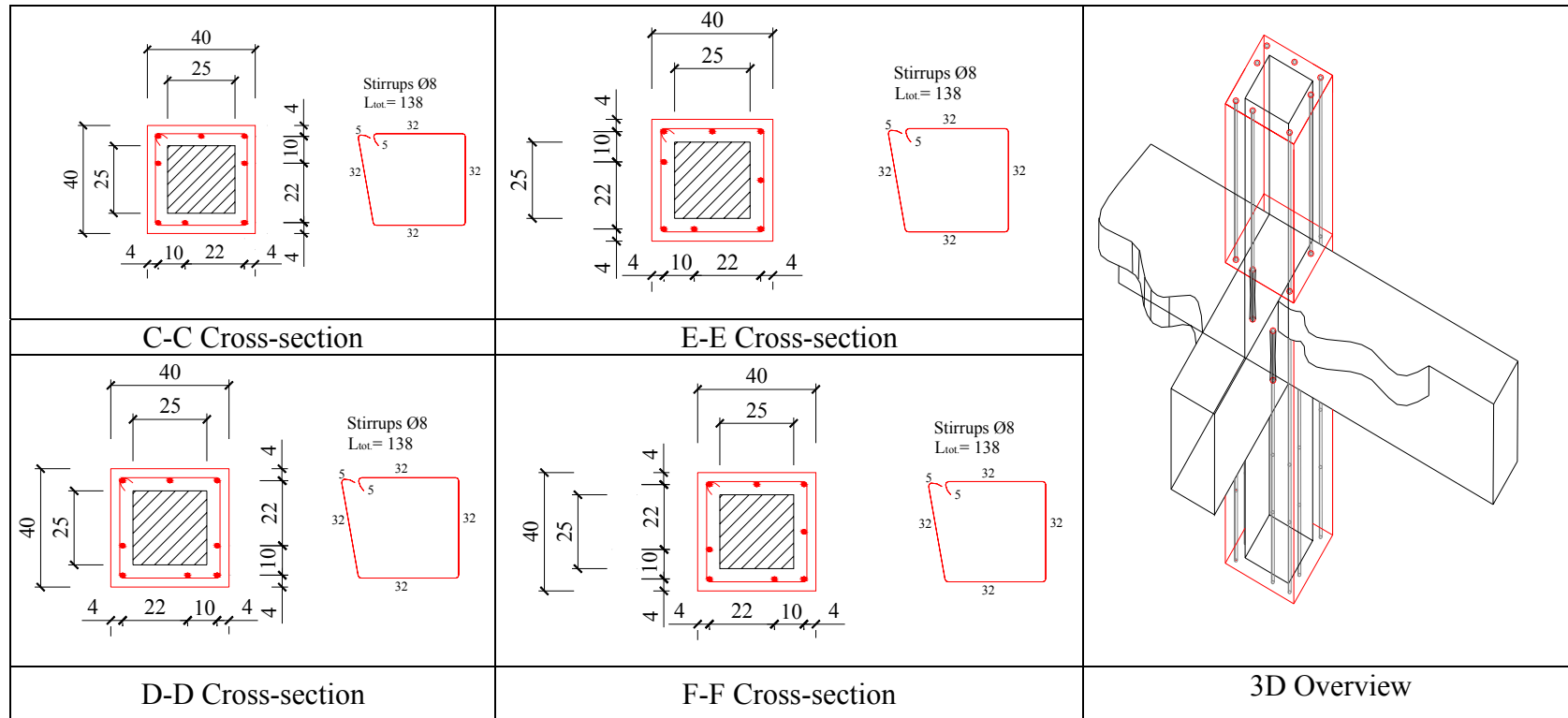


Figure 5.2-3 – RC jacketing reinforcement in proximity of the joints

According to the design drawings, to ensure the effectiveness of the retrofit, particular attention was paid in order to guarantee the reinforcement continuity in correspondence of the ends zone of the columns. Thus, the longitudinal reinforcement (8 bars 16 mm diameter) was passed trough holes drilled into the foundation and into the slab in the zone of the interior corners; moreover, for the bars in correspondence of the beams, holes were drilled into the beams starting to the upper and bottom side of the beams with an overlapping length equal to 250 mm. The detail of such intervention phases are reported in Figure 5.2-4.

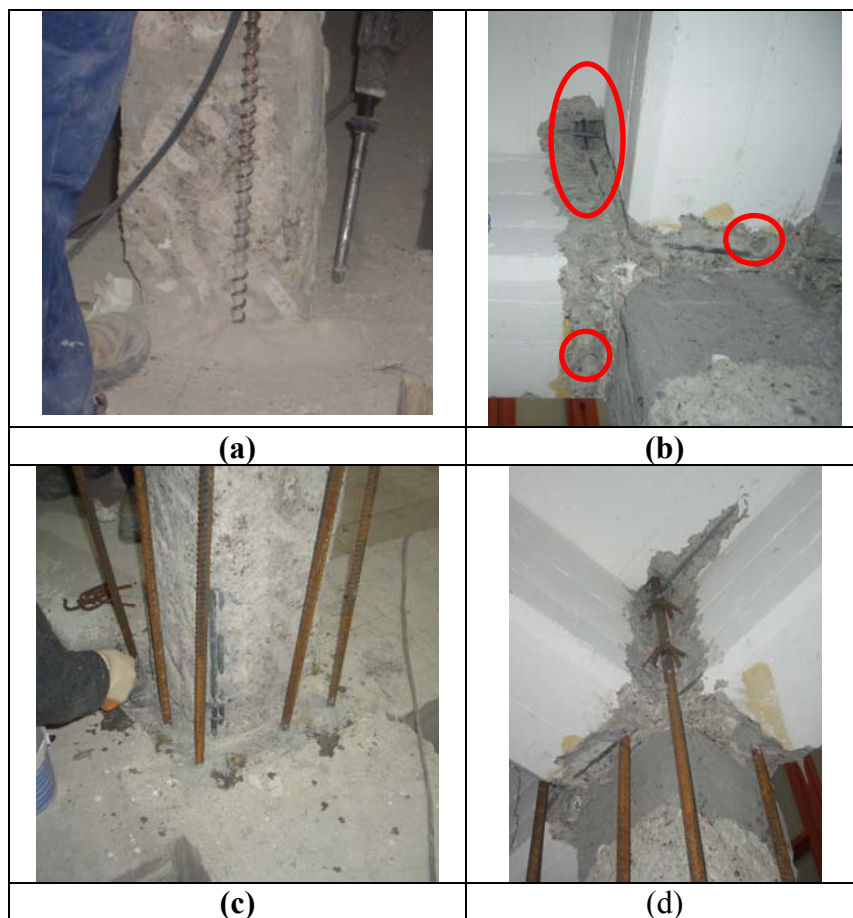


Figure 5.2-4 – Holes and longitudinal bars in correspondence of the foundation (a-c), and of the joint (b-d),

After that, added stirrups with the designed spacing were placed in correspondence of the joints where, due to the beams presence, L-shaped and C-shaped stirrups for column C4 and C1, respectively, were installed (see Figure 5.2-5).

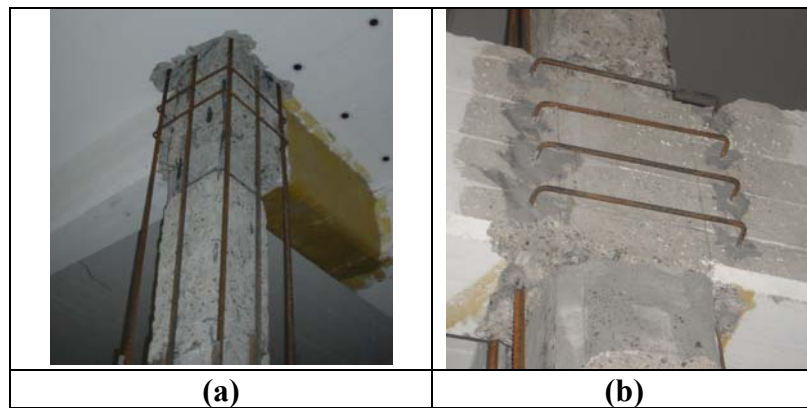


Figure 5.2-5 – Added stirrups in correspondence of joints of column C4 and C1.

Finally, once the longitudinal and transverse reinforcement was placed along each column (see Figure 5.2-6 (a) and (b)), the concrete jacket was cast in place providing the final jacketed cross-section (see Figure 5.2-6 (c)).

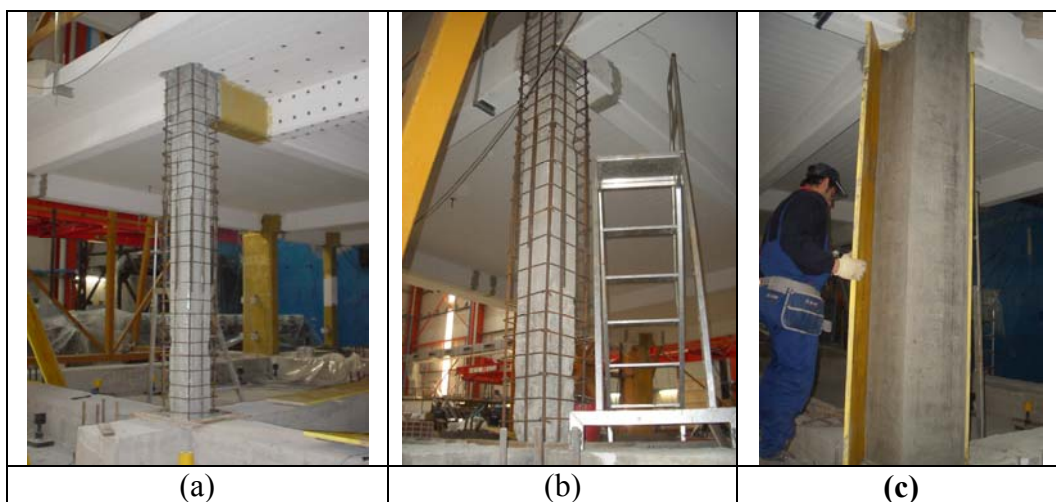


Figure 5.2-6 – Longitudinal and transverse reinforcement of column C4 (a) and C1 (b); RC jacketed column (c)

As concerns the other columns, after the laminates removing, the only intervention provided was the reconstruction of the original cross-section by using a shrinkage mortar.

5.3 EXPERIMENTAL BEHAVIOUR OF THE RC JACKETED STRUCTURE

Once the rehabilitation intervention was completed, the structure was again tested under the PGA level of 0.20g, and 0.30g. The main experimental outcomes recorded during such final rounds of tests are reported in the followings sections.

5.3.1 RC Jacketed structure: PGA = 0.20g

During the test on the RC jacketed structure at 0,20g PGA level the structure showed that the most significant damages were again detected especially in correspondence of columns ends. In particular column C3, where the axial load was maximum and thus the rotational capacity was limited, was the member with major damages mainly concentrated at the top ends of both first and second storey where a heavy concrete spalling was found; moreover, by removing the concrete cover after the test, it was observed the initiation of buckling of the longitudinal steel rebars due to the insufficient confinement provided by the stirrups (see Figure 5.3.1-1). A minor level of damage was founded at bottom end of the member (see Mola et. al., [22]).

As concern the jacketed columns, no significant damages were found on them, but some cracks were detected on the slab and beams connected to such members.

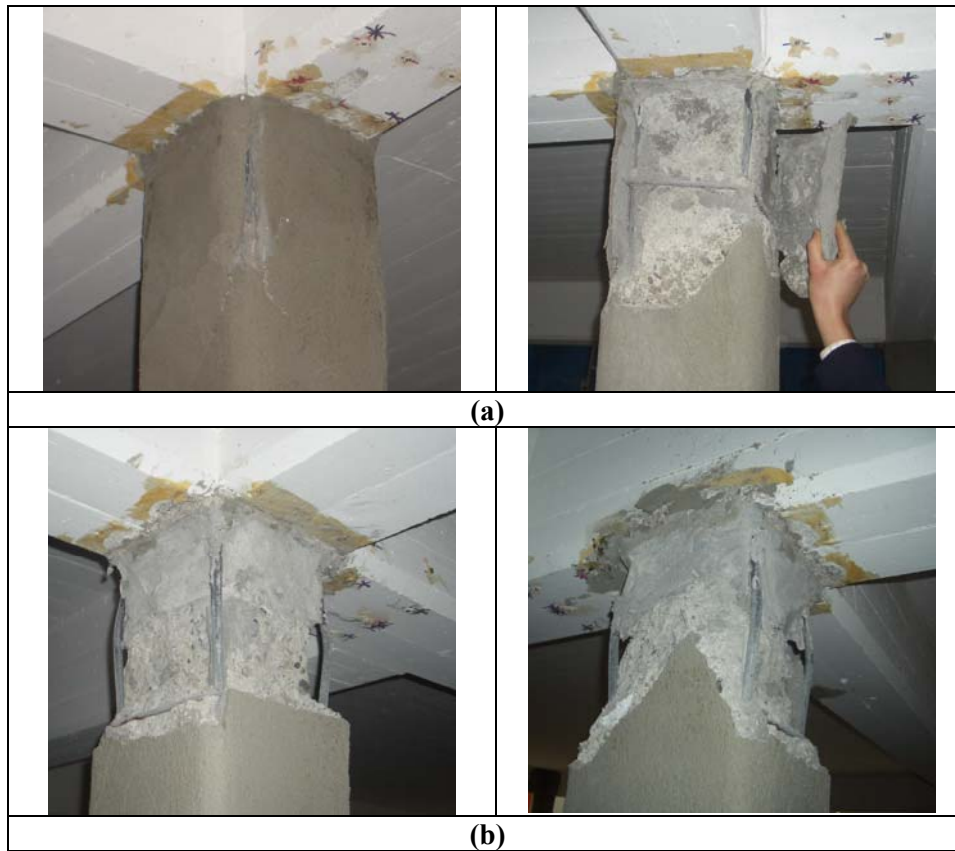


Figure 5.3.1-1 – Damages on the central column C3 at 1st (a) and 2nd storey (b)

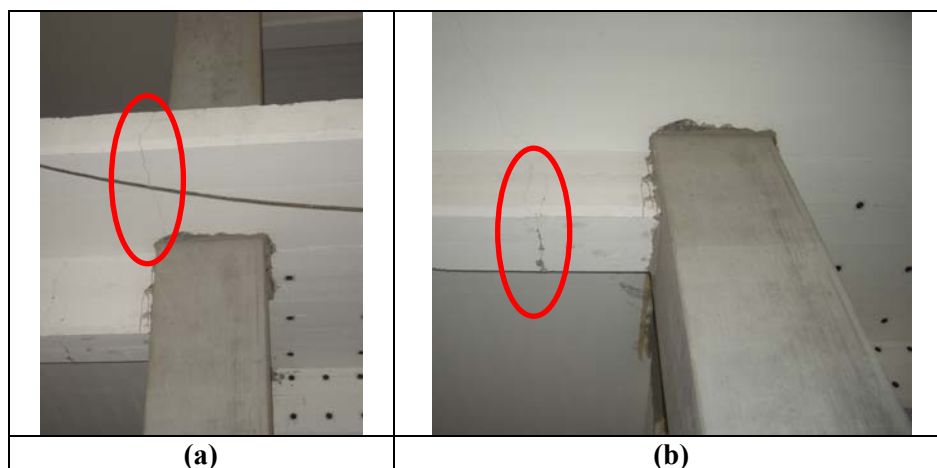


Figure 5.3.1-2 – Cracks on the slab (a) and beam (b) in proximity of column C3 at 1st storey.

In Figure 5.3.1-3, the base shear-top displacement curves related to such test for the X and Y direction are presented.

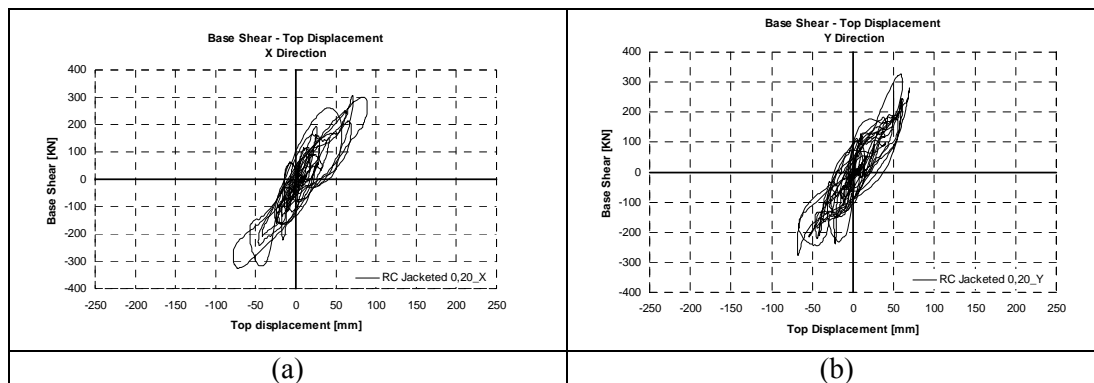


Figure 5.3.1-3– RC Jacketed structure, 0.20g: Base Shear-Top Displacement hysteresis loops; (a) X direction, (b) Y direction.

The same average slope of the two curves indicates that the rehabilitation intervention was able to strongly mitigate the stiffness difference between the X and Y direction; hence, the maximum base shear recorded along the two directions was the same and achieved a value of 325 kN. It is also noted that such maximum value of the base shear was about 25% larger than the maximum achieved on the ‘as-built’ structure (261 kN, in the Y direction) confirming that the rehabilitation intervention provided the structure with an increased global stiffness.

As a direct consequence, the maximum top displacement decreased with respect to the ‘as-built’ structure reaching 89,3 mm and 69,8 mm in the X and Y direction, respectively.

As for the energy dissipation, by totaling up the areas under the hysteretic cycles of the base shear-top displacement relationships of the two reported curves, comparable values were recorded in the two directions, 66 kJ in the X direction and 62 kJ in the Y one, equal to 52% and 48% of the total absorbed energy.

The torsional behaviour of the structure is represented in Figure 5.3.1-4 in which the base-torsion vs. top rotation is reported; the diagram shows that the maximum base torsion achieved during the test was equal to 1017 kNm and the maximum top rotation was equal to 13,66 mrad, that is much less than the value recorded on the original structure (19,91 mrad). Thus the rehabilitation intervention was able to reduce the torsional response of the structure by a factor of about 31%.

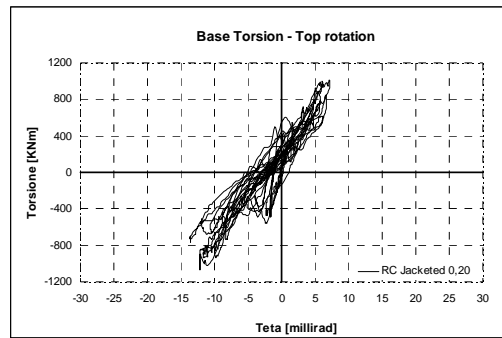


Figure 5.3.1-4 - Base Torsion-Top Rotation

A summary of the main experimental results recorded in such test are reported in Table 5.3.1-1 and Table 5.3.1-2.

DIRECTION	Total Absorbed Energy	Max Base Shear	Max Top Displ.	Level	Max I-S Shear	Max I-S Displ.
	[KJ]	[KN]	[mM]		[kN]	[mm]
X	66.00	PX: 325	PX: 78.2	1	325	33.1
		NX: 306	NX: 89.3	2	267	37.3
				3	169	20.3
Y	62.00	PY: 276	PY: 68.4	1	325	26
		NY: 325	NY: 69.8	2	256	30
				3	147	19.5

Table 5.3.1-1 – RC retrofitted structure: Experimental outcomes at 0,20g level.

	Max Base Torsion	Max Base Rotation	Level	Max I-S Torque	Max I-S Rotation
	[KNm]	[millirad]		[kNm]	[millirad]
TETA	Positive: 1012	Positive: 7.23	1	1017	4.78
	Negative: -1017	Negative: -13.66	2	805	5.96
			3	631	3.17

Table 5.3.1-2 - RC retrofitted structure: Experimental outcomes at 0,20g level

5.3.2 RC Jacketed structure PGA = 0,30g

Before starting with the last experimental test with a PGA level equal to 0,30g, considering that strong damages were already detected on the structure during the previous test, two steel columns were located in correspondence of the central column C3 so that in case of member collapse they could prevent the global collapse of the entire structure. During the execution of the test, the structural damages

became more and more evident especially on the central column C3, until even core concrete crushed and the complete member collapse was achieved.

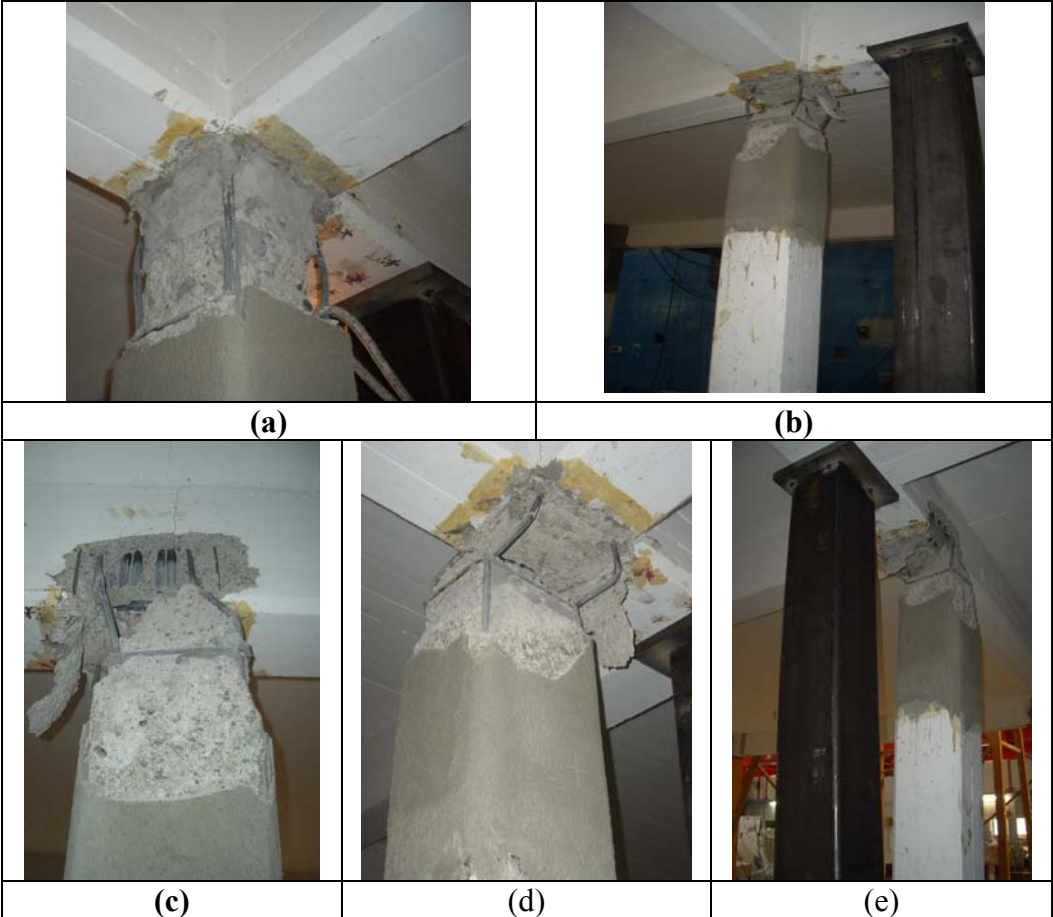


Figure 5.3.2-1 – Initial state of column C3 and its progressive damage pattern (b), (c), (d) and (e).

Immediately after the collapse of column C3, loads migrated to the nearest column C9 that showed a progressive increase of concrete spalling and buckling of longitudinal steel bars until its collapse (see Mola et. al., [21]). The progressive damages founded on such column are reported in Figure 5.3.2-2.



Figure 5.3.2-2 – Column C9 progressive damage.

At this stage, in order to avoid the complete collapse of the structure due to a soft storey mechanism, the test was interrupted. Thus, due to safety reasons, the test stopped in correspondence of 12.93 s of the accelerogram (the accelerogram original length was 15 s).

The global behaviour of the structure in terms of base shear-top displacement curves related to such test for the X and Y direction is presented in Figure 5.3.2-3.

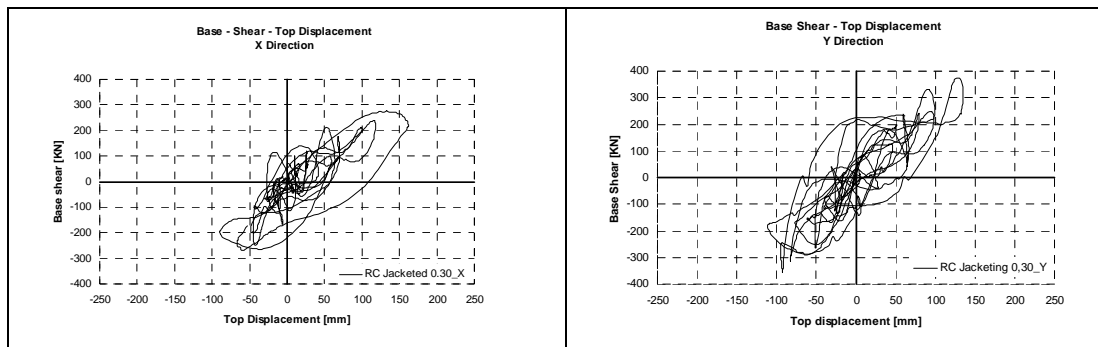


Figure 5.3.2-3– RC Jacketed structure, 0.20g: Base Shear-Top Displacement hysteresis loops; (a) X direction, (b) Y direction.

By assessing the average slope of the two curves it can be observed that the stiffness in the Y direction, during such test, was slightly greater than that recorded in the X one. In particular the maximum top displacement achieved in the Y direction (134.9 mm) resulted about 83 % of that reached in the X direction (161.6 mm).

As concerns the energy dissipation, the width of the base shear – top displacement hysteretic cycles showed that the plasticization of some members occurred inducing high values of energy adsorption: 82.5 kJ and 92.7 kJ in the X and Y direction,

respectively. It is also noted that in correspondence of such values of energy dissipation the structure was very close to the collapse while in the case of FRP strengthening the structure was able to adsorb more energy (up to 104.38 kJ in the Y direction at 0,30g PGA level) without showing any significant damage. Such consideration highlights the effectiveness of the laminates in increasing the local ductility of the member and thus the global deformation capacity of the entire structure.

The torsional behaviour of the structure is represented in Figure 5.3.2-4 in which the base-torsion vs. top rotation is reported; the diagram shows that the maximum base torsion achieved during the test was equal to 778 kNm and the maximum top rotation was equal to 23,21 mrad. However, it is noted that the base rotation was quite limited during the first stage of the test and had a strong increase when the first member starting to collapse; hence such value has to be ascribed to the formation of a structural mechanism rather than to the residual plan irregularity of the structure.

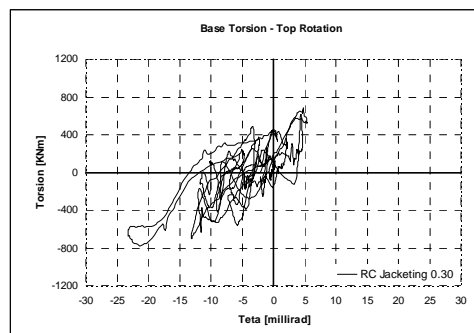


Figure 5.3.2-4 - Base Torsion-Top Rotation

Finally, with reference to the behavior of each storey of the structure, in Figure 5.3.2-5 the interstorey shears are plotted against the interstorey drifts. From the analysis of such curves, it can be noted that the maximum interstorey drifts were achieved at the second storey as observed in the ‘as-built’ structure.

The maximum interstorey drifts at the second storey were equal to 67.3 mm in the X direction and 54.9 mm in the Y one, with an increase of 14% and 29% with respect to the drifts recorded at the first storey along the two analysed direction. The comparison of the interstorey drifts of the second storey with those achieved at the third one shows a percentage increase of 85% and 6%, for X and Y direction respectively. Such data highlight that in this case, the first storey was involved in the

global mechanism almost as the second one while the third storey participated much less in the structural mechanism.

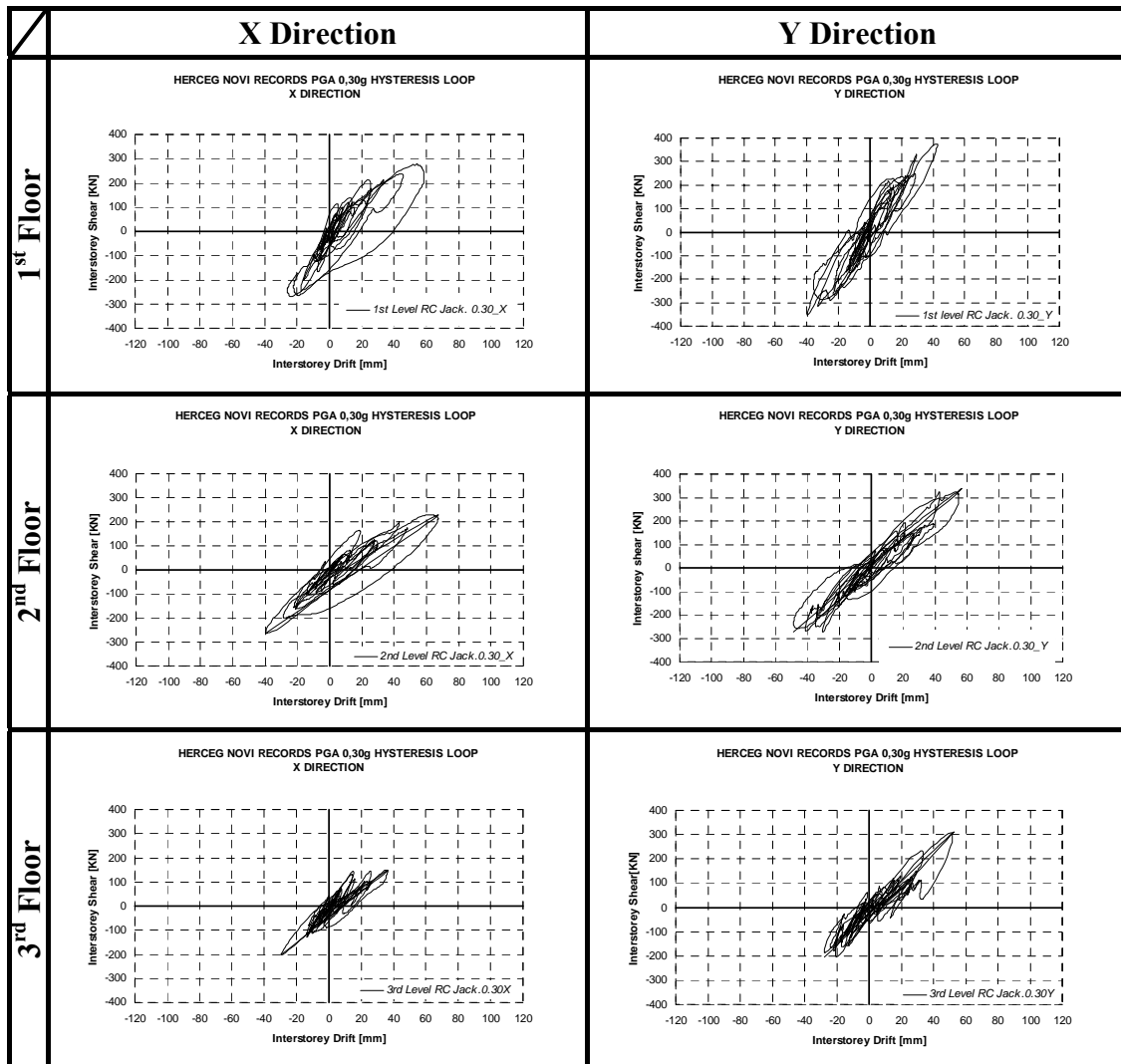


Figure 5.3.2-5 – RC Jacketed at 0,30g level: Interstorey Shear–Interstorey Drift hysteresis loops

The same trend was observed by plotting the curves related to the interstorey torque vs. the interstorey rotation (see Figure 5.3.2-6); the first and second floor were the most involved in the torsional behaviour; in particular at the second floor it was recorded a torsion increase equal to 80% with respect to the third storey.

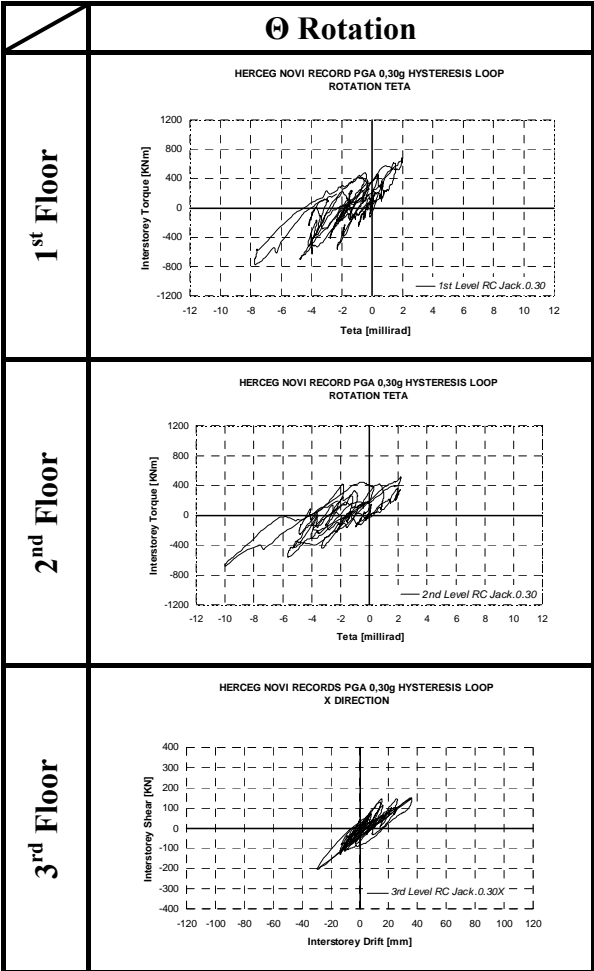


Figure 5.3.2-6 - FRP retrofitted at 0,30g level: Interstorey Torque – Rotation hysteresis loops

A summary of the main experimental results recorded during such test are reported in Table 5.3.2-1 and Table 5.3.2-2.

DIRECTION	Total Absorbed Energy	Max Base Shear	Max Top Displ.	Level	Max I-S Shear	Max I-S Displ.
	[KJ]	[KN]	[mM]		[kN]	[mm]
X	82.50	PX: 268	PX: 89.6	1	278	58.6
		NX: 278	NX: 161.6	2	263	67.3
				3	202	36.3
Y	97.7	PY: 355	PY: 111.7	1	375	42.7
				2	323	54.9
		NY: 375	NY: 134.9	3	308	52.0

Table 5.3.2-1 – RC retrofitted structure: Experimental outcomes at 0,30g level.

	Max Base Torsion	Max Base Rotation	Level	Max I-S Torque	Max I-S Rotation
	[KNm]	[millirad]		[kNm]	[millirad]
TETA	Positive: 687	Positive: 5.40	1	778	7.77
	Negative: -778	Negative: -23.21	2	688	10.03
			3	467	5.57

Table 5.3.2-2 - RC retrofitted structure: Experimental outcomes at 0,30g level

5.3.3 Theoretical vs. experimental results

The theoretical analysis was effective in predicting a strong mitigation of the torsional structural behaviour due to the reduction of the eccentricity between the stiffness and strength centre with respect to mass centre. Moreover, the experimental results confirmed the theoretical predictions indicating that the retrofit intervention, although increased both ductility and strength of the ‘as-built’ structure, was not completely able to provide the structure with the requested displacement. However, the experimental results have pointed out a damage level on the rehabilitated structure larger than that predicted by the theoretical analyses with the development of a soft storey mechanism; such divergence can be also explained considering that the full scale structure had been already tested several times before RC jacketing.

5.4 'AS-BUILT' vs. RC JACKETED: COMPARISON OF THE EXPERIMENTAL RESULTS

Both tests at 0.20g and 0.30g showed that the rotational component of the response was strongly reduced as expected according to the rehabilitation design. Such effect is clearly shown in Figure 5.4-1 in which the base-torsion vs. top rotation curve is plotted for both 'as-built' and RC jacketed structure at PGA level equal to 0.20g.

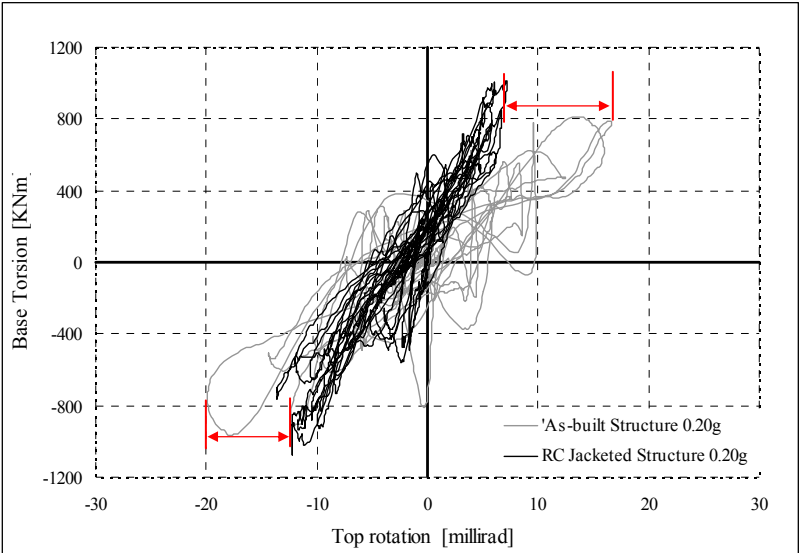


Figure 5.4-1 - Experimental Base torsion vs. top rotation: 'as-built' and RC jacketed structure at 0.20 PGA level

Furthermore, a comparison between the experimental results recorded on the 'as-built' structure and RC Jacketed one in terms of total adsorbed energy, maximum base shear and top displacement, maximum inter-storey shear and inter-storey displacement are reported in Table 5.4-1 and Table 5.4-2 for the X and Y directions, respectively.

Direction X	TEST	Total Absorbed Energy	Max Base Shear	Max Top Displ.	Level	Max I-S Shear	Max I-S Displ.
		[KJ]	[KN]	[mm]		[KN]	[mm]
	'As-Built' 0.15g	29.61	176	70.1	1	176	15.1
					2	161	36.2
					3	126	24.2
	'As-Built' 0.20g	44.00	195	105.7	1	195	24.6
					2	165	57.0
					3	112	35.8
	RC Jacketed 0.20g	66.0	325	89.3	1	325	33.1
					2	267	37.3
					3	169	20.3
RC Jacketed 0.30g	82.5	278	161.6	1	278	58.6	
				2	263	67.3	
				3	202	36.3	

Table 5.4-1– Experimental outcomes, X direction.

Direction Y	TEST	Total Absorbed Energy	Max Base Shear	Max Top Displ.	Level	Max I-S Shear	Max I-S Displ.
		[KJ]	[KN]	[mm]		[KN]	[mm]
	'As-Built' 0.15g	31.81	261	47.0	1	260	11.6
					2	235	19.9
					3	147	18.2
	'As-Built' 0.20g	65.00	276	103.1	1	276	30.6
					2	214	47.2
					3	167	32.6
	RC Jacketed 0.20g	62.0	325	69.8	1	325	26.0
					2	256	30.0
					3	147	19,5
RC Jacketed 0.30g	97.7	375	134.9	1	375	42.7	
				2	323	54.9	
				3	308	52.0	

Table 5.4-2- Experimental outcomes, Y direction.

By comparing the experimental outcomes provided by the tests on the ‘as-built’ and RC Jacketed structure, at the same PGA level equal to 0.20g, it is possible to immediately observe a very significant stiffness increase provided by the RC Jacketing of the two column C1 and C4; the maximum recorded base shear, in fact, became 325 kN in both X and Y direction against the values of 195 kN and 276 kN recorded in X direction and Y direction on the ‘as-built’ structure. As a consequence a strong difference in terms of maximum top displacement was observed; the

rehabilitated structure showed top displacements in the X and direction reduced by a factor of about 16% and 32%, respectively.

Moreover, an increase in terms of both strength and ductility was recorded even if the structure at 12.93 s of the accelerogram (the accelerogram original length was 15 s) showed the formation of a soft storey mechanism that induced to stop the test for safety reasons.

Chapter VI

6.1 COMPARISON BETWEEN LAMINATES AND RC JACKETING

The experimental activity validated the theoretical predictions and confirmed the effectiveness of the two rehabilitation methods investigated. In particular, the experimental campaign results allow underlying that FRP wrapping of the columns ends provides the structure with a very significant extra ductility if brittle failure collapses are prevented. Such result is clearly pointed out in Figure 6.1-1 where the pushover curves (up to the LSSD) referred to the NX direction are reported for the structure in each configuration.

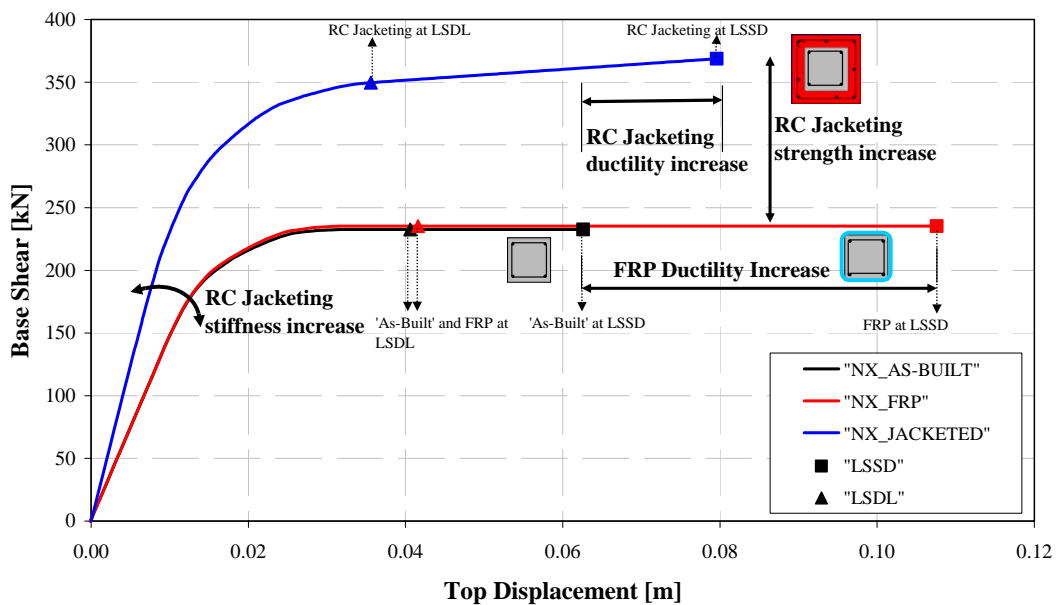


Figure 6.1-1– Pushover curves in the NX direction comparison.

The figure shows that the capacity curves of the ‘as-built’ and FRP rehabilitated structure are fitted together with the only difference of the increased plastic branch in the case of the FRP rehabilitation. The FRP column wrapping, in fact, allows strongly increasing the global ductility without affecting the global stiffness and strength of the structure. Thus, although the global displacement capacity of the structure is significantly enhanced, the seismic demand, depending by the elastic

period of the idealized bilinear system, remains substantially constant.

Moreover, such rehabilitation strategy appears very attractive for use in structural application as FRP laminates are very easy to install and effective also in the cases in which time or space restrictions exist. On the other hand, it is recognized that stiffness irregularities cannot be solved by applying FRP laminates. In such field, the columns RC jacketing intervention appears the most appropriate; such method allows minimizing the eccentricities between the centre of mass and stiffness and/or strength and thus can be used to mitigate the torsional effects due to building plan irregularities. Moreover also in the case of service condition problems the RC jacketing is more effective than FRP laminates as it induces a structural stiffness increase that reduces the elastic period of the structure and consequently the seismic demand request. Such effect is clearly pointed out in Figure 6.1-1 where it is shown that the global stiffness of the FRP rehabilitated structure is almost the same of the 'as-built' structure while it is significantly increased in the case of RC jacketed structure.

The RC jacketing intervention is also able to increase both the global strength and ductility of the structure (see Figure 6.1-1) if the added longitudinal reinforcement, placed in the jacket, passes through the beam-column joint ensuring in this way the reinforcement continuity.

As a drawback, such technique may results much more invasive and difficult from a constructability standpoint with a lengthy disruption of the function of the building and its occupants, especially in the case in which a foundation strengthening is needed. During the design, in fact, attention must be paid to the foundation systems as the increased seismic strength capacity leads to an overturning moments increase. When the intervention requires significant upgrade of the foundations its costs could become not affordable or its execution could be not doable.

6.2 CONCLUSIVE REMARKS

The doctoral thesis deals with full-scale tests of an under-designed RC structure retrofitted with two different techniques: FRP wrapping of columns and joints and RC jacketing of selected vertical elements. The rehabilitation strategies and criteria followed to improve the seismic performance of the structure were presented and discussed. Theoretical pushover analyses were conducted on both the retrofitted configurations in order to predict the seismic structural behaviour. By the experimental activity conducted on the structure in the three configurations it is possible to point out the following main conclusions:

- FRP laminates intervention (by columns ends wrapping and preventing brittle mechanisms) is a ductility based rehabilitation system: it provided a ductility increase equal to about 123% without varying the structural hierarchy of strength and the elastic period of the structure; it does not affect the torsional behaviour of the structure;
- RC jacketing intervention is a strength-ductility based rehabilitation system: it provided a ductility increase equal to about 76% and a strength increase equal to about 43% with an elastic period decrease of about 25%; it allowed reducing the torsional behaviour of the structure by a factor of about 56%
- FRP laminates intervention allowed the structure withstanding a level of excitation, in two directions, 1.5 times higher than that applied to the ‘as built’ structure without exhibiting significant damage or structural deterioration.
- the RC jacketing rehabilitation scheme was strongly effective in mitigating the torsional effects and increasing the seismic performance of the ‘as-built’ structure especially with regard to the damage limit state; on the other hand such intervention resulted insufficient to fully satisfy the seismic demand in terms of significant damage limitation limit state;

Seismic code provisions, theoretical assumption in the modelling of the structure and for the design of the rehabilitation were validated by the experimental activity

conducted on the full-scale structure, such validation provides the opportunity of selecting the most appropriate technique for the seismic retrofit of existing RC frames using either composite materials or traditional techniques.

REFERENCES

- [1] Legge 2/2/74, Provvedimenti per le costruzioni con particolari prescrizioni per le zone sismiche.

- [2] Ordinanza n. 3431, 3 maggio 2005, Ulteriori modifiche ed integrazioni all'ordinanza del Presidente del Consiglio dei Ministri n. 3274 del 20 marzo 2003, recante "Primi elementi in materia di criteri generali per la classificazione sismica del territorio nazionale e di normative tecniche per le costruzioni in zona sismica

- [3] EN 1998-1, 2003, Final Draft of Eurocode 8 "Design of Structures for Earthquake Resistance – Part 1: General rules, seismic actions and rules for buildings, European Committee for Standardization, Brussels.

- [4] Molina, F.J., Verzeletti, G., Magonette, G., Buchet, Ph., Geradin, M., "Bi-directional pseudodynamic test of a full-size three-storey building", *Earthquake Engineering and Structural Dynamic*, 28, 1999.

- [5] Molina, F. J., Buchet, Ph., Magonette, G.E., Hubert, O., Negro, P., "Bidirectional pseudodynamic technique for testing a three-storey reinforced concrete building", *Proc. of 13th World Conference on Earthquake Engineering*, Paper N. 75, 1-6 August 2004, Vancouver, Canada.

- [6] Jeong S.-H., Elnashi A.S., "Analytical assessment of an irregular RC frame for full-scale 3D pseudo-dynamic testing-Part II: Condition Assessment and test deployment", *Journal of Earthquake Engineering*, Vol. 9, No. 1, pp. 95- 128, 2005.

- [7] Jeong S.-H., Elnashi A.S., “Analytical assessment of an irregular RC frame for full-scale 3D pseudo-dynamic testing-Part I: Analytical model verification”, *Journal of Earthquake Engineering*, Vol. 9, No. 1, pp. 95- 128, 2005.
- [8] Fajfar P., Dolsek M., Marusic D., Stratan A., “Pre- and post-test mathematical modeling of the SPEAR building”, *Proc. of SPEAR (Seismic Performance Assessment and Rehabilitation) International Workshop*, 4-5 April 2005, Ispra, Italy, EU Publications office 2005.
- [9] Manuale SAP2000 versione 7.1, pubblicato da Computers and Structures Inc., traduzione di Brunetta e Perin Engineering Srl [2000].
- [10] Fardis, M.N., “Analysis and Design of Reinforced Concrete Buildings according to Eurocode 2 and 8”, Configuration 3, 5 and 6, Reports on Prenormative Research in Support of Eurocode 8, 1994.
- [11] Verderame, G., “Analisi sismica di edifici in C.A. progettati per carichi gravitazionali,” *PhD. Thesis*, XII ciclo, 1999.
- [12] European Standard, EN 1998-3, 2003, Eurocode 8, “Design of Structures for Earthquake Resistance” *Part 3: Strengthening and Repair of buildings*, Doc CEN/TC250/SC8/N343, Draft No. 3, January 2003
- [13] FEMA 356, 2000, Prestandard and Commentary for the Seismic Rehabilitation of Buildings, Federal Emergency Management Agency, Washington D.C:
- [14] Fajfar, P., “A Nonlinear Analysis Method for Performance Based Seismic Design”, *Earthquake Spectra*, Vol. 16, No. 3, pp.573-592, August 2000.
- [15] Sugano, S. “State-of-the-art in Techniques for Rehabilitation of Buildings”, *Proceedings of the Eleventh World Conference on Earthquake Engineering*, Acapulco, Mexico, June 23-28, 1996, <paper N. 2175.

- [16] CNR-DT 200/2004. Istruzioni per la Progettazione, l'Esecuzione ed il Controllo di Interventi di Consolidamenti di Intervento Statico mediante l'utilizzo di Compositi Fibrorinforzati.
- [17] Antonopoulos C.P., Triantafillou T.C., "Analysis of FRP-Strengthened RC Beam-Column Joints", *ASCE Journal of Composites for Construction*, Vol. 6, No. 1, pp. 41-51, 2002.
- [18] Balsamo A., Manfredi G., Mola E., Negro P. and Prota A. Seismic Rehabilitation of a Full-scale Structure using GFRP Laminates. *ACI Structural Journal*, Special Publication, Vol. 230, pp. 1325-1344, October 1, 2005.
- [19] Rutenberg A. Behaviour of irregular and complex structures, asymmetric structures. Proc. of 12th European Conference on Earthquake Engineering, Paper n. 832, London, 2002.
- [20] *Fib Bulletin* 24, Task Group 7.1. Seismic Assessment and Retrofit of Reinforced Concrete Buildings. May, 2003.
- [21] Kosmopoulos A., Fardis N. Conceptual design and evaluation of alternative drastic retrofitting schemes of the SPEAR 3-storey test structure. *Spear Report*, 2004.
- [22] Mola E., Negro P. Full scale PsD testing of the torsionally unbalanced SPEAR structure in the 'as-built' and retrofitted configurations. Proc. of the SPEAR International Workshop, Ispra, Italy, 4-5 April, 2005.

A. APPENDIX A: Beam Reinforcement details

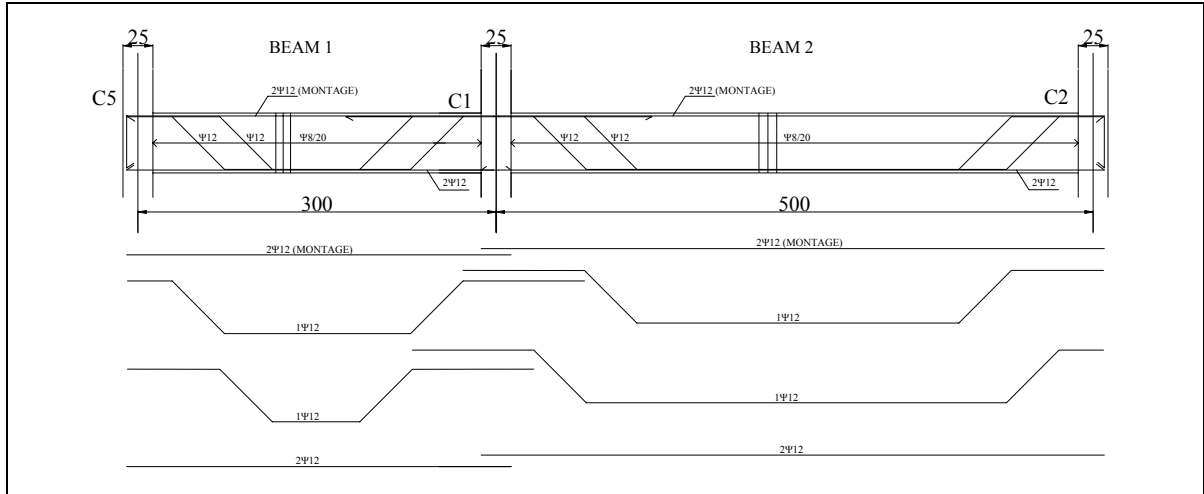


Figure A-1 –Beam 1 and beam 2 longitudinal reinforcement

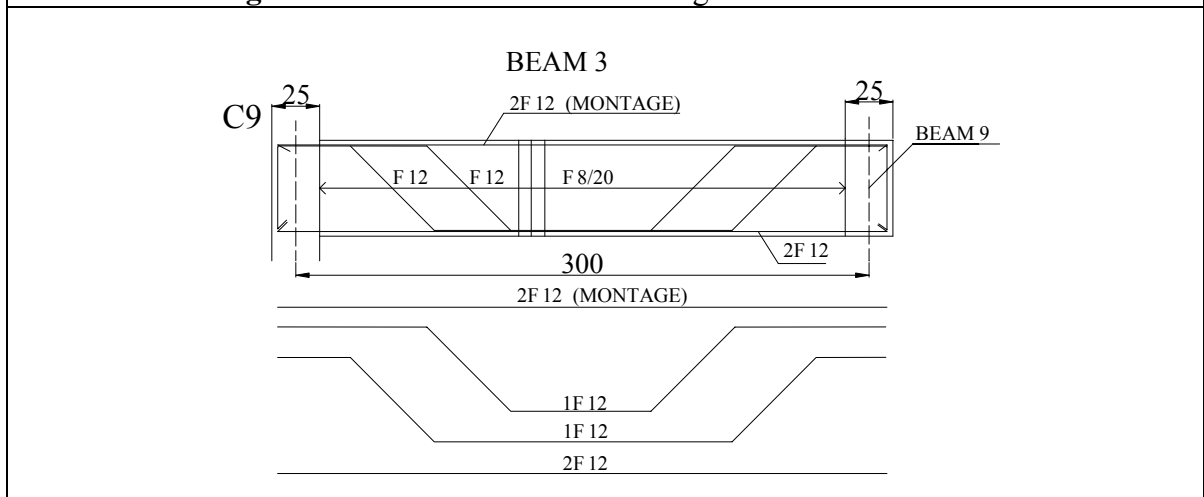


Figure A-2 - Beam 3 longitudinal reinforcement

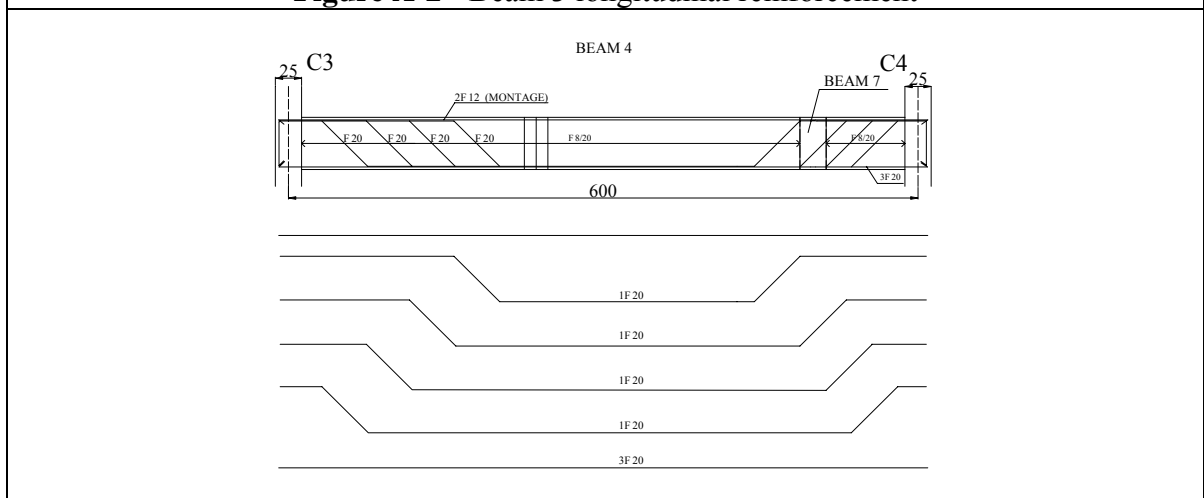


Figure A-3 - Beam 4 longitudinal reinforcement

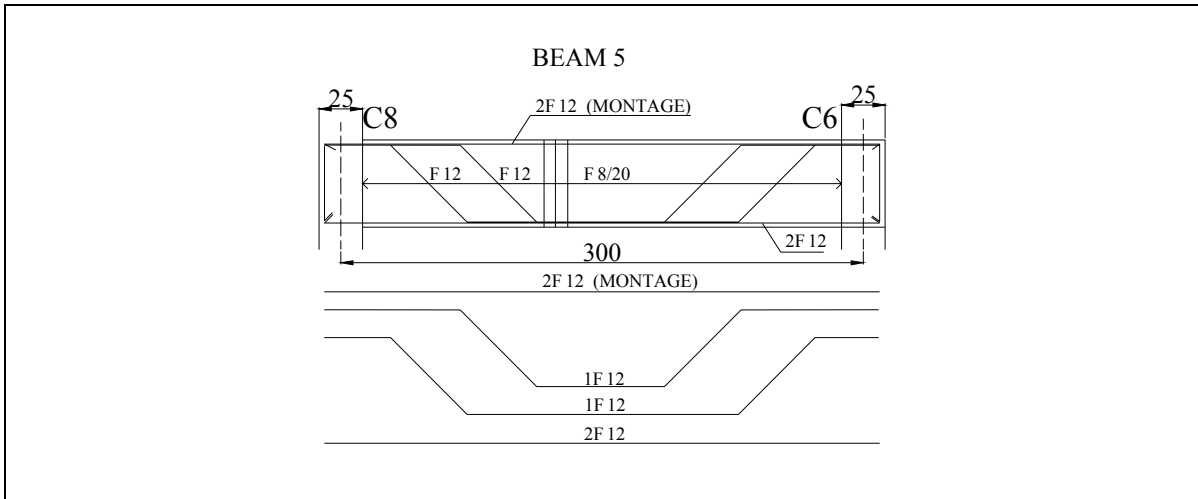


Figure A-4 - Beam 5 longitudinal reinforcement

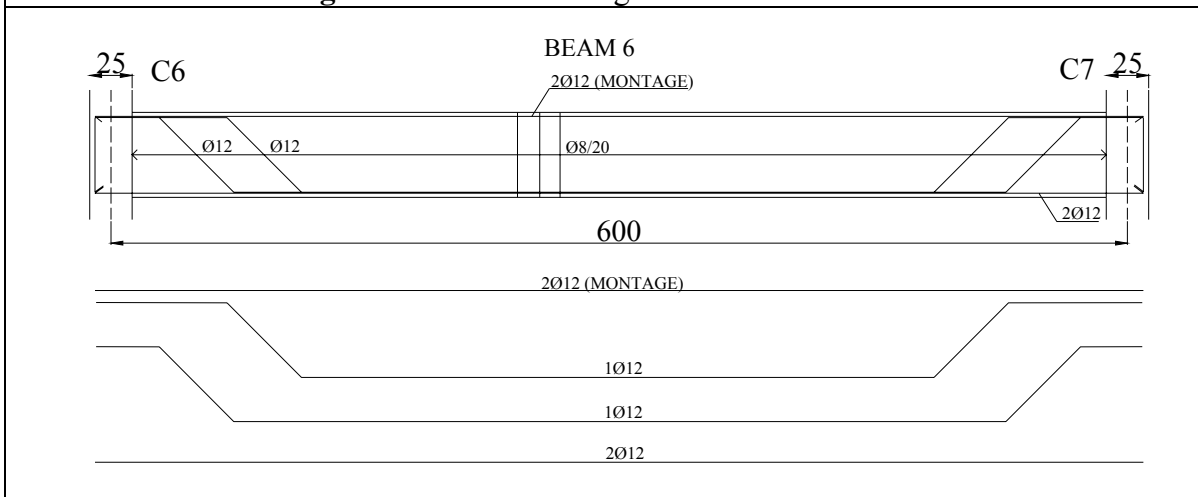


Figure A-5 - Beam 6 longitudinal reinforcement

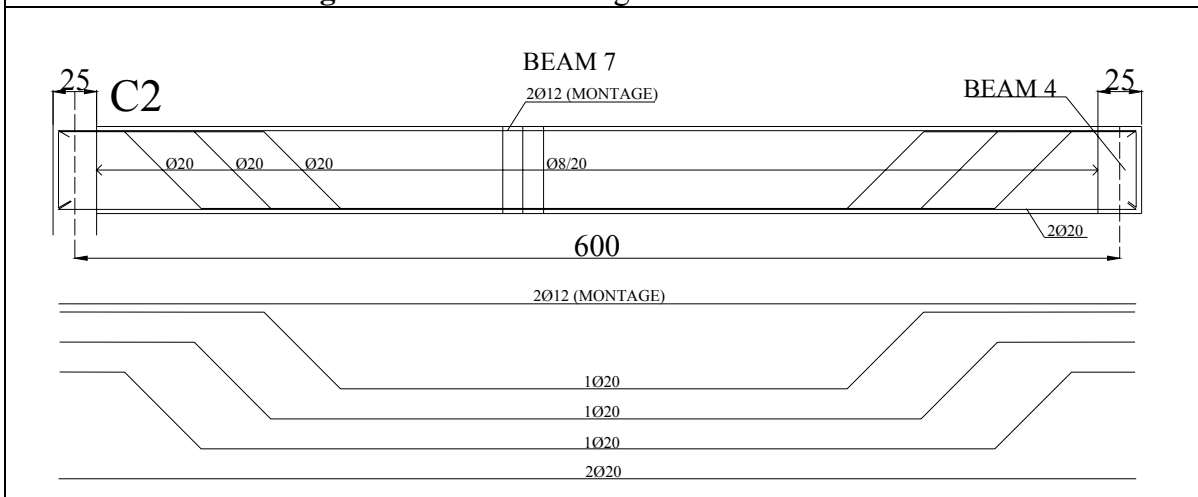


Figure A-6 - Beam 7 longitudinal reinforcement

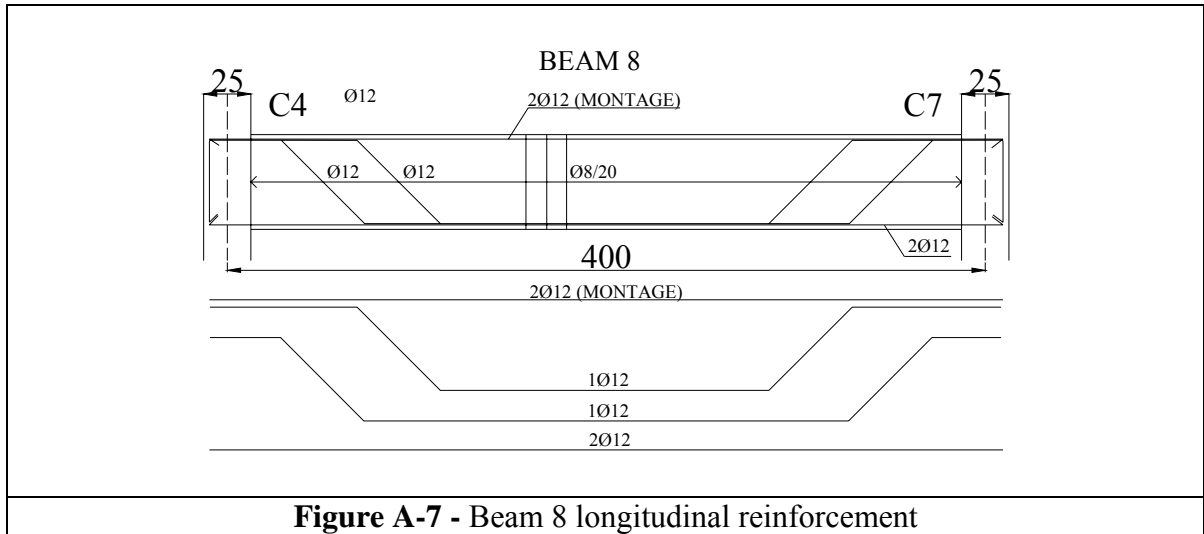


Figure A-7 - Beam 8 longitudinal reinforcement

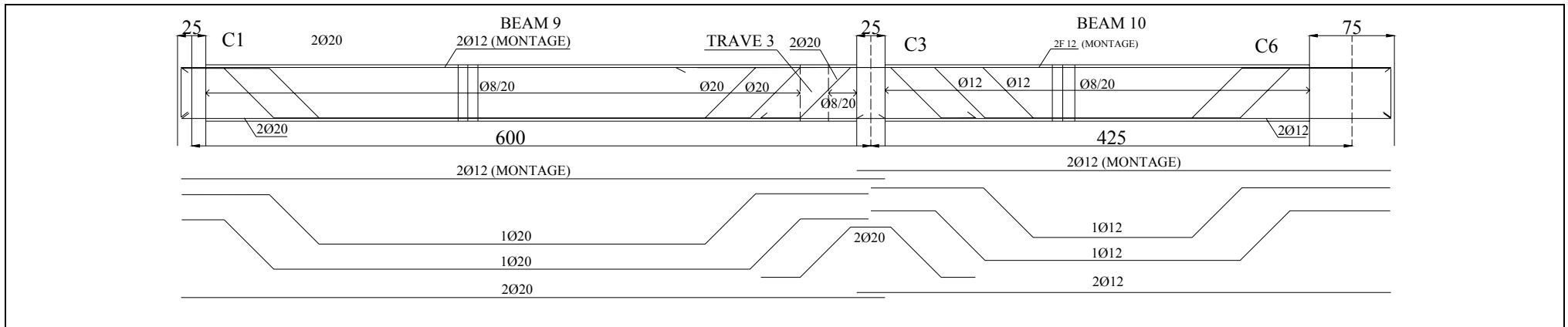


Figure A-8- Beam 9 and beam 10 longitudinal reinforcement

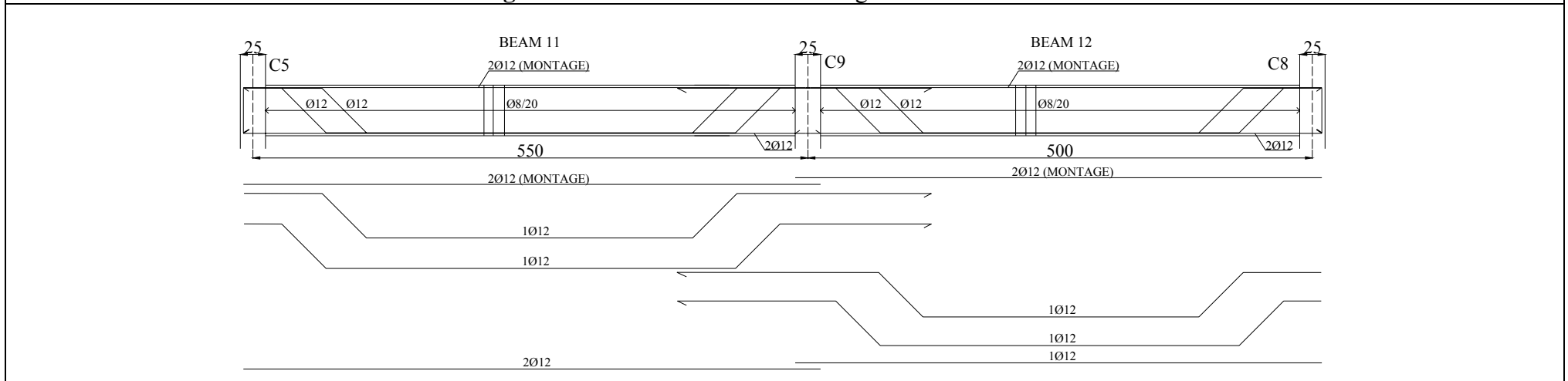


Figure A-9 - Beam 11 and beam 12 longitudinal reinforcement

B. APPENDIX B: Plastic Hinges Characterization

COLUMN	N [KN]
C1_1	-234,03
C1_2	-154,31
C1_3	-74,73
C2_1	-233,06
C2_2	-154,09
C2_3	-72,74
C3_1	-409,48
C3_2	-264,96
C3_3	-129,95
C4_1	-327,75
C4_2	-215,82
C4_3	-104,34
C5_1	-87,48
C5_2	-59,10
C5_3	-28,01
C6_1	-274,43
C6_2	-185,05
C6_3	-90,73
C7_1	-138,17
C7_2	-91,52
C7_3	-43,36
C8_1	-67,14
C8_2	-44,28
C8_3	-20,06
C9_1	-183,69
C9_2	-122,25
C9_3	-59,28

Table B-1- Axial load values for each column at each storey due to gravity loads

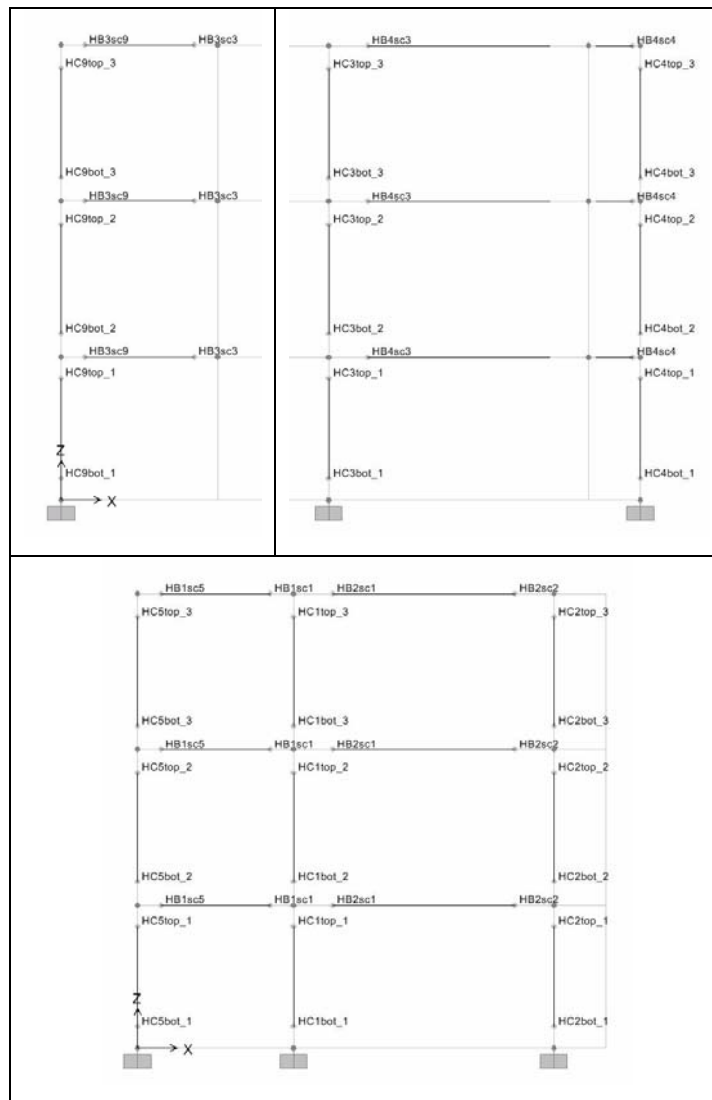


Figure B-1-Plane frame section, direction X.

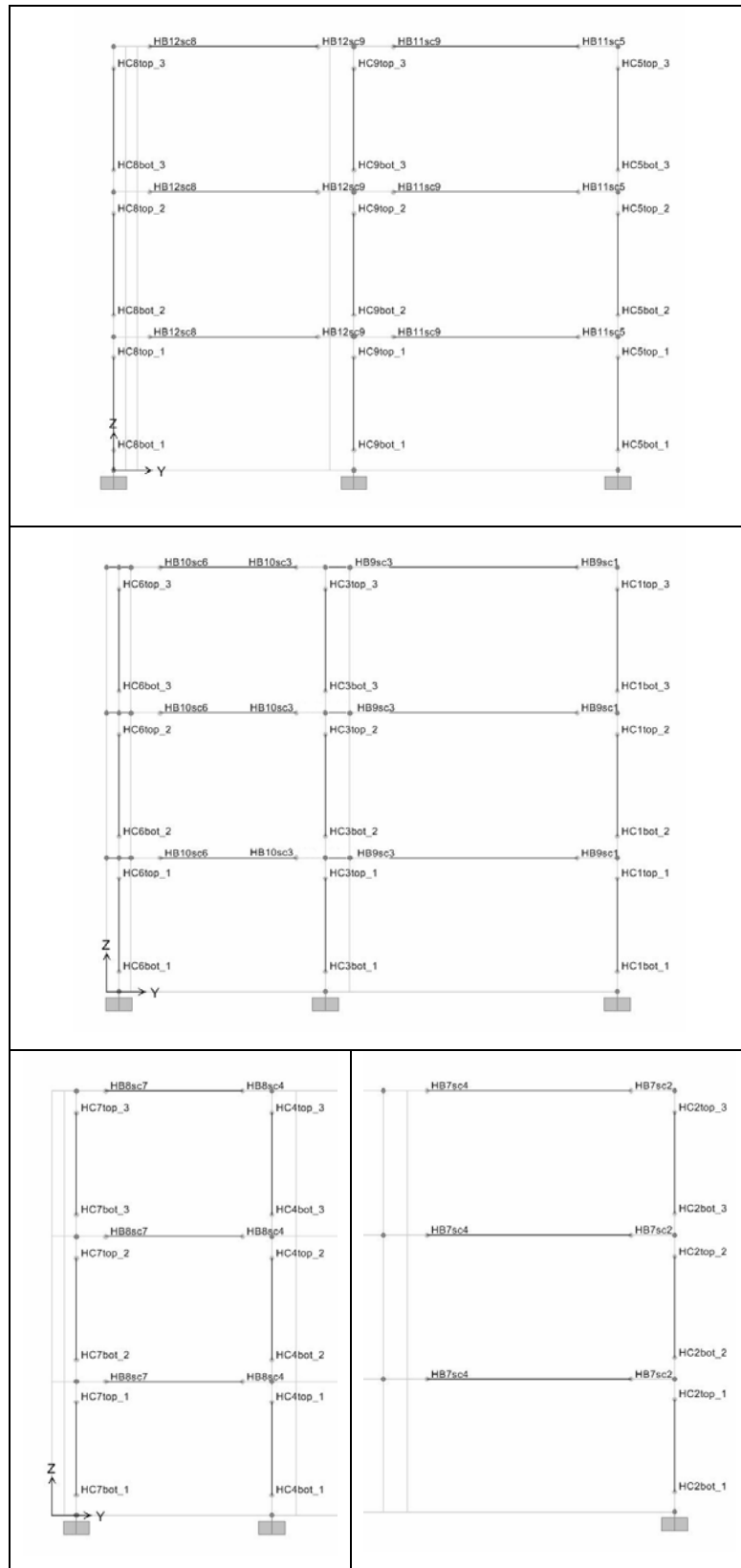


Figure B-2- Plane frame section, direction Y.

HINGE	b [mm]	h [mm]	N [KN]	M_y^+ [KNm]	M_y^- [KNm]	M_u^+ [KNm]	M_u^- [KNm]	θ_y^+ [rad]	θ_y^- [rad]	θ_u^+ [rad]	θ_u^- [rad]
HB1sc5	250	500	0	32,17	62,95	34,09	66,21	0,0042	0,0044	0,0235	0,0238
HB1sc1	250	500	0	32,19	93,06	34,16	98,32	0,0042	0,0046	0,0236	0,0242
HB2sc1	250	500	0	32,19	93,06	34,16	98,32	0,0052	0,0058	0,0303	0,0312
HB2sc2	250	500	0	32,17	62,95	34,09	66,21	0,0053	0,0056	0,0302	0,0306
HB3sc9	250	500	0	32,17	62,95	34,09	66,21	0,0042	0,0044	0,0235	0,0238
HB3sc3	250	500	0	32,17	62,95	34,09	66,21	0,0042	0,0044	0,0235	0,0238
HB4sc3	250	500	0	130,7	199,9	135,3	211,3	0,0066	0,0073	0,0383	0,0324
HB4sc4	250	500	0	130,7	199,9	135,3	211,3	0,0066	0,0073	0,0383	0,0324
HB5sc8	250	500	0	32,17	62,95	34,09	66,21	0,0042	0,0044	0,0235	0,0238
HB5sc6	250	500	0	32,17	62,95	34,09	66,21	0,0042	0,0044	0,0235	0,0238
HB6sc6	250	500	0	32,17	62,95	34,09	66,21	0,0058	0,0062	0,0335	0,0340
HB6sc7	250	500	0	32,17	62,95	34,09	66,21	0,0058	0,0062	0,0335	0,0340
HB7sc2	250	500	0	87,8	158	91,06	167,2	0,0064	0,0071	0,0376	0,0331
HB7sc4	250	500	0	87,8	158	91,06	167,2	0,0064	0,0071	0,0376	0,0331
HB8sc4	250	500	0	32,17	62,95	34,09	66,21	0,0047	0,0050	0,0269	0,0273
HB8sc7	250	500	0	32,17	62,95	34,09	66,21	0,0047	0,0050	0,0269	0,0273
HB9sc1	250	500	0	87,46	117,3	91,07	123,1	0,0064	0,0067	0,0371	0,0376
HB9sc3	250	500	0	88,05	198	91,05	210,8	0,0063	0,0074	0,0379	0,0281
HB10sc3	250	500	0	32,2	115,9	34,2	123	0,0048	0,0055	0,0297	0,0268
HB10sc6	250	500	0	32,17	62,95	34,09	66,21	0,0047	0,0050	0,0269	0,0273
HB11sc5	250	500	0	32,17	62,95	34,09	66,21	0,0055	0,0059	0,0319	0,0323
HB11sc9	250	500	0	32,19	93,06	34,16	98,32	0,0055	0,0061	0,0319	0,0329
HB12sc9	250	500	0	32,19	93,06	34,16	98,32	0,0052	0,0058	0,0303	0,0312
HB12sc8	250	500	0	32,17	62,95	34,09	66,21	0,0053	0,0056	0,0302	0,0306

Table B-2- Beams plastic hinge moments and rotations values

HINGE	b [mm]	h [mm]	N [KN]	M_y [KNm]	M_u [KNm]	θ_y [rad]	θ_u [rad]
HC1bot._1	250	250	-234,03	35,13	38,4	0,0084	0,0184
HC1top._1	250	250	-229,98	34,82	38,04	0,0084	0,0185
HC1bot._2	250	250	-154,31	28,66	31,13	0,0083	0,0234
HC1top._2	250	250	-149,89	28,29	30,17	0,0082	0,0236
HC1bot._3	250	250	-74,73	21,68	23,49	0,0076	0,0289
HC1top._3	250	250	-70,31	21,28	23,05	0,0076	0,0293
HC2bot._1	250	250	-233,06	35,06	38,31	0,0084	0,0184
HC2top._1	250	250	-229,01	34,74	37,96	0,0084	0,0186
HC2bot._2	250	250	-154,09	28,64	31,11	0,0083	0,0234
HC2top._2	250	250	-149,67	28,27	30,69	0,0082	0,0236
HC2bot._3	250	250	-72,74	21,5	23,29	0,0076	0,0291
HC2top._3	250	250	-68,32	21,1	22,86	0,0076	0,0294
HC3bot._1	250	250	-409,48	47,73	51,14	0,0097	0,0125
HC3top._1	250	250	-405,43	47,46	50,9	0,0096	0,0126
HC3bot._2	250	250	-264,96	37,52	41,07	0,0091	0,0180
HC3top._2	250	250	-260,54	32,95	35,95	0,0087	0,0205
HC3bot._3	250	250	-129,95	26,58	28,82	0,0081	0,0249
HC3top._3	250	250	-125,53	26,2	28,4	0,0081	0,0252
HC4bot._1	250	250	-327,75	42,14	45,88	0,0091	0,0146
HC4top._1	250	250	-323,70	41,85	45,59	0,0090	0,0148
HC4bot._2	250	250	-215,82	33,7	36,78	0,0087	0,0201
HC4top._2	250	250	-211,40	33,34	36,39	0,0087	0,0203
HC4bot._3	250	250	-104,34	24,34	26,36	0,0079	0,0267
HC4top._3	250	250	-99,92	23,95	25,93	0,0078	0,0270
HC5bot._1	250	250	-87,48	22,84	24,73	0,0074	0,0267
HC5top._1	250	250	-83,43	22,47	24,33	0,0073	0,0270
HC5bot._2	250	250	-59,10	20,25	21,96	0,0075	0,0302
HC5top._2	250	250	-54,69	19,84	21,53	0,0075	0,0306
HC5bot._3	250	250	-28,01	17,13	18,9	0,0072	0,0329
HC5top._3	250	250	-23,59	16,89	18,47	0,0072	0,0333
HC6bot._1	250	750	-274,43	172,1	217,5	0,0040	0,0125
HC6top._1	250	750	-259,11	168	212,8	0,0040	0,0129
HC6bot._2	250	750	-185,05	148,2	189,5	0,0040	0,0159
HC6top._2	250	750	-168,34	143,7	184,1	0,0040	0,0167
HC6bot._3	250	750	-90,73	122,1	158,3	0,0039	0,0175
HC6top._3	250	750	-74,02	117,4	152,6	0,0039	0,0174
HC6bot._1	750	250	-274,43	58,52	68,49	0,0073	0,0262
HC6top._1	750	250	-259,11	57,16	67	0,0073	0,0267
HC6bot._2	750	250	-185,05	50,48	59,73	0,0075	0,0303
HC6top._2	750	250	-168,34	48,95	58,08	0,0074	0,0309
HC6bot._3	750	250	-90,73	41,71	50,38	0,0072	0,0337
HC6top._3	750	250	-74,02	40,12	48,72	0,0071	0,0344
HC7bot._1	250	250	-138,17	27,29	29,6	0,0077	0,0233
HC7top._1	250	250	-134,12	26,94	29,22	0,0077	0,0236
HC7bot._2	250	250	-91,52	23,2	25,12	0,0078	0,0276

HC7top._2	250	250	-87,10	22,81	24,49	0,0077	0,0280
HC7bot._3	250	250	-43,36	18,77	20,41	0,0074	0,0315
HC7top._3	250	250	-38,94	18,36	19,98	0,0073	0,0319
HC8bot._1	250	250	-67,14	20,99	22,74	0,0072	0,0283
HC8top._1	250	250	-63,09	20,62	22,35	0,0072	0,0286
HC8bot._2	250	250	-44,28	18,86	20,5	0,0074	0,0314
HC8top._2	250	250	-39,86	18,44	20,07	0,0074	0,0318
HC8bot._3	250	250	-20,06	16,55	18,12	0,0072	0,0336
HC8top._3	250	250	-15,65	16,12	17,69	0,0071	0,0340
HC9bot._1	250	250	-183,69	31,1	33,86	0,0080	0,0207
HC9top._1	250	250	-179,64	30,77	33,49	0,0080	0,0209
HC9bot._2	250	250	-122,25	25,91	28,08	0,0080	0,0254
HC9top._2	250	250	-117,83	25,53	27,66	0,0080	0,0257
HC9bot._3	250	250	-59,28	20,26	21,98	0,0075	0,0302
HC9top._3	250	250	-54,87	19,85	21,54	0,0075	0,0305

Table B-3- Columns plastic hinge moments and rotations values

C. APPENDIX C: Pushover curves for a constant distribution of lateral loads

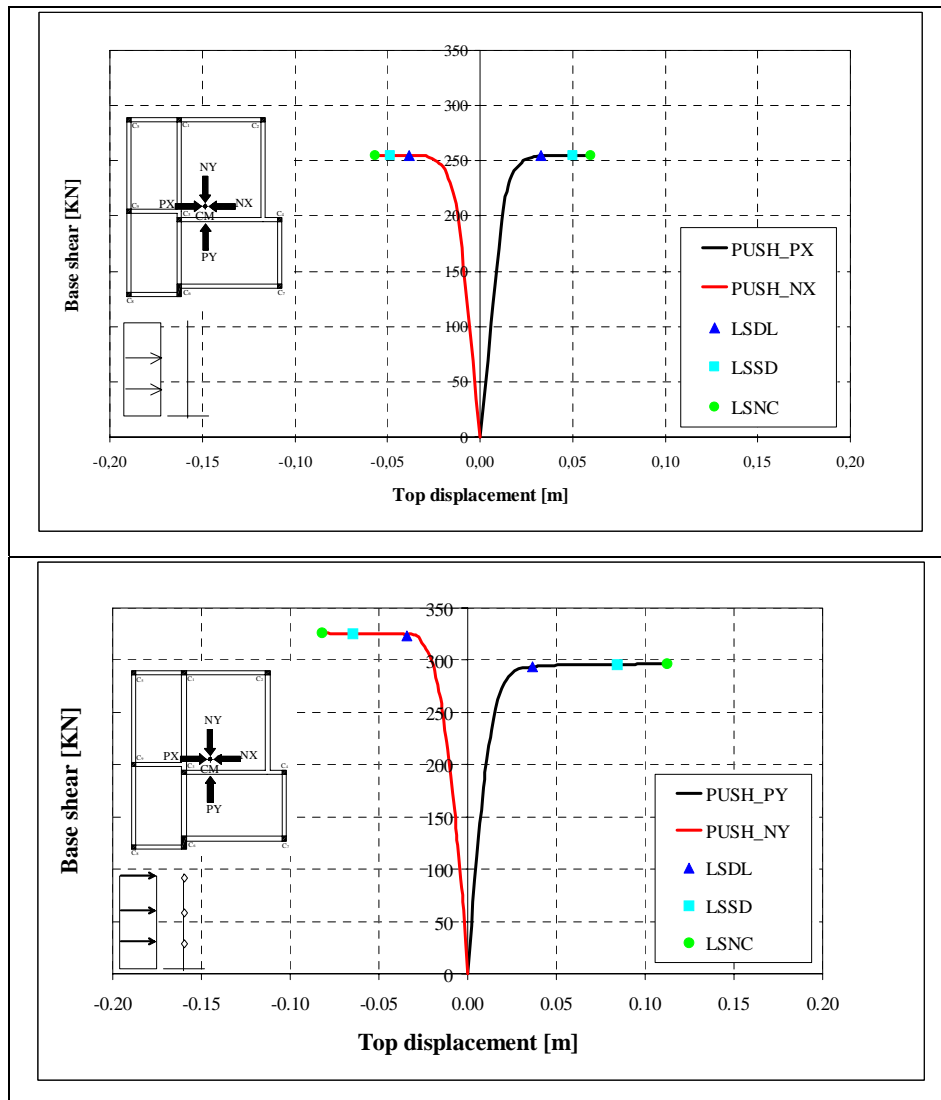


Figure C-1- Pushover curves in positive and negative X and Y direction.

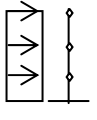
		CONSTANT LATERAL FORCE DISTRIBUTION							
		θ [rad]	MEMBER	F_{max} [KN]	d_{max} [m]	d_i [m]	h [m]	$I-D=d_i-d_{i-1}$ [m]	$\xi=I-D/h$
PUSH_PX	LSDL	B3_1	254,58	0,0329	0,0180	2,75	0,0180	0,007	
					0,0297	3,00	0,0117	0,004	
					0,0329	3,00	0,0032	0,001	
	LSSD	C3_1	254,85	0,0497	0,0344	2,75	0,0344	0,013	
					0,0465	3,00	0,0121	0,004	
					0,0497	3,00	0,0032	0,001	
	LSNC	C3_1	254,85	0,0585	0,0432	2,75	0,0432	0,016	
					0,0553	3,00	0,0121	0,004	
					0,0585	3,00	0,0032	0,001	
PUSH_NX	LSDL	C5_1	254,88	0,0373	-0,0238	2,75	-0,0238	-0,009	
					-0,0343	3,00	-0,0106	-0,004	
					-0,0373	3,00	-0,0030	-0,001	
	LSSD	C3_1	254,88	0,0469	-0,0334	2,75	-0,0334	-0,012	
					-0,0439	3,00	-0,0106	-0,004	
					-0,0469	3,00	-0,0030	-0,001	
	LSNC	C3_1	254,88	0,0557	-0,0422	2,75	-0,0422	-0,015	
					-0,0527	3,00	-0,0106	-0,004	
					-0,0557	3,00	-0,0030	-0,001	

Table C-1- Summary of the results in terms of capacity (direction X)

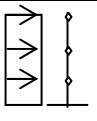
		CONSTANT LATERAL FORCE DISTRIBUTION							
		θ [rad]	MEMBER	F_{max} [KN]	d_{max} [m]	d_i [m]	h [m]	$I-D=d_i-d_{i-1}$ [m]	$\xi=I-D/h$
PUSH_PY	LSDL	B10_1	293,66	0,0361	0,0129	2,75	0,0129	0,005	
					0,0266	3,00	0,0137	0,005	
					0,0361	3,00	0,0095	0,003	
	LSSD	C6_1	295,89	0,0845	0,0283	2,75	0,0283	0,010	
					0,0587	3,00	0,0303	0,010	
					0,0845	3,00	0,0258	0,009	
	LSNC	C6_1	296,48	0,1113	0,0368	2,75	0,0368	0,013	
					0,0763	3,00	0,0395	0,013	
					0,1113	3,00	0,0350	0,012	
PUSH_NY	LSDL	C6_1	323,58	0,0334	-0,0136	2,75	-0,0136	-0,005	
					-0,0270	3,00	-0,0134	-0,004	
					-0,0334	3,00	-0,0063	-0,002	
	LSSD	C6_1	325,45	0,0634	-0,0279	2,75	-0,0279	-0,010	
					-0,0570	3,00	-0,0291	-0,010	
					-0,0634	3,00	-0,0064	-0,002	
	LSNC	C6_1	325,72	0,0814	-0,0365	2,75	-0,0365	-0,013	
					-0,0750	3,00	-0,0384	-0,013	
					-0,0814	3,00	-0,0064	-0,002	

Table C-2- Summary of the results in terms of capacity (direction Y)

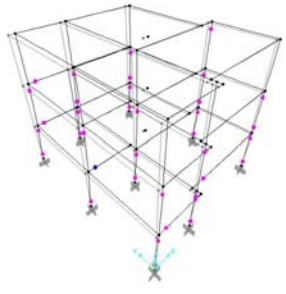
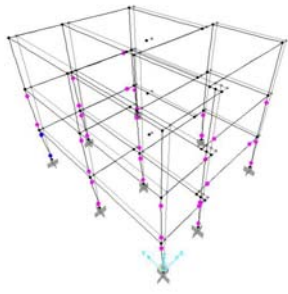
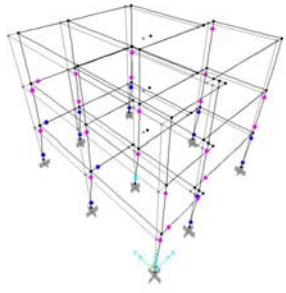
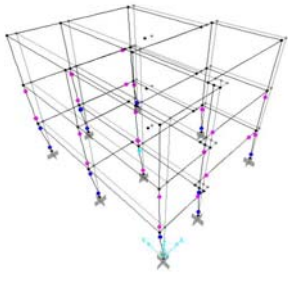
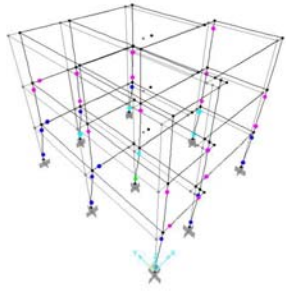
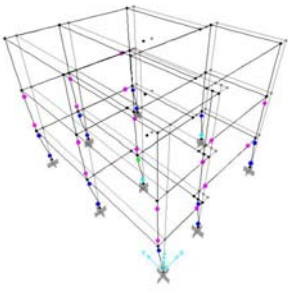
		CONSTANT LATERAL FORCE DISTRIBUTION	
		PUSHOVER_PX	PUSHOVER_NX
LSD	LSDL		
	LSSD		
	LSNC		

Figure C-2 – Plastic hinges distribution (constant lateral loads, direction X)

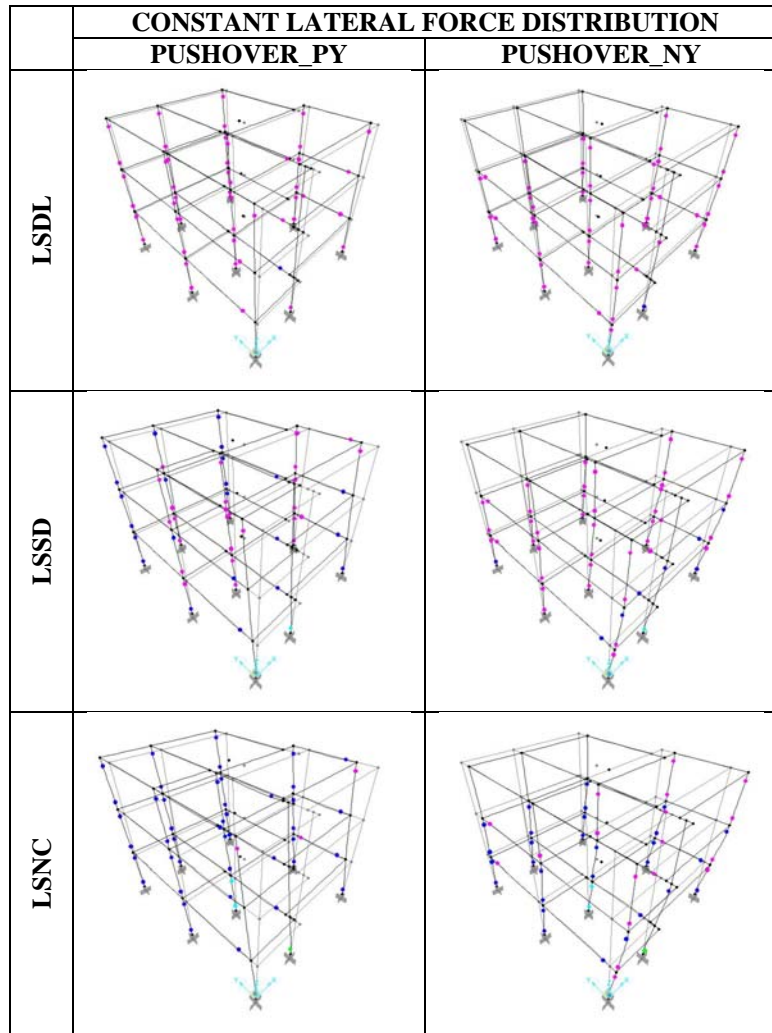


Figure C-3- Plastic hinges distribution (constant lateral loads, direction Y)

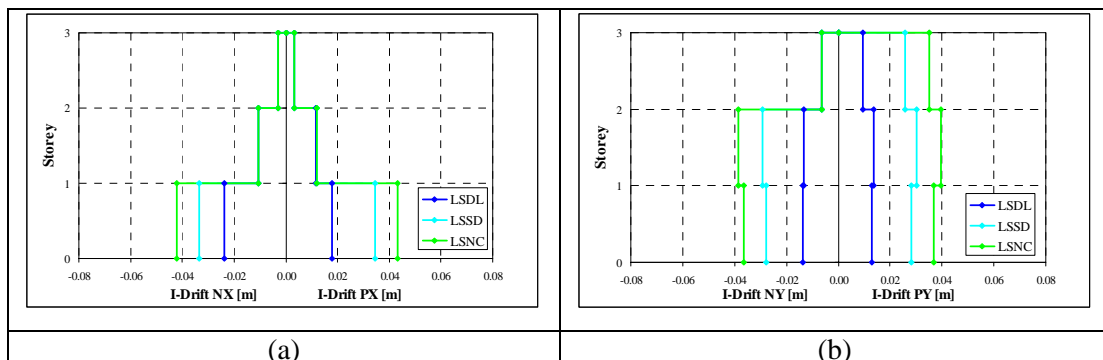


Figure C-4 – Interstorey displacements: (a) X direction, (b) Y direction

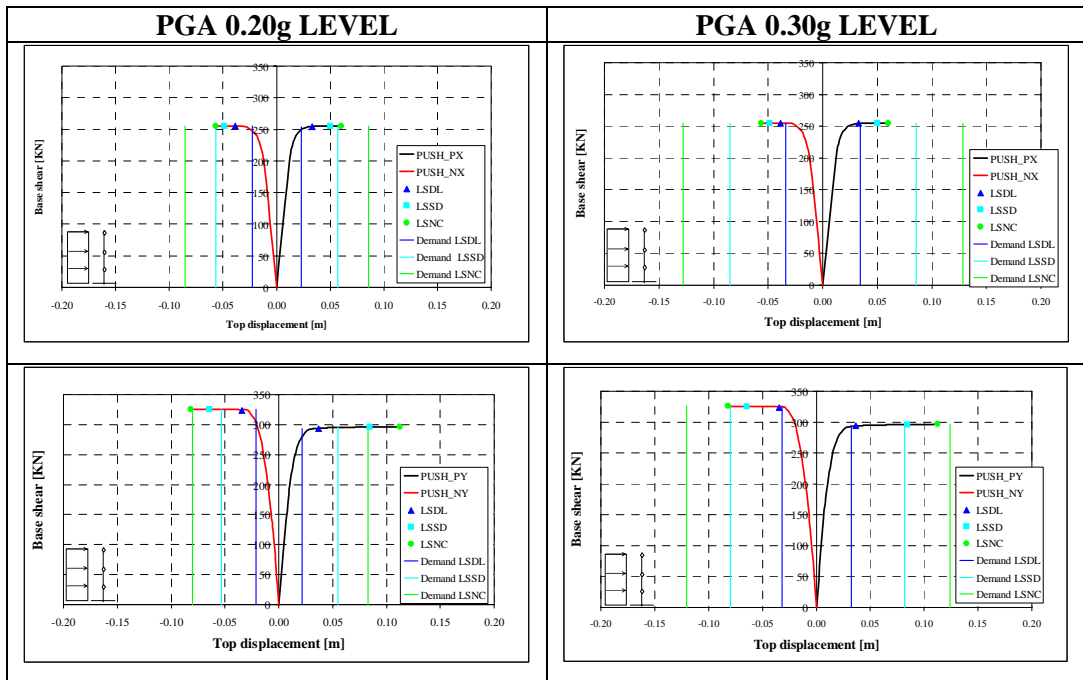
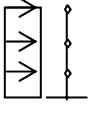
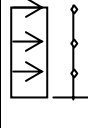


Figure C-5 – Demand vs. capacity comparison for PGA level equal to 0.20g and 0.30g at LSDL,LSSD and LSNC.

		CAPACITY	DEMAND	
			0,20g	0,30g
		d _{max} [m]	d _{max} [m]	d _{max} [m]
PUSH_PX	LSDL	0,0329	0,0228	0,0343*
	LSSD	0,0497	0,0572*	0,0858*
	LSNC	0,0585	0,0858*	0,1287*
PUSH_NX	LSDL	0,0373	0,0227	0,0341
	LSSD	0,0469	0,0568*	0,0852*
	LSNC	0,0557	0,0852*	0,1278*

		CAPACITY	DEMAND	
			0,20g	0,30g
		d _{max} [m]	d _{max} [m]	d _{max} [m]
PUSH_PY	LSDL	0,0361	0,0216	0,0324
	LSSD	0,0845	0,0548	0,0821
	LSNC	0,1113	0,0829	0,1243*
PUSH_NY	LSDL	0,0334	0,0213	0,0319
	LSSD	0,0634	0,0533	0,0800*
	LSNC	0,0814	0,0802	0,1202*

(*Demand displacements not satisfied by the structure)

Table C-3- Demand vs. capacity comparison for PGA level equal to 0.20g and 0.30g at LSDL,LSSD and LSNC

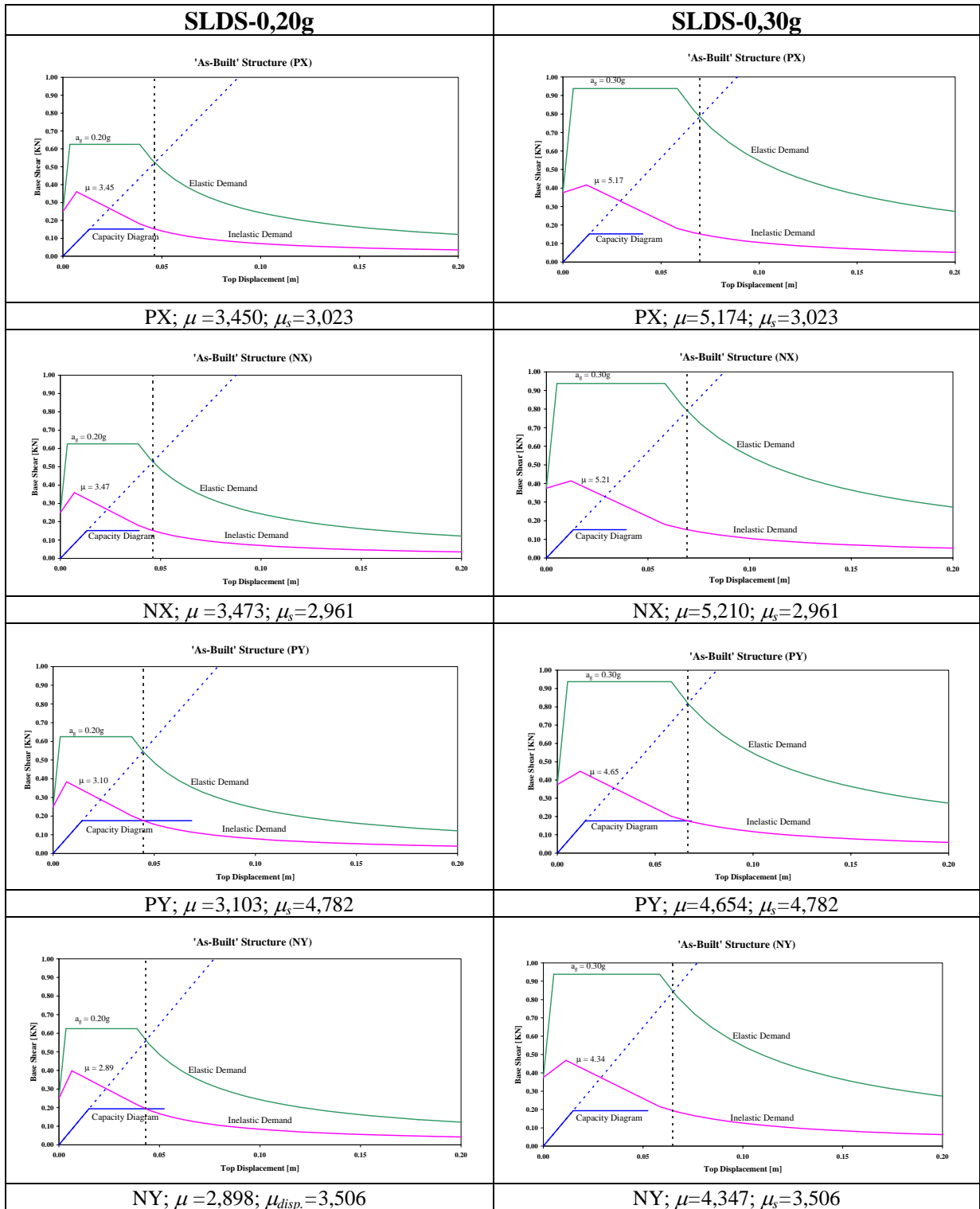


Figure C-6 - N2 method, capacity vs. demand

D. APPENDIX B: Plastic Hinges Characterization on the RC Jacketed Structure

COLUMN	N [KN]
C1_1	-286,69
C1_2	-192,34
C1_3	-93,74
C2_1	-212,71
C2_2	-139,00
C2_3	-65,85
C3_1	-345,55
C3_2	-221,26
C3_3	-109,49
C4_1	-378,67
C4_2	-250,68
C4_3	-121,24
C5_1	-87,79
C5_2	-58,15
C5_3	-26,86
C6_1	-278,54
C6_2	-188,21
C6_3	-92,55
C7_1	-135,69
C7_2	-89,34
C7_3	-42,27
C8_1	-80,10
C8_2	-53,71
C8_3	-23,94
C9_1	-189,70
C9_2	-126,27
C9_3	-61,04

Table D-1- Axial load values for each column at each storey due to gravity loads

HINGE	b [mm]	h [mm]	N [KN]	M_y^+ [KNm]	M_y^- [KNm]	M_u^+ [KNm]	M_u^- [KNm]	θ_y^+ [rad]	θ_y^- [rad]	θ_u^+ [rad]	θ_u^- [rad]
HB1sc5	250	500	0	32,17	62,95	34,09	66,21	0,0042	0,0044	0,0235	0,0238
HB1sc1	250	500	0	32,19	93,06	34,16	98,32	0,0042	0,0046	0,0236	0,0242
HB2sc1	250	500	0	32,19	93,06	34,16	98,32	0,0052	0,0058	0,0303	0,0312
HB2sc2	250	500	0	32,17	62,95	34,09	66,21	0,0053	0,0056	0,0302	0,0306
HB3sc9	250	500	0	32,17	62,95	34,09	66,21	0,0042	0,0044	0,0235	0,0238
HB3sc3	250	500	0	32,17	62,95	34,09	66,21	0,0042	0,0044	0,0235	0,0238
HB4sc3	250	500	0	130,70	199,90	135,30	211,30	0,0066	0,0073	0,0383	0,0324
HB4sc4	250	500	0	130,70	199,90	135,30	211,30	0,0066	0,0073	0,0383	0,0324
HB5sc8	250	500	0	32,17	62,95	34,09	66,21	0,0042	0,0044	0,0235	0,0238
HB5sc6	250	500	0	32,17	62,95	34,09	66,21	0,0042	0,0044	0,0235	0,0238
HB6sc6	250	500	0	32,17	62,95	34,09	66,21	0,0058	0,0062	0,0335	0,0340
HB6sc7	250	500	0	32,17	62,95	34,09	66,21	0,0058	0,0062	0,0335	0,0340
HB7sc2	250	500	0	87,80	158,00	91,06	167,20	0,0064	0,0071	0,0376	0,0331
HB7sc4	250	500	0	87,80	158,00	91,06	167,20	0,0064	0,0071	0,0376	0,0331
HB8sc4	250	500	0	32,17	62,95	34,09	66,21	0,0047	0,0050	0,0269	0,0273
HB8sc7	250	500	0	32,17	62,95	34,09	66,21	0,0047	0,0050	0,0269	0,0273
HB9sc1	250	500	0	87,46	117,30	91,07	123,10	0,0064	0,0067	0,0371	0,0376
HB9sc3	250	500	0	88,05	198,00	91,05	210,80	0,0063	0,0074	0,0379	0,0281
HB10sc3	250	500	0	32,20	115,90	34,20	123,00	0,0048	0,0055	0,0297	0,0268
HB10sc6	250	500	0	32,17	62,95	34,09	66,21	0,0047	0,0050	0,0269	0,0273
HB11sc5	250	500	0	32,17	62,95	34,09	66,21	0,0055	0,0059	0,0319	0,0323
HB11sc9	250	500	0	32,19	93,06	34,16	98,32	0,0055	0,0061	0,0319	0,0329
HB12sc9	250	500	0	32,19	93,06	34,16	98,32	0,0052	0,0058	0,0303	0,0312
HB12sc8	250	500	0	32,17	62,95	34,09	66,21	0,0053	0,0056	0,0302	0,0306

Table D-2- Beams plastic hinge moments and rotations values

HINGE	b [mm]	h [mm]	N [KN]	M_y [KNm]	M_u [KNm]	θ_y [rad]	θ_u [rad]
HC1bot._1	400	400	-286,69	135,80	162,00	0,0065	0,0152
HC1top._1	400	400	-276,33	134,40	160,40	0,0065	0,0154
HC1bot._2	400	400	-192,34	123,20	147,90	0,0066	0,0175
HC1top._2	400	400	-181,02	121,60	146,10	0,0066	0,0177
HC1bot._3	400	400	-93,74	109,70	139,20	0,0064	0,0195
HC1top._3	400	400	-82,43	108,10	131,10	0,0064	0,0197
HC2bot._1	250	250	-212,71	33,82	36,92	0,0083	0,0191
HC2top._1	250	250	-208,66	33,50	36,56	0,0083	0,0193
HC2bot._2	250	250	-139,00	27,66	30,02	0,0082	0,0241
HC2top._2	250	250	-134,59	27,28	29,60	0,0081	0,0244
HC2bot._3	250	250	-65,85	21,03	22,78	0,0076	0,0295
HC2top._3	250	250	-61,43	20,62	22,35	0,0075	0,0299
HC3bot._1	250	250	-345,55	44,29	47,97	0,0093	0,0137
HC3top._1	250	250	-341,50	44,01	47,70	0,0093	0,0138
HC3bot._2	250	250	-221,26	34,83	38,06	0,0088	0,0194
HC3top._2	250	250	-216,85	34,48	37,67	0,0088	0,0196
HC3bot._3	250	250	-109,49	25,23	27,33	0,0080	0,0260
HC3top._3	250	250	-105,07	24,84	26,91	0,0079	0,0263
HC4bot._1	400	400	-378,67	148,10	175,70	0,0067	0,0139
HC4top._1	400	400	-368,30	146,70	174,20	0,0066	0,0140
HC4bot._2	400	400	-250,68	131,40	157,00	0,0067	0,0164
HC4top._2	400	400	-239,37	129,80	155,30	0,0067	0,0166
HC4bot._3	400	400	-121,24	113,70	137,30	0,0065	0,0189
HC4top._3	400	400	-109,93	112,10	135,50	0,0065	0,0191
HC5bot._1	250	250	-87,79	22,90	24,79	0,0074	0,0267
HC5top._1	250	250	-83,74	22,53	24,40	0,0073	0,0270
HC5bot._2	250	250	-58,15	20,20	21,91	0,0075	0,0302
HC5top._2	250	250	-53,73	19,79	21,48	0,0075	0,0306
HC5bot._3	250	250	-26,86	17,23	18,81	0,0072	0,0330
HC5top._3	250	250	-22,44	16,80	18,38	0,0072	0,0334
HC6bot._1	250	750	-278,54	172,90	218,50	0,0041	0,0125
HC6top._1	250	750	-263,23	168,90	213,80	0,0040	0,0129
HC6bot._2	250	750	-188,21	148,90	190,30	0,0040	0,0158
HC6top._2	250	750	-171,50	144,30	184,90	0,0040	0,0166
HC6bot._3	250	750	-92,55	122,50	158,80	0,0039	0,0175
HC6top._3	250	750	-75,84	117,80	153,10	0,0039	0,0174
HC6bot._1	750	250	-278,54	58,80	68,80	0,0073	0,0261
HC6top._1	750	250	-263,23	57,44	67,31	0,0073	0,0266
HC6bot._2	750	250	-188,21	50,71	59,97	0,0075	0,0302
HC6top._2	750	250	-171,50	49,18	58,32	0,0074	0,0308
HC6bot._3	750	250	-92,55	41,84	50,52	0,0072	0,0337
HC6top._3	750	250	-75,84	40,25	48,85	0,0071	0,0343
HC7bot._1	250	250	-135,69	27,12	29,42	0,0077	0,0234
HC7top._1	250	250	-131,64	26,77	29,03	0,0077	0,0237

HC7bot._2	250	250	-89,34	23,04	24,95	0,0078	0,0277
HC7top._2	250	250	-84,92	22,65	24,52	0,0077	0,0281
HC7bot._3	250	250	-42,27	18,69	20,32	0,0074	0,0316
HC7top._3	250	250	-37,85	18,27	19,89	0,0073	0,0320
HC8bot._1	250	250	-80,10	21,97	23,79	0,0073	0,0274
HC8top._1	250	250	-76,05	21,60	23,39	0,0072	0,0278
HC8bot._2	250	250	-53,71	19,58	21,26	0,0075	0,0308
HC8top._2	250	250	-49,29	19,17	20,83	0,0074	0,0312
HC8bot._3	250	250	-23,94	16,85	18,43	0,0072	0,0333
HC8top._3	250	250	-19,52	16,42	17,99	0,0072	0,0337
HC9bot._1	250	250	-189,70	31,50	34,32	0,0081	0,0205
HC9top._1	250	250	-185,65	31,17	33,94	0,0080	0,0207
HC9bot._2	250	250	-126,27	26,20	28,39	0,0080	0,0252
HC9top._2	250	250	-121,85	25,81	27,97	0,0080	0,0255
HC9bot._3	250	250	-61,04	20,39	22,11	0,0075	0,0301
HC9top._3	250	250	-56,63	19,98	21,68	0,0075	0,0304

Table D-3- Columns plastic hinge moments and rotations values